Optical quantum error correction and detection against photon loss for qubits and beyond

Dissertation zur Erlangung des akademischen Grades

„Doktor der Naturwissenschaften"

am Fachbereich Physik, Mathematik und Informatik
der Johannes Gutenberg-Universität Mainz

Marcel Bergmann
geboren in Siegen

Mainz, Januar 2018

II

Abstract

The realization of optical quantum communication protocols is still one of the most challenging tasks in quantum information. To make specific tasks like quantum teleportation or quantum key distribution over large distances possible, the exponential decay of photonic quantum information has to be compensated. To achieve this, quantum repeaters exploiting quantum error detection and correction of photon losses have been proposed. In this thesis, new schemes to tackle the photon loss occurring in optical fibers are developed and applied in quantum communication scenarios.

The main part of this thesis is on quantum error correcting codes against photon loss. We develop exact codes based on NOON states and linear optics as well as approximate codes based on coherent state superpositions. For both classes of codes, we investigate suitable performance measures and show how to generalize them from logical qubits to general logical qudits. Furthermore, we apply the proposed codes in so-called one-way communication schemes to demonstrate their practical relevance.

Beside this, we propose a generalization of a known hybrid quantum repeater protocol for the distribution of material qubit-qubit entanglement mediated by coherent states of light to arbitrary finite dimensional material qudit-qudit entanglement distribution. Assuming perfect matter memories and deterministic entanglement swapping operations, we calculate the entanglement distribution rates and final fidelities for various total distances and repeater spacings.

Zusammenfassung

Die Umsetzung optischer Quantenkommunikationsprotokolle ist immer noch eine der größten Herausforderungen in der Quanteninformatik. Für die Realisierung von Quantenteleportation oder Quantenschlüsselaustauschverfahren über große Entfernungen muss der exponentielle Abfall der photonischen Quanteninformation kompensiert werden. Um dies zu erreichen wurden Quantenrepeaterprotokolle auf der Basis von Quantenfehlerdetektion und -korrektur der Photonenverluste vorgeschlagen. In dieser Arbeit werden neue Schemata zur Reduktion des Einflusses von Photonenverlusten in optischen Fasern entwickelt und im Umfeld der Quantenkommunikation angewandt.

Der Hauptteil dieser Arbeit handelt von Quantenfehlerkorrekturkodierungen gegen Photonenverluste. Es werden sowohl exakte Kodierungen auf der Basis von sogenannten NOON-Zuständen und linearer Optik als auch approximative Kodierungen basierend auf Superpositionen optischer kohärenter Zustände entwickelt. Für beide Klassen von Kodierungen werden geeignete Qualitätskriterien untersucht sowie Verallgemeinerungen der Kodierungen von logischen Qubits zu allgemeinen logischen Qudits (quantenmechanische „d-level"-Systeme) diskutiert. Um ihre Praxistauglichkeit zu demonstrieren, werden die vorgeschlagenen Kodierungen in Ein-Weg-Kommunikationsschemata angewandt, d.h. in Schemata, bei denen kodierte Quanteninformation direkt durch entsprechende Quantenkanäle gesendet wird ohne z.B. eine vorausgehende Verteilung verschränkter Zustände.

Desweiteren verallgemeinern wir ein bekanntes hybrides Quantenrepeaterprotokoll zur Verteilung materieller Qubit-Qubit-Verschränkung auf der Basis optischer kohärenter Zustände auf die Verteilung beliebig-endlichdimensionaler materieller Qudit-Qudit-Verschränkung. Unter der Annahme perfekter Speicher und deterministischem Verschränkungsaustausch werden die Raten und Güten dieses Repeaterprotokolls für diverse elementare Distanzen und Gesamtdistanzen berechnet.

List of publications and contributions

The results presented in this thesis have partially appeared in the following publications (see Chapters 5, 6 and 7, respectively):

1. **M. Bergmann** and P. van Loock: *Quantum error correction against photon loss using NOON states.* Phys. Rev. A 94, 012311 (2016)

2. **M. Bergmann** and P. van Loock: *Quantum error correction against photon loss using multicomponent cat states.* Phys. Rev. A 94, 042332 (2016)

3. **M. Bergmann** and P. van Loock: *A hybrid quantum repeater for qudits.* arXiv:1708.09322 (2017), (submitted to Physical Review A)

Besides that, my contribution to the following publication can be found in Appendix D of this thesis:

4. J. Yoshikawa, **M. Bergmann**, P. van Loock, M. Fuwa, M. Okada, K. Takase, T. Toyama, K. Makino, S. Takeda and A. Furusawa: *Heralded creation of photonic qudits from parametric down conversion using linear optics.* arXiv: 1710.08906 (2017), (submitted to Physical Review A)

This paper introduces an experimental scheme to generate an arbitrary superposition of two-mode optical states with fixed total photon number based on weak two-mode squeezed states of light and linear optics. Experimental results are provided for states of total photon number two, representing a qutrit. I calculated the transmission and reflection parameters as well as success probabilities for various examples, especially for the generation of a loss-protected qubit with total photon number 4.

So far unpublished results concerning quantum repeaters for continuous variables and ion-light interfaces can be found in Sections 7.1.2 and 7.2, respectively.

Not directly related to or discussed in this thesis are the following publications:

5. **M. Bergmann** and O. Gühne: *Entanglement criteria for Dicke states.* J. Phys. A: Math. Theor. 46, 385304 (2013)

6. F. Ewert, **M. Bergmann** and P. van Loock: *Ultrafast Long-Distance Quantum Communication with Static Linear Optics .* Phys. Rev. Lett. 117, 210501 (2016)

Contents

Chapter 1

Introduction

A future quantum internet promises a huge variety of possible features and applications [1, 2]. Not only are quantum networks expected to realize distributed quantum computing tasks [3] and to link future quantum computers. They can, in addition, also offer pure communication tasks like clock synchronization [4], the combination of telescopes [5] or the establishment of secret keys [6, 7] between two or more parties [8] for secure classical communication. Especially because of the latter, the field of quantum communication has created much interest during the last years.

Photons are fundamental carriers of quantum information [9]. Since they only very weakly interact with each other, they have been intensively investigated in the framework of optical quantum computing [10, 11]. Traveling at the speed of light, photons are furthermore the optimal choice for quantum communication.

Long-distance quantum communication protocols have been experimentally implemented in free-space scenarios, for instance by transmitting photonic states between an orbiting satellite and a telescope on Earth [12] or between the canary islands La Palma and Tenerife [13]. However, in free space quantum communication atmospheric losses induced by scattering and scintillation are, besides geometric losses related to the apertures of the telescopes, major issues which are extremely dependent on the weather conditions such as cloudiness.

Another approach, inspired by classical optical communication schemes, is the transmission of photonic quantum information by using more reliable optical fibers. Optical fibers are waveguides working on the principle of total reflection and routinely applied in many different technological fields.

The main problem in fiber-based quantum communication is the loss of photons due to atomic absorption. This results in an exponential decay of the transmission probability with the propagation distance of the photon inside the optical fiber. In classical optical communication schemes, this problem can be solved by reamplifying the signal. In the framework of quantum mechanics, cloning and amplification of an unknown quantum state is impossible [14, 15], such

that the classical approaches cannot be applied. To nevertheless avoid the exponential decay of photonic quantum information, quantum repeaters were proposed [16, 17, 18].

To date, quantum repeaters are characterized by the methods they employ to fight against the photon losses. This leads roughly to three different classes of quantum repeater protocols, also called quantum repeater generations [19].

Concerning photon losses, first- and second-generation quantum repeaters employ the distribution, purification [20] and swapping [21] of entangled states for quantum error detection [22], while in third-generation quantum repeaters, typically, encoded quantum information is sent directly using active quantum error correction [23].

Quantum error correction (QEC) [24, 22, 25] has been introduced to handle the fragility of quantum states in the presence of noise and decoherence. Decoherence leads, in general, to changes of the quantum states and induces errors in the stored quantum information. The aim of quantum error correction is to detect at least some of the errors and to recover the initial quantum information.

The basic unit of quantum information is, in analogy to a classical bit, the quantum bit or qubit. A qubit is a two-dimensional quantum system and the quantum information is stored in quantum states consisting in superpositions of the corresponding two orthogonal basis states usually denoted by $|0\rangle$ and $|1\rangle$. Mathematically, a qubit can be considered as a normalized vector in a two-dimensional Hilbert space and the physical operations are unitary operations in this space. Physical realizations of qubits are numerous, e.g. the two spin states of an electron, an atomic nucleus [26] or the stable electronic states of trapped ions [27] as well as the polarization of a single photon [9].

A single qubit alone can, thanks to the superposition principle, be utilized to transmit two bits of classical information which is referred to as superdense coding [28]. To realize, however, more interesting applications such as quantum teleportation [29, 30] or measurement-based quantum computation [31], entangled states of at least two qubits such as $\frac{1}{\sqrt{2}}(|00\rangle + |11\rangle)$ are a necessary resource. Being one of the most counterintuitive genuine quantum phenomena, quantum entanglement [32, 33] is a non-local correlation between two parties, e.g. two qubits, that can be proven to be stronger than any classical correlation. It is therefore not surprising that the distribution of entangled states of two qubits over large distances has been considered a key problem in quantum communication from the very beginning and is still a cornerstone of first-generation quantum repeaters.

In some situations, it is an advantage to generalize the notion of qubit to qudits, i.e. quantum systems of arbitrary finite dimension ("qudit" here refers to a "d-level" system). One can show that the usage of qudits makes fault-tolerant quantum computing not only more efficient [34, 35] but can also improve quantum communication protocols. More precisely, qudits lead to an increase in data transfer and especially to a higher security in quantum key distribution compared

to schemes involving only qubits [36, 37]. On the fundamental level qudits play an important role in closing of the detection loophole in Bell test experiments [38, 39]. Furthermore, the generation of a highly-entangled state between two ten-dimensional photonic quantum systems has been confirmed in [40]. An experimental scheme for generating arbitrary superpositions of photonic Fock states up to photon number three, which finally represents a qutrit, has been proposed in [41].

The notion of a qudit can be extended from finite to infinite dimensions. Since any observable of a quantum system either possesses a discrete or continuous spectrum, there is a priori a choice for employing the corresponding eigenstates as discrete or continuous bases for the description of the system. For example, the quantum harmonic oscillator can be described with the number basis as eigenstates of the discrete number operator $\hat{n} = \hat{a}^\dagger \hat{a}$, where $\hat{a}^\dagger$ and $\hat{a}$ are the usual creation and annihilation operator satisfying $[\hat{a}, \hat{a}^\dagger] = 1$. On the other hand, prominent examples of continuous-variable basis states in quantum optics [42, 43], where the light field is also described by a quantum harmonic oscillator, are position and momentum quadratures, $\hat{x} = \frac{1}{2}(\hat{a}^\dagger + \hat{a})$ and $\hat{p} = \frac{1}{2i}(\hat{a} - \hat{a}^\dagger)$, expressed by the ladder operators of a single mode of the electromagnetic field. Continuous superpositions of such basis states are then in analogy to qudits referred to as qumodes.

For such qumodes, measurements of position and momentum and, more general, quadratures can be performed very efficiently by homodyne detection, i.e. by mixing the qumode with a strong coherent state at a symmetric beam splitter and measuring the difference of photo currents in the output modes.

Despite the advantages of encoding quantum information into discrete qudits or continuous qumodes, rather little attention has so far been paid to exploiting qudits in long-distance quantum communication. From a conceptual point of view, first-generation repeater schemes for the distribution of qudit-qudit entanglement as well as higher-dimensional quantum error correction codes against photon loss are a necessity to fill this gap.

The topic of this thesis is the suppression and correction of photon losses occurring in optical fibers with a special focus on applications in long-distance quantum communication. All the developed schemes are silhouetted against existing schemes, because they also explicitly exploit the advantages of higher-dimensional quantum systems. The thesis is structured as follows.

In Chapter 2, we briefly review the physical origin of decoherence and give two different but equivalent descriptions to model photon loss in optical fibers. We furthermore discuss two prominent qubit-qubit entanglement purification schemes, which are key ingredients in first-generation quantum repeater protocols. The chapter closes with a brief introduction to quantum error detection codes.

The focus in Chapter 3 is on quantum error correction, especially in the context of photon loss. We state the Knill-Laflamme conditions [25, 22] for quantum error correction codes and explain

the difference between exact and approximate codes against photon loss. We give an overview of some of the most important known photon loss codes.

The three different classes of quantum repeaters are the topic of Chapter 4. We discuss the methods each class exploits to fight against photon losses and give examples of already proposed quantum repeater schemes for each class.

In Chapter 5, we show how so-called NOON states can be exploited for constructing exact quantum error correction codes against photon loss. Unlike existing photon loss codes, the codewords of these codes can systematically be obtained by means of experimentally obtainable NOON states and static linear optical manipulations alone. The proposed qubit codes are block codes with N photons per block. The total number of N^2 photons ensures that the corresponding logical qubit is protected exactly against $N-1$ photon losses. We furthermore show that this systematic approach can also be applied to qudit code constructions.

In the succeeding Chapter 6, we first consider a specific example of an approximate one-photon loss qubit code presented in [44] whose codewords are even cat states. After analyzing the properties of this code in a full loss channel, we generalize this code to higher losses. The possibility of a generalization of the one-loss cat code [45, 44] to higher losses has been briefly mentioned a couple of times in the literature (see the Conclusions of Ref. [45] and Section 4.2. on page 15 of Ref. [46]), including a few more detailed hints about the conceptual character of such an extension in a quite recent publication (Fig. 1 on page 4 and Section V.B. on page 10 of Ref. [47]). However, as far as we know, there is no detailed analysis of a generalized code that includes a complete and systematic definition of the codewords as well as a quantitative performance assessment of the code in a full amplitude-damping channel. In Chapter 6, we present such an analysis and give a very compact definition of the codewords for any number of correctable losses in terms of eigenvalue equations. It turns out that the eigenvalue equation approach is extendable to arbitrary approximate qudit codes.

The first part of Chapter 7 deals with first-generation quantum repeaters. We generalize a well-known hybrid quantum repeater (HQR) protocol for the long-distance distribution of qubit-qubit entanglement based on matter qubits and coherent-state light to the case of material qudit-qudit entanglement. The proposed protocol especially exploits both discrete and continuous variable quantum states and is, like the original qubit scheme, attractive for experimental realization.

In addition, we give a proposal for the faithful long-distance transmission of arbitrary continuous variable states by means of combining a known teleportation scheme and discrete variable quantum repeaters. Furthermore, we introduce a light-matter interface that allows to switch between noise-protected ionic quantum states and loss-protected photonic states. Such an ion-light interface could be employed in a second-generation quantum repeater.

Chapter 7 ends with the application of some of the codes developed in Chapters 5 and 6 in a

certain instance of a third-generation quantum repeater scheme, namely a so-called one-way scheme. We introduce and analyze performance measures adapted to both kinds of codes for various communication scenarios.

Concluding remarks and an outlook on future research directions can be found in Chapter 8. Due to the technically demanding flavor of this thesis, several appendices provide detailed calculations and additional information.

Chapter 2

Quantum error detection

In this chapter, we explain how photon loss in optical fibers can be modeled by means of an open system approach. The Kraus operators related to the photon loss channel, which play a major role in almost all parts of this thesis, are introduced. After clarifying the physical decoherence model, we discuss two important tools of quantum error detection that are typically included in quantum repeater schemes of the first kind, namely entanglement purification and the notion of quantum error detection codes. We consider two important entanglement purification schemes for qubit-qubit-entangled states and a dual-rail encoded photonic qubit as an example of a quantum error detection code.

2.1 Open system dynamics and photon loss

A quantum system is never completely isolated but interacts at least weakly with its environment [48]. While the evolution of the closed system is determined by solving the Schrödinger equation for the system Hamiltonian H_S, the open system dynamics is governed by two more Hamiltonians [49], namely the Hamiltonian of the environment H_E and an interaction Hamiltonian between the system and the environment H_I [1]. The total Hamiltonian H_{SE} of the system and the environment thus reads

$$H_{SE} = H_S + H_E + H_I. \tag{2.1}$$

At $t = 0$, the joint state is usually a product state $\rho_{SE}(t = 0) = \rho_S \otimes \rho_E$ with density operators ρ_S of the system and ρ_E of the environment. The total evolution of system and environment can be cast using the unitary global time-evolution operator $U_{SE}(t) = \exp(-\frac{i}{\hbar}H_{SE}t)$,

$$\rho_{SE}(t) = U_{SE}(t)\rho_{SE}(t = 0)U_{SE}^\dagger(t). \tag{2.2}$$

---

[1]To avoid unnecessary complications, we assume that the occurring Hamiltonians do not show explicit time-dependence.

Since the state of the environment is unobservable and the state of system S alone is anyway of particular interest, we build the trace over the environment to find

$$\rho_S(t) = \mathrm{Tr}_E[U_{SE}(t)\rho_{SE}(t=0)U_{SE}^\dagger(t)], \tag{2.3}$$

for the evolution of the quantum system S. Physically motivated, this approach is general and describes all kinds of open system dynamics such as decoherence, dissipation, ensembles of measurements and thermal relaxation.

In some situations, however, an equivalent approach via the notion of completely positive, trace-preserving (CPTP) maps is convenient [22]. From this point of view, we interpret the dynamics of a density matrix as a quantum operation. This operation is a map whose input is a density operator from an underlying Hilbert space and whose output is a density operator from a target Hilbert space. To ensure that the output is a density operator, i.e. a physical state, a map Φ has to fulfill three conditions.

First, Φ must be trace-preserving, i.e. $\Phi(\rho)$ has trace 1 for all input states ρ. This is an obvious criterion, since the output is desired to be a regular density operator[2]. Second, $\Phi(\rho)$ must be positive, i.e. it has non-negative eigenvalues which are to be interpreted as probabilities of the output state. The third required property is that Φ is completely positive, i.e. the map $(1 \otimes \Phi)(\rho')$ with support on density operators in a higher-dimensional Hilbert space leads to global output states that are still physical. Maps with these three properties are called completely positive, trace-preserving (CPTP) maps.

A first important observation following from a result in functional analysis [50] is that any CPTP map can be constructed as in Eq. (2.3). The three necessary operations to be performed are the tensor product with an arbitrary ancilla state, a joint unitary describing the interaction and the partial trace over the ancilla system.

Another very useful property of CPTP maps that we will exploit in Chapters 5 and 6 is the operator-sum representation [51, 52, 22]. It states that the action of any CPTP map Φ (and thus the non-unitary evolution of any open system) can be described as

$$\widetilde{\rho} := \Phi(\rho) = \sum_i E_i \rho E_i^\dagger, \tag{2.4}$$

where the so-called Kraus operators E_i are related to the so-called "positive operator-valued measure" (POVM) elements $E_i^\dagger E_i \geq 0$ with $\sum_{i=0}^\infty E_i^\dagger E_i = 1$.

So far, the description of the evolution of open quantum systems has been rather general. In this thesis, we are exclusively looking at photons traveling through an optical fiber. Since our goal is the faithful transmission of optical quantum information, the open system evolution

---

[2]Individual terms of a CPTP map written in the operator-sum representation (see below) are then trace-decreasing. Trace-decreasing maps may describe conditional evolutions depending on measurement outcomes.

described above leads to decoherence and loss of quantum information. For instance, photons can be scattered by flaws and impurities or be reflected by splices and connections. In addition, birefringence can occur that leads to photon pair generation. All these error sources are, however, minor issues and will be neglected in this thesis.

The main error source for photonic quantum information processing in optical fibers is photon loss due to atomic absorption. This is clearly a dissipation process that can be treated with the system-environment approach (2.3), leading to the so-called amplitude damping model (AD) [49, 52, 53]. The system in this case is a mode of a single harmonic oscillator expressible in the photon number basis ("Fock basis"), $\{|n\rangle, n = 0, 1, 2, ...\}$. The pure environmental state is assumed to be a vacuum state, $|0\rangle$. Physically, this corresponds to a zero-temperature environment. The interaction Hamiltonian will be represented by a beam splitter operation with transmittance χ (which plays the role of the coupling strength). The Hamiltonian in this case is given by

$$H_{BS} = \hbar\chi(\hat{a}^\dagger\hat{b} + \hat{b}^\dagger\hat{a}), \tag{2.5}$$

where $\hat{a}$ and $\hat{b}$ are the annihilation operators for the system and the environment, respectively. For special input states, this approach is rather easy to perform. This will be a main tool in Section 7.1.1 for the case of coherent states.

For calculations with discrete photon states, the Kraus operators of the AD channel are more suitable. These are given by [53]

$$A_k = \sum_{n=k}^{\infty} \sqrt{\binom{n}{k}} \sqrt{\gamma}^{n-k} \sqrt{1-\gamma}^k |n-k\rangle\langle n|, \tag{2.6}$$

$\forall k \in \{0, 1, \cdots, \infty\}$. For an optical fiber, the loss parameter $\gamma = \cos^2(\chi\Delta t)$ with an interaction time Δt, is given by $\exp(-L/L_{att})$, where L is the propagation distance of the photons in the optical fiber and $L_{att} = 22$ km is the attenuation length for photons at telecom wavelength.

The error operators in Eq. (2.6) can be equivalently cast in a different form that will be especially helpful in Chapter 6 for the no-loss and one-loss cases:

$$A_k = \sqrt{\frac{(1-\gamma)^k}{k!}} \sqrt{\gamma}^{\hat{n}} \hat{a}^k, \tag{2.7}$$

with the number operator $\hat{n}$.

Important for the code construction in Chapters 5 and 6 are systems consisting of many modes. For this scenario, we consider individual loss, i.e. each mode suffers from loss independent of all other modes. The corresponding multi-mode Kraus operators are thus given by tensor products of the single-mode Kraus operators, e.g. $A_0 \otimes A_1$ for a two-mode system corresponds to no loss on the first mode and one-photon loss on the second mode.

2.2 Entanglement purification

As directly obvious from Eq. (2.4), decoherence and errors turn a pure quantum state into a mixed quantum state. In general, mixed entangled states degrade the performance of quantum information processing tasks like teleportation or entanglement swapping (see Sections 4.1 and 4.2). Hence, the purification of a mixed state can be advantageous.

Entanglement purification aims at generating fewer high-fidelity copies from many noisy copies of a certain pure target state. By iterating this purification protocol, a fidelity arbitrarily close to unity can be achieved.

The purification of mixed qubit states was investigated by Bennett et.al [54] for the class of Werner states [55]. Nearly at the same time, Deutsch et al. [56] proposed a similar purification protocol for more general states diagonal in the Bell basis and with arbitrary Bell-state coefficients. Both protocols require two copies for each step, but the Deutsch protocol leads to a better efficiency compared to the Bennett scheme. The latter was demonstrated experimentally [57, 58] and generalized to arbitrary dimensions [59, 60].

We will use entanglement purification in the first generation quantum repeater protocols to be investigated in Chapter 7. Higher-dimensional extensions for special cases of the qubit purification schemes, as briefly presented in the next two sections, will be shown to lead to a better performance of the proposed protocols.

2.2.1 Bennett scheme

Bennett et al. [54] proposed a purification scheme where the non-maximally entangled resource states ρ are given in Werner form [55], i.e.

$$\rho = F|\phi^+\rangle\langle\phi^+| + \left(\frac{1-F}{3}\right)(|\psi^-\rangle\langle\psi^-| + |\psi^+\rangle\langle\psi^+| + |\phi^-\rangle\langle\phi^-|), \tag{2.8}$$

where $|\phi^\pm\rangle = \frac{1}{\sqrt{2}}(|00\rangle \pm |11\rangle)$, $|\psi^\pm\rangle = \frac{1}{\sqrt{2}}(|10\rangle \pm |01\rangle)$ are the four two-qubit Bell states and $F \equiv \langle\phi^+|\rho|\phi^+\rangle > 1/2$ is the initial fidelity with respect to the target state $|\phi^+\rangle$.

For a single purification step, two copies ρ_{12} and ρ_{34} of the state in Eq. (2.8) are required. A crucial point of purification protocols is that one is restricted to local operations and classical communication (LOCC). The physical reason is that the two parties sharing the entangled state are assumed to be spatially separated by a certain distance such that they do not have access to both qubits to perform joint measurements on them. Otherwise, the state in Eq. (2.8) could simply be purified by a non-local Bell measurement. So in this setting, it is assumed that one party has access to qubits 1 and 3, the other to qubits 2 and 4.

The joint state of four qubits is given by $\rho_{1234} = \rho_{12} \otimes \rho_{34}$. To obtain a two-qubit state with higher fidelity, both parties apply CNOT gates on their respective qubits, $CNOT_{13}$ and

$CNOT_{24}$. Finally, qubits 3 and 4 are measured in the Z-Basis and both parties compare their results. If the two results coincide, the state is purified. If not, the output state is discarded. If successful, this purification scheme results in a new mixed state whose fidelity F' with respect to the target state $|\phi^+\rangle$ is [54, 20]

$$F' = \frac{F^2 + \left(\frac{1-F}{3}\right)^2}{F^2 + \frac{2}{3}F(1-F) + \frac{5}{9}(1-F)^2}, \tag{2.9}$$

which corresponds to a fidelity gain provided that $F > 1/2$. Taking such states as new resource states, more rounds of purification can be performed to further increase the fidelity.

2.2.2 Deutsch scheme

Deutsch et al. [56] introduced a purification protocol where the resource states are given by a general mixture of the four Bell states,

$$\rho = F_1|\psi^+\rangle\langle\psi^+| + F_2|\psi^-\rangle\langle\psi^-| + F_3|\phi^+\rangle\langle\phi^+| + F_4|\phi^-\rangle\langle\phi^-|, \tag{2.10}$$

where $F_1 + F_2 + F_3 + F_4 = 1$ and $F_1 > 1/2$ is the initial fidelity with respect to $|\psi^+\rangle$.
Now given two copies of states like in Eq. (2.10), the first step of the purification protocol are unitary single-qubit transformations on qubits 1 and 3 as well as on 2 and 4. On qubits 1 and 3 the transformation

$$\begin{aligned} |0\rangle &\mapsto \frac{1}{\sqrt{2}}(|0\rangle - i|1\rangle), \\ |1\rangle &\mapsto \frac{1}{\sqrt{2}}(|1\rangle - i|0\rangle), \end{aligned} \tag{2.11}$$

is applied. A similar transformation is performed on qubits 2 and 4,

$$\begin{aligned} |0\rangle &\mapsto \frac{1}{\sqrt{2}}(|0\rangle + i|1\rangle), \\ |1\rangle &\mapsto \frac{1}{\sqrt{2}}(|1\rangle + i|0\rangle). \end{aligned} \tag{2.12}$$

After these unitary transformations, CNOT gates are applied on qubits 1 and 3 as well as on 2 and 4. As in the Bennett scheme, the final step is to measure qubits 3 and 4 in the Z-basis. Again, if the results coincide, purification has succeeded, or otherwise the state is discarded. The new fidelity with respect to the target state $|\psi^+\rangle$ in case of a successful purification reads

$$F_1' = \frac{F_1^2 + F_3^2}{(F_1 + F_3)^2 + (F_2 + F_4)^2}, \tag{2.13}$$

for which $F_1' > F_1$ holds if $F_1 > 1/2$.
In optical experiments, both the Bennett and the Deutsch scheme are difficult to realize with

single photons, since optical CNOT gates require high non-linearities and therefore efficient CNOT gates do not exist at the moment. However, the simpler task for the purification of mixed states that only consist of two Bell-state components, $|\phi^+\rangle$ and $|\psi^+\rangle$, has been performed experimentally [57, 58]. This scheme is based on polarization encoding and photon detection of four-fold detection events. Due to realistically inefficient measurements, the efficiency is far from those of the theoretical proposals with perfect gates and operations.

2.3   Quantum error detection codes

For applications like quantum computing or quantum communication, it is a crucial prerequisite to find out if a state has been successfully generated or received. In optical quantum information processing, it is therefore desired to find out if a photon was lost or not. This is the goal of quantum error detection codes [22].

An arbitrary "single-rail" qubit is denoted as $|\psi\rangle = \alpha|0\rangle + \beta|1\rangle$ with $|\alpha|^2 + |\beta|^2 = 1$. By applying A_1, one can easily verify that there is no way to find out if a loss has occurred because of the intial vacuum term. To circumvent this problem, it is useful to encode the qubit information into a dual-rail qubit, i.e. to perform the mapping

$$
\begin{aligned}
|0\rangle &\mapsto |\bar{0}\rangle = |10\rangle, \\
|1\rangle &\mapsto |\bar{1}\rangle = |01\rangle,
\end{aligned}
\tag{2.14}
$$

such that the encoded, logical qubit state reads $|\bar{\psi}\rangle = \alpha|10\rangle + \beta|01\rangle$. If now AD channels are applied to both modes simultaneously and independently, the resulting state becomes

$$
\rho = \gamma|\bar{\psi}\rangle\langle\bar{\psi}| + (1-\gamma)|00\rangle\langle00|.
\tag{2.15}
$$

Now, for instance, by means of a quantum non-demolition (QND) measurement of the total photon number on the two modes, we can infer whether a loss error has occurred or not. If we measure 1, then everything worked fine and we can further process the qubit. If we measure 0, we have to discard the state and start anew.

In general, a quantum error detection code is a subspace of some higher-dimensional Hilbert space that enables us to perform a measurement to find out if there was some error on the logical state. Note, however, that these errors cannot be corrected, but the state has to be prepared or sent again if an error was detected. To be more specific, states obtained from different errors are, in general, not necessarily distinguishable and therefore mapping them back to the original state is no longer possible. Moreover, even worse, the qubit information may be completely destroyed when the error occurs, although the error can be detected (like for the $|00\rangle\langle00|$-term in Eq. (2.15)). Correcting errors requires the qubit to remain intact in an orthogonal error

space. This requires quantum error correction codes (see Chapter 3).

Chapter 3

Quantum error correction (QEC)

This chapter introduces the notion of quantum error correction on which a large part of this thesis is based. We motivate and define quantum error correction codes and state the central Knill-Laflamme conditions. The fidelity as a measure of a quantum error correcting code's performance is introduced. Based on the error operators for photon loss (Eq. (2.6)), several existing photon loss codes and their performance are reviewed. By the example of these codes, we explain the differences between exact and approximate photon loss codes.

3.1 Quantum error correction and Knill-Laflamme conditions

The evolution of a quantum system following Eq. (2.4) is not always desired and at least some of the involved Kraus operators are considered as errors on the input state. By employing a quantum code, one is partially able to reverse the dynamics implied by Eq. (2.4) and, unlike the quantum error detection code in Section 2.3, to recover the original state.

A proper quantum code enables one to detect and correct a certain set of errors on the encoded state. A quantum code is a vector space spanned by basis codewords, denoted by $|\bar{0}\rangle \equiv |c_1\rangle$ and $|\bar{1}\rangle \equiv |c_2\rangle$ for a qubit code, and at the same time subspace of some higher-dimensional Hilbert space. Normalized elements of this vector space of the form $\alpha|\bar{0}\rangle + \beta|\bar{1}\rangle$ are called logical qubits (just as for the quantum error detection codes in Section 2.3). This notion can be extended to qudit codes, where there are more than two codewords $|c_1\rangle, \cdots, |c_d\rangle$ to encode a logical d-level system. To form a proper quantum code, the logical basis codewords have to fulfill certain conditions. We state the famous Knill-Laflamme conditions which are a set of necessary and sufficient conditions for the existence of a recovery operation [25, 22]:

Theorem 1. *(Knill-Laflamme)*

Let $C = span\{|c_1\rangle, |c_2\rangle, \cdots, |c_d\rangle\}$ be a quantum code, P be the projector onto C and $\{E_i\}$ the set of error operators. There exists an error-correction operation $\mathcal{R}$ that corrects the errors $\{E_i\}$ on C, iff

$$PE_i^\dagger E_j P = \Lambda_{ij} P, \quad \forall i, j \tag{3.1}$$

for some positive semi-definite, Hermitian matrix Λ with matrix elements Λ_{ij}.

For photon loss codes (in particular, the exact codes with a fixed total photon number), the matrix Λ is typically diagonal, i.e. $\Lambda_{ij} = g_i \delta_{ij}$. This defines a non-degenerate code with different loss errors (especially different numbers of photons lost, but also different modes subject to loss) corresponding to orthogonal error spaces. Nonetheless, certain instances of our NOON code to be developed in Chapter 5 do exhibit degeneracy for a given number of lost photons. The Knill-Laflamme (KL) conditions contain two basic notions. The first notion is the orthogonality of corrupted codewords, i.e.

$$\langle c_k | E_i^\dagger E_j | c_l \rangle = 0 \ \text{ if } \ k \neq l. \tag{3.2}$$

The second one is the non-deformability condition, i.e.

$$\langle c_l | E_i^\dagger E_i | c_l \rangle = g_i, \quad \forall l. \tag{3.3}$$

This means that the norm of a corrupted codeword only depends on the error operator and not on the codeword itself.

Our interest from now on is devoted to the Kraus operators for the AD channel, Eq. (2.6), describing photon loss. Before proceeding with an overview of already existing photon loss codes, we want to clarify how to quantify the performance of a photon loss code. A convenient measure for the quality of a quantum error correcting code is the worst-case fidelity, defined as [22, 53]

$$F = \min_{|\bar{\Psi}\rangle \in C} \langle \bar{\Psi} | \mathcal{R}(\bar{\rho}_f) | \bar{\Psi} \rangle, \tag{3.4}$$

where $\bar{\rho}_f$ is the final mixed state after multi-mode amplitude damping (with the only assumption that each AD channel acts independently on each mode) and $\mathcal{R}$ is the recovery operation. Note that the recovery operation always exists if the KL conditions are fulfilled. The fidelity defined in Eq.(3.4) is a suitable figure of merit to assess the performance of a quantum error correction code.[1] In particular, it also reveals if an encoding is not a proper code (see, e.g. the encodings in Eqs. (2.14) and (5.11)).

---

[1]The exact loss codes considered in this thesis have identical worst-case and average fidelities.

3.2 Review of some existing photon loss codes

3.2.1 Exact codes

In the first example, a logical qubit is encoded in a certain two-dimensional subspace of two bosonic modes. The basis codewords are chosen in the following way [53]:

$$|\bar{0}\rangle = \frac{1}{\sqrt{2}}(|40\rangle + |04\rangle),$$
$$|\bar{1}\rangle = |22\rangle, \tag{3.5}$$

i.e. any logical qubit has a total photon number $N^2 = 4$ [2]. This code corrects exactly $N - 1 = 1$ photon losses. The worst-case fidelity, as defined in Eq. (3.4), is found to be $F = \gamma^4 + 4\gamma^3(1 - \gamma) = 1 - 6(1 - \gamma)^2 + 8(1 - \gamma)^3 - 3(1 - \gamma)^4$. In the same reference [53], the following code is given:

$$|\bar{0}\rangle = \frac{1}{\sqrt{2}}(|70\rangle + |16\rangle),$$
$$|\bar{1}\rangle = \frac{1}{\sqrt{2}}(|52\rangle + |34\rangle). \tag{3.6}$$

This code corrects also all one-photon losses and its worst-case fidelity is

$$\gamma^7 + 7\gamma^6(1-\gamma) = 1 - 21(1-\gamma)^2 + 70(1-\gamma)^3 - 105(1-\gamma)^4 + 84(1-\gamma)^5 - 35(1-\gamma)^6 + 6(1-\gamma)^7. \tag{3.7}$$

Another example that encodes a qubit in three optical modes with a total photon number of 3 was proposed in [61]. The basis codewords are

$$|\bar{0}\rangle = \frac{1}{\sqrt{3}}(|300\rangle + |030\rangle + |003\rangle),$$
$$|\bar{1}\rangle = |111\rangle. \tag{3.8}$$

The fidelity in this case is $\gamma^3 + 3\gamma^2(1 - \gamma) = 1 - 3(1 - \gamma)^2 + 2(1 - \gamma)^3$. Moreover, note that all three codes given above are capable of exactly correcting only the loss of one photon, as can be easily seen by checking the KL conditions. An example for a proper two-photon-loss code is [53]

$$|\bar{0}\rangle = \frac{1}{2}|90\rangle + \frac{\sqrt{3}}{2}|36\rangle,$$
$$|\bar{1}\rangle = \frac{1}{2}|09\rangle + \frac{\sqrt{3}}{2}|63\rangle, \tag{3.9}$$

whose worst-case fidelity is found to be $F = \gamma^9 + 9\gamma^8(1 - \gamma) + 36\gamma^7(1 - \gamma)^2 \approx 1 - 84(1 - \gamma)^3$. What these codes also have in common is their small number of optical modes, at the expense

---

[2]In Appendix D, we present an experimentally feasible scheme to realize such a loss-protected qubit.

of having rather large maximal photon numbers in each mode (in order to obtain a sufficiently large Hilbert space). Conversely, codes that have at most one photon in any mode, but a correspondingly large total mode number, are, for example, the quantum parity codes (QPCs). The simplest non-trivial QPC, denoted as QPC(2,2), reads as follows [62]:

$$
\begin{aligned}
|\bar{0}\rangle &= \frac{1}{\sqrt{2}}(|10101010\rangle + |01010101\rangle), \\
|\bar{1}\rangle &= \frac{1}{\sqrt{2}}(|10100101\rangle + |01011010\rangle).
\end{aligned}
\tag{3.10}
$$

It also corrects exactly the loss of one photon.

3.2.2 Approximate codes

All exact codes presented in the last section consist of superpositions of states with a fixed photon number. Different from these is the following code [63]:

$$
\begin{aligned}
|\bar{0}\rangle &= \frac{1}{\sqrt{2}}(|0000\rangle + |1111\rangle), \\
|\bar{1}\rangle &= \frac{1}{\sqrt{2}}(|0011\rangle + |1100\rangle).
\end{aligned}
\tag{3.11}
$$

This code is conceptually distinct, because it does not satisfy the usual KL conditions. It satisfies certain relaxed conditions, which leads, in a more general setting, to approximate quantum error correcting schemes [63]. The above approximate code still satisfies the KL conditions up to linear order in $1 - \gamma$, corresponding to one-photon-loss correction, while it requires 4 physical qubits (single-rail qubits encoded as vacuum $|0\rangle$ and single-photon $|1\rangle$) instead of 5 physical qubits for the minimal universal one-qubit-error code [64, 65]. Note that for dual-rail physical qubits (i.e., the approximate Leung code [63] concatenated with standard optical dual-rail encoding), one obtains QPC(2,2), which is then an exact one-photon-loss code. Recently, also the concept of an approximate single-mode bosonic code was introduced whose codewords are finite superpositions of certain multiples of the photon number [47]. The easiest code which is an approximate one loss code reads as

$$
\begin{aligned}
|\bar{0}\rangle &= \frac{1}{\sqrt{2}}(|0\rangle + |4\rangle), \\
|\bar{1}\rangle &= |2\rangle,
\end{aligned}
\tag{3.12}
$$

where now only the average photon number in each codeword is equal, namely 2. The structural resemblance between this code and that in Eq. (3.5) is striking. But in terms of fidelity, this code equals the code in Eq. (3.11), because of the same average photon number.

Another approach to optical, loss-adapted QEC is to encode a logical qubit into the full Hilbert space of a single oscillator mode [66, 44, 45]. Such a code can make explicit use of the infinite-dimensional Hilbert space already available with just one optical, physical mode. Nonetheless, by sticking to a finite-dimensional (logical qubit) code space, such codes also circumvent existing no-go results for efficient QEC of logical continuous-variable Gaussian states encoded into physical, multi-mode Gaussian states [67, 68, 69, 70, 71] and subject to Gaussian error channels [72]. More precisely, non-Gaussian logical states alone, such as logical qubits, are actually not enough to circumvent those no-go results when both error and recovery channels are of Gaussian nature [73]. Note that the AD (photon-loss) channel is indeed a Gaussian channel. Nonetheless, non-Gaussian logical states subject to Gaussian error channels together with non-Gaussian ancilla states [66, 74] or with non-Gaussian operations [45, 44] for the recoveries do the trick. Similarly, Gaussian logical states subject to non-Gaussian error channels with only Gaussian recovery operations suffice to circumvent the no-go theorem [70, 71].

The qubit-into-oscillator codes are approximate codes based on non-orthogonal codewords that become perfect for infinite squeezing [66] or for infinitely large coherent-state amplitudes [45, 44]. Note that the Glancy-Knill-Preskill (GKP) code with codewords as superpositions of position (quadrature) eigenstates [66] is a universal code, whereas the "cat code" with codewords as even cat states (that is superpositions of even photon numbers) [45, 44] is specifically adapted to photon loss errors.

The codewords of the cat code presented in [44, 45] are given by

$$
\begin{aligned}
|\bar{0}_+\rangle &\sim |\alpha\rangle + |-\alpha\rangle, \\
|\bar{1}_+\rangle &\sim |i\alpha\rangle + |-i\alpha\rangle.
\end{aligned}
\tag{3.13}
$$

By writing the coherent states in the Fock basis, one can easily confirm that both codewords have only even photon number terms. If a photon gets lost, it is intuitively clear that the codewords will jump into the odd parity space. The idea is to detect the loss error via a parity measurement. A detailed analysis of the behavior of this approximate one-loss code under the AD channel as well as its performance in terms of fidelities is so far missing and therefore the topic of Section 6.1.

Chapter 4

Quantum repeaters (QRs)

The faithful transmission of photonic quantum information over large distances is one of the most challenging tasks in practical quantum information. As pointed out in Section 2.1, the transmission probability γ of a single photon decays exponentially with the length L of the optical fiber channel,

$$\gamma = \exp(-L/22\text{km}),$$

such that photon loss, represented by the AD channel, becomes a serious problem. Unlike classical information, quantum states cannot be amplified without adding extra noise due to the no-cloning theorem [14]. Quantum repeaters were therefore introduced to overcome the problem of transmission loss [16, 17, 18].

From the perspective of the most recent quantum repeater research, a quantum repeater protocol can be classified into three distinct categories, referred to as quantum repeater generations [19, 23]. We discuss all three generations in some detail in the next sections.

4.1   First-generation QR

In first-generation quantum repeaters, the total distance L to be covered is divided into 2^n segments of elementary length $L_0 = L/2^n$ (see Fig. 4.1).

In each segment, a maximally entangled state, e.g. $|10\rangle + |01\rangle$, covering the distance L_0 is generated. Neighboring links are then connected via entanglement swapping [21], i.e. a Bell measurement on adjacent repeater nodes. If two segments are successfully connected, an entangled state over the distance $2L_0$ is generated. Then these new neighboring links are again connected to create segments of length $4L_0$ and so on.

Since both the entanglement generation and the entanglement swapping are potentially probabilistic, it is important to perform both tasks in a heralded fashion. Moreover, the opportunity to store the successfully generated entangled states is a prerequisite, since neighboring links do not necessarily herald entanglement at the same time. In addition, the entanglement swapping
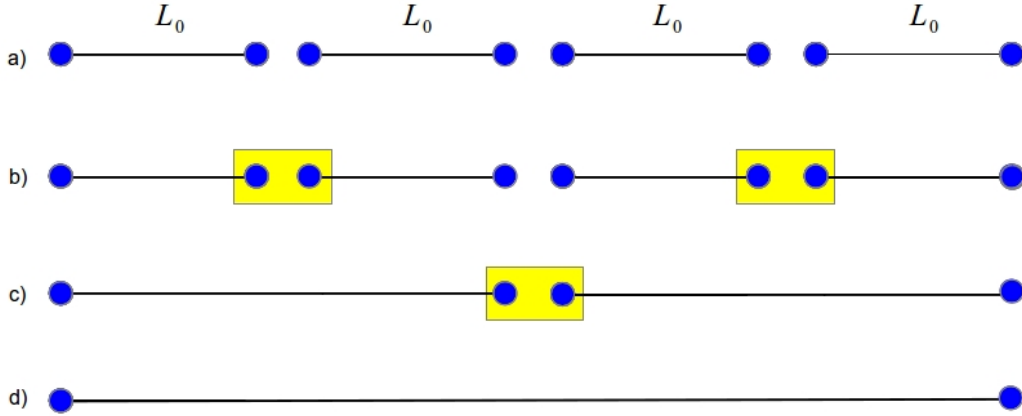
Figure 4.1: Basic principle of a first-generation quantum repeater: a) Entanglement is generated over a rather small distance L_0. b) Entanglement swapping is performed on adjacent repeater nodes (yellow boxes) to entangle the nodes over a distance $2L_0$. c) In the next step, the distance is increased by further entanglement swappings on the previously generated pairs. d) Finally, an entangled state over the distance $4L_0$ is generated. Note that the entanglement generation process a) as well as the swapping operation are usually non-deterministic and that at any time purification steps can be performed.

operation could fail and the corresponding segments have to be prepared anew, while other segments have to wait. To handle both scenarios, quantum memories with reasonable coherence times are required which limits the total communication distance.

In general, both transmission loss and memory errors lead to decoherence and instead of a pure maximally entangled Bell state, a mixed entangled state is generated over the distance L_0. Therefore, already on the elementary segments of length L_0, a few rounds of purification could be necessary to achieve reasonable initial fidelities before entanglement swapping operations are performed. Furthermore, after some rounds of entanglement swappings or at the very end, the obtained state can be further purified to increase the final fidelity.

For a given total distance L it is not trivial to find the right repeater strategy. The only fixed parameter is the success probability of the swapping p_{swap} operation. One is still free to choose the elementary distance L_0 which also determines the number of swappings, the number of necessary memories and at least partially the initial entanglement generation probability p_0. A crucial point is the number of rounds of purifications on each initial entangled state and if and when to do further purifications.

To assess the performance of a first-generation quantum repeater protocol in dependence of the free parameters and to compare different physical platforms, the average repeater rate is a suitable measure. The average repeater rate, in the following just called rate for short, is defined as the number of entangled pairs distributed over the distance L per unit time. It is therefore desired to choose the free parameters such that a maximal rate can be achieved. In general, however, the rate is limited by L/c [19].

Besides the rate that measures the time consumption of the repeater protocol, the quality of the final state in terms of fidelity is a second performance measure. Therefore, the goal is to achieve high rates and high fidelities.

As we will also see in our rate analysis in Section 7.1.1, there is typically a trade-off between rate and fidelity in first-generation quantum repeater protocols. High fidelities usually come at the cost of low rates and vice versa such that a happy medium has to be accepted. Many different physical systems and platforms have been investigated to realize first-generation quantum repeaters. Among these are single trapped ions [75], neutral atoms [76] and NV centers [77].

4.1.1 DLCZ-type quantum repeaters

One of the most prominent instances of a first-generation quantum repeater scheme is the well-known DLCZ protocol [78, 18] which uses atomic ensembles as quantum memories and single photons with linear optics for entanglement distribution and swapping. A remarkable feature of the DLCZ scheme is that entanglement purification is built into the process of initial entanglement distribution and swapping (purifying the entangled atomic ensembles from the effects of transmission and memory losses, respectively).

The entanglement generation between two atomic ensembles works by detecting a Stokes photon emitted by one of the two ensembles. The effective joint state of one ensemble and its Stokes mode can be described as a two-mode squeezed state in the limit of very small squeezing, i.e.

$$|\Psi\rangle_{al} = |00\rangle_{al} + r|11\rangle_{al} + \mathcal{O}(r^2), \tag{4.1}$$

where r is the squeezing parameter and labels "a" stand for the atomic ensemble and "l" for the light mode, respectively. Combining the two ensembles and their Stokes modes, the total state reads

$$|00>_{aa} |00\rangle_{ll} + r|01>_{aa} |01\rangle_{ll} + r|10>_{aa} |10\rangle_{ll} + \mathcal{O}(r^2)$$

where we reordered the modes and neglected higher order terms. The light modes are now sent over the desired distance, mixed at a symmetric beam splitter to erase which-path information and finally measured using a photon number resolving detector. We see that the two light modes are effectively encoded using the quantum error detection code presented in Eq. (2.14) in Section 2.3. A maximally entangled state between the two atomic ensembles is thus produced if and only if exactly one photon is detected after the beam splitter. Otherwise the generation process has to be repeated.

The same principle of error detection is automatically included in the entanglement swapping operation. If we are given two maximally entangled states of atomic ensembles next to each other, the swapping operation again works by mixing the Stokes modes of adjacent ensembles

at a symmetric beam splitter and again success is heralded when exactly one single photon is detected, otherwise the swapping failed and one has to start again with the entanglement generation.

Due to transmission and memory loss, the final distributed entangled state is a mixture of the target maximally entangled state and the two-mode vacuum state. The DLCZ protocol ensures that the vacuum component grows subexponentially with the total distance. Nevertheless, the statistical weight (later referred to as the fidelity) of the desired state is rather small for long distances. By using two repeater chains and two copies of noisy two-mode entangled states, the DLCZ protocol proposes postselection to create a four-mode entangled state containing two photons in total. This postselection procedure is probabilistic and could be realized by local QND measurements on each side of the links. More practical is the direct consumption of the corresponding photons for some application such as long-distance quantum cryptography. If successful, unit fidelity can be in principle achieved.

The DLCZ protocol has created much attention and various implementations, variations and generalizations have been proposed. In [79], a different qubit basis was chosen and active purification included. A similar approach was presented in [80] and [81]. Another variation [82] uses pair sources and multi-mode quantum memories while in [83] high-fidelity entangled pairs are locally prepared and long-distance entanglement is generated by means of two-photon detections.

4.1.2 Hybrid-type quantum repeaters

Another suitable first-generation "hybrid quantum repeater" protocol for the distribution of atomic qubit-qubit entanglement was given in [84, 85]. As in other hybrid quantum information-tion processing schemes [86], this protocol combines the advantages of discrete and continuous variable quantum states. Atomic two-level systems with long coherence time serve as quantum memories while optical coherent states are used to generate the initial entanglement between the atoms using dispersive light-matter interactions and highly efficient homodyne measurements. Employing such Gaussian measurements and Gaussian states as the initial resources appears very attractive from a practical point of view compared to repeater schemes based on the generation and detection of single photons. A particular experimental demonstration of this scheme is proposed in [87]. Another, similar hybrid quantum repeater protocol can be found in [88] and a recent hybrid approach to entanglement swapping using coherent states and linear optics can be found in [89].

The physical setup for a qubit HQR is as follows: the qubit is represented by the two spin states $|0\rangle$ and $|1\rangle$ of an atomic electron. The atom is placed into a cavity and the electronic spin interacts with a bright coherent light pulse. The situation at hand is theoretically described by the Jaynes-Cummings model in the limit of large detuning [90], i.e. the probe pulse and the

cavity are in resonance, but both are detuned from the resonance frequency of the electronic transition.

The interaction Hamiltonian in this model reads $H_{int}^{(2)} = \hbar g \sigma_z \hat{a}^\dagger \hat{a}$, where $\sigma_z = -\frac{1}{2}|0\rangle\langle 0| + \frac{1}{2}|1\rangle\langle 1|$ is the Pauli-operator on the spin state and $\hat{a}^\dagger \hat{a}$ is the photon number operator of the light mode. Furthermore, the parameter g describes the strength of the spin-light coupling.

Based on this interaction Hamiltonian, the corresponding unitary transformation is given by $U_2(\theta) = \exp(i\theta \sigma_z \hat{a}^\dagger \hat{a})$ (with $\theta = gt$ being an effective interaction time) and, up to an unconditional phase shift of the mode by $e^{i\theta/2}$, acts on the spin-light system effectively as a phase rotation, i.e.

$$U_2(\theta)[(|0\rangle + |1\rangle)|\alpha\rangle] = |0\rangle|\alpha\rangle + |1\rangle|\alpha e^{i\theta}\rangle. \tag{4.2}$$

In the literature, this interaction is also known as dispersive interaction [91].

For the generalization that we are aiming at, we consider the case $\theta = \pi$, corresponding to a strong interaction resulting in coherent states $|\pm\alpha\rangle$ on the light mode. Note that this is opposite to the original HQR-scheme of [84] where weak dispersive interactions are assumed.

The repeater protocol works as follows: the matter system is prepared in the state $|0\rangle + |1\rangle$ and interacts dispersively with a single-mode coherent state $|\alpha\rangle$ (referred to as "qubus") as described by Eq. (4.2). Note that this leads to a pure entangled state between the light mode and the matter system.

The light mode is then sent through an optical channel of length L where it inevitably suffers from photon loss. As pointed out in Section 2.1, the action of photon loss can be simulated by mixing the light mode with a vacuum state at a beam splitter with transmittance $\gamma = \exp\left(-\frac{L}{L_{att}}\right)$ (see the discussion below (2.6)).

After applying the beam splitter, the total pure state of the matter system, the qubus light mode and the loss mode reads as

$$\frac{1}{\sqrt{2}}(|0\rangle|\sqrt{\gamma}\alpha\rangle|\sqrt{1-\gamma}\alpha\rangle + |1\rangle|-\sqrt{\gamma}\alpha\rangle|-\sqrt{1-\gamma}\alpha\rangle). \tag{4.3}$$

The joint state of the matter system and the relevant light mode is obtained by tracing out the loss mode. Since the coherent states $|\alpha\rangle$ and $|-\alpha\rangle$ are not orthogonal, it is useful to transform these into an orthogonal basis. A suitable orthogonal basis in this case is the basis of even and odd cat states (throughout we assume $\alpha \in \mathbb{R}$),

$$|u\rangle = \frac{1}{\sqrt{N_u(\alpha)}}(|\alpha\rangle + |-\alpha\rangle), \tag{4.4}$$

$$|v\rangle = \frac{1}{\sqrt{N_v(\alpha)}}(|\alpha\rangle - |-\alpha\rangle), \tag{4.5}$$

with normalization constants $N_u(\alpha) = 2(1 + e^{-2\alpha^2})$ and $N_v(\alpha) = 2(1 - e^{-2\alpha^2})$. Expressed in this basis, one has

$$|\alpha\rangle = \frac{1}{2}(\sqrt{N_u(\alpha)}|u\rangle + \sqrt{N_v(\alpha)}|v\rangle), \tag{4.6}$$

$$|-\alpha\rangle = \frac{1}{2}(\sqrt{N_u(\alpha)}|u\rangle - \sqrt{N_v(\alpha)}|v\rangle). \tag{4.7}$$

After tracing out the loss mode in this basis, the resulting state of the matter system and the qubus light mode becomes

$$
\rho_{out} = \frac{N_u(\sqrt{1-\gamma}\alpha)}{4}\left[\frac{1}{2}\left(|0\rangle|\sqrt{\gamma}\alpha\rangle + |1\rangle|-\sqrt{\gamma}\alpha\rangle\right)\right] \times H.c.
$$
$$
+ \frac{N_v(\sqrt{1-\gamma}\alpha)}{4}\left[\frac{1}{2}\left(|0\rangle|\sqrt{\gamma}\alpha\rangle - |1\rangle|-\sqrt{\gamma}\alpha\rangle\right)\right] \times H.c.
\tag{4.8}
$$

This is a mixed entangled state between the matter system and the qubus. To study the entanglement of such a state, and also for later purposes, it is most convenient to use directly the $|\widetilde{u}\rangle, |\widetilde{v}\rangle$-basis on the light mode , where $\sim$ refers to the basis vectors in Eqs. (4.4) and (4.5) with damped amplitudes $\sqrt{\gamma}\alpha$.

In addition, a basis change on the matter system into the conjugate X-basis, $|\widetilde{0}\rangle = \frac{1}{\sqrt{2}}(|0\rangle + |1\rangle)$ and $|\widetilde{1}\rangle = \frac{1}{\sqrt{2}}(|0\rangle - |1\rangle)$, gives the expression

$$
\rho_{out} = \frac{N_u(\sqrt{1-\gamma}\alpha)}{4}\left[\frac{1}{2}(\sqrt{N_u(\sqrt{\gamma}\alpha)}|\widetilde{0}\rangle|\widetilde{u}\rangle + \sqrt{N_v(\sqrt{\gamma}\alpha)}|\widetilde{1}\rangle|\widetilde{v}\rangle)\right] \times H.c.
$$
$$
+ \frac{N_v(\sqrt{1-\gamma}\alpha)}{4}\left[\frac{1}{2}(\sqrt{N_u(\sqrt{\gamma}\alpha)}|\widetilde{1}\rangle|\widetilde{u}\rangle + \sqrt{N_v(\sqrt{\gamma}\alpha)}|\widetilde{0}\rangle|\widetilde{v}\rangle)\right] \times H.c.,
\tag{4.9}
$$

which represents the state in Eq. (4.8) in suitable binary orthogonal bases for both the matter system and the qubus. Note that this does not change the entanglement properties of the state, since any entanglement measure is invariant under local basis changes [92, 33].

Also note that this matter-light qubit-qubus entangled state effectively remains an entangled qubit-qubit state, since the two initial coherent states of the qubus span a two-dimensional qubit space and because individual coherent states remain pure after a loss channel.

After traveling through the optical fiber over the distance L_0, the light mode interacts dispersively with a second matter system, also prepared in the state $|0\rangle + |1\rangle$, but this time with the inverse angle, $\theta = -\pi$.

The joint tripartite state, written in the same basis as in Eq. (4.8), then becomes

$$
\rho_{out} = \frac{N_u(\sqrt{1-\gamma}\alpha)}{4}|C_0\rangle\langle C_0| + \frac{N_v(\sqrt{1-\gamma}\alpha)}{4}|C_1\rangle\langle C_1|, \tag{4.10}
$$

where

$$|C_0\rangle = \frac{1}{\sqrt{2}}(|\phi^+\rangle|\sqrt{\gamma}\alpha\rangle + |\psi^+\rangle| - \sqrt{\gamma}\alpha\rangle), \qquad (4.11)$$

and

$$|C_1\rangle = \frac{1}{\sqrt{2}}(|\phi^-\rangle|\sqrt{\gamma}\alpha\rangle + |\psi^-\rangle| - \sqrt{\gamma}\alpha\rangle). \qquad (4.12)$$

Here, $|\phi^\pm\rangle$ and $|\psi^\pm\rangle$ denote the four qubit Bell states already defined right after Eq. (2.8). The component $|C_0\rangle$ in Eq. (4.10) is the target component, whereas $|C_1\rangle$ is the loss component that vanishes in the loss-free case. Indeed, for $\gamma \to 1$, one observes $N_u(0) = 4$ and $N_v(0) = 0$ such that in this case the corresponding output density operator $\rho_{out} = |C_0\rangle\langle C_0|$ represents a pure state.

To achieve the goal of distributing entanglement between the two separated matter systems over the distance L_0, the final step is a measurement on the light mode, for instance, by homodyne detection.

Unlike in the original hybrid quantum repeater protocol where the dispersive interaction is assumed to be weak (and hence a p-homodyne detection is ultimately preferred over an x-homodyne detection with, respectively, state distinguishabilities $\sim \alpha\theta$ versus $\alpha\theta^2$ for small but otherwise unfixed θ), the suitable detection scheme in our case is a measurement of the quadrature $\hat{x} = \frac{1}{2}(\hat{a} + \hat{a}^\dagger)$ instead of $\hat{p} = \frac{1}{2i}(\hat{a} - \hat{a}^\dagger)$.

The position distribution of coherent states with complex amplitude β can be obtained by the square of their wave functions,

$$|\psi_\beta(x)|^2 = \sqrt{\frac{2}{\pi}} \exp\left(-2(x - \text{Re}(\beta))^2\right). \qquad (4.13)$$

Because of the finite overlap of the coherent states $|\sqrt{\gamma}\alpha\rangle$ and $| - \sqrt{\gamma}\alpha\rangle$, it is impossible to perfectly distinguish these states and an error due to this non-orthogonality has to be taken into account. Based on Eq. (4.13), it is obvious that $|\sqrt{\gamma}\alpha\rangle$ and $| - \sqrt{\gamma}\alpha\rangle$ have Gaussian position distributions around $\sqrt{\gamma}\alpha$ and $-\sqrt{\gamma}\alpha$, respectively. It is therefore useful to assign the result of the $\hat{x}$-measurement to one of three possible windows.

The first window is $w_0 = [\sqrt{\gamma}\alpha - \Delta, \infty]$ with $\sqrt{\gamma}\alpha > \Delta > 0$. If the measurement results fall into this range, then the light mode is effectively projected onto $|\sqrt{\gamma}\alpha\rangle$. Note that this is an approximate projection due to the non-orthogonality, i.e. the resulting state is still a superposition of $|\phi^+\rangle$ and $|\psi^+\rangle$ in the first component where the weight of the latter can be reduced by increasing the value of $\sqrt{\gamma}\alpha$. The same is true in the second component for $|\phi^-\rangle$ and $|\psi^-\rangle$.

As for the second window we define $w_1 = [-\infty, -\sqrt{\gamma}\alpha + \Delta]$ which is symmetric to w_0 and therefore represents the approximate projection on $| - \sqrt{\gamma}\alpha\rangle$. Unlike w_0, one has now $|\psi^\pm\rangle$ as the dominant terms in the superpositions in the two components. It is again true that the
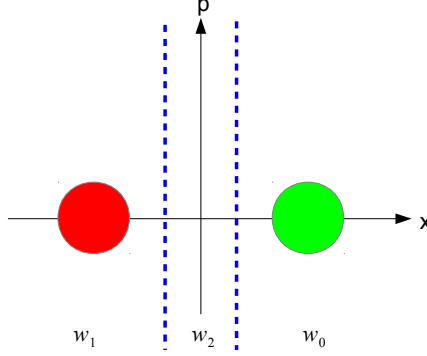
Figure 4.2: Phase space representation of the two coherent states $|\alpha\rangle$ and $|-\alpha\rangle$ to be distinguished by homodyne detection.

non-dominant term in the superposition can be made arbitrarily small by increasing $\sqrt{\gamma}\alpha$. A third window can be defined in between w_0 and w_1, and a measurement result in this range will be considered as a failure event to be discarded.

Valid measures for the performance of this entanglement distribution scheme are the success probabilities of the two non-failure windows w_0 and w_1 as well as the fidelity of the corresponding target state in the first component. As the fidelity, we define the overlap of the maximally entangled Bell states $|\phi^+\rangle$ (w_0) or $|\psi^+\rangle$ (w_1) with the mixed state (4.10) after the homodyne measurement.

The success probability for a measurement result to fall into the first window reads

$$p_{w_0} = \frac{1}{2} \int\limits_{\sqrt{\gamma}\alpha-\Delta}^{\infty} dx(|\psi_{\sqrt{\gamma}\alpha}(x)|^2 + |\psi_{-\sqrt{\gamma}\alpha}(x)|^2). \tag{4.14}$$

For the second window, we have

$$p_{w_1} = \frac{1}{2} \int\limits_{-\infty}^{-\sqrt{\gamma}\alpha+\Delta} dx(|\psi_{\sqrt{\gamma}\alpha}(x)|^2 + |\psi_{-\sqrt{\gamma}\alpha}(x)|^2), \tag{4.15}$$

which equals p_{w_0} for symmetry reasons. The same holds true for the two fidelities,

$$F_{w_0} = F_{w_1}$$

$$= \frac{N_u(\sqrt{1-\gamma}\alpha)}{4} \frac{\int\limits_{-\infty}^{-\sqrt{\gamma}\alpha+\Delta} dx|\psi_{\sqrt{\gamma}\alpha}(x)|^2}{\int\limits_{-\infty}^{-\sqrt{\gamma}\alpha+\Delta} dx(|\psi_{\sqrt{\gamma}\alpha}(x)|^2 + |\psi_{-\sqrt{\gamma}\alpha}(x)|^2)}. \tag{4.16}$$

25

The formulae for the fidelities and the success probabilities imply the crucial dependence of the performance on the choice of Δ and $\sqrt{\gamma}\alpha$: if we choose $\Delta = \Delta_0 := \sqrt{\gamma}\alpha$, then we have no failure window and every measurement result is assigned to one of the two coherent states $| \pm \sqrt{\gamma}\alpha\rangle$. The corresponding success probability equals unity at the expense of a rather low fidelity.

With $\Delta < \Delta_0$, the success probability is clearly less than unity and the fidelity correspondingly increases.

In general, the fidelity drops for too small $\sqrt{\gamma}\alpha$ due to the non-orthogonality and thus indistinguishability of the coherent states $| \pm \sqrt{\gamma}\alpha\rangle$. The overall effect becomes manifest in bit-flip errors in the target Bell state.

Though leading to near-orthogonality, large $\sqrt{\gamma}\alpha$ lead to a near-equally mixture of the state in Eq. (4.10) which then, after a near-deterministic discrimination, consists of one of the two possible Bell states in the first component and its phase-flipped version in the second. This state has therefore very low entanglement and hence is of limited practical interest.

So the task is to find a regime of α and distances L_0 such that both reasonable fidelities and success probabilities can be obtained.

Besides homodyne detection, unambiguous state discrimination (USD) has been considered for hybrid quantum repeaters in the literature. The advantage here is that the effects originating from the finite overlaps of the coherent states no longer appear in the fidelity thanks to an error-free state discrimination. The corresponding effects solely influence the success probabilities depending on the weights of the inconclusive discrimination results. Two-state USD for coherent states $| \pm \sqrt{\gamma}\alpha\rangle$ is well-known and can be optimally performed via a single beam splitter and on-off detections [93].

Further steps in the original repeater protocol address the purification of the mixed state in Eq. (4.10) after homodyne detection and entanglement swapping on the matter system or via the qubus to distribute the generated entanglement over longer distances. For more details, see [84].

We generalize the first-generation hybrid quantum repeater scheme presented in [84] to higher dimensions in Section 7.1.1.

4.2 Second-generation QR

A fundamental drawback in first-generation quantum repeaters is the necessity of rather long memory coherence times. The resulting restriction of the total communication distance has been first overcome with the introduction of second-generation quantum repeaters by Jiang et al. [94].

In [94], unlike first-generation quantum repeater protocols, the memories are protected by the

usage of quantum error correction codes against the specific memory errors.

In an elementary link, the goal is to distribute an encoded Bell state over a distance L_0. After entanglement generation, quantum error correction on the memories takes place to increase the initial fidelity of the entangled state. Using quantum error correction, some of the time-consuming purification steps can be avoided. Since the error correction steps are performed locally, no communication between different parties is necessary and thus the error correction scheme can be faster than schemes involving purification. Indeed, the rate of such a repeater scheme is limited by L_0/c [19].

After encoded entangled states in elementary links next to each other have successfully generated, entanglement swapping at the encoded level has to be performed. This requires gates and operations like CNOT gates which can further introduce errors. However, by a suitable choice of the quantum error correction code to be used, one is able to correct both, memory and operational errors. In [94], this is done by using Calderbank-Shore-Steane (CSS) codes [22], a special class of stabilizer codes which show the property of transversality and lead to the concept of error correcting teleportation [95]. It can be shown that quantum error correction and entanglement swapping can be done with the same set of gates.

Besides [94], not much attention has been paid to second-generation quantum repeater schemes. In [96], the hybrid quantum repeater protocol of reference [84] has been modified to tackle memory errors using CSS codes and repetition codes. Apart from that, a similar approach for the distribution of streams of entangled qubits in the framework of quantum networks has been considered [97].

4.3   Third-generation QR

Though suppressing memory and gate errors and possibly reducing the number of rounds of entanglement purification steps, second-generation quantum repeaters still need two-way communication between the repeater nodes for heralded entanglement generation. Apart from that, photon loss protection in both first and second-generation quantum repeater schemes is only implicitly included. The key idea of third-generation quantum repeater protocols is hence the employment of quantum error correction for both photon loss and operational errors.

As a specific instance of a third-generation quantum repeater, one-way quantum communication schemes were introduced [23] (see Fig. 4.3). Inspired by one-way quantum computing schemes [98], an encoded quantum state is sent from a sending station directly through an optical fiber of length L_0 to reach the first repeater station while suffering from a moderate amount of photon loss for sufficiently small L_0. In each intermediate station, teleportation-based error correction [95] is performed before the corrected state is sent to the next repeater station. For logical qubits, error correcting is realized by Bell-state preparation and Bell measurements at
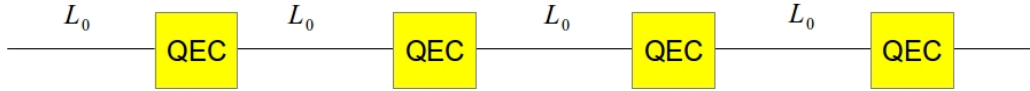
Figure 4.3: Except of a one-way quantum repeater: encoded quantum information is sent through an optical channel while losses are corrected by means of quantum error correction at intermediate stations separated by rather small distances L_0.

the encoded level, which requires encoded Pauli operations as well as encoded Hadamard and CNOT gates. This schemes uses QPCs for the loss protection and the syndrome identification and recovery process in every repeater station are realized in the framework of circuit quantum electrodynamics [99]. A similar and more practical scheme was presented in [100, 101] where the encoded Bell measurements are implemented with a static network of linear optical elements. As pointed out in [102], error correcting teleportation can be generalized to logical qudits using qudit Pauli and SUM gates together with qudit Hadamard gates.

The essential advantage of a third-generation repeater is that there is no need to temporarily store entangled states until neighboring entangled states have been distributed and purified, and there is also no need to send classical information back and forth between repeater stations. A third-generation repeater therefore only requires one-way classical communication and, in principle, no quantum memories are needed at all [103]. The rate is therefore only limited by the speed of local operations and quantum information can then be sent directly at rates that approach, in principle, those achievable in classical communication.

A conceptually distinct version of such a loss-error-correction-based repeater is the all-optical scheme of Azuma et al. [104] based on the distribution of entangled cluster states. This scheme also relies on sufficiently fast feedforward operations. Third-generation quantum repeater schemes play a crucial role in this thesis because quantum error correcting codes against photon loss are their key ingredient. We will apply the codes to be constructed in Section 5 and 6 directly in one-way communications schemes and determine the performance in terms of success probabilities and final fidelities.

Chapter 5

QEC against photon loss using NOON states

Based on the error operators for AD (Eq. (2.6)) and the KL-conditions for QEC (Eq. (3.1)), new explicit quantum codes against photon loss for logical qubits based on NOON states and beam splitter operations are systematically developed. The resulting codes are intermediate between QPCs and bosonic codes, because they use N^2 photons in $2N$ modes with at most N photons per mode. Our code is a block code like QPC and unlike the general bosonic code, with the same number of blocks as QPC, but with the N^2 photons distributed among a smaller number of modes in every block compared to QPC. It turns out that only in our scheme both the total mode number and the maximal photon number per mode scale linearly with N to achieve protection against $N - 1$ losses.

We then discuss the extension of this systematic scheme to logical qudits (d-level systems) in a natural manner by switching from beam splitters to general multi-port devices. It is shown that the scaling of the fidelity only depends on the total photon number and, especially, that it is independent of the dimension of the logical qudit. After that, we present an in-principle method for the generation of an arbitrary logical qubit state for the one-photon-loss qubit code based on linear optics and light-matter interactions.

Before deriving the different codes, we first provide a brief introduction to NOON states and the notion of linear-optical devices in the framework of quantum optics.

5.1 NOON states

So-called NOON states are an important resource in optical quantum information science [105, 106, 107, 108]. First introduced in 1996 [109], they are bipartite entangled, N-photon two-mode states where the N photons occupy either one of two optical modes,

$$\frac{1}{\sqrt{2}}(|N0\rangle + |0N\rangle). \tag{5.1}$$

NOON states have been widely used in quantum communication [110], quantum metrology [111] and quantum lithography [112], because they allow for super-sensitive measurements, e.g. in optical interferometry. This is related to the substandard quantum-limit behavior of NOON states, i.e. a factor $\sqrt{N}$ improvement to the shot noise limit can be achieved [113]. Due to their practical relevance, various schemes for NOON state generation based on strong non-linearities [114, 115] or measurement and feed-forward [116, 117, 118] have been proposed [1]. Unfortunately, NOON states are very fragile, which focused recent research on their entanglement and phase properties in noisy environments [119] or on the enhancements of NOON state sensitivity by non-Gaussian operations [120].

5.2 Linear optics

Passive linear optical devices such as beam splitters and their generalization are a basic ingredient for the NOON codes to be developed in the next sections. We therefore briefly review the notion of linear optics [10, 43].

In the general case, a linear optical device is best understood in the Heisenberg picture. A general optical device transforms d input modes into d output modes which can also be expressed as a transformation on the corresponding creation and annihilation operators of the modes. A linear optical device is defined by the linear relation between the annihilation operators of the input modes $\hat{a}_i, i = 0, ..., d-1$ and the annihilation operators of the output modes $\hat{b}_i$:

$$\hat{b}_i = \sum_{j=0}^{d-1} U_{ij} \hat{a}_j. \tag{5.2}$$

Here, the unitary matrix U, connecting the input and output modes and ensuring photon number preservation, is arbitrary. In the case $d = 2$, this transformation corresponds to a beam splitter [121] and the corresponding unitary is given by

$$U = \begin{pmatrix} \sqrt{\eta} & \sqrt{1-\eta} \\ \sqrt{1-\eta} & -\sqrt{\eta} \end{pmatrix}, \tag{5.3}$$

---

[1]In Appendix D, we present another experimentally feasible scheme to realize arbitrary NOON states.

such that the input annihilation operators $\hat{a}_1$ and $\hat{a}_2$ are transformed by a beam splitter with transmittance η according to $\hat{a}_1 \to \sqrt{\eta}\hat{a}_1 + \sqrt{1-\eta}\hat{a}_2$ and $\hat{a}_2 \to \sqrt{1-\eta}\hat{a}_1 - \sqrt{\eta}\hat{a}_2$. More general beam splitter transformations would include additional phase shifts.

By means of the linear input-output relation, the action of the above beam splitter transformation on any two-mode state can be calculated. Written in the Fock basis, the effect of the beam splitter transformation is described by

$$
|m,n\rangle \mapsto \sum_{j,k=0}^{m,n} \sqrt{\frac{(j+k)!(m+n-j-k)!}{m!n!}} \binom{m}{j}\binom{n}{k}
$$
$$
\times (-1)^k \sqrt{\eta}^{m+j-k} \sqrt{1-\eta}^{n-j+k} |m+n-j-k, j+k\rangle.
$$
(5.4)

In the case of a 50:50 beam splitter ($\sqrt{\eta} = \sqrt{1-\eta} = \frac{1}{\sqrt{2}}$), this reduces to

$$
|m,n\rangle \mapsto \sum_{j,k=0}^{m,n} \sqrt{\frac{1}{2}}^{n+m} \sqrt{\frac{(j+k)!(m+n-j-k)!}{m!n!}} \binom{m}{j}\binom{n}{k}(-1)^k |m+n-j-k, j+k\rangle,
$$
(5.5)

and we obtain in particular the expressions

$$
BS[|N0\rangle] = \sqrt{\frac{1}{2}}^N \sum_{j=0}^{N} \sqrt{\binom{N}{j}} |N-j, j\rangle,
$$
$$
BS[|0N\rangle] = \sqrt{\frac{1}{2}}^N \sum_{j=0}^{N} (-1)^j \sqrt{\binom{N}{j}} |N-j, j\rangle,
$$
(5.6)

which play a central role in the next section.

In the remainder of this chapter, we only need symmetric linear optical devices. In complete analogy to the 50:50 beam splitter, the symmetric tritter transformation T of the annihilation operators $\hat{a}_1$, $\hat{a}_2$ and $\hat{a}_3$ of three optical modes is given by

$$
\hat{a}_1 \mapsto \frac{1}{\sqrt{3}}(\hat{a}_1 + \hat{a}_2 + \hat{a}_3),
$$
$$
\hat{a}_2 \mapsto \frac{1}{\sqrt{3}}(\hat{a}_1 + e^{\frac{2\pi i}{3}}\hat{a}_2 + e^{-\frac{2\pi i}{3}}\hat{a}_3),
$$
$$
\hat{a}_3 \mapsto \frac{1}{\sqrt{3}}(\hat{a}_1 + e^{-\frac{2\pi i}{3}}\hat{a}_2 + e^{\frac{2\pi i}{3}}\hat{a}_3).
$$
(5.7)

By induction, one easily verifies that a symmetric d splitter on d optical modes with annihilation operators $\hat{a}_i$, $i = 0, 1, .., d-1$ can be described as

$$
\hat{a}_k \mapsto \sum_{j=0}^{d-1} e^{\frac{2\pi i k j}{d}} \hat{a}_j.
$$
(5.8)

General expressions for arbitrary multi-mode Fock states (as in Eq. (5.5) for $d = 2$) are not very insightful, so we do not display them here. Expressions for special cases similar to the input states in Eq. (5.6) are derived in Section 5.4.

5.3   Qubit codes

Let us consider the following qubit codewords defined in the three-dimensional Hilbert space of two photons distributed among two modes,

$$
|\bar{0}\rangle = \frac{1}{\sqrt{2}}(|20\rangle + |02\rangle),
$$
$$
|\bar{1}\rangle = |11\rangle.
$$
(5.9)

The action of the AD channels on the two modes of the logical qubit $|\bar{\Psi}\rangle = c_0|\bar{0}\rangle + c_1|\bar{1}\rangle$ is [2]

$$
\begin{aligned}
A_0 \otimes A_0|\bar{\Psi}\rangle &= \sqrt{\gamma^2}|\bar{\Psi}\rangle, \\
A_1 \otimes A_0|\bar{\Psi}\rangle &= \sqrt{\gamma(1-\gamma)}(c_0|10\rangle + c_1|01\rangle), \\
A_0 \otimes A_1|\bar{\Psi}\rangle &= \sqrt{\gamma(1-\gamma)}(c_0|01\rangle + c_1|10\rangle),
\end{aligned}
$$
(5.10)

including the first three error operators $E_1 = A_0 \otimes A_0$, $E_2 = A_1 \otimes A_0$ and $E_3 = A_0 \otimes A_1$, of which the last two describe the loss of a photon. Obviously, the one-photon-loss spaces are not orthogonal (they are even identical) and the qubit is subject to a random bit flip for the one-photon-loss case. A different choice would be:

$$
\begin{aligned}
|\bar{0}\rangle &= \frac{1}{2}|20\rangle + \frac{1}{2}|02\rangle + \frac{1}{\sqrt{2}}|11\rangle, \\
|\bar{1}\rangle &= \frac{1}{2}|20\rangle + \frac{1}{2}|02\rangle - \frac{1}{\sqrt{2}}|11\rangle.
\end{aligned}
$$
(5.11)

After AD, this becomes:

$$
A_0 \otimes A_0|\bar{\Psi}\rangle = \sqrt{\gamma^2}|\bar{\Psi}\rangle,
$$
(5.12)
$$
A_1 \otimes A_0|\bar{\Psi}\rangle = \sqrt{\gamma(1-\gamma)} \times (c_0\frac{1}{\sqrt{2}}(|10\rangle + |01\rangle) + c_1\frac{1}{\sqrt{2}}(|10\rangle - |01\rangle)),
$$
$$
A_0 \otimes A_1|\bar{\Psi}\rangle = \sqrt{\gamma(1-\gamma)} \times (c_0\frac{1}{\sqrt{2}}(|10\rangle + |01\rangle) - c_1\frac{1}{\sqrt{2}}(|10\rangle - |01\rangle)).
$$

Here, the phase flip in the last line corresponds to a violation of the KL criteria, $\langle\bar{0}|E_2^\dagger E_3|\bar{0}\rangle \neq \langle\bar{1}|E_2^\dagger E_3|\bar{1}\rangle$, preventing the encoding from being a proper quantum error correcting code. Indeed, again we have identical one-photon-loss spaces. One can easily verify that any choice of

---

[2]In the remainder of this chapter $c_0, c_1, .., c_{d-1} \in \mathbb{C}$ are the coefficients of our logical qudits.

codewords will either lead to overlapping one-photon-loss spaces or the qubit is completely lost. A possible remedy is to construct codes composed of blocks.

To demonstrate this, we first deal with the specific example for encoding a logical qubit. Define

$$
\begin{aligned}
|t_0^{2,2}\rangle &= BS[|20\rangle] = \frac{1}{2}|20\rangle + \frac{1}{2}|02\rangle + \frac{1}{\sqrt{2}}|11\rangle, \\
|t_1^{2,2}\rangle &= BS[|02\rangle] = \frac{1}{2}|20\rangle + \frac{1}{2}|02\rangle - \frac{1}{\sqrt{2}}|11\rangle,
\end{aligned}
\tag{5.13}
$$

as the "input states" for our encoding, where $BS[\ ]$ denotes a 50:50 beam splitter transformation. Now by means of a Hadamard-type operation on $|t_0^{2,2}\rangle$ and $|t_1^{2,2}\rangle$, the following states are obtained:

$$
\begin{aligned}
|\widetilde{0}\rangle &= \frac{1}{\sqrt{2}}(|t_0^{2,2}\rangle + |t_1^{2,2}\rangle) = \frac{1}{\sqrt{2}}(|20\rangle + |02\rangle), \\
|\widetilde{1}\rangle &= \frac{1}{\sqrt{2}}(|t_0^{2,2}\rangle - |t_1^{2,2}\rangle) = |11\rangle.
\end{aligned}
\tag{5.14}
$$

Note that $|\widetilde{1}\rangle$ equals $BS[\frac{1}{\sqrt{2}}(|20\rangle - |02\rangle)]$, whereas $|\widetilde{0}\rangle$ is the two-photon NOON state which is invariant under the beam splitter transformation. A logical qubit can now be encoded according to

$$
|\bar{\Psi}\rangle = c_0|\widetilde{0}\rangle|\widetilde{0}\rangle + c_1|\widetilde{1}\rangle|\widetilde{1}\rangle \equiv c_0|\bar{0}\rangle + c_1|\bar{1}\rangle.
\tag{5.15}
$$

We prove in the following that the codewords

$$
\begin{aligned}
|\bar{0}\rangle &= |\widetilde{0}\rangle|\widetilde{0}\rangle = \frac{1}{\sqrt{2}}(|20\rangle + |02\rangle)\frac{1}{\sqrt{2}}(|20\rangle + |02\rangle) = \frac{1}{2}(|2020\rangle + |2002\rangle + |0220\rangle + |0202\rangle), \\
|\bar{1}\rangle &= |\widetilde{1}\rangle|\widetilde{1}\rangle = |1111\rangle,
\end{aligned}
\tag{5.16}
$$

form a quantum error correcting code for the AD channel. Calculating the action of AD on the basis codewords and checking the KL conditions, we obtain

$$
\begin{aligned}
A_0 \otimes A_0 \otimes A_0 \otimes A_0|\bar{\Psi}\rangle &= \sqrt{\gamma^4}|\bar{\Psi}\rangle, \\
A_1 \otimes A_0 \otimes A_0 \otimes A_0|\bar{\Psi}\rangle &= \sqrt{\gamma^3(1-\gamma)}\left(\frac{c_0}{\sqrt{2}}(|1020\rangle + |1002\rangle) + c_1|0111\rangle\right), \\
A_0 \otimes A_1 \otimes A_0 \otimes A_0|\bar{\Psi}\rangle &= \sqrt{\gamma^3(1-\gamma)}\left(\frac{c_0}{\sqrt{2}}(|0120\rangle + |0102\rangle) + c_1|1011\rangle\right), \\
A_0 \otimes A_0 \otimes A_1 \otimes A_0|\bar{\Psi}\rangle &= \sqrt{\gamma^3(1-\gamma)}\left(\frac{c_0}{\sqrt{2}}(|2010\rangle + |0210\rangle) + c_1|1101\rangle\right), \\
A_0 \otimes A_0 \otimes A_0 \otimes A_1|\bar{\Psi}\rangle &= \sqrt{\gamma^3(1-\gamma)}\left(\frac{c_0}{\sqrt{2}}(|2001\rangle + |0201\rangle) + c_1|1110\rangle\right).
\end{aligned}
\tag{5.17}
$$

The KL conditions are obviously fulfilled for one-photon-loss errors. Note that, after losing any two or more photons, the logical qubit cannot be recovered anymore.

To be able to actively perform quantum error correction, it is a necessary task to determine the syndrome information, i.e. in our case the location (the mode) where a photon loss occurred. To get this information, we first measure the total photon number per block. If the result is "2" on each block, there is no photon missing and the logical qubit is unaffected. However, if for example a photon got lost on the first mode, the result is "1" for the first block and "2" for the other. This result is not unique, because there are still two possible corrupted states with this measurement pattern. In order to resolve this, inter-block photon number parity measurements with respect to modes 2+3 and 1+4 are suitable. The results "even-odd" and "odd-even" uniquely determine the corrupted state which can then be accordingly recovered. Note that all the measurements discussed here are assumed to be of QND-type such that also higher photon losses can be non-destructively detected. But so far these cannot be corrected by means of the encoding.

To assess the performance of this code, we use the worst-case fidelity, as defined in Eq. (3.4). A short calculation shows

$$F = \gamma^4 + 4\gamma^3(1 - \gamma) \approx 1 - 6(1 - \gamma)^2. \tag{5.18}$$

Note that this code has the same scaling as the four-photon-code of [53] described by Eq.(3.5). For higher losses, we can use NOON states with higher photon number to encode a logical qubit. For this purpose, let us define the input states for the codewords as

$$
\begin{aligned}
|t_0^{2,3}\rangle = BS[|30\rangle] &= \frac{1}{2\sqrt{2}}|03\rangle + \frac{1}{2}\sqrt{\frac{3}{2}}|12\rangle + \frac{1}{2}\sqrt{\frac{3}{2}}|21\rangle + \frac{1}{2\sqrt{2}}|30\rangle, \\
|t_1^{2,3}\rangle = BS[|03\rangle] &= -\frac{1}{2\sqrt{2}}|03\rangle + \frac{1}{2}\sqrt{\frac{3}{2}}|12\rangle - \frac{1}{2}\sqrt{\frac{3}{2}}|21\rangle + \frac{1}{2\sqrt{2}}|30\rangle,
\end{aligned}
\tag{5.19}
$$

such that this time

$$
\begin{aligned}
|\widetilde{0}\rangle &= \frac{1}{\sqrt{2}}(|t_0^{2,3}\rangle + |t_1^{2,3}\rangle) = \frac{1}{2}|30\rangle + \frac{\sqrt{3}}{2}|12\rangle = BS\left[\frac{1}{\sqrt{2}}(|30\rangle + |03\rangle)\right], \\
|\widetilde{1}\rangle &= \frac{1}{\sqrt{2}}(|t_0^{2,3}\rangle - |t_1^{2,3}\rangle) = \frac{1}{2}|03\rangle + \frac{\sqrt{3}}{2}|21\rangle = BS\left[\frac{1}{\sqrt{2}}(|30\rangle - |03\rangle)\right],
\end{aligned}
\tag{5.20}
$$

become the states after the Hadamard-type gate. We could now again build a qubit like in Eq.(5.15). However, we find that the resulting six-photon two-block (four-mode) code only corrects certain two-photon losses and therefore there is no significant enhancement compared to the $N = 2$ code above. This can be understood by looking at the corrupted logical qubit for losses of up to two photons. The details for this are presented in Appendix A.1. The conclusion

is that some of the orthogonality requirements are violated for certain two-photon losses which consequently cannot be corrected. To overcome this problem and to improve the code, instead we take the following codewords for $N = 3$ photons per block (with $N^2 = 9$ as the total number of photons):

$$
\begin{aligned}
|\bar{0}\rangle &= |\widetilde{0}\rangle|\widetilde{0}\rangle|\widetilde{0}\rangle, \\
|\bar{1}\rangle &= |\widetilde{1}\rangle|\widetilde{1}\rangle|\widetilde{1}\rangle,
\end{aligned} \tag{5.21}
$$

which are now composed of three blocks for a total number of six modes. To verify that this code corrects all losses up to two photons, we can calculate the action of AD on the logical qubit. Due to symmetry reasons, it is sufficient to calculate the action of only certain error operators on the codewords, because all other corrupted codewords with at most two lost photons can be obtained by permutations of the blocks. Therefore, if the KL conditions are fulfilled for the following error operators, then they are also satisfied by the block-permuted corrupted states. The relevant error operators are

$$
A_1 \otimes A_0 \otimes A_0 \otimes A_0 \otimes A_0 \otimes A_0|\bar{\Psi}\rangle = \sqrt{\frac{3}{2}\gamma^8(1-\gamma)}(\frac{c_0}{\sqrt{2}}(|20\rangle + |02\rangle)|\widetilde{0}\rangle|\widetilde{0}\rangle + c_1|11\rangle|\widetilde{1}\rangle|\widetilde{1}\rangle),
$$

$$
A_0 \otimes A_1 \otimes A_0 \otimes A_0 \otimes A_0 \otimes A_0|\bar{\Psi}\rangle = \sqrt{\frac{3}{2}\gamma^8(1-\gamma)}(c_0|11\rangle|\widetilde{0}\rangle|\widetilde{0}\rangle + \frac{c_1}{\sqrt{2}}(|20\rangle + |02\rangle)|\widetilde{1}\rangle|\widetilde{1}\rangle),
$$

$$
A_1 \otimes A_1 \otimes A_0 \otimes A_0 \otimes A_0 \otimes A_0|\bar{\Psi}\rangle = \sqrt{\frac{3}{2}\gamma^7(1-\gamma)^2}(c_0|01\rangle|\widetilde{0}\rangle|\widetilde{0}\rangle + c_1|10\rangle|\widetilde{1}\rangle|\widetilde{1}\rangle),
$$

$$
A_2 \otimes A_0 \otimes A_0 \otimes A_0 \otimes A_0 \otimes A_0|\bar{\Psi}\rangle = \frac{\sqrt{3}}{2}\sqrt{\gamma^7(1-\gamma)^2}(c_0|10\rangle|\widetilde{0}\rangle|\widetilde{0}\rangle + c_1|01\rangle|\widetilde{1}\rangle|\widetilde{1}\rangle),
$$

$$
A_0 \otimes A_2 \otimes A_0 \otimes A_0 \otimes A_0 \otimes A_0|\bar{\Psi}\rangle = \frac{\sqrt{3}}{2}\sqrt{\gamma^7(1-\gamma)^2}(c_0|10\rangle|\widetilde{0}\rangle|\widetilde{0}\rangle + c_1|01\rangle|\widetilde{1}\rangle|\widetilde{1}\rangle), \tag{5.22}
$$

$$
\begin{aligned}
A_1 \otimes A_0 \otimes A_1 \otimes A_0 \otimes A_0 \otimes A_0|\bar{\Psi}\rangle = \frac{3}{2}\sqrt{\gamma^7(1-\gamma)^2}(c_0\frac{1}{\sqrt{2}}(|20\rangle + |02\rangle)\frac{1}{\sqrt{2}}(|20\rangle + |02\rangle)|\widetilde{0}\rangle \\
+ c_1|11\rangle|11\rangle|\widetilde{1}\rangle),
\end{aligned}
$$

$$
\begin{aligned}
A_0 \otimes A_1 \otimes A_1 \otimes A_0 \otimes A_0 \otimes A_0|\bar{\Psi}\rangle = \frac{3}{2}\sqrt{\gamma^7(1-\gamma)^2}(c_0|11\rangle\frac{1}{\sqrt{2}}(|20\rangle + |02\rangle)|\widetilde{0}\rangle \\
+ c_1\frac{1}{\sqrt{2}}(|20\rangle + |02\rangle)|11\rangle|\widetilde{1}\rangle),
\end{aligned}
$$

$$
\begin{aligned}
A_0 \otimes A_1 \otimes A_0 \otimes A_1 \otimes A_0 \otimes A_0|\bar{\Psi}\rangle = \frac{3}{2}\sqrt{\gamma^7(1-\gamma)^2}(c_0|11\rangle|11\rangle|\widetilde{0}\rangle \\
+ c_1\frac{1}{\sqrt{2}}(|20\rangle + |02\rangle)\frac{1}{\sqrt{2}}(|20\rangle + |02\rangle)|\widetilde{1}\rangle),
\end{aligned}
$$

$$
\begin{aligned}
A_1 \otimes A_0 \otimes A_0 \otimes A_1 \otimes A_0 \otimes A_0|\bar{\Psi}\rangle = \frac{3}{2}\sqrt{\gamma^7(1-\gamma)^2}(c_0\frac{1}{\sqrt{2}}(|20\rangle + |02\rangle)|11\rangle|\widetilde{0}\rangle \\
+ c_1|11\rangle\frac{1}{\sqrt{2}}(|20\rangle + |02\rangle)|\widetilde{1}\rangle).
\end{aligned}
$$

One can easily verify that a recovery of the logical qubit is, in principle, possible by again detecting the photon number for each block with additional inter-block parity measurements. It is then also not difficult to see that the KL conditions are fulfilled for these operators, so indeed the corresponding two-photon loss errors can be corrected with this encoding. Note that the code is degenerate, i.e. the effect of some non-identical loss errors on the logical qubit is identical. For the loss of three or more photons, the code ceases to be a complete loss code. The corresponding worst-case fidelity is

$$
\begin{aligned}
F &= \gamma^9 + 9\gamma^8(1-\gamma) + 36\gamma^7(1-\gamma)^2 \\
&\approx 1 - 84(1-\gamma)^3.
\end{aligned}
\tag{5.23}
$$

This is the same result as for the bosonic code in Eq.(3.9). However, note that in order to promote the encoding from a one-photon-loss to a two-photon-loss code, in our scheme the maximal photon number per mode only needs to go up from two to three photons (as opposed to four versus nine photons in Eq.(3.5) and Eq.(3.9), respectively). Similarly, the two-photon-loss code QPC(3,3) requires as many as 18 optical modes compared to a modest number of six modes in our case.

Our procedure can be generalized for arbitrary N (i.e., N photons per block and N^2 total number of photons), setting

$$
\begin{aligned}
|t_0^{2,N}\rangle &= BS[|N0\rangle], \\
|t_1^{2,N}\rangle &= BS[|0N\rangle],
\end{aligned}
\tag{5.24}
$$

applying the Hadamard-type gate (using Eqs. (5.6) and (5.24)),

$$
\begin{aligned}
|\widetilde{0}\rangle &= \frac{1}{\sqrt{2}}\left(|t_0^{2,N}\rangle + |t_1^{2,N}\rangle\right) = \frac{1}{\sqrt{2}^{N-1}}\sum_{j=0}^{N}\sqrt{\binom{N}{2j}}|N-2j,2j\rangle \\
&= BS\left[\frac{1}{\sqrt{2}}\left(|N0\rangle + |0N\rangle\right)\right]
\end{aligned}
\tag{5.25}
$$

$$
\begin{aligned}
|\widetilde{1}\rangle &= \frac{1}{\sqrt{2}}\left(|t_0^{2,N}\rangle - |t_1^{2,N}\rangle\right) = \frac{1}{\sqrt{2}^{N-1}}\sum_{j=0}^{N}\sqrt{\binom{N}{2j+1}}|N-2j-1,2j+1\rangle \\
&= BS\left[\frac{1}{\sqrt{2}}\left(|N0\rangle - |0N\rangle\right)\right]
\end{aligned}
\tag{5.26}
$$

and finally introducing the N-block structure,

$$
\begin{aligned}
|\bar{0}\rangle &= |\widetilde{0}\rangle^{\otimes N}, \\
|\bar{1}\rangle &= |\widetilde{1}\rangle^{\otimes N}.
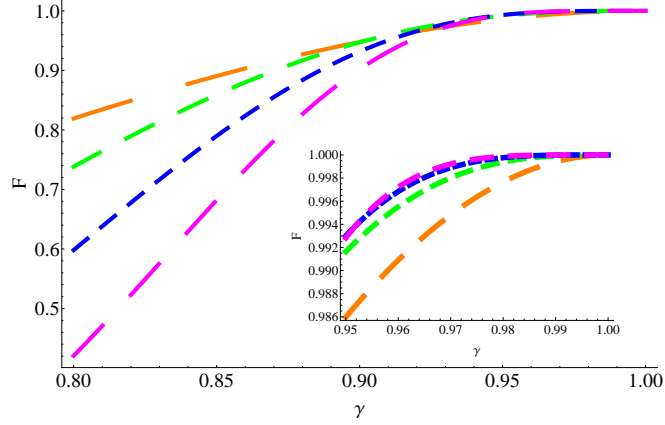\end{aligned}
\tag{5.27}
$$

Figure 5.1: Worst-case fidelities for different qubit loss NOON codes as a function of γ: $N^2 = 4$ (orange), $N^2 = 9$ (green), $N^2 = 16$ (blue) and $N^2 = 25$ (magenta), each correcting $N-1$ photon losses. Notice the change of ordering with higher-order codes beating the lower-order codes for small losses and the converse for larger losses [see inset]. The small-loss regime $\gamma \in [0.95, 1]$ would correspond to a communication channel length of ~ 1 km (see Section 2.1).

By construction (for more details, see the next section), this code corrects the loss of up to $N - 1$ photons using N^2 photons. For any order, i.e. photon number, the codewords of our NOON code can always be obtained from NOON state resources using beam splitters. The worst-case fidelities of different qubit codes are compared in Fig. 5.1 . One interesting feature of our qubit code construction is the interchangeability of the beam splitter transformation, Hadamard operation, and block building. For example, consider the $N^2 = 4$ case. In order to produce the codewords, we first apply the symmetric beam splitter transformation on $|20\rangle$ and $|02\rangle$, followed by the Hadamard gate, and finally build the blocks. The logical basis codewords obtained in this way are

$$
\begin{aligned}
|\bar{0}\rangle &= \left[\frac{1}{\sqrt{2}}(|20\rangle + |02\rangle)\right]^{\otimes 2} = \frac{1}{2}(|2020\rangle + |2002\rangle + |0220\rangle + |0202\rangle), \\
|\bar{1}\rangle &= \left[\frac{1}{\sqrt{2}}(|20\rangle - |02\rangle)\right]^{\otimes 2} = \frac{1}{2}(|2020\rangle - |2002\rangle - |0220\rangle + |0202\rangle),
\end{aligned}
\tag{5.28}
$$

which correspond to the codewords obtained as before up to a beam splitter transformation on each block. The details to verify that this encoding is also a proper code as well as its extension to qudits can be found in Appendix A.2 .

37

5.4 Generalization to qudit codes

Our method can be directly generalized to logical qudits. Let us again illustrate the idea by a specific example, namely that for a qutrit code ($d = 3$). Define the states

$$|t_0^{3,2}\rangle = T[|200\rangle] = \frac{1}{3}|200\rangle + \frac{1}{3}|020\rangle + \frac{1}{3}|002\rangle + \frac{\sqrt{2}}{3}|101\rangle + \frac{\sqrt{2}}{3}|011\rangle + \frac{\sqrt{2}}{3}|110\rangle, \qquad (5.29)$$

$$|t_1^{3,2}\rangle = T[|020\rangle] = \frac{1}{3}|200\rangle + \frac{1}{3}\exp(4\pi i/3)|020\rangle + \frac{1}{3}\exp(-4\pi i/3)|002\rangle + \frac{\sqrt{2}}{3}\exp(-2\pi i/3)|101\rangle$$

$$+ \frac{\sqrt{2}}{3}|011\rangle + \frac{\sqrt{2}}{3}\exp(2\pi i/3)|110\rangle,$$

$$|t_2^{3,2}\rangle = T[|002\rangle] = \frac{1}{3}|200\rangle + \frac{1}{3}\exp(-4\pi i/3)|020\rangle + \frac{1}{3}\exp(4\pi i/3)|002\rangle + \frac{\sqrt{2}}{3}\exp(2\pi i/3)|101\rangle$$

$$+ \frac{\sqrt{2}}{3}|011\rangle + \frac{\sqrt{2}}{3}\exp(-2\pi i/3)|110\rangle,$$

where T now represents a "tritter" transformation, i.e. a symmetric 3-splitter. The encoding works via a qutrit Hadamard-type gate:

$$|\widetilde{0}\rangle = \frac{1}{\sqrt{3}}(|t_0^{3,2}\rangle + |t_1^{3,2}\rangle + |t_2^{3,2}\rangle) = \frac{1}{\sqrt{3}}|200\rangle + \sqrt{\frac{2}{3}}|011\rangle,$$

$$|\widetilde{1}\rangle = \frac{1}{\sqrt{3}}(|t_0^{3,2}\rangle + \exp(2\pi i/3)|t_1^{3,2}\rangle + \exp(-2\pi i/3)|t_2^{3,2}\rangle) = \frac{1}{\sqrt{3}}|020\rangle + \sqrt{\frac{2}{3}}|101\rangle, \qquad (5.30)$$

$$|\widetilde{2}\rangle = \frac{1}{\sqrt{3}}(|t_0^{3,2}\rangle + \exp(-2\pi i/3)|t_1^{3,2}\rangle + \exp(2\pi i/3)|t_2^{3,2}\rangle) = \frac{1}{\sqrt{3}}|002\rangle + \sqrt{\frac{2}{3}}|110\rangle.$$

The logical qutrit state is then defined as

$$|\bar{\Psi}\rangle = c_0|\widetilde{0}\rangle|\widetilde{0}\rangle + c_1|\widetilde{1}\rangle|\widetilde{1}\rangle + c_2|\widetilde{2}\rangle|\widetilde{2}\rangle. \qquad (5.31)$$

The states obtained from the logical qutrit after the loss of exactly one photon are:

$$A_1 \otimes A_0 \otimes A_0 \otimes A_0 \otimes A_0 \otimes A_0|\bar{\Psi}\rangle = \sqrt{\frac{2}{3}}\gamma^3(1-\gamma)(c_0|100\rangle|\widetilde{0}\rangle + c_1|001\rangle|\widetilde{1}\rangle + c_2|010\rangle|\widetilde{2}\rangle),$$

$$A_0 \otimes A_1 \otimes A_0 \otimes A_0 \otimes A_0 \otimes A_0|\bar{\Psi}\rangle = \sqrt{\frac{2}{3}}\gamma^3(1-\gamma)(c_0|001\rangle|\widetilde{0}\rangle + c_1|010\rangle|\widetilde{1}\rangle + c_2|100\rangle|\widetilde{2}\rangle),$$

$$A_0 \otimes A_0 \otimes A_1 \otimes A_0 \otimes A_0 \otimes A_0|\bar{\Psi}\rangle = \sqrt{\frac{2}{3}}\gamma^3(1-\gamma)(c_0|010\rangle|\widetilde{0}\rangle + c_1|100\rangle|\widetilde{1}\rangle + c_2|001\rangle|\widetilde{2}\rangle),$$

$$A_0 \otimes A_0 \otimes A_0 \otimes A_1 \otimes A_0 \otimes A_0|\bar{\Psi}\rangle = \sqrt{\frac{2}{3}}\gamma^3(1-\gamma)(c_0|\widetilde{0}\rangle|100\rangle + c_1|\widetilde{1}\rangle|001\rangle + c_2|\widetilde{2}\rangle|010\rangle),$$

$$A_0 \otimes A_0 \otimes A_0 \otimes A_0 \otimes A_1 \otimes A_0 |\bar{\Psi}\rangle = \sqrt{\frac{2}{3}\gamma^3(1-\gamma)}(c_0|\widetilde{0}\rangle|001\rangle + c_1|\widetilde{1}\rangle|010\rangle + c_2|\widetilde{2}\rangle|100\rangle),$$

$$A_0 \otimes A_0 \otimes A_0 \otimes A_0 \otimes A_0 \otimes A_1 |\bar{\Psi}\rangle = \sqrt{\frac{2}{3}\gamma^3(1-\gamma)}(c_0|\widetilde{0}\rangle|010\rangle + c_1|\widetilde{1}\rangle|100\rangle + c_2|\widetilde{2}\rangle|001\rangle).$$

$$(5.32)$$

Again, the KL conditions are obviously fulfilled, so the code can correct the loss of up to one single photon. As before, the error spaces can be discriminated by identifying in which block the photon was lost and by measuring global inter-block observables (while simple inter-block parities no longer work). An extension to higher photon numbers and to higher dimensional quantum systems is natural,

$$|t_0^{d,N}\rangle = S_d[|N00...0\rangle], ..., |t_{d-1}^{d,N}\rangle = S_d[|000...0N\rangle]. \tag{5.33}$$

Here, S_d represents a d-splitter, i.e. a symmetric d-port device where d is the number of modes. It is the multi-mode generalization of a symmetric beam splitter and the tritter as discussed above (thus $S_2 = BS$ and $S_3 = T$).

Then we define the following states:

$$|\widetilde{k}\rangle = \frac{1}{\sqrt{d}} \sum_{j=0}^{d-1} \exp(2\pi i k j/d)|t_j^{d,N}\rangle, \tag{5.34}$$

for $k = 0, ..., d-1$. A general logical qudit is then expressed by the dN-mode, N^2-photon state

$$|\bar{\Psi}\rangle = c_0|\widetilde{0}\rangle^{\otimes N} + c_1|\widetilde{1}\rangle^{\otimes N} + ... + c_{d-1}|\widetilde{d-1}\rangle^{\otimes N}. \tag{5.35}$$

By construction, this code can correct up to $N-1$ photon losses. The orthogonality of corrupted codewords, required by the KL conditions, is easy to check, because the codewords are built blockwise. The non-deformation criterion, however, requires a more rigorous check. Let us first calculate the input state $|t_0^{d,N}\rangle$ for general N and d,

$$\begin{aligned}
|N00\cdots\rangle &= \frac{\hat{a}_1^{\dagger N}}{\sqrt{N!}}|000...\rangle \rightarrow S_d[|N000...\rangle] \\
&= \frac{1}{\sqrt{N!}}\sqrt{\frac{1}{d}}^N (\hat{a}_1^\dagger + \hat{a}_2^\dagger + \cdots + \hat{a}_d^\dagger)^N |000\cdots\rangle \\
&= \frac{1}{\sqrt{N!}}\sqrt{\frac{1}{d}}^N \sum_{\vec{k}\in\mathcal{A}} \binom{N}{k_1, k_2, \cdots, k_d} \hat{a}_1^{\dagger k_1}\hat{a}_2^{\dagger k_2}\cdots\hat{a}_d^{\dagger k_d}|000\rangle
\end{aligned} \tag{5.36}$$

$$= \frac{1}{\sqrt{N!}} \sqrt{\frac{1}{d}}^N \sum_{\vec{k} \in \mathcal{A}} \binom{N}{k_1, k_2, \cdots, k_d} \times \sqrt{k_1!}\sqrt{k_2!}\cdots\sqrt{k_d!}|k_1, k_2, \cdots, k_d\rangle$$

$$= \frac{1}{\sqrt{N!}} \sqrt{\frac{1}{d}}^N \sum_{\vec{k} \in \mathcal{A}} \frac{N!}{\sqrt{k_1!k_2!\cdots k_d!}}|k_1, k_2, \cdots, k_d\rangle.$$

In the third line, we used the multinomial theorem, bearing in mind that all the creation operators commute with each other. Furthermore, we defined the multinomial coefficient,

$$\binom{N}{k_1, k_2, \cdots, k_d} = \frac{N!}{k_1!k_2!\cdots k_d!}, \tag{5.37}$$

as the number of arrangements of N objects in which there are k_j objects of type j, k_q objects of type q and so on. We also introduced the set of d-dimensional vectors with fixed column sum, i.e. $\mathcal{A} \equiv \{\vec{k} \in \mathbb{N}_0^d | \sum_{i=1}^d k_i = N\}$, to parametrize the set of all d-mode Fock states with fixed photon number N. Furthermore, we define $\mathcal{A}' \equiv \{\vec{k} \in \mathbb{N}_0^d | \sum_{i=1}^d k_i = N \text{ and } k_1 \geq 1\}$ and $\mathcal{A}'' \equiv \{\vec{k} \in \mathbb{N}_0^d | \sum_{i=1}^d k_i = N - 1\}$.

We consider the loss of exactly one photon in the first mode, i.e. we apply the operator $A_1 \otimes A_0^{\otimes d-1}$:

$$A_1 \otimes A_0^{\otimes d-1} S_d[|N00...\rangle]$$

$$= \frac{1}{\sqrt{N!}} \sqrt{\frac{1}{d}}^N \sum_{\vec{k} \in \mathcal{A}} \frac{N!}{\sqrt{k_1!}\sqrt{k_2!}\cdots\sqrt{k_d!}} A_1 \otimes A_0^{\otimes d-1}|k_1, k_2, \cdots, k_d\rangle$$

$$= \frac{1}{\sqrt{N!}} \sqrt{\frac{1}{d}}^N \sum_{\vec{k} \in \mathcal{A}'} \frac{N!}{\sqrt{k_1!}\sqrt{k_2!}\cdots\sqrt{k_d!}} \sqrt{\gamma}^{N-1}\sqrt{1-\gamma}\sqrt{k_1}|k_1 - 1, k_2, \cdots, k_d\rangle$$

$$= \frac{1}{\sqrt{N!}} \sqrt{\frac{1}{d}}^N \sqrt{\gamma}^{N-1}\sqrt{1-\gamma} \sum_{\vec{k} \in \mathcal{A}'} \frac{N!}{\sqrt{(k_1-1)!}\sqrt{k_2!}\cdots\sqrt{k_d!}}|k_1 - 1, k_2, \cdots, k_d\rangle$$

$$= \frac{1}{\sqrt{N!}} \sqrt{\frac{1}{d}}^N \sqrt{\gamma}^{N-1}\sqrt{1-\gamma} \sum_{\vec{q} \in \mathcal{A}''} \frac{N!}{\sqrt{q_1!}\sqrt{q_2!}\cdots\sqrt{q_d!}}|q_1, q_2, \cdots, q_d\rangle$$

$$= \sqrt{N}\sqrt{\frac{1}{d}}\sqrt{\gamma}^{N-1}\sqrt{1-\gamma}S_d(|N-1, 0, 0, \cdots\rangle). \tag{5.38}$$

For symmetry reasons, the loss of a photon in a different mode acts identically. The same is true for the other input states, i.e. $S_d[|0, 0, \cdots, N, 0, 0, \cdots\rangle]$ decays into $S_d[|0, 0, \cdots, N-1, 0, 0, \cdots\rangle]$ after losing one photon. Higher losses can be treated by induction. Because the blocks of the

basis codewords are exactly superpositions of these states, no deformation can take place after photon loss. Together with the orthogonality of corrupted codewords, this proves our qudit encoding to be a quantum error correction code.

5.5 Physical implementation of the qubit code

In order to substantiate the importance of the encodings, we describe a scheme how to generate an arbitrary logical qubit for the simplest code with just two photons per block ($N = 2$). We assume that the states $\frac{1}{\sqrt{2}}(|20\rangle \pm |02\rangle)$ are experimentally accessible from two single-photon states $|1\rangle \otimes |1\rangle$ with a phase-free and an appropriately phase-inducing, 50:50 beam splitter. In addition, we need one auxiliary photon in two ancilla modes to produce the following states:

$$
\begin{aligned}
|\psi_1\rangle &= |0\rangle \frac{1}{\sqrt{2}}(|20\rangle + |02\rangle)|1\rangle, \\
|\psi_2\rangle &= |1\rangle \frac{1}{\sqrt{2}}(|20\rangle - |02\rangle)|0\rangle.
\end{aligned}
\tag{5.39}
$$

As pointed out in [122], by employing an ancilla ion-trap system, the generation of a symmetric entangled state, $\frac{1}{\sqrt{2}}(|\phi_1\rangle|\phi_2\rangle + |\phi_2\rangle|\phi_1\rangle)$, is, in principle, possible for arbitrary photonic input states $|\phi_1\rangle$ and $|\phi_2\rangle$. Applied to $|\psi_1\rangle$ and $|\psi_2\rangle$, one obtains

$$
\frac{1}{\sqrt{2}} \left(\frac{1}{\sqrt{2}}(|20\rangle + |02\rangle)\frac{1}{\sqrt{2}}(|20\rangle - |02\rangle)|0110\rangle) + \frac{1}{\sqrt{2}}(|20\rangle - |02\rangle)\frac{1}{\sqrt{2}}(|20\rangle + |02\rangle)|1001\rangle \right),
\tag{5.40}
$$

where we already reordered the modes. The next step is to apply a general beam splitter with complex transmittance t and reflectivity r, with the coefficients in the desired superposition determined later, to the first and second pair of the ancilla modes. This leads to

$$
\begin{aligned}
\frac{1}{\sqrt{2}} \Big(&\frac{1}{\sqrt{2}}(|20\rangle + |02\rangle)\frac{1}{\sqrt{2}}(|20\rangle - |02\rangle))(r|10\rangle - t|01\rangle)(t|10\rangle + r|01\rangle) \\
&+ \frac{1}{\sqrt{2}}(|20\rangle - |02\rangle)\frac{1}{\sqrt{2}}(|20\rangle + |02\rangle)(t|10\rangle + r|01\rangle)(r|10\rangle - t|01\rangle) \Big).
\end{aligned}
\tag{5.41}
$$

Measuring the photons after the beam splitter and detecting '1001' projects the state onto

$$
\begin{aligned}
&\frac{r^2}{\sqrt{|r|^4 + |t|^4}}\frac{1}{\sqrt{2}}(|20\rangle + |02\rangle)\frac{1}{\sqrt{2}}(|20\rangle - |02\rangle)) \\
&- \frac{t^2}{\sqrt{|r|^4 + |t|^4}}\frac{1}{\sqrt{2}}(|20\rangle - |02\rangle)\frac{1}{\sqrt{2}}(|20\rangle + |02\rangle)).
\end{aligned}
\tag{5.42}
$$

Finally, a phase shift of $\pi/2$ on the last mode (i.e., applying $\exp\left(\frac{i\pi\hat{n}}{2}\right)$ to it) gives the logical

qubit

$$
\begin{aligned}
|\bar{\Psi}\rangle &= \frac{r^2}{\sqrt{|r|^4 + |t|^4}} \frac{1}{\sqrt{2}}(|20\rangle + |02\rangle)\frac{1}{\sqrt{2}}(|20\rangle + |02\rangle)) \\
&\quad - \frac{t^2}{\sqrt{|r|^4 + |t|^4}} \frac{1}{\sqrt{2}}(|20\rangle - |02\rangle)\frac{1}{\sqrt{2}}(|20\rangle - |02\rangle)) \\
&= c_0 \frac{1}{\sqrt{2}}(|20\rangle + |02\rangle)\frac{1}{\sqrt{2}}(|20\rangle + |02\rangle)) + c_1 \frac{1}{\sqrt{2}}(|20\rangle - |02\rangle)\frac{1}{\sqrt{2}}(|20\rangle - |02\rangle)),
\end{aligned}
\tag{5.43}
$$

similar to Eq.(5.15). Because $|t|^2 + |r|^2 = 1$, this means that with an appropriate choice of t and r and with a final symmetric beam splitter transformation on the blocks, any superposition of the logical codewords can be generated. Note that the logical qubit in Eq.(5.43) (without the final symmetric beam splitter) corresponds to the four-photon, alternative NOON code qubit [see Section 5.3 and Appendix A.2].

Chapter 6

QEC against photon loss using multicomponent cat states

In this chapter, we start with a discussion of the known approximate one-loss qubit cat code [44, 45] (see Eq. (3.13)) and its properties when subject to individual photon loss events as well as its behavior in a full loss channel. Following this, we present a generalisation of this code to a higher number of losses. We present a detailed analysis of a generalized code that includes a complete and systematic definition of the codewords as well as a quantitative performance assessment of the code in a full photon loss channel. We will give a very compact definition of the codewords in terms of eigenvalue equations, expressed in terms of powers of the mode annihilation operators, for any loss order. In this way we will also define the canonical codewords for the respective error spaces, which satisfy the same eigenvalue equations, but differ from the code space-codewords and the codewords from the other error spaces in their (generalized) number parities. Thus, a certain instance of the cat code (corresponding to a certain coherent-state amplitude α, a certain loss order L, and also a certain logical dimension d for general logical qudits living in the code and error spaces) is defined by two sets of eigenvalue equations: one to determine the space (and hence the error syndrome) and another one to define (together with the former set) the codewords. We will demonstrate that for the right choice of codewords there is no deformation of the initial logical qubit (not even for small coherent-state amplitudes, in which case, however, the codewords begin to overlap significantly). This no-deformation property results in a rather simple and well structured output density matrix when the encoded state is subject to a complete loss channel. This feature is also similar to the cyclic behavior of the one-loss-code in the simplified photon-annihilation ("photon-jump") error model [44, 45], but here extended to higher losses and for the full, physical photon loss channel.

6.1 One-loss cat code

It is rather well-known that there is a two-fold effect when a cat state, i.e., a superposition of two distinct coherent states such as $\propto |\alpha\rangle + |-\alpha\rangle$ is subject to a full photon loss (amplitude damping) channel. On the one hand, the coherent-state amplitude α in each term is attenuated depending on the channel transmission parameter, $\sqrt{\gamma}\alpha$, corresponding to an exponential amplitude decay with distance. On the other hand, a random phase flip occurs that incoherently mixes the initial cat state with its phase-flipped version such as $\propto |\alpha\rangle - |-\alpha\rangle$, where the flip probability also depends on the channel transmission γ and on the initial amplitude α. In a cat-state qubit encoding [62, 123], a loss-induced phase flip of a logical qubit could be corrected when the qubit is encoded into an additional layer of a multi-qubit repetition code composed of three or more logical cat qubits (i.e., by adding two or more physical oscillator modes) [124, 125, 126]. A conceptually more innovative approach, however, would stick to a single oscillator mode and instead exploit more than just two (near-)orthogonal coherent-state components of that mode (i.e., exploiting a manifold with dimension larger than two in the oscillator's phase space). While it is obvious that this approach enables one to reach higher dimensions, it is not immediately clear how this can provide protection against photon losses. In Refs. [44, 45], however, it was shown that by constructing two (near-)orthogonal codewords both in the form of even cat states (those with only even photon-number terms) a logical qubit can be encoded that remains intact under the effect of a lost photon, as the qubit is then mapped onto an orthogonal error space that is spanned by two (near-)orthogonal codewords both in the form of odd cat states (those with only odd photon-number terms).

Formally, for the even cat code given in [44, 45], the basic codewords are certain $+1$ eigenstates of the number parity operator $(-1)^{\hat{n}}$:

$$
\begin{aligned}
|\bar{0}_+\rangle &= \frac{1}{\sqrt{N_+}}(|\alpha\rangle + |-\alpha\rangle), \\
|\bar{1}_+\rangle &= \frac{1}{\sqrt{N_+}}(|i\alpha\rangle + |-i\alpha\rangle),
\end{aligned}
\tag{6.1}
$$

with normalization constant $N_\pm = 2 \pm 2\exp(-2\alpha^2)$ (N_- for later). Throughout we assume $\alpha \in \mathbb{R}$. By writing the coherent states in the Fock basis, one can easily confirm that both codewords have only even photon number terms,

$$
\begin{aligned}
|\bar{0}_+\rangle &= \frac{2e^{-\alpha^2/2}}{\sqrt{N_+}}\left(|0\rangle + \frac{\alpha^2}{\sqrt{2}}|2\rangle + \frac{\alpha^4}{2\sqrt{6}}|4\rangle + ...\right), \\
|\bar{1}_+\rangle &= \frac{2e^{-\alpha^2/2}}{\sqrt{N_+}}\left(|0\rangle - \frac{\alpha^2}{\sqrt{2}}|2\rangle + \frac{\alpha^4}{2\sqrt{6}}|4\rangle - ...\right).
\end{aligned}
\tag{6.2}
$$

These two so-called even cat states are, in general, not orthogonal, but for large α, as $e^{-\alpha^2/2}\alpha^k \to 0$, an infinite superposition of nearly equally weighted even number states is obtained for each codeword, $|\bar{0}_+\rangle \propto |0\rangle + |2\rangle + |4\rangle + ...$ and $|\bar{1}_+\rangle \propto |0\rangle - |2\rangle + |4\rangle - ...$ and thus $\langle \bar{0}_+|\bar{1}_+\rangle \approx 0$ (notice the alternating sign in $|\bar{1}_+\rangle$). For general α, their overlap is (see App. B.1)

$$\langle \bar{0}_+|\bar{1}_+\rangle = \frac{1}{N_+}\left(\langle\alpha|i\alpha\rangle + \langle\alpha|-i\alpha\rangle + \langle-\alpha|i\alpha\rangle + \langle-\alpha|-i\alpha\rangle\right) = \frac{\cos(\alpha^2)}{\cosh(\alpha^2)}, \tag{6.3}$$

which indeed goes to zero in the limit $\alpha \to \infty$. Instead of the codewords in Eq. (6.1), as an alternative qubit basis, we may also use the two *orthogonal* states

$$|\bar{0}_+ \pm \bar{1}_+\rangle = \frac{1}{\sqrt{N'_\pm}}(|\alpha\rangle + |-\alpha\rangle \pm |i\alpha\rangle \pm |-i\alpha\rangle), \tag{6.4}$$

which span the same (even) code space as $\{|\bar{0}_+\rangle, |\bar{1}_+\rangle\}$ do and hence represent the same (even) cat code ($N'_\pm$ are some normalization constants). Their exact orthogonality (for any α) can be immediately seen in the Fock basis:

$$\begin{aligned}
|\bar{0}_+ + \bar{1}_+\rangle &= \frac{4e^{-\alpha^2/2}}{\sqrt{N'_+}}\left(|0\rangle + \frac{\alpha^4}{2\sqrt{6}}|4\rangle + \frac{\alpha^8}{24\sqrt{70}}|8\rangle + ...\right), \\
|\bar{0}_+ - \bar{1}_+\rangle &= \frac{4e^{-\alpha^2/2}}{\sqrt{N'_-}}\left(\frac{\alpha^2}{\sqrt{2}}|2\rangle + \frac{\alpha^6}{12\sqrt{5}}|6\rangle + \frac{\alpha^{10}}{720\sqrt{7}}|10\rangle + ...\right).
\end{aligned} \tag{6.5}$$

Here we refer to the non-orthogonal codewords $|\bar{0}_+\rangle$ and $|\bar{1}_+\rangle$ as the (approximate) logical Pauli-$\bar{Z}$ basis, and in this sense, the states $|\bar{0}_+ \pm \bar{1}_+\rangle$ can be thought of a logical Pauli-$\bar{X}$ basis obtained by taking an equally weighted sum or difference of the two $\bar{Z}$ eigenstates. This is similar to the cat-qubit encoding of Ref.[123] when two non-orthogonal phase-rotated coherent states $\{|\pm\alpha\rangle\}$ form the computational $\bar{Z}$ basis, while the two orthogonal even and odd cat states $\{|\alpha\rangle \pm |-\alpha\rangle\}$ correspond to the Hadamard-transformed, logical $\bar{X}$ basis (this encoding, however, does not represent a loss code that allows to correct a certain non-zero number of photon losses and it corresponds to the 0th order of our family of generalized cat codes, see next section).

Although $\{|\bar{0}_+\rangle, |\bar{1}_+\rangle\}$ and $\{|\bar{0}_+ \pm \bar{1}_+\rangle\}$ represent the same code, we will see that, nonetheless, the choice of codewords, for example the $\bar{Z}$ or $\bar{X}$ basis, does make a difference when assessing the code's performance in a physical loss channel. This is related to the fact that the code is an approximate code, for which there is not a clear distinction between correctable errors (exactly satisfying the Knill-Laflamme (KL) conditions [22], see App. B.1) and uncorrectable errors (violating the KL conditions) like for an exact code. For the approximate cat code, those errors that are, in principle, correctable may still give violations of the KL conditions, however, these violations go away in the limit of large amplitudes α. For general α values, it then depends

on the choice of codewords what particular KL conditions are violated and, as a result, what particular logical errors occur. These logical errors reduce the (input-state-dependent qubit) fidelity, which is further reduced by the uncorrectable errors (which remain uncorrectable even when $\alpha \to \infty$ and which occur more frequently when α is large, see below).

As one type of violation of the KL conditions can be avoided at least in the 0th order (i.e., the orthogonality condition of the initial codewords) for the basis $\{|\bar{0}_+ \pm \bar{1}_+\rangle\}$, independently of α, it appears beneficial to choose this basis. However, for finite α, these codewords lead to a deformation of the logical qubit, i.e., the norms of the codewords after an otherwise correctable error (such as a one-loss-error for the one-loss-code) change depending on the specific codeword. This latter effect of qubit deformation turns out to be highly undesirable when the full photon loss channel is considered and so our choice of codewords will be the non-orthogonal $\{|\bar{0}_+\rangle, |\bar{1}_+\rangle\}$-basis. These codewords do not lead to a qubit deformation, i.e., the change in the norm of either codeword after a one-loss-error (or any other correctable error such as 0,4,8,12,... or 5,9,13,... losses of photons, see below) is independent of the codeword for any α. This no-deformation property of the codewords means that the nice cyclicity feature of the cat code for a simplified, unphysical photon-loss error model, as we discuss next, can be effectively taken over to the physical model of a full loss channel. The only remaining effects that have to be dealt with then come from the non-orthogonality of the codewords $|\bar{0}_+\rangle$ and $|\bar{1}_+\rangle$ before and after an error (i.e., in the code and the error spaces, as it becomes manifest through violations of the corresponding KL conditions). In App. B.1, we present a detailed discussion of the KL criteria for the various error models.

In order to understand the behavior of the codewords under photon loss, it is conceptually useful to first model the effects of the channel by individual photon loss and simply apply the annihilation operator $\hat{a}$ to the codewords. Higher losses are analogously represented by higher powers of $\hat{a}$. It also turns out to be advantageous to look at even and odd powers separately:

$$
\begin{aligned}
\hat{a}^{2k}|\bar{0}_+\rangle &= \alpha^{2k} \frac{1}{\sqrt{N_+}}(|\alpha\rangle + |-\alpha\rangle), \\
\hat{a}^{2k}|\bar{1}_+\rangle &= (-1)^k \alpha^{2k} \frac{1}{\sqrt{N_+}}(|i\alpha\rangle + |-i\alpha\rangle), \\
\hat{a}^{2k+1}|\bar{0}_+\rangle &= \alpha^{2k+1} \frac{1}{\sqrt{N_+}}(|\alpha\rangle - |-\alpha\rangle), \\
\hat{a}^{2k+1}|\bar{1}_+\rangle &= i(-1)^k \alpha^{2k+1} \frac{1}{\sqrt{N_+}}(|i\alpha\rangle - |-i\alpha\rangle),
\end{aligned}
\tag{6.6}
$$

where $k = 0, 1, 2, ...$ According to this simplified loss model, a logical qubit of the (unnormalized) form $|\bar{\psi}\rangle = a|\bar{0}_+\rangle + b|\bar{1}_+\rangle$ evolves cyclically into the following four (unnormalized) states [44, 45],

$$|\bar{\psi}\rangle_{4k} = a|\bar{0}_+\rangle + b|\bar{1}_+\rangle,$$
$$|\bar{\psi}\rangle_{4k+1} = a|\bar{0}_-\rangle + ib|\bar{1}_-\rangle,$$
$$|\bar{\psi}\rangle_{4k+2} = a|\bar{0}_+\rangle - b|\bar{1}_+\rangle, \quad (6.7)$$
$$|\bar{\psi}\rangle_{4k+3} = a|\bar{0}_-\rangle - ib|\bar{1}_-\rangle,$$

depending on whether the number of lost photons is 0,4,8,... or 1,5,9,... or 2,6,10,... or 3,7,11,..., respectively. Here, we defined the non-orthogonal basic codewords for the error space as

$$|\bar{0}_-\rangle = \frac{1}{\sqrt{N_-}}(|\alpha\rangle - |-\alpha\rangle),$$
$$|\bar{1}_-\rangle = \frac{1}{\sqrt{N_-}}(|i\alpha\rangle - |-i\alpha\rangle), \quad (6.8)$$

which are two so-called odd cat states with only odd photon number terms,

$$|\bar{0}_-\rangle = \frac{2e^{-\alpha^2/2}\alpha}{\sqrt{N_-}} \left(|1\rangle + \frac{\alpha^2}{\sqrt{6}}|3\rangle + \frac{\alpha^4}{2\sqrt{30}}|5\rangle + ... \right),$$
$$|\bar{1}_-\rangle = \frac{2e^{-\alpha^2/2}i\alpha}{\sqrt{N_-}} \left(|1\rangle - \frac{\alpha^2}{\sqrt{6}}|3\rangle + \frac{\alpha^4}{2\sqrt{30}}|5\rangle - ... \right). \quad (6.9)$$

Again, these two codewords approach an orthogonal qubit basis, this time in the odd-parity error space, when α is sufficiently large (notice the alternating sign in $|\bar{1}_-\rangle$ inherited from $|\bar{1}_+\rangle$). In fact, the overlap between $|\bar{0}_-\rangle$ and $|\bar{1}_-\rangle$ is

$$\langle\bar{0}_-|\bar{1}_-\rangle = \frac{1}{N_-} \left(\langle\alpha|i\alpha\rangle - \langle\alpha|-i\alpha\rangle - \langle-\alpha|i\alpha\rangle + \langle-\alpha|-i\alpha\rangle \right) = \frac{i\sin(\alpha^2)}{\sinh(\alpha^2)}, \quad (6.10)$$

which again can be made arbitrarily small by increasing α. The code and error spaces can be characterized by their photon number parity (even/odd) and thus are perfectly distinguishable. However, there can be uncorrectable phase-flip errors of the logical qubit when it is mapped back to the even code space after half a cycle, $|\bar{\psi}\rangle_{4k+2} = a|\bar{0}_+\rangle - b|\bar{1}_+\rangle$, or when it is mapped again onto the odd error space before the end of a cycle, $|\bar{\psi}\rangle_{4k+3} = a|\bar{0}_-\rangle - ib|\bar{1}_-\rangle$. Otherwise the qubit remains intact either in the code space, $|\bar{\psi}\rangle_{4k} = a|\bar{0}_+\rangle + b|\bar{1}_+\rangle$, or in the error space, $|\bar{\psi}\rangle_{4k+1} = a|\bar{0}_-\rangle + ib|\bar{1}_-\rangle$ (in which case it is transformed by a known and fixed phase gate). Once the parity is detected, the qubit is recovered and no further correction step is needed. The uncorrectable errors lead to a non-unit fidelity, when the actual physical loss channel is considered which we do next.

The full loss channel is described by the error operators in Eq. (2.6) and represents a (complete-positive) trace-preserving map that incorporates all possible individual photon loss events as well as the effect of amplitude decay.

Let us now study the action of AD on the encoding in Eq. (6.1). The somewhat lengthy calculations are presented in App. B.1 and the channel evolution of a normalized logical qubit $|\bar{\psi}\rangle$ is found to be

$$
\begin{aligned}
\bar{\rho} = \; &\widetilde{p}_0 \left(\frac{a|\widetilde{0}_+\rangle + b|\widetilde{1}_+\rangle}{\sqrt{1 + 2\operatorname{Re}(ab^*)\frac{\cos(\gamma\alpha^2)}{\cosh(\gamma\alpha^2)}}} \right) \times H.c. \\
+ \; &\widetilde{p}_1 \left(\frac{a|\widetilde{0}_-\rangle + ib|\widetilde{1}_-\rangle}{\sqrt{1 - 2\operatorname{Re}(ab^*)\frac{\sin(\gamma\alpha^2)}{\sinh(\gamma\alpha^2)}}} \right) \times H.c. \\
+ \; &\widetilde{p}_2 \left(\frac{a|\widetilde{0}_+\rangle - b|\widetilde{1}_+\rangle}{\sqrt{1 - 2\operatorname{Re}(ab^*)\frac{\cos(\gamma\alpha^2)}{\cosh(\gamma\alpha^2)}}} \right) \times H.c. \\
+ \; &\widetilde{p}_3 \left(\frac{a|\widetilde{0}_-\rangle - ib|\widetilde{1}_-\rangle}{\sqrt{1 + 2\operatorname{Re}(ab^*)\frac{\sin(\gamma\alpha^2)}{\sinh(\gamma\alpha^2)})}} \right) \times H.c. \quad .
\end{aligned}
\tag{6.11}
$$

The statistical weights in this mixture are given by

$$
\begin{aligned}
\widetilde{p}_0 &= \frac{1 + 2\operatorname{Re}(ab^*)\frac{\cos(\gamma\alpha^2)}{\cosh(\gamma\alpha^2)}}{1 + 2\operatorname{Re}(ab^*)\frac{\cos(\alpha^2)}{\cosh(\alpha^2)}} p_0, \\
\widetilde{p}_1 &= \frac{1 - 2\operatorname{Re}(ab^*)\frac{\sin(\gamma\alpha^2)}{\sinh(\gamma\alpha^2)}}{1 + 2\operatorname{Re}(ab^*)\frac{\cos(\alpha^2)}{\cosh(\alpha^2)}} p_1, \\
\widetilde{p}_2 &= \frac{1 - 2\operatorname{Re}(ab^*)\frac{\cos(\gamma\alpha^2)}{\cosh(\gamma\alpha^2)}}{1 + 2\operatorname{Re}(ab^*)\frac{\cos(\alpha^2)}{\cosh(\alpha^2)}} p_2, \\
\widetilde{p}_3 &= \frac{1 + 2\operatorname{Re}(ab^*)\frac{\sin(\gamma\alpha^2)}{\sinh(\gamma\alpha^2)}}{1 + 2\operatorname{Re}(ab^*)\frac{\cos(\alpha^2)}{\cosh(\alpha^2)}} p_3,
\end{aligned}
\tag{6.12}
$$

where

$$
\begin{aligned}
p_0 &= \frac{\cosh(\gamma\alpha^2)}{2\cosh(\alpha^2)} \left(\cos[\alpha^2(1-\gamma)] + \cosh[\alpha^2(1-\gamma)] \right), \\
p_1 &= \frac{\sinh(\gamma\alpha^2)}{2\cosh(\alpha^2)} \left(\sin[\alpha^2(1-\gamma)] + \sinh[\alpha^2(1-\gamma)] \right), \\
p_2 &= \frac{\cosh(\gamma\alpha^2)}{2\cosh(\alpha^2)} \left(-\cos[\alpha^2(1-\gamma)] + \cosh[\alpha^2(1-\gamma)] \right), \\
p_3 &= \frac{\sinh(\gamma\alpha^2)}{2\cosh(\alpha^2)} \left(-\sin[\alpha^2(1-\gamma)] + \sinh[\alpha^2(1-\gamma)] \right),
\end{aligned}
\tag{6.13}
$$

are the loss probabilities for the individual codewords. The states in the mixture above are damped compared to the input states $(\alpha \to \sqrt{\gamma}\alpha)$, which is denoted by the transition $|\bar{0}_+\rangle \to |\widetilde{0}_+\rangle$ etc. throughout. Although the complex coefficients of the logical input qubit state are
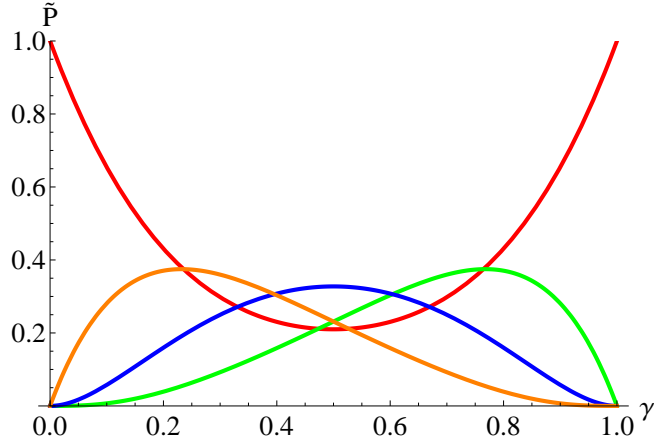
Figure 6.1: Statistical weights for $\alpha = 2$ and $a = b = \frac{1}{\sqrt{2}}$ (from top to bottom at $\gamma = 1$): $\widetilde{p}_0$ (red), $\widetilde{p}_1$ (green), $\widetilde{p}_2$ (blue), $\widetilde{p}_3$ (orange) as a function of the damping parameter γ (no damping means $\gamma = 1$). Thus, the red and the green curves represent the weights of the correctable errors (0,4,8,... and 1,5,9,... losses), while the blue and orange curves correspond to the uncorrectable errors (2,6,10,... and 3,7,11,... losses). Note that the a, b-dependence can lead to a different qualitative behavior of the probabilities for different logical qubits.

normalized as usual, $|a|^2 + |b|^2 = 1$, note that because of the finite overlap between the codewords in the code and error spaces, an extra factor depending on the input qubit state occurs in the probabilities. This is also related to the fact that the encoding is not an exact quantum error correction code, but only an approximate one (see Chapter 3). The channel output state $\bar{\rho}$ in Eq. (6.11) still reflects the cyclic behavior of the code[1] under individual photon loss events owing to the use of the $\bar{Z}$-basis codewords for the logical qubit (thus, avoiding its deformation and a resulting mixture of infinitely many deformed qubits corresponding to infinitely many different loss events). The choice of the logical basis becomes irrelevant only when $\alpha \to \infty$ [2]. Besides the damping of α, an uncorrectable phase flip occurs whenever $2, 6, 10, ...$ or $3, 7, 11, ...$ photons are lost. Any other loss errors belong to the correctable set.

The error correction works by a QND-type parity measurement which distinguishes between even and odd photon numbers. For this encoding, the probability to correctly identify the error

---

[1]Note that even for $L = 0$, i.e. when we consider the simple coherent state encoding $|\pm\alpha\rangle$ (see the notation for generalized cat codes in Section 6.2), the resulting density matrix $\bar{\rho}$ intrinsically contains such a cyclic behavior (see Eq. (B.44) for $L = 0$). In this well-known case [124], the resulting mixture has only two terms, of which one corresponds to all even losses containing the initial (damped) qubit and the other one corresponds to all odd losses containing a phase-flipped version of the initial (damped) qubit. Since in either case, even or odd losses, the qubit lives in the same space spanned by the damped versions of $|\pm\alpha\rangle$, already a one-photon-loss error cannot be distinguished from zero loss and thus the qubit phase flip must be regarded as random.

[2]Of course, we may also rewrite a logical (unnormalized) qubit initially expressed in the $\bar{Z}$-basis, $|\bar{\Psi}\rangle = a|\bar{0}_+\rangle + b|\bar{1}_+\rangle$, as the same qubit expressed in the $\bar{X}$-basis, $|\bar{\Psi}\rangle = \frac{a}{2}[(|\bar{0}_+\rangle + |\bar{1}_+\rangle) + (|\bar{0}_+\rangle - |\bar{1}_+\rangle)] + \frac{b}{2}[(|\bar{0}_+\rangle + |\bar{1}_+\rangle) - (|\bar{0}_+\rangle - |\bar{1}_+\rangle)] = \frac{a+b}{2}\sqrt{N'_+}|\bar{0}_+ + \bar{1}_+\rangle + \frac{a-b}{2}\sqrt{N'_-}|\bar{0}_+ - \bar{1}_+\rangle$.
As said, this choice of basis leads to a deformation of the qubit for finite α (while the codewords are exactly orthogonal). Calculating the worst-case fidelity in this case is rather complicated, because every loss event leads to a differently deformed qubit in the resulting output density matrix.
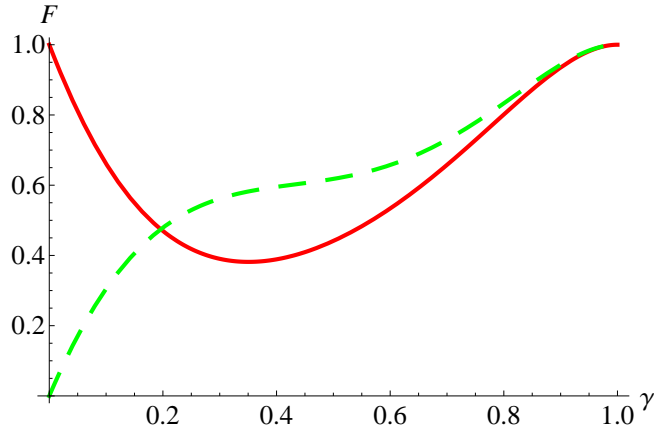
Figure 6.2: Probability $F(a,b)$ with a logical qubit $a = b = \frac{1}{\sqrt{2}}$ (red, solid line) and $a = -b = \frac{1}{\sqrt{2}}$ (green, dashed line) for $\alpha = 2$ as a function of the damping parameter γ (no damping means $\gamma = 1$). The actual lower bound on F_{wc} is given by the minimum of the two curves for each γ.

syndrome is the sum of the statistical weights of the correctable components in the mixture,

$$F(a,b) = \widetilde{p}_0(a,b) + \widetilde{p}_1(a,b). \tag{6.14}$$

The worst-case fidelity F_{wc} (see Eq. (3.4)) is then lower-bounded as

$$F_{wc} \geq \min_{a,b} F(a,b) \equiv F. \tag{6.15}$$

This bound F is the minimum of the probabilities of correctable errors over all input states. How this lower bound can be understood is explained in App. B.2.

The bound F for the one-loss cat code (for a balanced logical qubit minimizing $F(a,b)$, see App. B.2) is shown in Fig. 6.2. The actual F_{wc} is at least as large as plotted there, so that the minimal performance can be inferred. The statistical weights from Eq. (6.12) are shown in Fig. 6.1, also for a balanced logical qubit.

6.2   Generalized cat codes

Let us now generalize the one-loss code to include higher losses and state the defining equations for the codewords $|\bar{0}\rangle$ and $|\bar{1}\rangle$ of an approximate qubit QECC that is capable of correcting L losses:

$$\exp\left(\frac{2\pi i\hat{n}}{L+1}\right)|\bar{0}\rangle = |\bar{0}\rangle,$$

$$\exp\left(\frac{2\pi i\hat{n}}{L+1}\right)|\bar{1}\rangle = |\bar{1}\rangle,$$

$$(\hat{a}^{L+1} - \alpha^{L+1})|\bar{0}\rangle = 0,$$

$$(\hat{a}^{L+1} + \alpha^{L+1})|\bar{1}\rangle = 0. \tag{6.16}$$

Here, $\hat{n} = \hat{a}^\dagger\hat{a}$ is again the number operator. We will refer to the first two equations as the "parity conditions" that determine the error syndrome and hence the subspace in which the qubit resides after an error occurred (one code space and L error spaces). The current choice of eigenvalue $+1$ for the two parity conditions in Eq. (6.16) corresponds to (the codewords of) the original code space. The error spaces spanned by two codewords with another parity are described by parity conditions with other phase factors as eigenvalues, see below and App. B.3. This is reminiscent of the stabilizer formalism for QEC in terms of Pauli operators [127, 128]. The last two equations in Eq. (6.16) define the codewords in every subspace and remain unchanged for different parities (subspaces), i.e., both codewords are always zero-eigenstates of the corresponding (generally nonlinear) expressions for the mode operator $\hat{a}$.

As shown in App. B.3 , the (unnormalized) solutions for general L can be written as superpositions of coherent states,

$$|\bar{0}\rangle = \sum_{k=0}^{L} |\alpha\exp\left(\frac{2k\pi i}{L+1}\right)\rangle,$$

$$|\bar{1}\rangle = \sum_{k=1}^{L+1} |\alpha\exp\left(\frac{(2k-1)\pi i}{L+1}\right)\rangle. \tag{6.17}$$

For $L = 0$, one obtains the coherent-state encoding $|\bar{0}\rangle = |\alpha\rangle$ and $|\bar{1}\rangle = |-\alpha\rangle$ presented in Refs. [123, 62] that provides no intrinsic loss protection. The $L = 1$ case corresponds to the one-loss cat code reviewed in Section 6.1. Setting $L = 2$ corresponds to a two-loss code, for which the unnormalized codewords become

$$|\bar{0}\rangle = |\alpha\rangle + |\alpha\exp\left(\frac{2\pi i}{3}\right)\rangle + |\alpha\exp\left(-\frac{2\pi i}{3}\right)\rangle,$$

$$|\bar{1}\rangle = |\alpha\exp\left(\frac{\pi i}{3}\right)\rangle + |\alpha\exp\left(\pi i\right)\rangle + |\alpha\exp\left(-\frac{\pi i}{3}\right)\rangle. \tag{6.18}$$

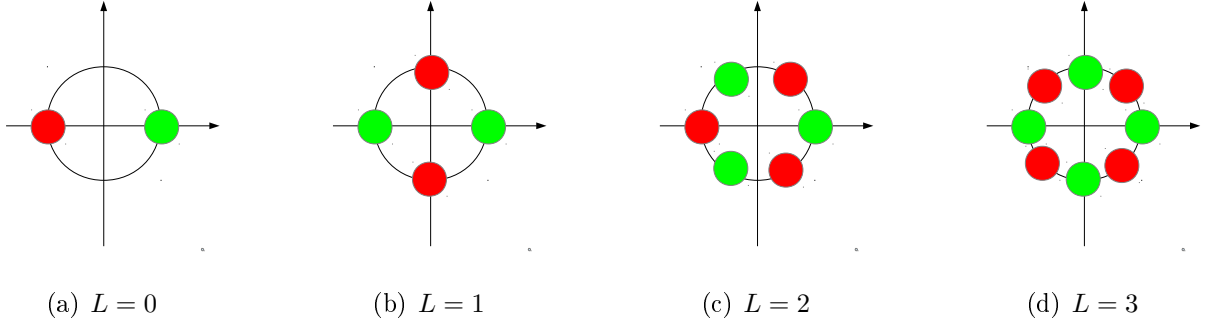(a) $L = 0$ (b) $L = 1$ (c) $L = 2$ (d) $L = 3$

Figure 6.3: Illustration of the lowest qubit ($d = 2$) loss codes in phase space. The binary codewords are represented by green ($|\bar{0}\rangle$) and red ($|\bar{1}\rangle$) circles which are to be superimposed.

These are both superpositions of number terms of multiples of three (see App. B.4). As can easily be checked using the defining equations in Eq.(6.16), a logical qubit $|\bar{\psi}\rangle = a|\bar{0}\rangle + b|\bar{1}\rangle$ then evolves cyclically under the simplified error model (similar to Section 6.1) as

$$\hat{a}^{3k}|\bar{0}\rangle = \alpha^{3k}|\bar{0}\rangle,$$
$$\hat{a}^{3k}|\bar{1}\rangle = (-1)^k \alpha^{3k}|\bar{1}\rangle,$$
$$\hat{a}^{3k+1}|\bar{0}\rangle = \alpha^{3k+1}(|\alpha\rangle + \exp\left(\frac{2\pi i}{3}\right)|\alpha\exp\left(\frac{2\pi i}{3}\right)\rangle + \exp\left(-\frac{2\pi i}{3}\right)|\alpha\exp\left(-\frac{2\pi i}{3}\right)\rangle),$$
$$\hat{a}^{3k+1}|\bar{1}\rangle = (-1)^k \alpha^{3k+1} \exp\left(\frac{\pi i}{3}\right)(|\alpha\exp\left(\frac{\pi i}{3}\right)\rangle + \exp\left(\frac{2\pi i}{3}\right)|\alpha\exp\left(\pi i\right)\rangle$$
$$+ \exp\left(-\frac{2\pi i}{3}\right)|\alpha\exp\left(-\frac{\pi i}{3}\right)\rangle), \tag{6.19}$$
$$\hat{a}^{3k+2}|\bar{0}\rangle = \alpha^{3k+2}(|\alpha\rangle + \exp\left(-\frac{2\pi i}{3}\right)|\alpha\exp\left(\frac{2\pi i}{3}\right)\rangle + \exp\left(\frac{2\pi i}{3}\right)|\alpha\exp\left(-\frac{2\pi i}{3}\right)\rangle),$$
$$\hat{a}^{3k+2}|\bar{1}\rangle = (-1)^k \alpha^{3k+2} \exp\left(\frac{2\pi i}{3}\right)(|\alpha\exp\left(\frac{\pi i}{3}\right)\rangle + \exp\left(-\frac{2\pi i}{3}\right)|\alpha\exp\left(\pi i\right)\rangle$$
$$+ \exp\left(\frac{2\pi i}{3}\right)|\alpha\exp\left(-\frac{\pi i}{3}\right)\rangle),$$

where again $k = 0, 1, 2, \dots$. Similar to $L = 1$, we encounter a cyclic behavior. For even k (especially $k = 0$ corresponding to 0, 1 and 2 losses), there are no k-dependent phase flips (the factors $(-1)^k$ in front of the transformed $|\bar{1}\rangle$-codewords in lines 2, 4 and 6 on the rhs of Eq.(6.19), see also below) and only fixed, k-independent phase factors (in front of the transformed $|\bar{1}\rangle$-codewords). The parities for the one- and two-loss cases change compared to the zero-loss case from 0,3,6,... to 2,5,8,... and 1,4,7,..., respectively (see App. B.4).
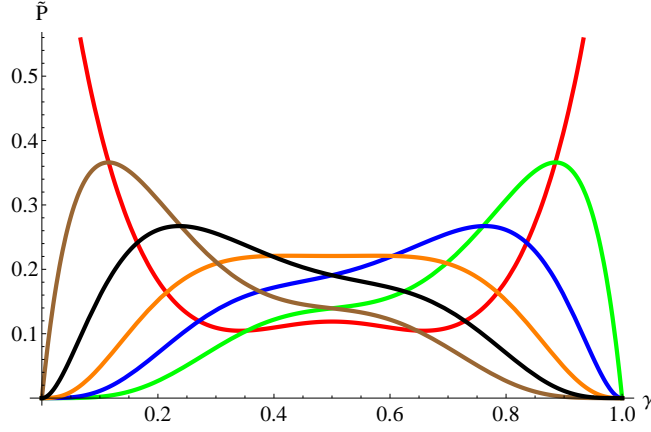
Figure 6.4: Statistical weights with $\alpha = 3$ and $a = b = \frac{1}{\sqrt{2}}$ for $L = 2$ (from top to bottom at $\gamma = 1$): $\widetilde{p}_0$ (red), $\widetilde{p}_1$ (green), $\widetilde{p}_2$ (blue), $\widetilde{p}_3$ (orange), $\widetilde{p}_4$ (black), $\widetilde{p}_5$ (brown) as a function of γ. Note that the a, b-dependence can lead to a different qualitative behavior of the probabilities for different logical qubits.

The calculations for the complete, physical AD channel are presented in App.B.4. Besides the basic codewords in the initial code space, we define the (unnormalized) codewords in all the three orthogonal subspaces (one code space, and two error spaces for one- and two-photon losses, etc.) as

$$
\begin{aligned}
|\bar{0}_0\rangle_2 &= |\alpha\rangle + |\alpha \exp\left(\frac{2\pi i}{3}\right)\rangle + |\alpha \exp\left(-\frac{2\pi i}{3}\right)\rangle, \\
|\bar{1}_0\rangle_2 &= |\alpha \exp\left(\frac{\pi i}{3}\right)\rangle + |\alpha \exp\left(\pi i\right)\rangle + |\alpha \exp\left(-\frac{\pi i}{3}\right)\rangle, \\
|\bar{0}_1\rangle_2 &= |\alpha\rangle + \exp\left(\frac{2\pi i}{3}\right)|\alpha \exp\left(\frac{2\pi i}{3}\right)\rangle + \exp\left(-\frac{2\pi i}{3}\right)|\alpha \exp\left(-\frac{2\pi i}{3}\right)\rangle, \\
|\bar{1}_1\rangle_2 &= |\alpha \exp\left(\frac{\pi i}{3}\right)\rangle + \exp\left(\frac{2\pi i}{3}\right)|\alpha \exp\left(\pi i\right)\rangle + \exp\left(-\frac{2\pi i}{3}\right)|\alpha \exp\left(-\frac{\pi i}{3}\right)\rangle, \\
|\bar{0}_2\rangle_2 &= |\alpha\rangle + \exp\left(-\frac{2\pi i}{3}\right)|\alpha \exp\left(\frac{2\pi i}{3}\right)\rangle + \exp\left(\frac{2\pi i}{3}\right)|\alpha \exp\left(-\frac{2\pi i}{3}\right)\rangle, \\
|\bar{1}_2\rangle_2 &= |\alpha \exp\left(\frac{\pi i}{3}\right)\rangle + \exp\left(-\frac{2\pi i}{3}\right)|\alpha \exp\left(\pi i\right)\rangle + \exp\left(\frac{2\pi i}{3}\right)|\alpha \exp\left(-\frac{\pi i}{3}\right)\rangle.
\end{aligned}
\tag{6.20}
$$

Here, we introduced the notation $\{|\bar{0}_q\rangle_L, |\bar{1}_q\rangle_L\}$ to specify the order of the loss code (L) and the corresponding error space (q) ($q = 0$ for no loss, $q = 1$ for one-photon loss, and $q = 2$ for two-photon loss, plus cyclic loss events, see below). With these definitions for the canonical codewords in the code and error spaces, Eq. (6.19) simplifies to
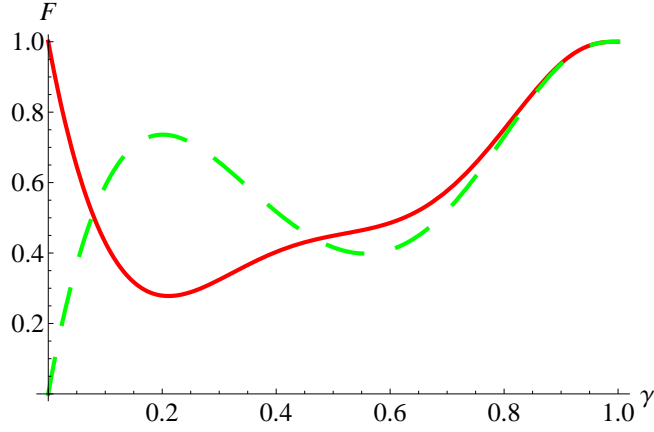
Figure 6.5: Probability $F(a,b)$ as a function of γ for $\alpha = 3$ with $a = b = \frac{1}{\sqrt{2}}$ (red, solid line) and $a = -b = \frac{1}{\sqrt{2}}$ (green, dashed line) where $L = 2$. The actual lower bound on F_{wc} is given by the minimum of the two curves for each γ.

$$
\begin{aligned}
\hat{a}^{3k}|\bar{0}_0\rangle_2 &= \alpha^{3k}|\bar{0}_0\rangle_2, \\
\hat{a}^{3k}|\bar{1}_0\rangle_2 &= (-1)^k \alpha^{3k}|\bar{1}_0\rangle_2, \\
\hat{a}^{3k+1}|\bar{0}_0\rangle_2 &= \alpha^{3k+1}|\bar{0}_1\rangle_2, \\
\hat{a}^{3k+1}|\bar{1}_0\rangle_2 &= (-1)^k \alpha^{3k+1} \exp\left(\frac{\pi i}{3}\right)|\bar{1}_1\rangle_2, \\
\hat{a}^{3k+2}|\bar{0}_0\rangle_2 &= \alpha^{3k+2}|\bar{0}_2\rangle_2, \\
\hat{a}^{3k+2}|\bar{1}_0\rangle_2 &= (-1)^k \alpha^{3k+2} \exp\left(\frac{2\pi i}{3}\right)|\bar{1}_2\rangle_2.
\end{aligned}
\tag{6.21}
$$

As shown in App. B.4, a logical qubit $a|\bar{0}_0\rangle_2 + b|\bar{1}_0\rangle_2$ subject to AD becomes a mixture of six components, which can be cast in the form (omitting proper normalizations of the qubits),

$$
\begin{aligned}
\bar{\rho} = &\; p_0(a|\widetilde{0}_0\rangle_2 + b|\widetilde{1}_0\rangle_2) \times H.c. \\
&+ p_1(a|\widetilde{0}_1\rangle_2 + e^{\frac{i\pi}{3}} b|\widetilde{1}_1\rangle_2) \times H.c. \\
&+ p_2(a|\widetilde{0}_2\rangle_2 + e^{\frac{2i\pi}{3}} b|\widetilde{1}_2\rangle_2) \times H.c. \\
&+ p_3(a|\widetilde{0}_0\rangle_2 - b|\widetilde{1}_0\rangle_2) \times H.c. \\
&+ p_4(a|\widetilde{0}_1\rangle_2 - e^{\frac{i\pi}{3}} b|\widetilde{1}_1\rangle_2) \times H.c. \\
&+ p_5(a|\widetilde{0}_2\rangle_2 - e^{\frac{2i\pi}{3}} b|\widetilde{1}_2\rangle_2) \times H.c. \quad .
\end{aligned}
\tag{6.22}
$$

Recall again the additional damping of the amplitude due to the AD channel ($\alpha \to \sqrt{\gamma}\alpha$) and correspondingly the adapted notation $\{|\bar{0}_q\rangle_2, |\bar{1}_q\rangle_2\} \to \{|\widetilde{0}_q\rangle_2, |\widetilde{1}_q\rangle_2\}$ for $q = 0, 1, 2$. Now the first three terms in Eq. (6.22) correspond to correctable logical qubits with, besides some fixed phase gates for $q = 1$ and $q = 2$, photon number parities of 0,3,6... or 2,5,8,... or 1,4,7,...
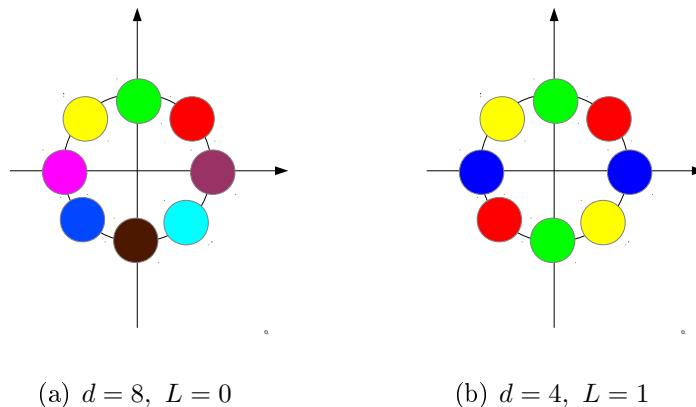
54

(a) $d = 8$, $L = 0$ (b) $d = 4$, $L = 1$

Figure 6.6: Illustration of some qudit codes in phase space realized through coherent-state superpositions (every color indicates another codeword) with in total 8 components (for $d = 2$, $L = 3$, see Fig 2.)

.

corresponding to the loss of 0,6,12,... ($q = 0$) or 1,7,13,...($q = 1$) or 2,8,14,... ($q = 2$) photons, respectively. The additional terms each mix in uncorrectable phase-flip errors for every subspace corresponding to the loss of 3,9,15,... or 4,10,16,... or 5,11,17,... photons. Again, like for the one-loss code, the cyclic behavior of the simplified model is recovered for the full channel (for more details, see App. B.4). Thus, for the $L = 2$ case, among the dominating loss errors, those from one- and two-photon losses can be corrected (i.e., the qubit is still intact in the corresponding error space), whereas those from three-, four- and five-photon losses cannot (i.e., the qubit is subject to a phase error). For six- and higher photon losses, the cycle starts again. In general, an L-code can correct up to L photon losses plus other cycles and each codeword has $(L + 1)$ coherent-state components living in a $2(L + 1)$-dimensional manifold.

The lowest cat codes $L = 0, 1, 2, 3$ encoding a logical qubit are illustrated in Fig. 6.3. In Figs. 6.4 and 6.5, the statistical weights and the fidelity bound on F_{wc}, respectively, are shown as functions of the damping (loss) parameter γ.

6.3 Extension to qudit codes

Another generalisation that goes beyond the qubit codes presented in the last section is to define equations for the encoding of an arbitrary qudit of d dimensions:

$$\exp\left(\frac{2\pi i \hat{n}}{L + 1}\right)|\bar{k}\rangle = |\bar{k}\rangle,$$
$$(\hat{a}^{L+1} - \exp\left(\frac{2\pi i k}{d}\right)\alpha^{L+1})|\bar{k}\rangle = 0 \ \text{ for } \ k = 0, 1, .., d - 1. \tag{6.23}$$

For $d = 2$, Eq. (6.16) for logical qubits is obtained. The simplest encoding for general d with $L = 0$ corresponds to $|\bar{k}\rangle = |\alpha e^{\frac{2\pi i k}{d}}\rangle$ for $k = 0, 1, ..., d-1$, which is referred to as "coherent states on a ring" in Ref. [129]. Phase space illustrations of two distinct instances of qudit codes are shown in Fig. 6.6.

For $d = 3$ and $L = 1$, i.e. the simplest loss code beyond $d = 2$, one finds the (unnormalized) solutions

$$
\begin{aligned}
|\bar{0}\rangle &\equiv |\bar{0}_+\rangle = |\alpha\rangle + |-\alpha\rangle, \\
|\bar{1}\rangle &\equiv |\bar{1}_+\rangle = |e^{\frac{i\pi}{3}}\alpha\rangle + |-e^{\frac{i\pi}{3}}\alpha\rangle, \\
|\bar{2}\rangle &\equiv |\bar{2}_+\rangle = |e^{-\frac{i\pi}{3}}\alpha\rangle + |-e^{-\frac{i\pi}{3}}\alpha\rangle.
\end{aligned}
\tag{6.24}
$$

The three-dimensional code space is spanned by three (generally non-orthogonal) even cat states, similar to the $L = 1$ qubit code which has two even cat states as codewords. In the simplified error model, we also find a similar cyclic behavior of the codewords,

$$
\begin{aligned}
\hat{a}^{2k}|\bar{0}\rangle &= \alpha^{2k}|\bar{0}_+\rangle, \\
\hat{a}^{2k}|\bar{1}\rangle &= \exp\left(\frac{i\pi}{3}\right)^{2k}\alpha^{2k}|\bar{1}_+\rangle, \\
\hat{a}^{2k}|\bar{2}\rangle &= \exp\left(-\frac{i\pi}{3}\right)^{2k}\alpha^{2k}|\bar{2}_+\rangle, \\
\hat{a}^{2k+1}|\bar{0}\rangle &= \alpha^{2k+1}|\bar{0}_-\rangle, \\
\hat{a}^{2k+1}|\bar{1}\rangle &= \exp\left(\frac{i\pi}{3}\right)^{2k+1}\alpha^{2k+1}|\bar{1}_-\rangle, \\
\hat{a}^{2k+1}|\bar{2}\rangle &= \exp\left(-\frac{i\pi}{3}\right)^{2k+1}\alpha^{2k+1}|\bar{2}_-\rangle,
\end{aligned}
\tag{6.25}
$$

where $|\bar{0}_-\rangle = |\alpha\rangle - |-\alpha\rangle$, $|\bar{1}_-\rangle = |e^{\frac{i\pi}{3}}\alpha\rangle - |-e^{\frac{i\pi}{3}}\alpha\rangle$ and $|\bar{2}_-\rangle = |e^{-\frac{i\pi}{3}}\alpha\rangle - |-e^{-\frac{i\pi}{3}}\alpha\rangle$. Depending on the number of lost photons $m = 0, 1, 2, 3, 4, 5$, the logical qudit $a|\bar{0}\rangle + b|\bar{1}\rangle + c|\bar{2}\rangle$ suffers from random relative phases (the phase factors $(e^{\pm\frac{i\pi}{3}})^{2k}$ in front of the transformed codewords $|\bar{1}_\pm\rangle$ and $|\bar{2}_\pm\rangle$). In fact, only for $k = 0, 3, 6, ...$ no phase errors occur and a fixed phase gate (the phase factor $e^{\pm\frac{i\pi}{3}}$ in front of $|\bar{1}_-\rangle$ and $|\bar{2}_-\rangle$) is either applied (1,7,13,.. losses) or not (0,6,12,...losses). Subject to the full AD channel, the mixed output state for a logical qutrit $a|\bar{0}\rangle + b|\bar{1}\rangle + c|\bar{2}\rangle$ has six components,

$$
\begin{aligned}
|\bar{\psi}_0\rangle &= a|\bar{0}_+\rangle + b|\bar{1}_+\rangle + c|\bar{2}_+\rangle, \\
|\bar{\psi}_1\rangle &= a|\bar{0}_-\rangle + b\exp\left(\frac{i\pi}{3}\right)|\bar{1}_-\rangle + c\exp\left(-\frac{i\pi}{3}\right)|\bar{2}_-\rangle, \\
|\bar{\psi}_2\rangle &= a|\bar{0}_+\rangle + b\exp\left(\frac{2i\pi}{3}\right)|\bar{1}_+\rangle + c\exp\left(-\frac{2i\pi}{3}\right)|\bar{2}_+\rangle,
\end{aligned}
\tag{6.26}
$$

$$|\bar{\psi}_3\rangle = a|\bar{0}_-\rangle - b|\bar{1}_-\rangle - c|\bar{2}_-\rangle,$$

$$|\bar{\psi}_4\rangle = a|\bar{0}_+\rangle - b\exp\left(\frac{i\pi}{3}\right)|\bar{1}_+\rangle - c\exp\left(-\frac{i\pi}{3}\right)|\bar{2}_+\rangle,$$

$$|\bar{\psi}_5\rangle = a|\bar{0}_-\rangle - b\exp\left(\frac{2i\pi}{3}\right)|\bar{1}_-\rangle - c\exp\left(-\frac{2i\pi}{3}\right)|\bar{2}_-\rangle,$$

with some statistical weights. Here, only $|\bar{\psi}_0\rangle$ and $|\bar{\psi}_1\rangle$ correspond to correctable qutrits (corresponding to 0,6,12,... and 1,7,13,.. losses, respectively). All the remaining qutrits $|\bar{\psi}_2\rangle, |\bar{\psi}_3\rangle, |\bar{\psi}_4\rangle$ and $|\bar{\psi}_5\rangle$ have suffered from phase errors (corresponding to 2,8,14,... or 3,9,15... or 4,10,16,... or 5,11,17,.. losses, respectively). After six losses a new cycle starts.

In general, for a general L-code the period of a cycle depends on the total number of coherent-state components of the code (that is $d(L+1)$), e.g. a 4-cycle (i.e., 4 terms in $\bar{\rho}$) for $d = 2|L = 1$ or a 6-cycle (6 terms in $\bar{\rho}$) for both $d = 2|L = 2$ and $d = 3|L = 1$.

Chapter 7

Quantum repeater protocols for qubits and beyond

Based on the hybrid quantum repeater protocol for qubits discussed in Section 4.1.2, we generalize this scheme to the case of three-level systems (qutrits) in Section 7.1.1. After proposing a generalized dispersive atomic qutrit-light interaction, we discuss the process of entanglement generation in elementary links using this interaction. We consider both homodyne detection and photon-detection-based unambiguous state discrimination (USD) for the measurement on the light mode. Including entanglement purification for the initial qutrit-qutrit entangled states, we calculate the final rates and fidelities for our generalized entanglement distribution scheme in various scenarios. Based on these results, we discuss a generalization to arbitrarily dimensional quantum systems.

Following this, a scheme in the direction of a quantum repeater for continuous variables is considered. We adapt the continuous-variable teleportation scheme proposed in [130] to the long-distance scenario. Instead of using noisy single-photon entangled pairs, we use discrete-variable first-generation quantum repeaters to distribute perfect resource states. The overall effect is shown to be an increase of the fidelity at the expense of a decreasing rate of the protocol. Furthermore, we propose a light-matter interface that enables one to switch between decoherence-free subspaces of ions and QPC(2,2) encoded photonic states. We explicitly describe how this can be done with feasible transformations on ionic qubits.

The last part of the chapter is dedicated to applications of the qudit codes developed in Chapters 5 and 6 to one-way communication schemes. For the qudit codes of Chapter 5, we show that this scheme does not intrinsically provide an optimal rate between physical versus logical qubits like another recent approach [102], but nonetheless allows for sending more quantum information at each time step with the same loss protection. For the approximate cat codes of Chapter 6, we also show in addition to the qubit recovery how the decay of the coherent-state amplitude can be, in principle, dealt with at large distances.

7.1 First-generation quantum repeaters

7.1.1 A hybrid quantum repeater for qudits

Qutrit hybrid quantum repeater

Dispersive interaction   The dispersive interaction (see Eq. (4.2)) lies at the heart of the hybrid quantum repeater for qubits and therefore, as a first step to extend this repeater scheme to qutrits, a generalization of the dispersive interaction to the qutrit case is necessary.

In analogy to the dispersive interaction for qubits, we define the interaction Hamiltonian for qutrits as

$$H_{int}^{(3)} = \hbar g \hat{S}_z^{(3)} \hat{a}^\dagger \hat{a}, \tag{7.1}$$

where the operator $\hat{S}_z^{(3)}$ acts on the qutrit basis states $|0\rangle$, $|1\rangle$ and $|2\rangle$ as

$$\begin{aligned}
\hat{S}_z^{(3)}|0\rangle &= -1 \cdot |0\rangle, \\
\hat{S}_z^{(3)}|1\rangle &= 0 \cdot |1\rangle, \\
\hat{S}_z^{(3)}|2\rangle &= 1 \cdot |2\rangle.
\end{aligned} \tag{7.2}$$

The matter system could be, for example, realized by a spin-1 particle where the basis states are the eigenstates to the corresponding magnetic quantum numbers, $m_z = -1, 0, 1$. Such a spin realization of a qutrit has been demonstrated in the framework of nuclear magnetic resonance (NMR) for various applications [35, 131].

Similar to the qubit case, the corresponding unitary transformation is $U_3(\theta) = \exp\left(i\theta \hat{S}_z^{(3)} \hat{a}^\dagger \hat{a}\right)$ which again corresponds to a conditional phase rotation on the light-matter system (up to an unconditional phase shift of the qubus mode by $e^{i\theta}$), i.e.

$$U_3(\theta)(|0\rangle + |1\rangle + |2\rangle)|\alpha\rangle = |0\rangle|\alpha\rangle + |1\rangle|\alpha e^{i\theta}\rangle + |2\rangle|\alpha e^{2i\theta}\rangle. \tag{7.3}$$

For our purposes, we will choose $\theta = \frac{2\pi}{3}$ to obtain a rather strong dispersive interaction.

Loss-free case   The qutrit hybrid repeater protocol works in complete analogy to the qubit case. To illustrate the concept, we neglect the photon losses in the optical fiber and assume a noiseless quantum channel.

The repeater protocol works as follows: First, the matter system is initiated in the state $\frac{1}{\sqrt{3}}(|0\rangle + |1\rangle + |2\rangle)$ and interacts with a light mode in a coherent state $|\alpha\rangle$ via the qutrit dispersive interaction with $\theta = \frac{2\pi}{3}$. This results in the entangled matter-qubus state

$$\frac{1}{\sqrt{3}}\left(|0\rangle|\alpha\rangle + |1\rangle|\alpha e^{\frac{2\pi i}{3}}\rangle + |2\rangle|\alpha e^{-\frac{2\pi i}{3}}\rangle\right). \tag{7.4}$$

The light mode is then sent to a second matter system, separated from the first one by a distance L_0 and also prepared in the state $\frac{1}{\sqrt{3}}(|0\rangle + |1\rangle + |2\rangle)$. The incoming light mode interacts dispersively with the second matter system, but this time with the reverse angle $\theta = -\frac{2\pi}{3}$. The resulting pure state is

$$
\frac{1}{\sqrt{3}} \left(\frac{1}{\sqrt{3}} (|00\rangle + |11\rangle + |22\rangle)|\alpha\rangle \right.
$$
$$
+ \frac{1}{\sqrt{3}} (|01\rangle + |12\rangle + |20\rangle)|\alpha e^{-\frac{2\pi i}{3}}\rangle \tag{7.5}
$$
$$
\left. + \frac{1}{\sqrt{3}} (|02\rangle + |10\rangle + |21\rangle)|\alpha e^{\frac{2\pi i}{3}}\rangle \right).
$$

To keep the notation short and also for later purposes, it it useful to define the set of maximally entangled qutrit Bell states,

$$
|\phi_{kj}\rangle = \frac{1}{\sqrt{3}} \sum_{m=0}^{2} \exp\left(\frac{2\pi i k m}{3} \right) |m, m \ominus j\rangle, \tag{7.6}
$$

where "$\ominus$" denotes subtraction modulo 2. Eq. (7.5) can therefore be rewritten as

$$
\frac{1}{\sqrt{3}} \left(|\phi_{00}\rangle|\alpha\rangle + |\phi_{02}\rangle|\alpha e^{-\frac{2\pi i}{3}}\rangle + |\phi_{01}\rangle|\alpha e^{\frac{2\pi i}{3}}\rangle \right). \tag{7.7}
$$

To generate a maximally entangled state between the matter systems, a homodyne measurement is performed on the light mode to distinguish the three coherent states of the mode. Unlike the qubit case, here a measurement of $\hat{p}$ is useful, because it allows one to (almost) discriminate all three coherent states (as opposed to the case of an $\hat{x}$-measurement). Moreover, for an ideal loss-free channel, increasing the amplitude α leads to near-orthogonality of the coherent states such that a maximally entangled qutrit-qutrit state can be distributed over the distance L_0. This state is referred to as the elementary repeater link. To further distribute entanglement, two elementary links next to each other are connected by entanglement swapping, via a Bell measurement on adjacent repeater nodes. By one such successful entanglement swapping, qutrit-qutrit entanglement can thus be established over the distance $2L_0$, and so forth.

We will address all the steps of the repeater protocol in detail in the next sections and also explain which subtleties and necessary generalizations occur compared to the loss-free case discussed here.

Matter-light qutrit-qubus hybrid entanglement At the beginning of the qutrit HQR protocol, the matter system is prepared in the state $\frac{1}{\sqrt{3}}(|0\rangle + |1\rangle + |2\rangle)$. The dispersive interaction with a coherent state leads to the state in Eq. (7.4).

In the realistic case, the light mode is sent through an optical loss channel which is again simulated by an interaction of the mode with an ancilla vacuum state (see Section 4.1.2). The

application of the beam splitter leads to

$$\frac{1}{\sqrt{3}}(|0\rangle|\sqrt{\gamma}\alpha\rangle|\sqrt{1-\gamma}\alpha\rangle + |1\rangle|\sqrt{\gamma}\alpha e^{\frac{2\pi i}{3}}\rangle|\sqrt{1-\gamma}\alpha e^{\frac{2\pi i}{3}}\rangle + |2\rangle|\sqrt{\gamma}\alpha e^{-\frac{2\pi i}{3}}\rangle|\sqrt{1-\gamma}\alpha e^{-\frac{2\pi i}{3}}\rangle).$$
(7.8)

To trace out the loss mode, it is again useful to switch to an orthogonal basis. While in the qubit case that basis is given by a kind of qubit Hadamard transform, the qutrit basis is given by a qutrit Hadamard gate to yield

$$|u\rangle = \frac{1}{\sqrt{N_u(\alpha)}}(|\alpha\rangle + |\alpha e^{\frac{2\pi i}{3}}\rangle + |\alpha e^{-\frac{2\pi i}{3}}\rangle),$$

$$|v\rangle = \frac{1}{\sqrt{N_v(\alpha)}}(|\alpha\rangle + e^{\frac{2\pi i}{3}}|\alpha e^{\frac{2\pi i}{3}}\rangle + e^{-\frac{2\pi i}{3}}|\alpha e^{-\frac{2\pi i}{3}}\rangle),$$
(7.9)

$$|w\rangle = \frac{1}{\sqrt{N_w(\alpha)}}(|\alpha\rangle + e^{-\frac{2\pi i}{3}}|\alpha e^{\frac{2\pi i}{3}}\rangle + e^{\frac{2\pi i}{3}}|\alpha e^{-\frac{2\pi i}{3}}\rangle),$$

with normalization constants

$$N_u(\alpha) = 3 + 6e^{-\frac{3}{2}\alpha^2}\cos\left(\sqrt{\frac{3}{4}}\alpha^2\right),$$

$$N_v(\alpha) = 3 - e^{-\frac{3}{2}\alpha^2}\left(3\cos\left(\sqrt{\frac{3}{4}}\alpha^2\right) + \sqrt{3}\sin\left(\sqrt{\frac{3}{4}}\alpha^2\right)\right),$$
(7.10)

$$N_w(\alpha) = 3 - e^{-\frac{3}{2}\alpha^2}\left(3\cos\left(\sqrt{\frac{3}{4}}\alpha^2\right) - \sqrt{3}\sin\left(\sqrt{\frac{3}{4}}\alpha^2\right)\right).$$

The coherent states above can thus be written as

$$|\alpha\rangle = \frac{1}{3}(\sqrt{N_u(\alpha)}|u\rangle + \sqrt{N_v(\alpha)}|v\rangle + \sqrt{N_w(\alpha)}|w\rangle),$$

$$|\alpha e^{\frac{2\pi i}{3}}\rangle = \frac{1}{3}(\sqrt{N_u(\alpha)}|u\rangle + e^{-\frac{2\pi i}{3}}\sqrt{N_v(\alpha)}|v\rangle + e^{\frac{2\pi i}{3}}\sqrt{N_w(\alpha)}|w\rangle),$$
(7.11)

$$|\alpha e^{-\frac{2\pi i}{3}}\rangle = \frac{1}{3}(\sqrt{N_u(\alpha)}|u\rangle + e^{\frac{2\pi i}{3}}\sqrt{N_v(\alpha)}|v\rangle + e^{-\frac{2\pi i}{3}}\sqrt{N_w(\alpha)}|w\rangle).$$

Substituting this into Eq. (7.8) for the loss mode and tracing out the loss mode gives the three-component mixed state

$$\rho_{out} = \frac{N_u(\sqrt{1-\gamma}\alpha)}{9}\frac{1}{\sqrt{3}}(|0\rangle|\sqrt{\gamma}\alpha\rangle + |1\rangle|\sqrt{\gamma}\alpha e^{\frac{2\pi i}{3}}\rangle + |2\rangle|\sqrt{\gamma}\alpha e^{-\frac{2\pi i}{3}}\rangle) \times H.c.$$

$$+ \frac{N_v(\sqrt{1-\gamma}\alpha)}{9}\frac{1}{\sqrt{3}}(|0\rangle|\sqrt{\gamma}\alpha\rangle + e^{-\frac{2\pi i}{3}}|1\rangle|\sqrt{\gamma}\alpha e^{\frac{2\pi i}{3}}\rangle + e^{\frac{2\pi i}{3}}|2\rangle|\sqrt{\gamma}\alpha e^{\frac{-2\pi i}{3}}\rangle) \times H.c.$$ (7.12)

$$+ \frac{N_w(\sqrt{1-\gamma}\alpha)}{9}\frac{1}{\sqrt{3}}(|0\rangle|\sqrt{\gamma}\alpha\rangle + e^{\frac{2\pi i}{3}}|1\rangle|\sqrt{\gamma}\alpha e^{\frac{2\pi i}{3}}\rangle + e^{-\frac{2\pi i}{3}}|2\rangle|\sqrt{\gamma}\alpha e^{-\frac{2\pi i}{3}}\rangle) \times H.c.$$

This represents an entangled state between the matter system and the qubus. Similar to the qubit case, the resulting density matrix still effectively represents a state of two qutrits (one optical and one material), since the three coherent states $\{|\sqrt{\gamma}\alpha\rangle, |\sqrt{\gamma}\alpha e^{\pm\frac{2\pi i}{3}}\rangle\}$ effectively span a three-dimensional Hilbert space.

For studying the entanglement properties, it is helpful to express the light mode in the $\{|u\rangle, |v\rangle, |w\rangle\}$-basis and the matter system in the qutrit (generalized Pauli) X-basis,

$$
\begin{aligned}
|\widetilde{0}\rangle &= \frac{1}{\sqrt{3}}(|0\rangle + |1\rangle + |2\rangle), \\
|\widetilde{1}\rangle &= \frac{1}{\sqrt{3}}(|0\rangle + e^{\frac{2\pi i}{3}}|1\rangle + e^{-\frac{2\pi i}{3}}|2\rangle), \\
|\widetilde{2}\rangle &= \frac{1}{\sqrt{3}}(|0\rangle + e^{-\frac{2\pi i}{3}}|1\rangle + e^{\frac{2\pi i}{3}}|2\rangle).
\end{aligned} \tag{7.13}
$$

Eq. (7.12) can thus be rewritten as

$$
\begin{aligned}
\rho_{out} = {}& \frac{N_u(\sqrt{1-\gamma}\alpha)}{9} \cdot \left[\frac{1}{3}\left(\sqrt{N_u(\sqrt{\gamma}\alpha)}|\widetilde{0}\rangle|\widetilde{u}\rangle + \sqrt{N_v(\sqrt{\gamma}\alpha)}|\widetilde{1}\rangle|\widetilde{v}\rangle + \sqrt{N_w(\sqrt{\gamma}\alpha)}|\widetilde{2}\rangle|\widetilde{w}\rangle\right)\right] \times H.c. \\
&+ \frac{N_v(\sqrt{1-\gamma}\alpha)}{9} \cdot \left[\frac{1}{3}\left(\sqrt{N_u(\sqrt{\gamma}\alpha)}|\widetilde{2}\rangle|\widetilde{u}\rangle + \sqrt{N_v(\sqrt{\gamma}\alpha)}|\widetilde{1}\rangle|\widetilde{v}\rangle + \sqrt{N_w(\sqrt{\gamma}\alpha)}|\widetilde{0}\rangle|\widetilde{w}\rangle\right)\right] \times H.c. \\
&+ \frac{N_w(\sqrt{1-\gamma}\alpha)}{9} \cdot \left[\frac{1}{3}\left(\sqrt{N_u(\sqrt{\gamma}\alpha}|\widetilde{1}\rangle|\widetilde{u}\rangle + \sqrt{N_v(\sqrt{\gamma}\alpha)}|\widetilde{0}\rangle|\widetilde{v}\rangle + \sqrt{N_w(\sqrt{\gamma}\alpha)}|\widetilde{2}\rangle|\widetilde{w}\rangle\right)\right] \times H.c. ,
\end{aligned}
$$

where $|\widetilde{u}\rangle, |\widetilde{v}\rangle$ and $|\widetilde{w}\rangle$ denote the basis vectors in Eq. (7.9) with amplitudes $\sqrt{\gamma}\alpha$.

To quantify the qutrit-qutrit entanglement of this state, we choose the so-called entanglement negativity [33] as our figure of merit. The negativity $\mathcal{N}$ of a bipartite quantum state of a system AB is defined as

$$
\mathcal{N}(\rho) = \frac{||\rho^{T_A}|| - 1}{2} \tag{7.14}
$$

where ρ^{T_A} is the partial transposition of the bipartite state with respect to system A and $||\circ||$ denotes the trace norm.

A plot of the negativities for different α and various distances is shown in Fig. 7.1. The orange line indicates the entanglement negativity of a pure maximally entangled qubit Bell state. Up to a distance L_0 of approximately 10 km, it is possible to generate matter-qubus entanglement stronger than any, even ideal qubit-qubit entanglement. Taking into account that the distribution of qubit-qubit entanglement is also subject to loss, the difference in entanglement negativity will be even more significant. However, a crucial step still is to transfer this entanglement to a sufficient extent from the matter-light system to a matter-matter system for storage.
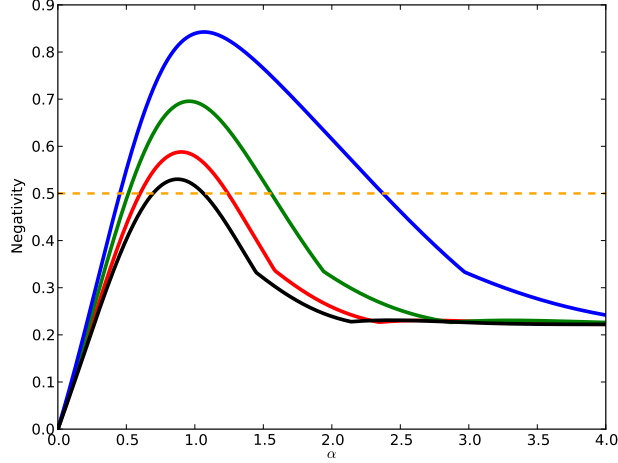
Figure 7.1: Negativity of the effective qutrit-qutrit state in dependence of α for various distances: 10 km (black), 8 km (red), 5 km (green) and 2 km (blue) (from bottom to top). The dashed, orange line indicates the negativity of a maximally entangled pure two-qubit Bell state.

Matter-matter qutrit-qutrit entanglement To establish entanglement between two matter qutrits, the light mode of the state in Eq. (7.12) interacts with a second matter system, initialized in the state $\frac{1}{\sqrt{3}}(|0\rangle + |1\rangle + |2\rangle)$. This time, similar to the qubit case, the controlled phase rotation takes place with the opposite angle, $\theta = -\frac{2\pi}{3}$. One obtains

$$\rho_{out} = \frac{N_u(\sqrt{1-\gamma}\alpha)}{9}|C_0\rangle\langle C_0| + \frac{N_v(\sqrt{1-\gamma}\alpha)}{9}|C_1\rangle\langle C_1| + \frac{N_w(\sqrt{1-\gamma}\alpha)}{9}|C_2\rangle\langle C_2|, \qquad (7.15)$$

where the individual components are given by

$$|C_0\rangle = \frac{1}{\sqrt{3}}(|\phi_{00}\rangle|\sqrt{\gamma}\alpha\rangle + |\phi_{02}\rangle|\sqrt{\gamma}\alpha e^{-\frac{2\pi i}{3}}\rangle + |\phi_{01}\rangle|\sqrt{\gamma}\alpha e^{\frac{2\pi i}{3}}\rangle), \qquad (7.16)$$

$$|C_1\rangle = \frac{1}{\sqrt{3}}(|\phi_{20}\rangle|\sqrt{\gamma}\alpha\rangle + |\phi_{22}\rangle|\sqrt{\gamma}\alpha e^{-\frac{2\pi i}{3}}\rangle + |\phi_{21}\rangle|\sqrt{\gamma}\alpha e^{\frac{2\pi i}{3}}\rangle), \qquad (7.17)$$

and

$$|C_2\rangle = \frac{1}{\sqrt{3}}(|\phi_{10}\rangle|\sqrt{\gamma}\alpha\rangle + |\phi_{12}\rangle|\sqrt{\gamma}\alpha e^{-\frac{2\pi i}{3}}\rangle + |\phi_{11}\rangle|\sqrt{\gamma}\alpha e^{\frac{2\pi i}{3}}\rangle), \qquad (7.18)$$

with the Bell states from Eq. (7.6). In order to establish entanglement between the two matter systems, the coherent states $|\sqrt{\gamma}\alpha\rangle, |\sqrt{\gamma}\alpha e^{-\frac{2\pi i}{3}}\rangle$, and $|\sqrt{\gamma}\alpha e^{\frac{2\pi i}{3}}\rangle$ have to be distinguished (see Fig. 7.2). Like in the loss-free case, this can be done using a homodyne measurement on the light mode. Unlike the qubit case, an $\hat{x}$-measurement is not suitable here, because $|\sqrt{\gamma}\alpha e^{\frac{2\pi i}{3}}\rangle$ and $|\sqrt{\gamma}\alpha e^{-\frac{2\pi i}{3}}\rangle$ cannot be distinguished. Therefore, we choose the quadrature $\hat{p}$ whose Gaussian momentum distribution for coherent states with complex amplitude β reads
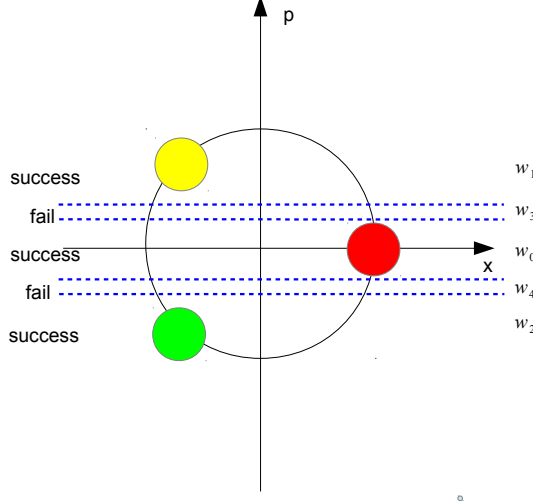
Figure 7.2: Phase space representation of the three coherent states $|\alpha\rangle$ and $|\alpha e^{\pm \frac{2\pi i}{3}}\rangle$ to be distinguished by USD.

$$|\psi_\beta(p)|^2 = \sqrt{\frac{2}{\pi}} \exp\left(-2(p - \text{Im}(\beta))^2\right). \tag{7.19}$$

This time, it is useful to define at least three windows to which a measurement result is assigned when the light mode of the output state in Eq. (7.15) is measured. The first window is a symmetric interval around $p = 0$, $w_0 = [-\Delta, \Delta]$. A measurement result in this interval, similar to the qubit case, corresponds to an approximate projection on $|\alpha\rangle$. A projection onto the states $|\sqrt{\gamma}\alpha e^{\pm \frac{2\pi i}{3}}\rangle$ is assumed if a value falls into $w_1 = [\frac{\sqrt{3}}{2}\sqrt{\gamma}\alpha - \Delta, \infty]$ or $w_2 = [-\infty, -\frac{\sqrt{3}}{2}\sqrt{\gamma}\alpha + \Delta]$, respectively. Note that we need $\Delta \leq \frac{1}{2}\sqrt{\frac{3}{4}}\sqrt{\gamma}\alpha =: \Delta_0$ to exclude overlapping windows. We may decide to add two extra windows w_3 and w_4 to include the possibility of discarding measurement results (see Fig. 7.2). Inclusion of such failure events renders our qutrit entanglement distribution probabilistic.

Using the momentum wave functions for the coherent states, the qutrit-qutrit-qumode $|C_0\rangle$-component of ρ_{out} after measuring the value p in the homodyne detection of the qubus has the following conditional state for the two matter qutrits,

$$\text{Tr}_{qubus}(|p\rangle\langle p|C_0\rangle\langle C_0|p\rangle\langle p|) = \frac{1}{3}\Big(|\phi_{00}\rangle\langle\phi_{00}| \cdot |\psi_{\sqrt{\gamma}\alpha}(p)|^2 + |\phi_{02}\rangle\langle\phi_{02}| \cdot |\psi_{\sqrt{\gamma}\alpha e^{-\frac{2\pi i}{3}}}(p)|^2$$

$$+|\phi_{01}\rangle\langle\phi_{01}| \cdot |\psi_{\sqrt{\gamma}\alpha e^{\frac{2\pi i}{3}}}(p)|^2 + |\phi_{00}\rangle\langle\phi_{02}| \cdot \psi_{\sqrt{\gamma}\alpha}(p)\psi^*_{\sqrt{\gamma}\alpha e^{-\frac{2\pi i}{3}}}(p) + |\phi_{00}\rangle\langle\phi_{01}| \cdot \psi_{\sqrt{\gamma}\alpha}(p)\psi^*_{\sqrt{\gamma}\alpha e^{\frac{2\pi i}{3}}}(p)$$

$$+ |\phi_{02}\rangle\langle\phi_{00}| \cdot \psi_{\sqrt{\gamma}\alpha e^{-\frac{2\pi i}{3}}}(p)\psi^*_{\sqrt{\gamma}\alpha}(p) + |\phi_{02}\rangle\langle\phi_{01}| \cdot \psi_{\sqrt{\gamma}\alpha e^{-\frac{2\pi i}{3}}}(p)\psi^*_{\sqrt{\gamma}\alpha e^{\frac{2\pi i}{3}}}(p)$$

$$+ |\phi_{01}\rangle\langle\phi_{00}| \cdot \psi_{\sqrt{\gamma}\alpha e^{\frac{2\pi i}{3}}}(p)\psi^*_{\sqrt{\gamma}\alpha}(p) + |\phi_{00}\rangle\langle\phi_{02}| \cdot \psi_{\sqrt{\gamma}\alpha e^{\frac{2\pi i}{3}}}(p)\psi^*_{\sqrt{\gamma}\alpha e^{-\frac{2\pi i}{3}}}(p)\Big). \tag{7.20}$$
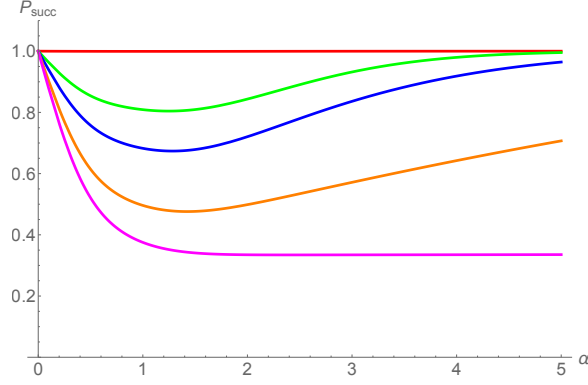
64

Figure 7.3: Success probability for the homodyne-based distribution of qutrit-qutrit entanglement over a distance of 5 km for various Δ: $\Delta = \Delta_0$ (red), $\Delta = 0.7\Delta_0$ (green), $\Delta = 0.5\Delta_0$ (blue), $\Delta = 0.2\Delta_0$ (orange) and $\Delta = 0.001\Delta_0$ (magenta) (from top to bottom).

If we only accept the selection window $w_0 = [-\Delta, \Delta]$, the resulting unnormalized state is obtained by doing the p-integration,

$$\sigma_{w_0}^{C_0} = \int\limits_{-\Delta}^{\Delta} dp \ \sigma_p^{C_0}. \tag{7.21}$$

For carefully chosen Δ, α and distance L_0, the contribution of the off-diagonal terms in Eq. (7.20) can be neglected such that we obtain the effective unnormalized state

$$\widetilde{\rho}_{w_0}^{C_0} = \frac{1}{3} \left(|\phi_{00}\rangle\langle\phi_{00}| \cdot \int\limits_{-\Delta}^{\Delta} dp \ |\psi_{\sqrt{\gamma}\alpha}(p)|^2 + |\phi_{02}\rangle\langle\phi_{02}| \cdot \int\limits_{-\Delta}^{\Delta} dp \ |\psi_{\sqrt{\gamma}\alpha e^{-\frac{2\pi i}{3}}}(p)|^2 \right.$$
$$\left. + |\phi_{01}\rangle\langle\phi_{01}| \cdot \int\limits_{-\Delta}^{\Delta} dp \ |\psi_{\sqrt{\gamma}\alpha e^{\frac{2\pi i}{3}}}(p)|^2 \right). \tag{7.22}$$

The same calculation as above for $|C_0\rangle$ can be made for the other two components in ρ_{out} of Eq. (7.15), $|C_1\rangle$ and $|C_2\rangle$. The total conditional (unnormalized) density matrix then becomes

$$\widetilde{\rho}_{w_0} = \frac{N_u(\sqrt{1-\gamma}\alpha)}{9} \widetilde{\rho}_{w_0}^{C_0} + \frac{N_v(\sqrt{1-\gamma}\alpha)}{9} \widetilde{\rho}_{w_0}^{C_1} + \frac{N_w(\sqrt{1-\gamma}\alpha)}{9} \widetilde{\rho}_{w_0}^{C_2}, \tag{7.23}$$

whose norm is the success probability

$$p_{w_0} = \text{Tr}[\widetilde{\rho}_{w_0}] = \frac{1}{3} \left(\int\limits_{-\Delta}^{\Delta} dp \ \left(|\psi_{\sqrt{\gamma}\alpha}(p)|^2 + |\psi_{\sqrt{\gamma}\alpha e^{-\frac{2\pi i}{3}}}(p)|^2 + |\psi_{\sqrt{\gamma}\alpha e^{\frac{2\pi i}{3}}}(p)|^2 \right) \right), \tag{7.24}$$

where we used $\text{Tr}[\rho_{out}] = 1$ and $\text{Tr}[\widetilde{\rho}_{w_0}^{C_0}] = \text{Tr}[\widetilde{\rho}_{w_0}^{C_1}] = \text{Tr}[\widetilde{\rho}_{w_0}^{C_2}]$. The corresponding fidelity for the

target state is then calculated as

$$
\begin{aligned}
F_{w_0} &= \frac{\langle \phi_{00} | \widetilde{\rho}_{w_0} | \phi_{00} \rangle}{p_{w_0}} \\[2mm]
&= \frac{N_u(\sqrt{1-\gamma}\alpha)}{9} \; \frac{\frac{1}{3} \int\limits_{-\Delta}^{\Delta} dp \; |\psi_{\sqrt{\gamma}\alpha}(p)|^2}{p_{w_0}}.
\end{aligned}
\tag{7.25}
$$

The success probabilities for the other two selection windows are obtained in complete analogy,

$$
\begin{aligned}
p_{w_1} &= \frac{1}{3} \left(\int\limits_{\frac{\sqrt{3}}{2}\sqrt{\gamma}\alpha - \Delta}^{\infty} dp \; \left(|\psi_{\sqrt{\gamma}\alpha}(p)|^2 + |\psi_{\sqrt{\gamma}\alpha e^{-\frac{2\pi i}{3}}}(p)|^2 + |\psi_{\sqrt{\gamma}\alpha e^{\frac{2\pi i}{3}}}(p)|^2 \right) \right), \\[2mm]
p_{w_2} &= \frac{1}{3} \left(\int\limits_{-\infty}^{-\frac{\sqrt{3}}{2}\sqrt{\gamma}\alpha + \Delta} dp \; \left(|\psi_{\sqrt{\gamma}\alpha}(p)|^2 + |\psi_{\sqrt{\gamma}\alpha e^{-\frac{2\pi i}{3}}}(p)|^2 + |\psi_{\sqrt{\gamma}\alpha e^{\frac{2\pi i}{3}}}(p)|^2 \right) \right).
\end{aligned}
\tag{7.26}
$$

The corresponding fidelities with respect to $|\phi_{02}\rangle$ and $|\phi_{01}\rangle$ are, respectively,

$$
F_{w_1} = \frac{N_v(\sqrt{1-\gamma}\alpha)}{9} \; \frac{\frac{1}{3} \int\limits_{\frac{\sqrt{3}}{2}\sqrt{\gamma}\alpha - \Delta}^{\infty} |\psi_{\sqrt{\gamma}\alpha}(p)|^2}{p_{w_1}},
\tag{7.27}
$$

and

$$
F_{w_2} = \frac{N_w(\sqrt{1-\gamma}\alpha)}{9} \; \frac{\frac{1}{3} \int\limits_{-\infty}^{-\frac{\sqrt{3}}{2}\sqrt{\gamma}\alpha + \Delta} |\psi_{\sqrt{\gamma}\alpha}(p)|^2}{p_{w_2}}.
\tag{7.28}
$$

To estimate the performance of this entanglement generation scheme, we define the average fidelity as

$$
F_{av} = \frac{\sum\limits_{i=0}^{2} p_{w_i} F_{w_i}}{P_{succ}},
\tag{7.29}
$$

where $P_{succ} = \sum\limits_{i=0}^{2} p_{w_i}$ is the total success probability. The α-dependence of the success proba-
bility and the average fidelity for various values of Δ is shown in Figs. 7.3 and 7.4 for $L_0=5$km.
Clearly, if $\Delta = \Delta_0$, then there is no failure window at all and all measurement results are
accepted. This results in unit success probability, $P_{succ} = 1$. On the other hand, for smaller
(but not too small) Δ, i.e. $\Delta < \Delta_0$, the success probability still tends to unity for increasing α,
as long as the three coherent states remain well within their respective selection windows. The
fidelity, however, shows an opposite behavior. The smaller Δ is chosen, the higher the final

Figure 7.4: Average fidelity for the homodyne-based distribution of qutrit-qutrit entanglement over a distance of 5 km for various Δ: $\Delta = \Delta_0$ (red), $\Delta = 0.7\Delta_0$ (green), $\Delta = 0.5\Delta_0$ (blue), $\Delta = 0.2\Delta_0$ (orange) and $\Delta = 0.001\Delta_0$ (magenta) (from bottom to top).
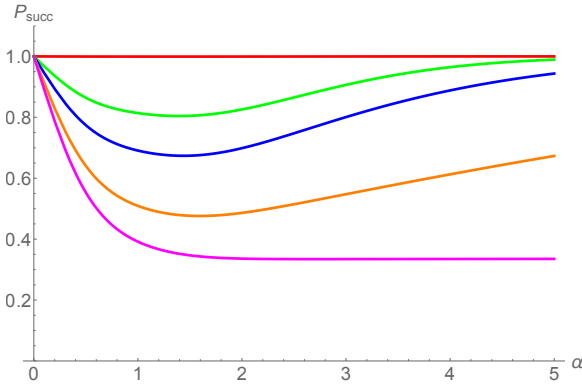
Figure 7.5: Success probability for the homodyne-based distribution of qutrit-qutrit entanglement over a distance of 10 km for various Δ: $\Delta = \Delta_0$ (red), $\Delta = 0.7\Delta_0$ (green), $\Delta = 0.5\Delta_0$ (blue), $\Delta = 0.2\Delta_0$ (orange) and $\Delta = 0.001\Delta_0$ (magenta) (from top to bottom).

average fidelity for moderate values of α. Increasing α makes the fidelity finally drop to $1/3$, which is a direct consequence of the loss channel whose mixed output becomes more and more balanced for larger α. For each chosen value of Δ, there is an optimal value for α leading to a maximal fidelity. For instance, choosing $\Delta = 0.2\Delta_0$ and $\alpha \approx 1$ leads to an average fidelity of $F_{av} \approx 0.7$ at a very reasonable success probability of $P_{succ} \approx 0.4$. The corresponding plots for elementary distances of $L_0 = 10$ km are shown in Figs. 7.5 and 7.6.

A possible ququart scheme for distributing ququart-ququart entanglement is explicitly discussed in App. C.2.

Unambiguous state discrimination In this section, we will consider an alternative measurement scheme for a qutrit hybrid repeater based upon so-called unambiguous state discrimination (USD). Compared to the homodyne-based scheme, the conceptual difference in the USD-based scheme is that the non-orthogonality of the coherent states only affects P_{succ} and
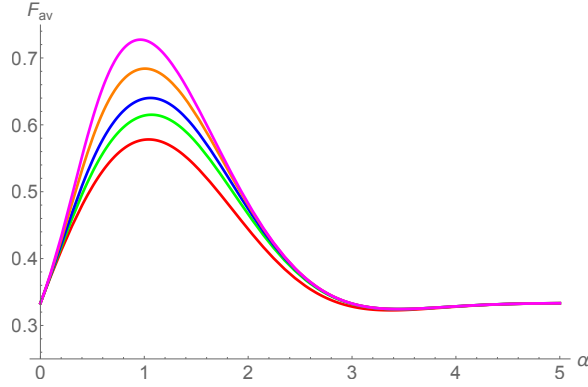
Figure 7.6: Average fidelity for the homodyne-based distribution of qutrit-qutrit entanglement over a distance of 10 km for various Δ: $\Delta = \Delta_0$ (red), $\Delta = 0.7\Delta_0$ (green), $\Delta = 0.5\Delta_0$ (blue), $\Delta = 0.2\Delta_0$ (orange) and $\Delta = 0.001\Delta_0$ (magenta) (from bottom to top).
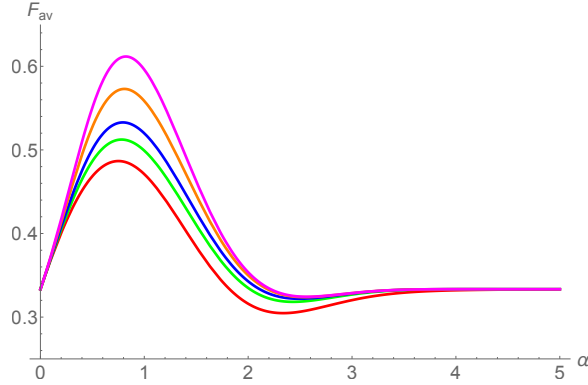
no longer F_{av}, as USD enables one to discriminate non-orthogonal states probabilistically in an error-free fashion. The idea is that a successful and error-free projection onto one of the states $|\sqrt{\gamma}\alpha\rangle$ or $|\sqrt{\gamma}\alpha e^{\pm\frac{2\pi i}{3}}\rangle$ would lead to maximally entangled states in all components in Eq.(7.15). The task is therefore to find the most efficient possible scheme in the framework of quantum theory for unambiguously discriminating between the three coherent states above.

This problem was treated by Chefles [132] who derived the optimal success probability as

$$P_D \leq \min_r \sum_{j=0}^{2} e^{-\frac{2\pi ijr}{3}} e^{\gamma\alpha^2(e^{\frac{2\pi ij}{3}}-1)}, \tag{7.30}$$

with $r = 0, 1, 2$ (see also Refs. [133, 134]). The relation between this optimal probability and the corresponding fidelity of the final maximally entangled state is shown in Fig. 7.7.

Entanglement purification   After the homodyne detection, the conditional state state resulting from Eq. (7.15) still represents a mixed state. Depending on the channel distance, the selection window and the amplitude α, the resulting state in the first component is a mixture of the dominant target state $|\phi_{00}\rangle$ with small extra components of $|\phi_{02}\rangle$ and $|\phi_{01}\rangle$ (if the result belongs to window w_0). This is similar for the other two components of the mixture with their rotated Bell states. Thus, effectively, the state after homodyne detection reads (up to local qutrit rotations in case of the other two windows)

$$\rho_{eff} = \frac{N_u(\sqrt{1-\gamma}\alpha)}{9}|\widetilde{C}_0\rangle\langle\widetilde{C}_0| + \frac{N_v(\sqrt{1-\gamma}\alpha)}{9}|\widetilde{C}_1\rangle\langle\widetilde{C}_1| + \frac{N_w(\sqrt{1-\gamma}\alpha)}{9}|\widetilde{C}_2\rangle\langle\widetilde{C}_2|, \tag{7.31}$$

where
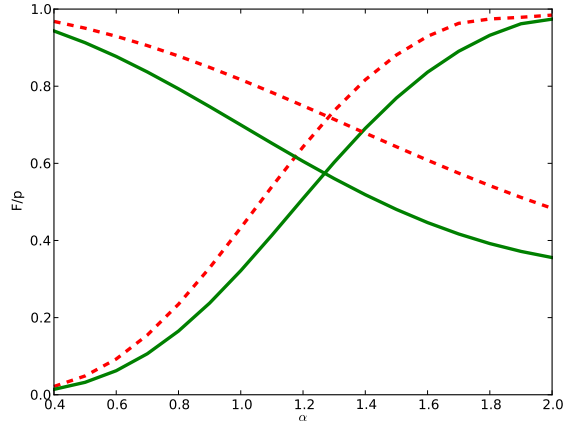
Figure 7.7: Success probability and fidelity for the USD-based scheme for 5 km (red, dotted) and 10 km (green, solid) in dependence of α.

$$|\widetilde{C_0}\rangle = \frac{1}{\sqrt{3}}(|00\rangle + |11\rangle + |22\rangle),$$

$$|\widetilde{C_1}\rangle = \frac{1}{\sqrt{3}}(|00\rangle + e^{-\frac{2\pi i}{3}}|11\rangle + e^{\frac{2\pi i}{3}}|22\rangle), \qquad (7.32)$$

$$|\widetilde{C_2}\rangle = \frac{1}{\sqrt{3}}(|00\rangle + e^{+\frac{2\pi i}{3}}|11\rangle + e^{-\frac{2\pi i}{3}}|22\rangle).$$

Note that in the case of USD, Eqs. (7.31) and (7.32) are exact and there are no extra terms from the rotated Bell states (which nonetheless can be neglected for the case of homodyne detection provided the selection window-based state discrimination works sufficiently well). In general, mixed entangled states degrade the performance of quantum information processing tasks like teleportation or the entanglement swapping operation discussed in the next section. Hence, a purification of the above mixed state is required (see Section 2.2).

To perform a purification of our relevant state, i.e. to increase the statistical weight of $|\widetilde{C_0}\rangle$ in Eq. (7.31), at least two copies of the matter-matter output state are required.

On each matter system of each copy, the following transformations are performed: The first matter system is subject to the transformation

$$|0\rangle \mapsto \frac{1}{\sqrt{3}}(|0\rangle + |1\rangle + |2\rangle),$$

$$|1\rangle \mapsto \frac{1}{\sqrt{3}}(|0\rangle + e^{i\phi}|1\rangle + e^{-i\phi}|2\rangle), \qquad (7.33)$$

$$|2\rangle \mapsto \frac{1}{\sqrt{3}}(|0\rangle + e^{-i\phi}|1\rangle + e^{i\phi}|2\rangle),$$

while on the second system

$$|0\rangle \mapsto \frac{1}{\sqrt{3}}(|0\rangle + |1\rangle + |2\rangle),$$

$$|1\rangle \mapsto \frac{1}{\sqrt{3}}(|0\rangle + e^{-i\phi}|1\rangle + e^{i\phi}|2\rangle), \qquad (7.34)$$

$$|2\rangle \mapsto \frac{1}{\sqrt{3}}(|0\rangle + e^{i\phi}|1\rangle + e^{-i\phi}|2\rangle),$$

is performed. The components of the mixture are then transformed as

$$|\widetilde{C}_0\rangle \mapsto \frac{1}{\sqrt{3}}(|00\rangle + |11\rangle + |22\rangle),$$

$$|\widetilde{C}_1\rangle \mapsto \frac{1}{\sqrt{3}}(|01\rangle + |20\rangle + |12\rangle), \qquad (7.35)$$

$$|\widetilde{C}_2\rangle \mapsto \frac{1}{\sqrt{3}}(|10\rangle + |02\rangle + |21\rangle).$$

A mixture of $|\widetilde{C}_0\rangle$, $|\widetilde{C}_1\rangle$, and $|\widetilde{C}_2\rangle$ with statistical weights p_0,p_1, and p_2, $p_0 + p_1 + p_2 = 1$, can now be purified as follows. One needs two copies of the state that is shared between two parties A and B. As proven in Section 6.3 for arbitrary dimensions, a local subtraction gate is applied on the qutrits belonging to A and B, respectively. After this, A and B choose one of the two copies and measure the spin. Equal spin results lead to the new mixed state

$$\rho' = \frac{\sum_{j=0}^{2} p_j^2 |\widetilde{C}_j\rangle\langle\widetilde{C}_j|}{\sum_{j=0}^{2} p_j^2}, \qquad (7.36)$$

whose fidelity with respect to the target state $|C_0\rangle$ is now increased, provided $p_0 > 1/3$ and $p_1, p_2 < p_0$.

Entanglement swapping In the previous sections, we have shown how to entangle two qutrits over a distance L_0. The distance L_0, however, is in general too short for applications in quantum communication. It is therefore necessary to further distribute entanglement over larger distances. This can be done by entanglement swapping.

To perform entanglement swapping, two entangled qutrit-qutrit pairs are generated next to each other, covering a total distance of $2L_0$. To connect the two pairs and thus establish entanglement over two times the initial distance, a Bell measurement is carried out on the two adjacent matter systems. A successful Bell measurement projects the remaining two matter systems onto a maximally entangled state.

In analogy to the qubit case, a Bell measurement on two qutrits can be performed by applying a qudit sum gate (CNOT) and measurements in the X- and in the Z-basis (see Eq. (7.2)). As

pointed out in [135], Hadamard transformations and a CPHASE gate suffice to implement the sum gate.

In the following, we assume that arbitrary single qutrit rotations and measurements can be performed on the matter systems and show how to construct the sum gate from these assumptions.

In our framework, a CPHASE gate is represented by the unitary

$$U_{CS} = \exp\left(-\frac{2\pi i}{3}\hat{S}_{z_1}^{(3)}\hat{S}_{z_2}^{(3)}\right),\tag{7.37}$$

where the operators $\hat{S}_{z_i}^{(3)}$ represent the operations introduced in Eq. (7.2) on the ith qutrit. Like in the qubit case, a decomposition for the CSHIFT gate reads

$$\text{CSHIFT} = (H \otimes 1)\,\text{CPHASE}(H \otimes 1),\tag{7.38}$$

where H is the qutrit Hadamard transformation. Indeed, one observes by direct calculation $(H \otimes 1)\,\text{CSIGN}(H \otimes 1)|x, y\rangle = |x \ominus y, y\rangle$ for $x, y \in \mathbb{Z}_2$. Note that $\ominus$ denotes subtraction modulo 3. A more formal proof of this decomposition for arbitrary dimensions is given in Section 6.3. With hybrid quantum repeater protocols for qubits and qutrits in mind, an extension to ququarts, i.e. 4-level systems, is straightforward. As a bridge to the general qudit case, as presented in the next section, it is nonetheless useful to explicitly consider the ququart case including the optical qubus measurements adapted to this case. This is presented in App. C.1.

Rate analysis

Methods and assumptions   In this section, we quantify the performance of our hybrid qutrit HQR protocol for the generation of entanglement over the total distance. The performance can be cast by the entanglement generation rate, i.e. the number of entangled pairs over the entire distance per unit time. Besides this, the fidelity of the generated state is of particular interest. We assume matter systems with infinite coherence time, i.e. perfect memories, as well as deterministic and error-free gates on them. Especially, the entanglement swapping operation is treated as deterministic. Strictly speaking, photon loss is the only error source entering our rate analysis and the resulting rates have to be understood as upper bounds of the actual rates. For this scenario, analytical formulae for the rates in dependence of the number of elementary links as well as the number of purifications performed on each link have been derived in [136]. Note that we include one to several rounds of entanglement purification only right after the initial entangled-state distributions.

We consider 2^n links of elementary distance L_0, covering a total distance $L = 2^n L_0$. Entanglement is generated in each link with a probability P_0. If the obtained state is not further

purified, the resulting rate reads

$$R_n = \frac{c}{2L_0} \frac{1}{Z_n(P_0)}, \tag{7.39}$$

where

$$Z_n(p) = \sum_{j=1}^{2^n} \binom{2^n}{j} \frac{(-1)^{j+1}}{1 - (1-p)^j}, \tag{7.40}$$

is the average total number of attempts it takes for all segments to eventually share an entangled pair (recall that initially shared pairs can be stored as long as needed), $T_0 = \frac{2L_0}{c}$ is the elementary time unit for sending the quantum states and also the classical information to confirm their successful distribution (as well as purification), and c is the speed of light in the optical fiber.

If one round of purification is performed, the same formula can be applied, but now P_0 has to be substituted by an effective probability,

$$Q_1(L_0) = P_0 P_1 \left(\frac{2 - P_0}{3 - 2P_0} \right), \tag{7.41}$$

where P_1 is the probability for the first round of purification to succeed. Furthermore, the rates with two and three rounds of purification can be calculated using the effective probabilities

$$Q_2(L_0) = Q_1(L_0) P_2 \left(\frac{2 - Q_1(L_0)}{3 - 2Q_1(L_0)} \right), \tag{7.42}$$

and

$$Q_3(L_0) = Q_2(L_0) P_3 \left(\frac{2 - Q_2(L_0)}{3 - 2Q_2(L_0)} \right), \tag{7.43}$$

where P_2 and P_3 are the success probabilities for two and three rounds of purification, respectively. Note that without the use of quantum memories, Q_3 would scale as $P_0^8 P_1^4 P_2^2 P_3$, which (assuming small probabilities) is turned into a scaling like $P_0 P_1 P_2 P_3$ with the help of the quantum memories. Higher rounds of purification can be considered in a recursive fashion. We analyze the rates for the USD- and homodyne-based scheme separately in the next two sections.

USD-based scheme For USD-scheme, P_0 is given by the optimal probability in Eq. (7.30) to distinguish the three coherent states $|\alpha\rangle$ and $|\alpha e^{\frac{2\pi i}{3}}\rangle$. The resulting state is the normalized version of Eq. (7.22) and the initial fidelity of the target state reads

$$F_0 = \frac{N_u(\sqrt{1-\gamma}\alpha)}{9}, \tag{7.44}$$

and

$$F_1 = \frac{N_v(\sqrt{1-\gamma}\alpha)}{9},$$
$$F_2 = \frac{N_w(\sqrt{1-\gamma}\alpha)}{9}, \tag{7.45}$$

for the other two components. One round of purification succeeds with probability

$$P_1 = F_0^2 + F_1^2 + F_2^2, \tag{7.46}$$

and the resulting improved fidelity is

$$F_0' = \frac{F_0^2}{F_0^2 + F_1^2 + F_2^2}. \tag{7.47}$$

For more rounds of purification, the fidelities and success probabilities can be obtained recursively.

After entanglement swapping, the final fidelity of the entangled state distributed over the total distance is lower bounded by $(\widetilde{F_0})^{2^n}$, where $\widetilde{F_0}$ is the final fidelity on each link, possibly obtained after some rounds of purification.

Homodyne scheme An exact rate analysis for the entanglement distribution based on homodyne detection is much more demanding than for the USD-case. This is due to the fact that at adjacent elementary links potentially different mixed quantum states are generated depending on the corresponding measurement result. As already pointed out, these states can be brought into a similar form, i.e. the components are equal, but the statistical weights are not necessarily equal. An exact rate analysis is therefore hard to perform.

To nevertheless assess the performance of that scheme, we model the situation with an effective state on each elementary link. This effective state has the average fidelity $F_{av}(\alpha, \gamma)$ as the statistical weight of the first component, whereas the other two components are equally weighted with $F_1 = F_2 = \frac{1}{2}(1 - F_{av}(\alpha, \gamma))$. For an elementary distance of $L_0 = 5$ km, we choose $\alpha \approx 1$, which leads to a maximum initial fidelity of ≈ 0.7. As the generation probability P_0, we insert the average success probability, $P_{succ} = \sum_{i=0}^{2} p_{w_i}$, for obtaining a result in the success windows (see Section 7.1.1) which equals ≈ 0.4 in this case. For $L_0 = 5$ km, we also have $\alpha \approx 1$, but now $F_{av} \approx 0.6$ and $P_0 \approx 0.39$.

Using these initial values, the formulae for the rates and fidelities, including possible rounds of purification, can directly be applied. For quantitative examples and an illustration of the trade-off between repeater rates and fidelities, see App. C.1.

To summarize some of the results presented there, for elementary distances as short as $L_0 = 5$ km, the USD-based scheme and the homodyne-based scheme perform comparably. In either

case at least three rounds of purification are needed in order to obtain reasonable fidelities and rates for distances as large as 640 km.

For $L_0 = 10$ km according to our calculations, the USD-based scheme performs slightly better than the homodyne-based scheme, such that in both scenarios rather high fidelities can be achieved for distances as large as 1280 km (the rates are comparable and again three rounds of purification are necessary). However, note that our results for the homodyne-based scheme only hold under the assumptions that the off-diagonal terms in Eq. (7.20) are negligible and that the conditional state after homodyne detection can be modeled via an effective state with fidelity F_{av}. Thus, the numbers presented in App. C.1 may overestimate the homodyne-based scheme compared to the USD-based scheme.

Results for a situation with a more practical repeater spacing, $L_0 = 20$ km, indicate that for $L = 1280$ km near-unit fidelities at rates $\approx$ Hz are only achievable using USD, because in the homodyne-based scheme the output fidelities drop below 0.5 for such large elementary distances. Note that a similar observation was made for the original qubit scheme based on homodyne detection [85].

The general qudit case

Based on the results obtained in the last sections for specific examples, we are now in turn to propose HQR protocols for arbitrary finite dimensional quantum systems.

The dispersive interaction between a general qudit, i.e. a d-level system, and a light mode can be realized by the Hamiltonian

$$H_{int}^{(d)} = \hbar g \hat{S}_z^{(d)} \hat{a}^\dagger \hat{a},$$ (7.48)

with $\hat{S}_z^{(d)}|k\rangle = \left(\frac{2k-d+1}{2}\right)|k\rangle$ for $k = \{0, 1, .., d-1\}$, and where $\hat{S}_z^{(2)} = \sigma_z$. The corresponding unitary is $U_d(\theta) = \exp(i\theta \hat{S}_z^{(d)} \hat{a}^\dagger \hat{a})$ and the relevant case of a strong interaction is obtained by setting $\theta = \frac{2\pi}{d}$.

The first step in the protocol is the preparation of the matter state $\frac{1}{\sqrt{d}} \sum_{k=0}^{d-1} |k\rangle$, which then interacts with an optical coherent state $|\alpha\rangle$ via the strong dispersive interaction. This results in a hybrid entangled qudit-light (qudit-qubus) state,

$$\frac{1}{\sqrt{d}} \sum_{k=0}^{d-1} |k\rangle |\alpha e^{\frac{2k\pi i k}{d}}\rangle.$$ (7.49)

After locally generating qudit-light entanglement, the light mode is sent through an optical channel of length L_0 where it is subject to photon loss. Including again an ancilla vacuum mode and mixing it with the optical mode results in

$$\frac{1}{\sqrt{d}} \sum_{q=0}^{d-1} |q\rangle |\sqrt{\gamma}\alpha e^{\frac{2\pi i q}{d}}\rangle |\sqrt{1-\gamma}\alpha e^{\frac{2\pi i q}{d}}\rangle.$$ (7.50)

As in the specific examples above, the crucial point is now to find a suitable basis for tracing out the loss mode. Here, in the general case, this basis consists of the d vectors

$$|v_m\rangle = \frac{1}{\sqrt{N_{v_m}(\alpha)}} \sum_{k=0}^{d-1} e^{\frac{2\pi i k m}{d}} |\alpha e^{\frac{2\pi i k}{d}}\rangle, \tag{7.51}$$

with $m = 0, 1, .., d-1$. We can thus recast the coherent states of the ancilla light mode in Eq. (7.50) as

$$|\alpha e^{\frac{2\pi i k}{d}}\rangle = \frac{1}{d} \sum_{m=0}^{d-1} \sqrt{N_{v_m}(\alpha)} e^{-\frac{2\pi i k m}{d}} |v_m\rangle, \tag{7.52}$$

and find for Eq. (7.50):

$$\frac{1}{d\sqrt{d}} \sum_{q,m=0}^{d-1} \sqrt{N_{v_m}(\sqrt{1-\gamma}\alpha)} e^{-\frac{2\pi i q m}{d}} |q\rangle |\sqrt{\gamma}\alpha e^{\frac{2\pi i q}{d}}\rangle |v_m\rangle. \tag{7.53}$$

Tracing out the loss mode in this basis is now a trivial task and one obtains

$$\rho_{out} = \sum_{m=0}^{d-1} \frac{N_{v_m}(\sqrt{1-\gamma}\alpha)}{d^2} \left[\left(\frac{1}{\sqrt{d}} \sum_{q=0}^{d-1} e^{-\frac{2\pi i q m}{d}} |q\rangle |\sqrt{\gamma}\alpha e^{\frac{2\pi i q}{d}}\rangle \right) \times H.c. \right], \tag{7.54}$$

for the d-component qudit-light output state.

Again, this can be further simplified by basis transformations on both the light mode and the matter system. The light mode can be expressed in the basis given in Eq. (7.51), while the matter system can be written in the (generalized Pauli) qudit X-basis,

$$|\widetilde{k}\rangle = \frac{1}{\sqrt{d}} \sum_{m=0}^{d-1} e^{\frac{2\pi i k m}{d}} |m\rangle, \tag{7.55}$$

for $k = 0, 1, ..., d-1$. This gives the expression

$$\rho_{out} = \sum_{m=0}^{d-1} \frac{N_{v_m}(\sqrt{1-\gamma}\alpha)}{d^2} \left[\left(\frac{1}{d} \sum_{r=0}^{d-1} \sqrt{N_{v_r}} |\widetilde{m \oplus r}\rangle |\widetilde{v}_r\rangle \right) \times H.c. \right], \tag{7.56}$$

for Eq. (7.54) where $\oplus$ denotes addition modulo d. Note that $\sim$ again indicates basis vectors with damped amplitude $\sqrt{\gamma}\alpha$ on the light mode and the X-basis on the matter system.

After traveling through the loss channel over a distance L_0, the light mode reaches a second matter system, also prepared in the state $\frac{1}{\sqrt{d}} \sum_{k=0}^{d-1} |k\rangle$. The light mode interacts dispersively with the second matter system, this time with the inverse angle $\theta = -\frac{2\pi}{d}$. The resulting state becomes

$$\rho = \sum_{m=0}^{d-1} \frac{N_{v_m}}{d^2} |T_m\rangle\langle T_m|, \tag{7.57}$$

75
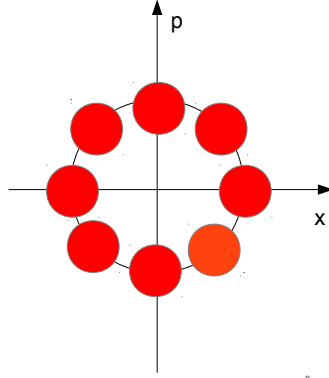
Figure 7.8: Phase space representation of the qubus mode for $d = 8$.

with the components

$$|T_m\rangle = \frac{1}{d} \sum_{q=0}^{d-1} \sum_{l=0}^{d-1} e^{-\frac{2\pi i q m}{d}} |q\rangle |l\rangle |\sqrt{\gamma}\alpha e^{\frac{2\pi i (q-l)}{d}}\rangle, \tag{7.58}$$

written in the original basis (like in Eq.(7.54)).

The state discrimination in the general case involves the d coherent states $|\sqrt{\gamma}\alpha\rangle, ..., |\sqrt{\gamma}\alpha e^{\frac{2\pi i (d-1)}{d}}\rangle$ which can be graphically represented as coherent states "on a ring" (see Fig. 7.8 for $d = 8$). A projection onto one of the d coherent states collapses each component onto a maximally entangled state. However, by increasing the dimension d, a projection scheme based on homodyne detection becomes more and more futile since no direction is uniquely specified any more.

A scheme for unambiguously discriminating exactly these d coherent states was derived in [132] for arbitrary dimensions (for $d = 3$, recall Section 7.1.1). An upper bound for the success probability is given by

$$P_D \leq \min_r \sum_{j=0}^{d-1} e^{-\frac{2\pi i j r}{d}} e^{\gamma \alpha^2 (e^{\frac{2\pi i j}{d}} - 1)}, \tag{7.59}$$

$r = 0, 1, .., d-1$, where Eq.(7.30) is recovered for $d = 3$. Since the upper bound on the right-hand side depends on both α and γ the minimization with respect to r is hard analytically. We therefore calculate the bound numerically.

After the USD, the resulting mixed state will be a mixture of $d - 1$ maximally entangled Bell states of the form

$$|\phi_{kj}\rangle = \frac{1}{\sqrt{d}} \sum_{y=0}^{d-1} e^{\frac{2\pi i k y}{d}} |y, y \ominus j\rangle, \tag{7.60}$$

for one fixed $j = 0, ..., d-1$, according to the specific identified coherent state. If $j \neq 0$, a j-fold application of $X = \sum_{k=0}^{d-1} |k+1\rangle\langle k|$ transforms all these states to

$$|\phi_{k0}\rangle = \frac{1}{\sqrt{d}} \sum_{y=0}^{d-1} e^{\frac{2\pi i k y}{d}} |y, y\rangle. \tag{7.61}$$

By means of local unitaries, the different components of the mixtures with $|\phi_{k0}\rangle$ can always be transformed to a mixture of the states

$$|\psi_j\rangle \equiv |\phi_{0j}\rangle = \frac{1}{\sqrt{d}} \sum_{y=0}^{d-1} |y, y \ominus j\rangle, \tag{7.62}$$

with now all j included. We therefore obtain

$$\rho = \sum_{j=0}^{d-1} p_j |\psi_j\rangle\langle\psi_j|, \tag{7.63}$$

for the state to be purified.

The purification now works as follows. We prepare two copies of the state in Eq. (7.63) such that the total joint four-qudit state reads

$$\rho \otimes \rho = \sum_{j=0}^{d-1} \sum_{k=0}^{d-1} p_j p_k |\psi_j\rangle|\psi_k\rangle\langle\psi_j|\langle\psi_k|, \tag{7.64}$$

where the individual terms are

$$|\psi_j\rangle|\psi_k\rangle = \frac{1}{d} \sum_{y=0}^{d-1} \sum_{y'=0}^{d-1} |y, y \ominus j\rangle|y', y' \ominus k\rangle. \tag{7.65}$$

One applies a local CSHIFT gate on systems 1 and 3 as well 2 and 4 in order to obtain

$$\frac{1}{d} \sum_{y=0}^{d-1} \sum_{y'=0}^{d-1} |y - y', y \ominus y' \oplus k \ominus j\rangle|y', y' \ominus k\rangle. \tag{7.66}$$

After that, the first spins of the first two systems are measured. If the spins are parallel, it follows $k = j$ such that only diagonal parts contribute. As a consequence, the second two systems collapse to $|\psi_k\rangle$.

The new state then becomes

$$\rho' = \frac{\sum_{j=0}^{d-1} p_j^2 |\psi_j\rangle\langle\psi_j|}{\sum_{j=0}^{d-1} p_j^2}. \tag{7.67}$$

The fidelity with respect to the target state $|\psi_0\rangle$ is thus

$$F' = \frac{p_0^2}{\sum\limits_{j=0}^{d-1} p_j^2}, \qquad (7.68)$$

which is increased compared to the initial fidelity p_0 if $p_0 > \frac{1}{d}$ and $p_i < p_0$ for $i = 1, ..., d - 1$.

After possibly several rounds of purification, a high-fidelity entangled state can be obtained between the two separated qudits. This is referred to as the initial entanglement generation or distribution.

To further extend the entanglement, two elementary segments next to each other are connected via entanglement swapping through Bell measurements on adjacent repeater nodes, i.e., a projection on maximally entangled qudit-qudit states is performed.

Generalizing the qutrit case, we show that the CSHIFT gate lies at the heart of such Bell measurements and that these can be realized by a CPHASE gate based on the generalized dispersive interaction.

The CPHASE gate for an arbitrary dimension d is realized by the two-qudit unitary transformation

$$U_d = \exp\left(-\frac{2\pi i}{d} \hat{S}_{z_1}^{(d)} \hat{S}_{z_2}^{(d)}\right), \qquad (7.69)$$

with the generalized spin operator $\hat{S}_i^{(d)}$ acting on qudit i. We show by direct calculation that the sequence $H \otimes 1 \to \text{CPHASE} \to H \otimes 1$ acts as a controlled phase shift gate on an arbitrary two-qudit state:

$$
\begin{aligned}
(H \otimes 1) \cdot \text{CPHASE} \cdot (H \otimes 1)|xy\rangle &= (H \otimes 1) \cdot \text{CPHASE} \frac{1}{\sqrt{d}} \sum_{k=0}^{d-1} \exp\left(\frac{2\pi i k x}{d}\right) |ky\rangle \\
&= (H \otimes 1) \frac{1}{\sqrt{d}} \sum_{k=0}^{d-1} \exp\left(\frac{2\pi i k (x - y)}{d}\right) |ky\rangle \\
&= |x - y, y\rangle.
\end{aligned}
\qquad (7.70)
$$

Together with arbitrary qudit rotations and measurements in the qudit X and Z basis, this suffices to implement a deterministic Bell state analyzer for qudits [135].
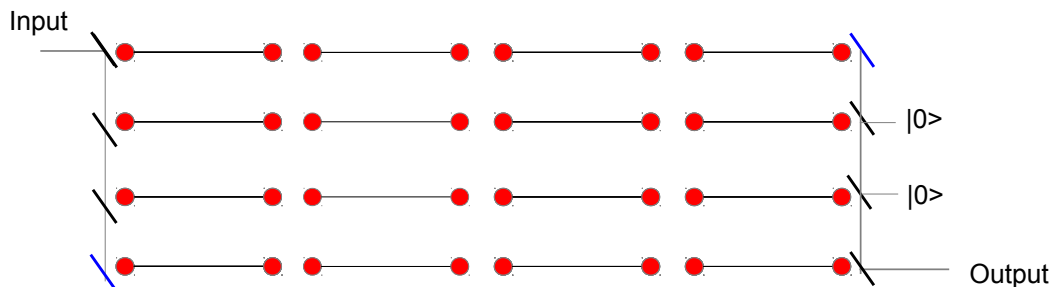
Figure 7.9: Teleporter with $N = 2$ scissors: The resource Bell states for the teleportation are generated using first-generation qubit quantum repeaters. Each segment is individually generated with some probability p_0 (depending on the protocol) and then connected via entanglement swapping on adjacent repeater nodes (red dots). For the teleporter protocol, see the description in the text.

7.1.2   Quantum repeaters for continuous variables

A proper first-generation continuous-variable quantum repeater requires the generation of bipartite entangled continuous-variable states in elementary segments whose distances are then enlarged by continuous-variable entanglement swapping. Unfortunately, continuous-variable teleportation and swapping requires infinite energy to achieve unit fidelity. Therefore, it is not surprising that except the works of [137] and [138] not much has been done on this topic.

In this section, we propose a repeater protocol for continuous-variable states based on quantum teleportation using delocalized single photons. The basic scheme was originally introduced in [130] to demonstrate high-fidelity continuous-variable teleportation (see Fig. 7.9).This scheme works as follows.

The single-mode pure input state is first divided at a symmetric N-splitter (see Eq. (5.8) in Section 5.2) together with $N - 1$ ancillary vacuum modes at the other input ports. Each of the modes is then individually teleported using a maximally entangled resource state $|r\rangle = \frac{1}{\sqrt{2}}(|10\rangle + |01\rangle)$. After that, the modes are recombined at another symmetric N-splitter. Finally, measuring no photons in any of the ancilla output modes approximately teleports the input state.

One can show that the output state for an arbitrary input state $|\psi\rangle = \sum\limits_{k=0}^{\infty} c_k |k\rangle$ reads as

$$|\widetilde{\psi}\rangle = \mathcal{N} \sum_{k=0}^{N} c_k \binom{N}{k} \frac{k!}{N^k} |k\rangle, \tag{7.71}$$

with some normalization constant $\mathcal{N}$. This teleportation scheme therefore effectively returns a truncated version of the state whose norm corresponds to the success probability.

In the following, we consider the teleportation of a coherent state $|\alpha\rangle$ with $\alpha \in \mathbb{R}$ over large distances. In Ref. [130], the output states and probabilities for the teleportation scheme with lossy resource states, i.e.

$$\rho = \gamma|r\rangle\langle r| + (1-\gamma)|00\rangle\langle 00|, \tag{7.72}$$

have been derived. The unnormalized output state reads

$$\rho_{out} = \sum_{n=0}^{N} \binom{N}{n} \frac{\gamma^{N-n}(1-\gamma)^n \alpha^{2n} \exp(-|\alpha|^2)}{2^{N-n} N^n} \tag{7.73}$$

$$\times \sum_{k,k'}^{N-n} \binom{N-n}{k}\binom{N-n}{k'} \left(\frac{\alpha}{N}\right)^k \sqrt{k!}|k\rangle\langle k'|\sqrt{k'!}\left(\frac{\alpha^*}{N}\right)^{k'}, \tag{7.74}$$

and its normalization is the success probability

$$p_{succ}(\gamma, N, \alpha) = \sum_{n=0}^{N} \binom{N}{n} \frac{\gamma^{N-n}(1-\gamma)^n \alpha^{2n} \exp(-|\alpha|^2)}{2^{N-n} N^n} \sum_{k=0}^{N-n} \binom{N-n}{k}^2 \left(\frac{|\alpha|^2}{N^2}\right)^k k!. \tag{7.75}$$

The fidelity after the teleportation with respect to the input state $|\alpha\rangle$ is (using $\langle k|\alpha\rangle = \exp(-|\alpha|^2/2)\frac{\alpha^k}{\sqrt{k!}}$)

$$F(\gamma, \alpha, N) = \langle\alpha|\rho_{out}|\alpha\rangle/p_{succ}(\gamma, N, \alpha)$$

$$= \sum_{n=0}^{N} \binom{N}{n} \frac{\gamma^{N-n}(1-\gamma)^n \alpha^{2n} \exp(-2|\alpha|^2)}{2^{N-n} N^n} \left(\sum_{k}^{N-n} \binom{N-n}{k} \left(\frac{|\alpha|^2}{N}\right)^k\right)^2 /p_{succ}(\gamma, N, \alpha). \tag{7.76}$$

Since the lossy resource state in Eq. (7.72) is obtained when each mode of the pure resource state is sent from a fictitious middle station through halves of the channel in opposite directions, it appears meaningful to substitute each lossy resource state in the teleporter by the successful output of a first-generation quantum repeater to achieve a better scaling of the fidelity.

We consider a first-generation quantum repeater protocol where two-mode entangled single-photon states are distributed over a large distance. For illustration, we assume perfect memories and deterministic entanglement swapping to keep the analysis manageable. We furthermore let $N = 2^q$ be an even number with q an arbitrary positive integer.

The first step is to determine the probability that, given a generation probability p_0 for one elementary segment of length L_0, $2^n = L/L_0$ segments next to each other are created which cover the total distance L. As mentioned in Section 7.1.1, the average number of steps to create 2^n links is $Z_n(p_0)$. Since the swapping is deterministic, we can therefore define an

effective probability,

$$\langle p_{gen} \rangle = \frac{1}{Z_n(p_0)},\tag{7.77}$$

for the generation of one entangled link covering the total distance L. For the creation of $N = 2^q$ entangled links in series, we find in analogy

$$\langle p_{ser} \rangle = \frac{1}{Z_q(\langle p_{gen} \rangle)},\tag{7.78}$$

for the effective probability. The total success probability for teleporting an unknown coherent state is then

$$P_{tot}(N, \alpha, p_0) = P_{tele}(\alpha, N)\langle p_{ser}(p_0)\rangle,\tag{7.79}$$

where

$$P_{tele}(\alpha, N) = \frac{e^{-\alpha^2}}{2^N} \sum_{k=0}^{N} \binom{N}{k}^2 \left(\frac{\alpha^2}{N^2}\right) k!,\tag{7.80}$$

is the success probability of the loss-free teleporter [130]. Since memories and entanglement swapping operations are assumed perfect, the loss only affects the generation probability but not the final fidelity of the generated Bell pairs. Therefore, after generating entanglement in each line, our scheme works effectively as a loss-free teleporter. The only drawback is that our scheme is slower compared to a direct transmission of the Bell pairs.

The only implementation-specific part is the generation probability p_0. For a dual-rail entangled Bell state, $p_0 = \exp(-L_0/L_{att})$. For the DLCZ protocol (see Section 4.1.1), one has $p_0 = r\gamma = r\exp(-L_0/2L_{att})$ where the squeezing parameter r is chosen sufficiently small to avoid multiple excitations of the atomic ensembles.

7.2   An ionic matter-light interface for quantum repeaters

A basic requirement for first-generation quantum repeaters are efficient quantum memories with a reasonably long coherence time in order to faithfully store quantum information. Just as important as the storage of the quantum state encoding the information are the write-in and read-out processes on the quantum memories [139].

The interconversion of stationary qubits and flying qubits has been declared as a fundamental ingredient for quantum communication networks [140], at least as long as third-generation quantum repeater schemes are experimentally out of reach.

Second-generation quantum repeater schemes actively use quantum error correction for protecting the quantum memories against errors. It is therefore an important question in which way a memory can be encoded and, at the same, the encoded information can be converted into photonic quantum states which can be used for processing.

In the following, we consider trapped ions, for example, Calcium or Beryllium, as quantum memories. The ionic qubit could be realized by two of its hyperfine states, which we denote by $|\uparrow\rangle$ and $|\downarrow\rangle$. A main error source in the ionic quantum memory is collective dephasing, i.e. the transformation

$$
\begin{aligned}
|\uparrow\rangle &\mapsto |\uparrow\rangle, \\
|\downarrow\rangle &\mapsto -|\downarrow\rangle
\end{aligned}
\tag{7.81}
$$

on the basis states which causes a phase-flip on the ionic qubit. A way to circumvent this undesired phase flip is to encode the qubit in a decoherence-free subspace [141]. To see what this means, let us say we encode the qubit by means of two ions, such that the logical basis states read as

$$
\begin{aligned}
|\bar{0}\rangle &= |\uparrow\rangle|\uparrow\rangle, \\
|\bar{1}\rangle &= |\downarrow\rangle|\downarrow\rangle.
\end{aligned}
\tag{7.82}
$$

It is now easy to see that both logical codewords are invariant under the collective dephasing acting separately on each ion. The description as a correlated error is justified since the origin are usually intensity fluctuations of electromagnetic fields that are, for example, needed to manipulate the quantum state of the system or to compensate background fields [142]. Such fields are typically generated outside the actual experimental setting and can therefore be considered as spatially homogeneous on the scale of the ion trap. This means that a variation of the field strength affects all trapped ions in the same way, which explains the correlated error model.

Using this decoherence-free subspace encoding, the corresponding logical qubit remains also unaffected and is automatically protected without any further error correction steps. Another suitable decoherence-free subspace encoding using four ions is

$$
\begin{aligned}
|\bar{0}\rangle &= |\uparrow\rangle|\uparrow\rangle|\uparrow\rangle|\uparrow\rangle, \\
|\bar{1}\rangle &= |\downarrow\rangle|\downarrow\rangle|\downarrow\rangle|\downarrow\rangle.
\end{aligned}
\tag{7.83}
$$

Our goal is now to write in a loss-encoded flying photonic qubit into a decoherence-free subspace encoded ionic quantum memory.

We consider photonic qubits encoded into horizontal ($|H\rangle$) and vertical ($|V\rangle$) polarization. We need the following experimentally feasible light-matter interaction [143] that transforms an unencoded ionic qubit into an optical polarization qubit,

$$
(\alpha|\uparrow\rangle + \beta|\downarrow\rangle)_{ion} \otimes |0\rangle_{light} \to |D\rangle_{ion} \otimes (\alpha|H\rangle + \beta|V\rangle)_{light},
\tag{7.84}
$$

where $|0\rangle_{light}$ is the photonic vacuum state and $|D\rangle_{ion}$ denotes some additional ionic level. Especially, we need the special cases

$$
\begin{aligned}
|\uparrow\rangle \otimes |0\rangle_{light} &\rightarrow |D\rangle \otimes |H\rangle, \\
|\downarrow\rangle \otimes |0\rangle_{light} &\rightarrow |D\rangle \otimes |V\rangle.
\end{aligned}
\tag{7.85}
$$

The key observation for our scheme is that the codewords of the quantum parity code QPC(2,2) (see Eq. (3.10)) can be equivalently expressed as

$$
\begin{aligned}
|\bar{0}\rangle &= \frac{1}{\sqrt{2}} \left(|HHHH\rangle + |VVVV\rangle \right), \\
|\bar{1}\rangle &= \frac{1}{\sqrt{2}} \left(|HHVV\rangle + |VVHH\rangle \right).
\end{aligned}
\tag{7.86}
$$

Here, the one-to-one-correspondence $|H\rangle \equiv |10\rangle$ and $|V\rangle \equiv |01\rangle$ ensures the equivalence of both expressions.

Assume that an arbitrary optical logical QPC(2,2)-encoded flying qubit can be prepared and is sent to a memory consisting of four ions, all initially prepared in the state $|D\rangle$. The reverse interaction of Eq. (7.84) then gives

$$
|D\rangle|D\rangle|D\rangle|D\rangle \otimes (\alpha|\bar{0}\rangle + \beta|\bar{1}\rangle) \rightarrow (\alpha \frac{1}{\sqrt{2}} (|\uparrow\uparrow\uparrow\uparrow\rangle + |\downarrow\downarrow\downarrow\downarrow\rangle) + \beta \frac{1}{\sqrt{2}} (|\uparrow\uparrow\downarrow\downarrow\rangle + |\downarrow\downarrow\uparrow\uparrow\rangle)) \otimes |0\rangle,
\tag{7.87}
$$

where $|0\rangle$ is the four-mode photonic vacuum.

The described protocol is therefore effectively a state transfer from optical loss-protected qubits to ion qubits living in the decoherence-free subspace defined in Eq. (7.83) where the quantum information can be efficiently stored [144]. Using the inverse operation, a read-out of the ionic quantum state is also possible.

7.3 Third-generation quantum repeaters

7.3.1 NOON codes
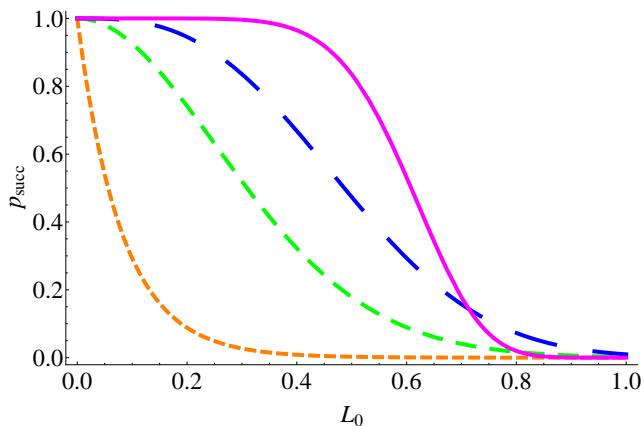
Figure 7.10: Success probabilities for the one-way scheme with different encodings: $N^2 = 4$ (orange, ultrafine dashed), $N^2 = 9$ (green, fine dashed), $N^2 = 16$ (blue, dashed) and $N^2 = 100$ (magenta, solid) total photons for $L = 1000$ km (L_0 in km).

Now we shall demonstrate the performance of the exact QECC developed in Chapter 5 when applied in third-generation quantum repeaters (see Section 4.3).

Based on the results of Chapter 5, the success probability for one-way communication over a total distance L with repeater spacings L_0 of an (N^2, d) encoded qudit is [1]

$$P_{succ} = \left(\sum_{k=0}^{N-1} \binom{N^2}{k} \gamma^{N^2-k}(1-\gamma)^k \right)^{L/L_0}. \tag{7.88}$$

Here, the damping parameter is given by $\gamma = \exp\left(-\frac{L_0}{L_{att}}\right)$ with the attenuation length $L_{att} = 22$ km for telecom fibers and photons at telecom wavelengths. Note that P_{succ} only depends on N and especially not on d. The success probability for the one-way scheme over a total distance of 1000 km using various codes is shown in Fig. 7.10.

To assess the resources needed in a scheme with our qudit codes, we furthermore define a (spatial) cost function as [23]

$$C(N, d) = \frac{N^2}{P_{succ} \log_2(d) L_0}, \tag{7.89}$$

which depends on the photon number N per block and the dimension of the qudit d [2]. Fixing the

---

[1]The success probability corresponds to a multiple of the fidelity determined in Section 5.3, $P_{succ} = [F(L_0)]^{L/L_0}$.

[2]Compared to [23], here we shall only consider the cost for transmitting logical qubits over a total distance

(a) $N^2 = 1$ (b) $N^2 = 9$ (c) $N^2 = 16$ (d) $N^2 = 25$
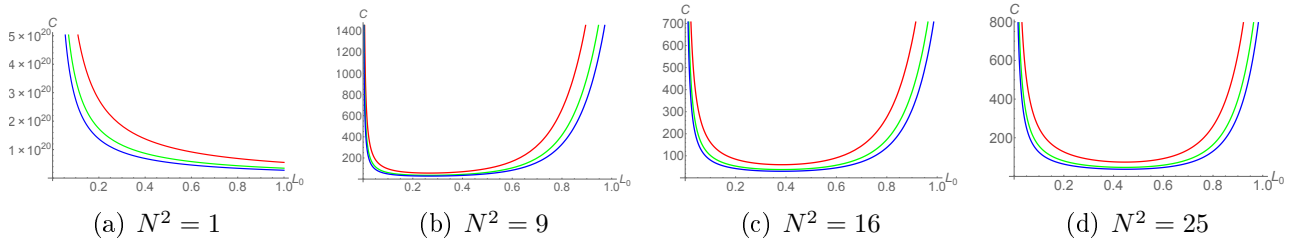
Figure 7.11: Cost function for codes with different photon numbers and dimensions for $L = 1000$ km: $d = 2$ (red), $d = 3$ (green), $d = 4$ (blue) (from top to bottom, L_0 in km).

total photon number, the cost is obviously suppressed by the inverse of the binary logarithm of the qudit dimension (corresponding to the effective number of encoded logical qubits) such that qudit encodings make the one-way scheme more efficient. More interesting is the comparison of different qudit encodings with different total photon numbers, as shown in Fig. 7.11 . The plot shows the cost functions of various codes. The cost decreases with N as P_{succ} is increasing at the same time for a suitably chosen L_0.

Note that also $N^2 = 1$ can be realized in the so-called multiple-rail qudit encoding, where a single photon occupies one of d modes, i.e. $|\bar{0}\rangle = |1000..\rangle, |\bar{1}\rangle = |0100..\rangle, ..., |\overline{d-1}\rangle = |00...01\rangle$. Since the scaling of the transmission probability with the loss parameter γ only depends on the total photon number (and especially not on the qudit dimension d), a cost reduction can be achieved already in this case by increasing d. However, the multiple-rail encoding is not a quantum error correction code; it is only a quantum error detection code (see Section 2.3) that can detect but not correct loss errors. By including the number of modes into the cost function, e.g. $C(N, d) = \frac{N^3 d}{P_{succ} \log_2(d) L_0}$ [19, 145], we no longer get a cost reduction by increasing the logical dimension d.

In our illustrative example here, we have assumed that adding extra modes is cheap compared to adding extra photons and hence used the cost function in Eq. (7.89) as a figure of merit. This point of view is different compared to the usual, information theoretical secret-key analysis, where the key rate is calculated per mode [145].

L, instead of secure classical bits eventually obtained via quantum communication.

(a) "old" scheme   (b) improved, "new" scheme

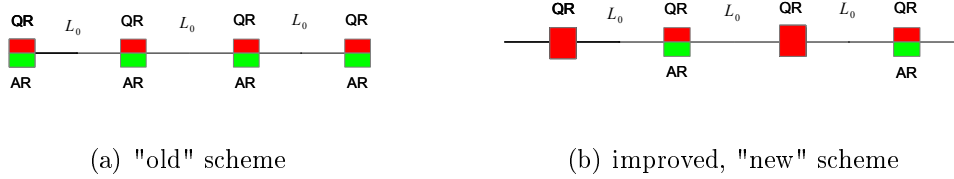Figure 7.12: Schematic of a one-way quantum repeater with qubit recovery (QR, red) as well as amplitude restoration (AR, green) at every repeater station (a) or with QR at every repeater station and AR only at every second station (b).

7.3.2 Cat codes

We now examine the performance of the cat codes developed in Chapter 6 in third-generation quantum repeaters.

As loss-protected qubits are usually encoded into multi-mode states [23], an attractive feature of the cat loss code of Chapter 6 would be that only a single optical mode must be sent.

In the case of cat codes, the first step at each repeater station is a QND-type parity measurement that determines the corresponding error space. After fixing the parity, the logical state is recovered to a great extent and the initial logical qubit resides in some error space with high, but non-unit fidelity.

As already mentioned in Section 6.1, a special problem that occurs with the transmission of cat-code qubits is the distance-dependent damping of the amplitude. In addition to the qubit recovery (QR) at each repeater station, the amplitude has to be restored as well. A probabilistic scheme for this amplitude restoration (AR) is presented in App. B.5. In our AR scheme, we use quantum teleportation and choose to teleport the qubit back into the code space, while restoring the amplitude. A schematic is depicted in Fig. 7.12 a). After each repeater station, the qubit is recovered as well as the amplitude is restored. Figure 7.12 b) shows an improved scheme in which the qubit is still recovered at each repeater station, but the amplitude is restored at every second repeater station only. The total success probability for this improved scheme is shown in Fig. 7.13. One observes that the total success probability initially increases with the elementary distance L_0 before reaching a maximum and tending to zero again. Indeed, doing AR at the end of the total channel at distance $\mathcal{L}$ corresponds to an exponentially small success probability, while a scheme in which AR is performed too frequently also means that the probabilistic element introduced via AR accumulates over the total distance. We expect that a further improvement compared to the results shown in Fig. 7.13 can be obtained by doing AR even less frequently than at every second repeater station. Here, we shall only demonstrate an in-principle improvement when QR and AR are not always performed synchronously, without intending to find an optimal scheme.
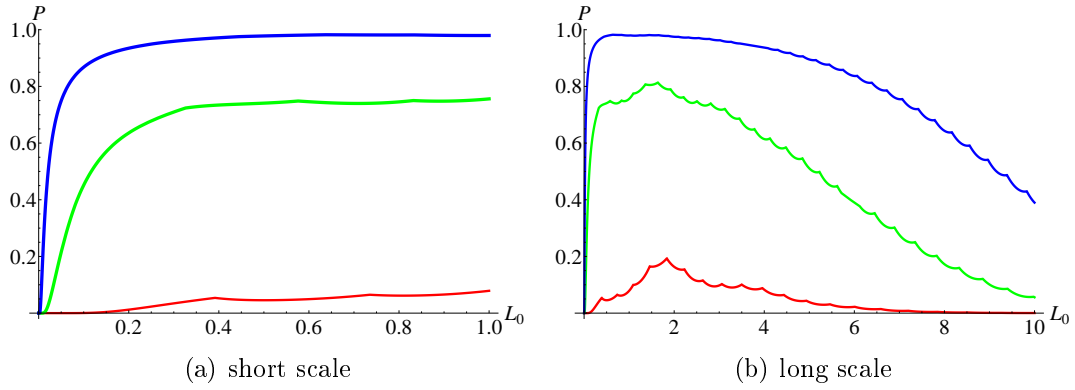
(a) short scale   (b) long scale

Figure 7.13: Total success probability P of amplitude restoration as a function of the elementary distance L_0 (in km) in an improved ("new") one-way scheme over a total distance of 1000 km for $L = 4$ and various α (from top to bottom): $\alpha = 8$ (blue), $\alpha = 7$ (green), $\alpha = 6$ (red).

The fidelity bound

$$F = \left[\min_{a,b} [\widetilde{p}_0(a,b) + \widetilde{p}_1(a,b) + ... + \widetilde{p}_L(a,b)] \right]^{\mathcal{L}/L_0}, \tag{7.90}$$

however, is near unity for short elementary distances and decreases with increasing L_0 (see Fig. 7.14). Note that this bound does not include those events (occurring with probabilities $\widetilde{p}_{L+1}, ..., \widetilde{p}_{2L+1}$) where the qubit gets "self-corrected" after a suitable sequence of uncorrectable errors.

To summarize, qubit recovery is necessary after sufficiently short distances, whereas amplitude restoration seems to be beneficial after longer but not too long distances. That the logical qubits must be recovered frequently after short distances is also expected, since the loss code does not tolerate too large losses for the quantum information to remain intact. A comparison of the success probabilities and fidelities for the "old" and the improved "new" scheme with different cat codes and different amplitudes is shown in Tables 7.1-7.3. Besides the significantly higher success probabilities, the improved scheme also gives slightly better fidelities.

In general, the expected trade-off is recovered: for too large amplitudes α, the photon loss probability goes up (and hence the fidelity decreases) while the codewords become more orthogonal (and hence the filter probabilities, see App. B.5, and thus the AR probabilities increase). Conversely, for smaller α, the AR becomes less likely to succeed, while larger fidelities can be obtained. A non-trivial result is to find a code L and a protocol, for which an α-regime exists that allows for both reasonable success probabilities ($\sim 1\% - 10\%$) and near-unit fidelities at some elementary distances L_0. For $L = 3$ using the "old" scheme such an α-regime does not seem to exist (see Table 7.1). With the "new", improved scheme, however, the $L = 3$-code may suffice for elementary distances of $L_0 \sim 100$ m. For the $L = 4$- and $L = 5$-codes, both schemes can work at elementary distances of $L_0 \sim 10 - 100$ m. A general observation is that elementary

87
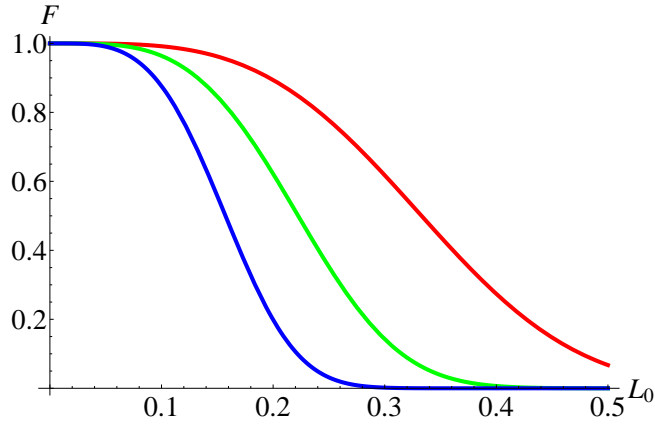
Figure 7.14: Bound F on worst-case fidelity as a function of the elementary distance L_0 (in km) for a one-way scheme over a total distance of 1000 km with $L = 4$ for various α (from top to bottom): $\alpha = 6$ (red) $\alpha = 7$ (green) $\alpha = 8$ (blue).

distances as large as ~ 1 km result in very bad fidelities. Thus, a cat-encoded logical qubit is more sensitive to too large losses and too large L_0 than, for instance, a single-photon-based, multi-mode, QPC-encoded qubit for which $L_0 \sim 1$ km works [23, 100]. However, the fact that a cat-encoded qubit only requires a single optical mode means that low success probabilities in a single repeater chain could be efficiently compensated via (e.g. broadband) parallelization or multiplexing.

α	L_0	F_{new}	P_{new}	F_{old}	P_{old}
4.0	0.01	0.99998900	≈ 0	0.999989	≈ 0
4.0	0.10	0.98944600	≈ 0	0.989275	10^{-76}
4.0	1.00	0.00473919	$3 \cdot 10^{-8}$	0.00232537	10^{-12}
4.5	0.01	0.99997000	≈ 0	0.99997	10^{-42}
4.5	0.10	0.97327800	0.00830884	0.972789	$7 \cdot 10^{-5}$
4.5	1.00	$9 \cdot 10^{-6}$	0.00880618	10^{-6}	$3 \cdot 10^{-3}$
5.0	0.01	0.99993100	≈ 0	0.999931	10^{-67}
5.0	0.10	0.94012200	$5 \cdot 10^{-4}$	0.87604	$2 \cdot 10^{-7}$
5.0	1.00	≈ 0	0.16894200	$6 \cdot 10^{-22}$	0.0847453
6.0	0.01	0.99970600	$5 \cdot 10^{-4}$	0.999705	$3 \cdot 10^{-7}$
6.0	0.10	0.77462700	0.46871500	0.771153	0.221926
6.0	1.00	≈ 0	0.89348900	$3 \cdot 10^{-36}$	0.843821

Table 7.1: Comparison between the "old" and the "new" schemes for a total distance of $\mathcal{L} = 1000$ km with the $L = 3$-code, L_0 in km. Color indicates near-feasible regimes. Here, "≈ 0" corresponds to $\lesssim 10^{-100}$.

α	L_0	F_{new}	P_{new}	F_{old}	P_{old}
6	0.01	0.999999	$3 \cdot 10^{-31}$	0.999999	10^{-61}
6	0.1	0.991757	$4 \cdot 10^{-4}$	0.991574	$4 \cdot 10^{-7}$
6	1.00	10^{-9}	0.0787418	$4 \cdot 10^{-11}$	0.0455329
7	0.01	0.999996	$6 \cdot 10^{-4}$	0.999996	$3 \cdot 10^{-7}$
7	0.1	0.963915	0.451687	0.96314	0.214877
7	1.00	$6 \cdot 10^{-28}$	0,755955	$3 \cdot 10^{-22}$	0.740854
8	0.01	0.999983	0.230988	0.999983	0.0531004
8	0.1	0.876309	0.867937	0.873809	0.74901
8	1.00	10^{-66}	0.979637	10^{-75}	0.977982

Table 7.2: Comparison between the "old" and the "new" schemes for a total distance of $\mathcal{L} = 1000$ km with the $L = 4$-code, L_0 in km. Color indicates feasible regimes.

α	L_0	F_{new}	P_{new}	F_{old}	P_{old}
6	0.01	1	≈ 0	1	≈ 0
6	0.1	0.999781	$4 \cdot 10^{-24}$	0.999776	10^{-47}
6	1.00	0.00639287	$3 \cdot 10^{-5}$	$3 \cdot 10^{-3}$	$6 \cdot 10^{-6}$
7	0.01	1	$3 \cdot 10^{-50}$	1	≈ 0
7	0.1	0.998659	$\cdot 10^{-5}$	0.998624	10^{-10}
7	1.00	$2 \cdot 10^{-9}$	0.06615	$4 \cdot 10^{-11}$	0.0759747
8	0.01	1	10^{-7}	1	$2 \cdot 10^{-14}$
8	0,1	0.99371	0.194448	0.993546	0.0417406
8	1.00	$4 \cdot 10^{-27}$	0.691036	10^{-31}	0.659869
9	0.01	1	$4 \cdot 10^{-3}$	1	$1.75 \cdot 10^{-5}$
9	0.1	0.975983	0.578119	0.97537	0.334447
9	1.00	$5 \cdot 10^{-64}$	0.963224	$4 \cdot 10^{-74}$	0.89103

Table 7.3: Comparison between the "old" and the "new" schemes for a total distance of $\mathcal{L} = 1000$ km with the $L = 5$-code, L_0 in km. Color indicates feasible regimes. Here, "≈ 0" corresponds to $\lesssim 10^{-100}$.

Chapter 8

Discussion and Conclusions

The main topic of this thesis is the possibility of suppressing and correcting the effect of photon loss on quantum optical states in optical fibers. We investigated various approaches for quantum error correction and detection.

We proposed a systematic approach for constructing a class of exact quantum error correcting codes for the amplitude-damping channel. Based on quantum optical NOON state resources, logical qubits can be encoded in a block code consuming a total of N^2 photons in N blocks. These codes are capable of correcting $N-1$ photon losses, which is the same scaling obtainable with existing exact loss codes for the same fixed total photon number. Nonetheless, only our codes have a total mode number and a maximal photon number per mode that both scale linearly with N.

All the presented exact codes have logical codewords that can be built from NOON states with linear optics. A method for the experimental generation of the $N^2 = 4$ qubit code including arbitrary logical qubits was also proposed. This method relies on the presence of an ion-trap ancilla system. Furthermore, the NOON code approach can be generalized to logical qudits of arbitrary dimension by increasing the mode number per block without losing the loss robustness, i.e. the fidelity always only depends on the total photon number N^2 and not on the dimension of the logical qudit. As for an application, this feature has been exploited in a one-way communication scheme in Section 7.3.1 where general qudit codes turn out to be beneficial in terms of the spatial resource cost.

We furthermore analyzed a generalized quantum error correction code against photon loss that is based on superpositions of coherent states. Our generalisation includes instances of such a cat code where errors from more than one-photon loss can be, in principle, approximately corrected. For the higher loss codes, however, the overlap of the codewords increases and must be compensated by an increasing coherent-state amplitude which results in a growing error rate. Thus, one encounters the usual trade-offs when a continuous-variable encoding is employed. We illustrated such an effect for the example of a one-way quantum communication scheme for

large distances based on cat codes in Section 7.3.2.

The non-orthogonality of the codewords could be entirely avoided by choosing a particular logical basis in the code space (the $\bar{X}$- instead of the $\bar{Z}$-basis), however, this would be at the expense of a deformation of the logical qubits for finite coherent-state amplitudes leading to a complicated and undesirable output density matrix. Our choice of the $\bar{Z}$-basis circumvents this deformation at the expense of non-zero codeword overlap. Another generalisation that we discussed for cat codes is for a higher-dimensional code space beyond logical qubits, i.e., qudits. Besides the above-mentioned two new types of loss codes, we introduced a hybrid quantum repeater protocol for the distribution of arbitrary finite-dimensional bipartite entangled states over large distances with a specific focus on qutrit entanglement. A generalization of the dispersive light-matter interaction from the qubit to the general qudit case is the essential ingredient of our protocol and can be expressed by higher spin operators. The distribution of matter-matter entanglement between neighboring repeater stations is mediated via coherent states interacting dispersively and subsequently with the matter systems. We investigated both unambiguous state discrimination and homodyne detection of the light mode and compared the entangled-state distribution rates and final fidelities. By exploiting entanglement purification on the elementary segments, sufficiently high initial fidelities can be achieved to cover distances up to 1280 km with final fidelities close to unity. With three rounds of entanglement purification directly after the initial entanglement distributions, rates ~ 100 Hz are, in principle, possible. This number corresponds to an upper bound on the performance of the quantum repeater, as we assumed perfect memories and local operations.

We furthermore generalized a teleportation-based scheme for the transmission of an unknown coherent state to large distances by exploiting chains of qubit quantum repeaters for the generation of long-distance resource entangled states. With this scheme, the same fidelity as in a loss-free scenario is obtained at the expense of a lower total success probability.

As another scheme, a light-matter interface between decoherence-free subspaces of trapped ions and QPC(2,2)-encoded photonic states is proposed on the basis of routinely available ion-light operations. Fragile photonic quantum information can therefore be faithfully stored in the ionic quantum memory.

There may be several drawbacks of the approaches presented in this thesis that will be part of future research. The main practical limitation for our proposed codes is that there is no simple and efficient method known for the experimental generation of qubit codes with higher loss resistance and for that of arbitrary qudit codes (including arbitrary logical quantum states). For NOON codes, this is, however, necessary for the presented one-way scheme, because for achieving a useful success probability at moderate intermediate distances $L_0 \sim 1$ km, a code with a total photon number of $N^2 = \mathcal{O}(100)$ will be required. In addition, the proposed QND-type measurement for syndrome identification and the corresponding recovery operation, possibly

implemented via encoded qudit quantum teleportation, are experimentally hard to achieve. In addition, for the cat codes, practical ways to achieve the coherent-state amplitude restorations (either by creating the encoded, entangled ancilla states, as proposed here, or by employing an alternative method) are still unknown.

Despite the usage of very efficient homodyne detection, the proposed qudit hybrid quantum repeater protocol relies upon idealizations. For example, the assumption of perfect memories with infinite coherence time may turn problematic in the realistic scenario. In fact, almost all quantum memories that have been demonstrated so far perform worse compared to a simple optical fiber loop [146]. Therefore, realistic imperfections for the quantum memories can be taken into account which might also be tackled by quantum error correction, as has been already considered for the qubit hybrid repeater protocol [96].

Besides the fact that a sufficiently strong dispersive matter-light interaction is already difficult to obtain in the qubit scenario,the physical mechanism behind our proposed generalization of this interaction to general qudits using spin operators is not entirely clear. For both cornerstones of the qudit hybrid quantum repeater, the memories and the interaction, considerably more research on the quantum optics side is necessary. Nonetheless, from a quantum information perspective, our scheme represents a step forward, because, as far as we know, it is the only existing proposal for an implementation of a quantum repeater that aims at distributing entanglement beyond that of qubits.

Though there are still a lot of things to be further explored, our research has already made a clear impact on the quantum communication community. After publication, our NOON codes have been, amongst the traditional bosonic codes and some other kinds of codes, recently referred to as a specific (sub-)class of codes within the framework of existing loss codes [47, 147, 148]. Sometimes, this subclass is denoted as `noon`.

The same is true for our cat codes, which form a superclass in the set of photon loss codes. However, opposite to our convention, usually the class of cat codes for which the codewords are expressed in the $\bar{X}$-basis (whereas our basis of choice is $\bar{Z}$) are denoted by `cat`. The main reason for this is the orthogonality of the codewords which allows for a deterministic recovery operation (as opposed to our probabilistic scheme).

On the conceptual level, photon loss codes protecting continuous-variable states would be, in addition, highly desired to overcome the inefficiency of typical schemes like the proposed long-distance teleporter and to make continuous-variable third-generation quantum repeaters possible.

The future certainly offers more interesting research directions in the field of optical quantum error correction and communication, not only limited to pure applications but also including exciting physical effects and environments [149].

Appendix A

Appendices to Chapter 5

A.1   Inefficiency of the N=3 two-block code

By calculating the corrupted codewords, the violation of the KL conditions becomes manifest:

$$A_0 \otimes A_0 \otimes A_0 \otimes A_0 |\bar{\Psi}\rangle = \sqrt{\gamma^6}|\bar{\Psi}\rangle,$$

$$A_1 \otimes A_0 \otimes A_0 \otimes A_0 |\bar{\Psi}\rangle = \sqrt{\frac{3}{2}\gamma^5(1-\gamma)}\left(c_0\frac{1}{\sqrt{2}}(|20\rangle + |02\rangle)|\widetilde{0}\rangle + c_1|11\rangle|\widetilde{1}\rangle\right),$$

$$A_0 \otimes A_1 \otimes A_0 \otimes A_0 |\bar{\Psi}\rangle = \sqrt{\frac{3}{2}\gamma^5(1-\gamma)}\left(c_0|11\rangle|\widetilde{0}\rangle + c_1\frac{1}{\sqrt{2}}(|20\rangle + |02\rangle)|\widetilde{1}\rangle\right),$$

$$A_0 \otimes A_0 \otimes A_1 \otimes A_0 |\bar{\Psi}\rangle = \sqrt{\frac{3}{2}\gamma^5(1-\gamma)}\left(c_0|\widetilde{0}\rangle\frac{1}{\sqrt{2}}(|20\rangle + |02\rangle) + c_1|\widetilde{1}\rangle|11\rangle\right),$$

$$A_0 \otimes A_0 \otimes A_0 \otimes A_1 |\bar{\Psi}\rangle = \sqrt{\frac{3}{2}\gamma^5(1-\gamma)}\left(c_0|\widetilde{0}\rangle|11\rangle + c_1|\widetilde{1}\rangle\frac{1}{\sqrt{2}}(|20\rangle + |02\rangle)\right),$$

$$A_1 \otimes A_1 \otimes A_0 \otimes A_0 |\bar{\Psi}\rangle = \sqrt{\frac{3}{2}\gamma^4(1-\gamma)^2}\left(c_0|01\rangle|\widetilde{0}\rangle + c_1|10\rangle|\widetilde{1}\rangle\right),$$

$$A_0 \otimes A_0 \otimes A_1 \otimes A_1 |\bar{\Psi}\rangle = \sqrt{\frac{3}{2}\gamma^4(1-\gamma)^2}\left(c_0|\widetilde{0}\rangle|01\rangle + c_1|\widetilde{1}\rangle|10\rangle\right),$$

$$A_2 \otimes A_0 \otimes A_0 \otimes A_0 |\bar{\Psi}\rangle = \frac{\sqrt{3}}{2}\sqrt{\gamma^4(1-\gamma)^2}\left(c_0|10\rangle|\widetilde{0}\rangle + c_1|01\rangle|\widetilde{1}\rangle\right),$$

$$A_0 \otimes A_2 \otimes A_0 \otimes A_0 |\bar{\Psi}\rangle = \frac{\sqrt{3}}{2}\sqrt{\gamma^4(1-\gamma)^2}\left(c_0|10\rangle|\widetilde{0}\rangle + c_1|01\rangle|\widetilde{1}\rangle\right),$$

$$A_0 \otimes A_0 \otimes A_2 \otimes A_0 |\bar{\Psi}\rangle = \frac{\sqrt{3}}{2}\sqrt{\gamma^4(1-\gamma)^2}\left(c_0|\widetilde{0}\rangle|10\rangle + c_1|\widetilde{1}\rangle|01\rangle\right), \tag{A.1}$$

$$A_0 \otimes A_0 \otimes A_0 \otimes A_2 |\bar{\Psi}\rangle = \frac{\sqrt{3}}{2}\sqrt{\gamma^4(1-\gamma)^2}\left(c_0|\widetilde{0}\rangle|10\rangle + c_1|\widetilde{1}\rangle|01\rangle\right),$$

$$A_1 \otimes A_0 \otimes A_1 \otimes A_0 |\bar{\Psi}\rangle = \frac{3}{2}\sqrt{\gamma^4(1-\gamma)^2}\left(c_0\frac{1}{\sqrt{2}}(|20\rangle + |02\rangle)\frac{1}{\sqrt{2}}(|20\rangle + |02\rangle)) + c_1|1111\rangle\right),$$

$$A_0 \otimes A_1 \otimes A_0 \otimes A_1 |\bar{\Psi}\rangle = \frac{3}{2}\sqrt{\gamma^4(1-\gamma)^2}\left(c_1\frac{1}{\sqrt{2}}(|20\rangle + |02\rangle)\frac{1}{\sqrt{2}}(|20\rangle + |02\rangle) + c_0|1111\rangle\right),$$

$$A_0 \otimes A_1 \otimes A_1 \otimes A_0 |\bar{\Psi}\rangle = \frac{3}{2}\sqrt{\gamma^4(1-\gamma)^2}\left(c_0|11\rangle\frac{1}{\sqrt{2}}(|20\rangle + |02\rangle) + c_1\frac{1}{\sqrt{2}}(|20\rangle + |02\rangle)|11\rangle\right),$$

$$A_1 \otimes A_0 \otimes A_0 \otimes A_1 |\bar{\Psi}\rangle = \frac{3}{2}\sqrt{\gamma^4(1-\gamma)^2}\left(c_1|11\rangle\frac{1}{\sqrt{2}}(|20\rangle + |02\rangle) + c_0\frac{1}{\sqrt{2}}(|20\rangle + |02\rangle)|11\rangle\right).$$

Note that, for example, the corrupted logical basis states in the last two lines are, in general, not orthogonal such that a recovery is not possible. This means that, besides all one-photon losses, only certain two-photon-loss errors are correctable which gives a worst-case fidelity of $F \approx 1 - 9(1-\gamma)^2$. This result is still worse compared to our $N = 2$ four-photon, two-block code.

A.2 Alternative NOON code construction

A.2.1 Qubit codes

The action of the AD channel on the codewords $|\bar{0}\rangle = \left[\frac{1}{\sqrt{2}}(|20\rangle + |02\rangle)\right]^{\otimes 2} = \frac{1}{2}(|2020\rangle + |2002\rangle + |0220\rangle + |0202\rangle)$ and $|\bar{1}\rangle = \left[\frac{1}{\sqrt{2}}(|20\rangle - |02\rangle)\right]^{\otimes 2} = \frac{1}{2}(|2020\rangle - |2002\rangle - |0220\rangle + |0202\rangle)$ is

$$
\begin{aligned}
A_0 \otimes A_0 \otimes A_0 \otimes A_0 |\bar{0}\rangle &= \sqrt{\gamma^4}|\bar{0}\rangle, \\
A_0 \otimes A_0 \otimes A_0 \otimes A_0 |\bar{1}\rangle &= \sqrt{\gamma^4}|\bar{1}\rangle, \\
A_1 \otimes A_0 \otimes A_0 \otimes A_0 |\bar{0}\rangle &= \sqrt{\gamma^3(1-\gamma)}\frac{1}{\sqrt{2}}(|1020\rangle + |1002\rangle), \\
A_1 \otimes A_0 \otimes A_0 \otimes A_0 |\bar{1}\rangle &= \sqrt{\gamma^3(1-\gamma)}\frac{1}{\sqrt{2}}(|1020\rangle - |1002\rangle), \\
A_0 \otimes A_1 \otimes A_0 \otimes A_0 |\bar{0}\rangle &= \sqrt{\gamma^3(1-\gamma)}\frac{1}{\sqrt{2}}(|0120\rangle + |0102\rangle), \\
A_0 \otimes A_1 \otimes A_0 \otimes A_0 |\bar{1}\rangle &= \sqrt{\gamma^3(1-\gamma)}\frac{1}{\sqrt{2}}(-|0120\rangle + |0102\rangle), \quad\quad (A.2)\\
A_0 \otimes A_0 \otimes A_1 \otimes A_0 |\bar{0}\rangle &= \sqrt{\gamma^3(1-\gamma)}\frac{1}{\sqrt{2}}(|0210\rangle + |2010\rangle), \\
A_0 \otimes A_0 \otimes A_1 \otimes A_0 |\bar{1}\rangle &= \sqrt{\gamma^3(1-\gamma)}\frac{1}{\sqrt{2}}(-|0210\rangle + |2010\rangle), \\
A_0 \otimes A_0 \otimes A_0 \otimes A_1 |\bar{0}\rangle &= \sqrt{\gamma^3(1-\gamma)}\frac{1}{\sqrt{2}}(|2001\rangle + |0201\rangle), \\
A_0 \otimes A_0 \otimes A_0 \otimes A_1 |\bar{1}\rangle &= \sqrt{\gamma^3(1-\gamma)}\frac{1}{\sqrt{2}}(-|2001\rangle + |0201\rangle).
\end{aligned}
$$

Obviously, this also defines a quantum error correcting code which can correct the loss of one photon. Since the fidelity only depends on the photon number in the codewords, one obtains the same result as for the other $N^2 = 4$ code.

Similar to the code construction presented in the main text, the extension to codes with higher loss protection works by building blocks of NOON states with higher photon number. For a total photon number $N^2 = 9$, the logical basis states read

$$|\bar{0}\rangle = \left(\frac{1}{\sqrt{2}}(|30\rangle + |03\rangle)\right)^{\otimes 3} \tag{A.3}$$

$$= \frac{1}{2\sqrt{2}}(|303030\rangle + |303003\rangle + |300330\rangle + |300303\rangle + |033030\rangle + |033003\rangle$$

$$+ |030330\rangle + |030303\rangle),$$

$$|\bar{1}\rangle = \left(\frac{1}{\sqrt{2}}(|30\rangle - |03\rangle)\right)^{\otimes 3} \tag{A.4}$$

$$= \frac{1}{2\sqrt{2}}(|303030\rangle - |303003\rangle - |300330\rangle + |300303\rangle - |033030\rangle + |033003\rangle$$

$$+ |030330\rangle - |030303\rangle).$$

It is not difficult to show that this encoding also represents a quantum error correction code, this time capable of correcting up to two-photon losses.

In general,

$$|\bar{0}\rangle = \left(\frac{1}{\sqrt{2}}(|N0\rangle + |0N\rangle)\right)^{\otimes N},$$

$$|\bar{1}\rangle = \left(\frac{1}{\sqrt{2}}(|N0\rangle - |0N\rangle)\right)^{\otimes N}, \tag{A.5}$$

defines a quantum code correcting $N - 1$ photon losses using N^2 total photons.

A.2.2   Qudit codes

The idea for the qubit code construction can be directly generalized to arbitrary qudit codes. Consider $d = 3$ and $N = 2$ and the qutrit Hadamard transformation H_3. Then we choose

$$|\widetilde{0}\rangle = H_3(|200\rangle) = \frac{1}{\sqrt{3}}(|200\rangle + |020\rangle + |002\rangle),$$

$$|\widetilde{1}\rangle = H_3(|020\rangle) = \frac{1}{\sqrt{3}}(|200\rangle + \exp\left(\frac{2\pi i}{3}\right)|020\rangle + \exp\left(\frac{4\pi i}{3}\right)|002\rangle), \tag{A.6}$$

$$|\widetilde{2}\rangle = H_3(|002\rangle) = \frac{1}{\sqrt{3}}(|200\rangle + \exp\left(\frac{4\pi i}{3}\right)|020\rangle + \exp\left(\frac{8\pi i}{3}\right)|002\rangle),$$

and build the blocks to construct the basis codewords,

$$\begin{aligned} |\bar{0}\rangle &= |\widetilde{0}\rangle|\widetilde{0}\rangle, \\ |\bar{1}\rangle &= |\widetilde{1}\rangle|\widetilde{1}\rangle, \\ |\bar{2}\rangle &= |\widetilde{2}\rangle|\widetilde{2}\rangle. \end{aligned} \tag{A.7}$$

It is easy to check that this is a qutrit quantum error correction code, because the loss of a single photon on an individual block gives

$$\begin{aligned} A_1 \otimes A_0 \otimes A_0 |\widetilde{0}\rangle &= A_1 \otimes A_0 \otimes A_0 |\widetilde{1}\rangle, = A_1 \otimes A_0 \otimes A_0 |\widetilde{2}\rangle = \frac{1}{\sqrt{3}}\sqrt{\gamma^3(1-\gamma)}|100\rangle, \\ A_0 \otimes A_1 \otimes A_0 |\widetilde{0}\rangle &= \frac{1}{\sqrt{3}}\sqrt{\gamma^3(1-\gamma)}|010\rangle, \\ A_0 \otimes A_1 \otimes A_0 |\widetilde{1}\rangle &= \frac{1}{\sqrt{3}}\sqrt{\gamma^3(1-\gamma)}\exp\left(\frac{2\pi i}{3}\right)|010\rangle, \\ A_0 \otimes A_1 \otimes A_0 |\widetilde{2}\rangle &= \frac{1}{\sqrt{3}}\sqrt{\gamma^3(1-\gamma)}\exp\left(\frac{4\pi i}{3}\right)|010\rangle, \\ A_0 \otimes A_0 \otimes A_1 |\widetilde{0}\rangle &= \frac{1}{\sqrt{3}}\sqrt{\gamma^3(1-\gamma)}|001\rangle, \\ A_0 \otimes A_0 \otimes A_1 |\widetilde{1}\rangle &= \frac{1}{\sqrt{3}}\sqrt{\gamma^3(1-\gamma)}\exp\left(\frac{4\pi i}{3}\right)|001\rangle, \\ A_0 \otimes A_0 \otimes A_1 |\widetilde{2}\rangle &= \frac{1}{\sqrt{3}}\sqrt{\gamma^3(1-\gamma)}\exp\left(\frac{8\pi i}{3}\right)|001\rangle, \end{aligned} \tag{A.8}$$

which proves the non-deformation of corrupted codewords. The orthogonality is ensured by the block structure.

To construct a general qudit code, we set

$$\begin{aligned} |\bar{0}\rangle_{N,d} &= [H_d(|N000...\rangle)]^{\otimes N}, \\ |\bar{1}\rangle_{N,d} &= [H_d(|0N00...\rangle)]^{\otimes N}, \\ &\vdots \\ |\overline{d-1}\rangle_{N,d} &= [H_d(|000...0N\rangle)]^{\otimes N}, \end{aligned} \tag{A.9}$$

which is again a qudit code correcting $N-1$ photon losses using N^2 total photons.

Appendix B

Appendices to Chapter 6

B.1 Full loss channel and KL conditions for the one-loss cat code

Let us first consider the simplified set of errors $\mathcal{E} = \{\hat{a}^{4k}, \hat{a}^{4k+1}, k \in \mathbb{N}_0\}$. For the even-cat codewords of Eq. (6.1) (i.e., the "$\bar{Z}$-basis"), we have the following KL conditions:

$$
\begin{aligned}
\langle \bar{0}_+|(\hat{a}^{4k})^\dagger \hat{a}^{4k}|\bar{1}_+\rangle =& i^{4k}(\alpha^2)^{4k} \frac{1}{\sqrt{N_+}}(\langle\alpha| + \langle-\alpha|) \cdot \frac{1}{\sqrt{N_+}}(|i\alpha\rangle + |-i\alpha\rangle) \\
=& \frac{(\alpha^2)^{4k}}{N_+} \left(\langle\alpha|i\alpha\rangle + \langle\alpha|-i\alpha\rangle + \langle-\alpha|i\alpha\rangle + \langle-\alpha|-i\alpha\rangle \right) \\
=& \frac{(\alpha^2)^{4k}}{N_+} \left(\exp(-\alpha^2)\exp(i\alpha^2) + \exp(-\alpha^2)\exp(-i\alpha^2) + \exp(-\alpha^2)\exp(-i\alpha^2) \right. \\
& \left. + \exp(-\alpha^2)\exp(i\alpha^2) \right) \\
=& \frac{2(\alpha^2)^{4k}\exp(-\alpha^2)}{N_+} \left(\exp(i\alpha^2) + \exp(-i\alpha^2) \right) \\
=& \frac{4(\alpha^2)^{4k}\exp(-\alpha^2)}{N_+}\cos(\alpha^2) \\
=& \frac{4(\alpha^2)^{4k}\exp(-\alpha^2)}{4\exp(-\alpha^2)\cosh(\alpha^2)}\cos(\alpha^2) = \frac{(\alpha^2)^{4k}\cos(\alpha^2)}{\cosh(\alpha^2)},
\end{aligned}
\tag{B.1}
$$

$$
\langle \bar{0}_+|(\hat{a}^{4k})^\dagger \hat{a}^{4k}|\bar{0}_+\rangle = \langle \bar{1}_+|(\hat{a}^{4k})^\dagger \hat{a}^{4k}|\bar{1}_+\rangle = (\alpha^2)^{4k},
\tag{B.2}
$$

$$
\begin{aligned}
\langle \bar{0}_+|(\hat{a}^{4k})^\dagger \hat{a}^{4k+1}|\bar{0}_+\rangle &= \langle \bar{0}_+|(\hat{a}^{4k})^\dagger \hat{a}^{4k+1}|\bar{1}_+\rangle \\
&= \langle \bar{1}_+|(\hat{a}^{4k})^\dagger \hat{a}^{4k+1}|\bar{1}_+\rangle = \langle \bar{1}_+|(\hat{a}^{4k})^\dagger \hat{a}^{4k+1}|\bar{0}_+\rangle = 0,
\end{aligned}
\tag{B.3}
$$

$$\langle\bar{0}_+|(\hat{a}^{4k+1})^\dagger \hat{a}^{4k+1}|\bar{1}_+\rangle = \frac{1}{N_+}(\langle\alpha| + \langle-\alpha|)(\hat{a}^{4k+1})^\dagger \hat{a}^{4k+1}(|i\alpha\rangle + |-i\alpha\rangle)$$

$$= \frac{i(\alpha^2)^{4k+1}}{N_+}(\langle\alpha| - \langle-\alpha|)(|i\alpha\rangle - |-i\alpha\rangle)$$

$$= \frac{i(\alpha^2)^{4k+1}}{N_+}\left(\exp(-\alpha^2)\exp(i\alpha^2) - \exp(-\alpha^2)\exp(-i\alpha^2)\right.$$

$$\left. - \exp(-\alpha^2)\exp(-i\alpha^2) + \exp(-\alpha^2)\exp(i\alpha^2)\right) \qquad \text{(B.4)}$$

$$= \frac{2i(\alpha^2)^{4k+1}\exp(-\alpha^2)}{N_+}\left(\exp(i\alpha^2) - \exp(-i\alpha^2)\right)$$

$$= -\frac{4(\alpha^2)^{4k+1}\exp(-\alpha^2)}{N_+}\sin(\alpha^2)$$

$$= -\frac{(\alpha^2)^{4k+1}\sin(\alpha^2)}{\cosh(\alpha^2)},$$

$$\langle\bar{0}_+|(\hat{a}^{4k+1})^\dagger \hat{a}^{4k+1}|\bar{0}_+\rangle = \langle\bar{1}_+|(\hat{a}^{4k+1})^\dagger \hat{a}^{4k+1}|\bar{1}_+\rangle = \frac{(\alpha^2)^{4k+1}N_-}{N_+}, \qquad \text{(B.5)}$$

Written in the Fock basis, the basic codewords read

$$|\bar{0}_+\rangle = \frac{1}{\sqrt{\cosh(\alpha^2)}}\sum_{n=0}^{\infty}\frac{\alpha^{2n}}{\sqrt{(2n)!}}|2n\rangle,$$

$$|\bar{1}_+\rangle = \frac{1}{\sqrt{\cosh(\alpha^2)}}\sum_{n=0}^{\infty}\frac{(-1)^n\alpha^{2n}}{\sqrt{(2n)!}}|2n\rangle. \qquad \text{(B.6)}$$

Like in the annihilation operator model, it is useful to study even and odd losses on the codewords separately:

$$A_{2m}|\bar{0}_+\rangle = \frac{1}{\sqrt{\cosh(\alpha^2)}}\sum_{n=m}^{\infty}\frac{\alpha^{2n}}{\sqrt{(2n)!}}\sqrt{\gamma}^{2n-2m}\sqrt{1-\gamma}^{2m}\sqrt{\frac{(2n)!}{(2n-2m)!(2m)!}}|2n-2m\rangle$$

$$= \frac{1}{\sqrt{\cosh(\alpha^2)}}\sum_{n=m}^{\infty}\frac{\alpha^{2n}}{\sqrt{(2n-2m)!(2m)!}}\sqrt{\gamma}^{2n-2m}\sqrt{1-\gamma}^{2m}|2n-2m\rangle$$

$$= \frac{1}{\sqrt{(2m)!}\sqrt{\cosh(\alpha^2)}}\sqrt{1-\gamma}^{2m}\alpha^{2m}\sum_{l=0}^{\infty}\frac{\alpha^{2l}}{\sqrt{(2l)!}}\sqrt{\gamma}^{2l}|2l\rangle \qquad \text{(B.7)}$$

$$= \sqrt{\frac{\cosh(\alpha^2\gamma)}{\cosh(\alpha^2)}}\frac{\sqrt{1-\gamma}^{2m}\alpha^{2m}}{\sqrt{(2m)!}}|\widetilde{0}_+\rangle,$$

$$A_{2m}|\bar{1}_+\rangle = \frac{1}{\sqrt{\cosh(\alpha^2)}} \sum_{n=m}^{\infty} \frac{i^{2n}\alpha^{2n}}{\sqrt{(2n)!}} \sqrt{\gamma}^{2n-2m} \sqrt{1-\gamma}^{2m} \sqrt{\frac{(2n)!}{(2n-2m)!(2m)!}} |2n-2m\rangle$$

$$= \frac{1}{\sqrt{\cosh(\alpha^2)}} \sum_{n=m}^{\infty} \frac{i^{2n}\alpha^{2n}}{\sqrt{(2n-2m)!(2m)!}} \sqrt{\gamma}^{2n-2m} \sqrt{1-\gamma}^{2m} |2n-2m\rangle$$

$$= \frac{1}{\sqrt{(2m)!}\sqrt{\cosh(\alpha^2)}} \sqrt{1-\gamma}^{2m} \alpha^{2m} i^{2m} \sum_{l=0}^{\infty} (-1)^l \frac{\alpha^{2l}}{\sqrt{(2l)!}} \sqrt{\gamma}^{2l} |2l\rangle$$

$$= \sqrt{\frac{\cosh(\alpha^2\gamma)}{\cosh(\alpha^2)}} \frac{\sqrt{1-\gamma}^{2m}\alpha^{2m}i^{2m}}{\sqrt{(2m)!}} |\widetilde{1}_+\rangle, \tag{B.8}$$

$$A_{2m+1}|\bar{0}_+\rangle = \frac{1}{\sqrt{\cosh(\alpha^2)}}$$

$$\times \sum_{n=m+1}^{\infty} \frac{\alpha^{2n}}{\sqrt{(2n)!}} \sqrt{\gamma}^{2n-2m-1} \sqrt{1-\gamma}^{2m+1} \sqrt{\frac{(2n)!}{(2n-2m-1)!(2m+1)!}} |2n-2m-1\rangle$$

$$= \frac{1}{\sqrt{\cosh(\alpha^2)}} \sum_{n=m+1}^{\infty} \frac{\alpha^{2n}}{\sqrt{(2n-2m-1)!(2m+1)!}} \sqrt{\gamma}^{2n-2m-1} \sqrt{1-\gamma}^{2m+1} |2n-2m-1\rangle$$

$$= \frac{1}{\sqrt{(2m)!}\sqrt{\cosh(\alpha^2)}} \sqrt{1-\gamma}^{2m+1} \alpha^{2m+1} \sum_{l=0}^{\infty} \frac{\alpha^{2l+1}}{\sqrt{(2l+1)!}} \sqrt{\gamma}^{2l+1} |2l+1\rangle$$

$$= \sqrt{\frac{\sinh(\alpha^2\gamma)}{\cosh(\alpha^2)}} \frac{\sqrt{1-\gamma}^{2m+1}\alpha^{2m+1}}{\sqrt{(2m+1)!}} |\widetilde{0}_-\rangle, \tag{B.9}$$

$$A_{2m+1}|\bar{1}_+\rangle = \frac{1}{\sqrt{\cosh(\alpha^2)}}$$

$$\times \sum_{n=m+1}^{\infty} \frac{i^{2n}\alpha^{2n}}{\sqrt{(2n)!}} \sqrt{\gamma}^{2n-2m-1} \sqrt{1-\gamma}^{2m+1} \sqrt{\frac{(2n)!}{(2n-2m-1)!(2m+1)!}} |2n-2m-1\rangle$$

$$= \frac{1}{\sqrt{\cosh(\alpha^2)}} \sum_{n=m}^{\infty} \frac{i^{2n}\alpha^{2n}}{\sqrt{(2n-2m-1)!(2m+1)!}} \sqrt{\gamma}^{2n-2m-1} \sqrt{1-\gamma}^{2m+1} |2n-2m-1\rangle$$

$$= \frac{1}{\sqrt{(2m)!}\sqrt{\cosh(\alpha^2)}} \sqrt{1-\gamma}^{2m+1} \alpha^{2m+1} i^{2m+1} \sum_{l=0}^{\infty} (-1)^l \frac{\alpha^{2l+1}}{\sqrt{(2l+1)!}} \sqrt{\gamma}^{2l} |2l+1\rangle$$

$$= \sqrt{\frac{\sinh(\alpha^2\gamma)}{\cosh(\alpha^2)}} \frac{\sqrt{1-\gamma}^{2m+1}\alpha^{2m+1}i^{2m+1}}{\sqrt{(2m+1)!}} |\widetilde{1}_-\rangle. \tag{B.10}$$

One can easily verify that the norms of corrupted codewords are identical, i.e. the logical

qubits are not deformed after loss. Qualitatively, we find the same cyclic behavior as in the simplified loss model. Note however, that the logical codewords in the different error spaces are not orthogonal for finite α. The encoding presented here is therefore not an exact QEC but can be regarded as an approximate QECC, provided α is taken sufficiently large to ensure near-orthogonality.

From the expressions above, the probabilities for individual losses on the codewords can easily be determined by calculating the corresponding squared norm:

$$
\begin{aligned}
p_0 &= \frac{\cosh(\alpha^2\gamma)}{\cosh(\alpha^2)} \sum_{m=0,2,4,}^{\infty} \frac{((1-\gamma)|\alpha|^2)^{2m}}{(2m)!} \\
&= \frac{\cosh(\gamma\alpha^2)}{2\cosh(\alpha^2)} \left(\cos(\alpha^2(1-\gamma)) + \cosh(\alpha^2(1-\gamma))\right), \\
p_1 &= \frac{\sinh(\alpha^2\gamma)}{\cosh(\alpha^2)} \sum_{m=0,2,4,}^{\infty} \frac{((1-\gamma)\alpha^2)^{2m+1}}{(2m+1)!} \\
&= \frac{\sinh(\gamma\alpha^2)}{2\cosh(\alpha^2)} \left(\sin(\alpha^2(1-\gamma)) + \sinh(\alpha^2(1-\gamma))\right), \\
p_2 &= \frac{\cosh(\alpha^2\gamma)}{\cosh(\alpha^2)} \sum_{m=1,3,5,}^{\infty} \frac{((1-\gamma)\alpha^2)^{2m}}{(2m)!} \\
&= \frac{\cosh(\gamma\alpha^2)}{2\cosh(\alpha^2)} \left(-\cos(\alpha^2(1-\gamma)) + \cosh(\alpha^2(1-\gamma))\right), \\
p_3 &= \frac{\sinh(\alpha^2\gamma)}{\cosh(\alpha^2)} \sum_{m=1,3,5,}^{\infty} \frac{((1-\gamma)\alpha^2)^{2m+1}}{(2m+1)!} \\
&= \frac{\sinh(\gamma\alpha^2)}{2\cosh(\alpha^2)} \left(-\sin(\alpha^2(1-\gamma)) + \sinh(\alpha^2(1-\gamma))\right).
\end{aligned}
\tag{B.11}
$$

Note that p_0 contains the probability for no loss, four losses, eight losses and so on.

We are interested in the evolution of a logical qubit subject to photon loss. Taking the finite overlap of the codewords into account, a properly normalized qubit reads as

$$
|\bar{\psi}\rangle = \frac{a|\bar{0}_+\rangle + b|\bar{1}_+\rangle}{\sqrt{1 + 2\operatorname{Re}(ab^*)\langle\bar{0}_+|\bar{1}_+\rangle}}.
\tag{B.12}
$$

The codewords are not deformed, such that after a loss, say one loss and the cyclic equivalents, a global factor p_1 arises. In addition to that, we have to take the non-orthogonality of the codewords in the error spaces into account, i.e. we have to properly renormalize the erroneous state. In this example, we get a relative phase of i which changes the norm of the qubit as well as the damped amplitude:

$$
A_1|\bar{\psi}\rangle = \sqrt{\frac{1 - 2\operatorname{Re}(a^*b)\frac{\sin(\gamma\alpha^2)}{\sinh(\gamma\alpha^2)}}{1 + 2\operatorname{Re}(ab^*)\frac{\cos(\alpha^2)}{\cosh(\alpha^2)}} p_1} \left(\frac{a|\widetilde{0}_-\rangle + ib|\widetilde{1}_-\rangle}{\sqrt{1 - 2\operatorname{Re}(a^*b)\frac{\sin(\gamma\alpha^2)}{\sinh(\gamma\alpha^2)}}}\right).
\tag{B.13}
$$

The loss probability is therefore

$$\widetilde{p}_1 = \frac{1 - 2\operatorname{Re}(a^*b)\frac{\sin(\gamma\alpha^2)}{\sinh(\gamma\alpha^2)}}{1 + 2\operatorname{Re}(ab^*)\frac{\cos(\alpha^2)}{\cosh(\alpha^2)}} p_1. \tag{B.14}$$

and the normalized state reads

$$\left(\frac{a|\widetilde{0}_-\rangle + ib|\widetilde{1}_-\rangle}{\sqrt{1 - 2\operatorname{Re}(a^*b)\frac{\sin(\gamma\alpha^2)}{\sinh(\gamma\alpha^2)}}} \right). \tag{B.15}$$

The analogous results for the loss probabilities and the total final mixed states are summarized in the main text.

For comparison, let us investigate the KL conditions for the codewords in the $\bar{X}$-basis (see also the discussion after Eq. (6.4) in the main text):

$$\begin{aligned}
|\bar{0}_+ + \bar{1}_+\rangle &= \frac{1}{\sqrt{N'_+}}(|\bar{0}_+\rangle + |\bar{1}_+\rangle), \\
|\bar{0}_+ - \bar{1}_+\rangle &= \frac{1}{\sqrt{N'_-}}(|\bar{0}_+\rangle - |\bar{1}_+\rangle).
\end{aligned} \tag{B.16}$$

We consider again the error set $\mathcal{E} = \{\hat{a}^{4k}, \hat{a}^{4k+1}, k \in \mathbb{N}_0\}$. The action on the $\bar{X}$-basis codewords can be easily calculated based on the results of the $\bar{Z}$-basis analysis:

$$\begin{aligned}
\hat{a}^{4k}|\bar{0}_+ + \bar{1}_+\rangle &= \alpha^{4k}|\bar{0}_+ + \bar{1}_+\rangle = \frac{\alpha^{4k}}{\sqrt{N'_+}}(|\bar{0}_+\rangle + |\bar{1}_+\rangle), \\
\hat{a}^{4k}|\bar{0}_+ - \bar{1}_+\rangle &= \alpha^{4k}|\bar{0}_+ - \bar{1}_+\rangle = \frac{\alpha^{4k}}{\sqrt{N'_-}}(|\bar{0}_+\rangle - |\bar{1}_+\rangle), \\
\hat{a}^{4k+1}|\bar{0}_+ + \bar{1}_+\rangle &= \frac{\alpha^{4k+1}}{\sqrt{N'_+}}(|\bar{0}_-\rangle + i|\bar{1}_-\rangle), \\
\hat{a}^{4k+1}|\bar{0}_+ + \bar{1}_+\rangle &= \frac{\alpha^{4k+1}}{\sqrt{N'_-}}(|\bar{0}_-\rangle - i|\bar{1}_-\rangle).
\end{aligned} \tag{B.17}$$

The orthogonality requirements are fulfilled, as

$$\begin{aligned}
\langle\bar{0}_+ + \bar{1}_+|(\hat{a}^{4k})^\dagger\hat{a}^{4k}|\bar{0}_+ - \bar{1}_+\rangle &= \langle\bar{0}_+ + \bar{1}_+|(\hat{a}^{4k+1})^\dagger\hat{a}^{4k+1}|\bar{0}_+ - \bar{1}_+\rangle \\
&= \langle\bar{0}_+ + \bar{1}_+|(\hat{a}^{4k+1})^\dagger\hat{a}^{4k}|\bar{0}_+ - \bar{1}_+\rangle \\
&= \langle\bar{0}_+ - \bar{1}_+|(\hat{a}^{4k+1})^\dagger\hat{a}^{4k}|\bar{0}_+ + \bar{1}_+\rangle.
\end{aligned} \tag{B.18}$$

The non-deformation criterion for $\hat{a}^{4k}$ reads

$$\langle\bar{0}_+ + \bar{1}_+|(\hat{a}^{4k})^\dagger\hat{a}^{4k}|\bar{0}_+ - \bar{1}_+\rangle = \langle\bar{0}_+ - \bar{1}_+|(\hat{a}^{4k})^\dagger\hat{a}^{4k}|\bar{0}_+ - \bar{1}_+\rangle = (\alpha^2)^{4k}. \tag{B.19}$$

101

However, for $\hat{a}^{4k+1}$, we have

$$
\begin{aligned}
\langle \bar{0}_+ + \bar{1}_+ | (\hat{a}^{4k+1})^\dagger \hat{a}^{4k+1} | \bar{0}_+ + \bar{1}_+ \rangle &= \frac{2(\alpha^2)^{4k+1}}{N'_+} \left(1 - \frac{\sin(\alpha^2)}{\sinh(\alpha^2)} \right), \\
\langle \bar{0}_+ - \bar{1}_+ | (\hat{a}^{4k+1})^\dagger \hat{a}^{4k+1} | \bar{0}_+ - \bar{1}_+ \rangle &= \frac{2(\alpha^2)^{4k+1}}{N'_-} \left(1 + \frac{\sin(\alpha^2)}{\sinh(\alpha^2)} \right),
\end{aligned}
\tag{B.20}
$$

which shows a violation of the non-deformation criterion. This can only be overcome with sufficiently large α.

B.2 Error correction steps and lower bound on fidelity

We discuss the error correction procedure and the fidelity as a figure of merit for the example of the one-loss cat code. An extension to the higher-loss codes is straightforward.

The first step for correcting loss-induced errors on an incoming logical qubit is to determine its photon number parity (even or odd) and hence the subspace in which the qubit resides (code or error space). After this first error-correction step, i.e., the number parity measurement that projects $\bar{\rho}$ either onto the even space with the normalized conditional density matrix

$$
\begin{aligned}
\rho^{(+)} = \frac{1}{P^+} \Bigg[&\widetilde{p}_0 \left(\frac{a|\widetilde{0}_+\rangle + b|\widetilde{1}_+\rangle}{\sqrt{1 + 2\operatorname{Re}(ab^*)\frac{\cos(\gamma\alpha^2)}{\cosh(\gamma\alpha^2)}}} \right) \times H.c. \\
+ &\widetilde{p}_2 \left(\frac{a|\widetilde{0}_+\rangle - b|\widetilde{1}_+\rangle}{\sqrt{1 - 2\operatorname{Re}(ab^*)\frac{\cos(\gamma\alpha^2)}{\cosh(\gamma\alpha^2)}}} \right) \times H.c. \Bigg],
\end{aligned}
\tag{B.21}
$$

or onto the odd space with the corresponding density matrix

$$
\begin{aligned}
\rho^{(-)} = \frac{1}{P^-} \Bigg[&\widetilde{p}_1 \left(\frac{a|\widetilde{0}_-\rangle + ib|\widetilde{1}_-\rangle}{\sqrt{1 - 2\operatorname{Re}(ab^*)\frac{\sin(\gamma\alpha^2)}{\sinh(\gamma\alpha^2)}}} \right) \times H.c. \\
+ &\widetilde{p}_3 \left(\frac{a|\widetilde{0}_-\rangle - ib|\widetilde{1}_-\rangle}{\sqrt{1 + 2\operatorname{Re}(ab^*)\frac{\sin(\gamma\alpha^2)}{\sinh(\gamma\alpha^2)}}} \right) \times H.c. \Bigg],
\end{aligned}
\tag{B.22}
$$

as a second step, the amplitudes are probabilistically restored, $|\widetilde{0}_+\rangle \to |\bar{0}_+\rangle$, etc. (see App. B.5). Here, P^+ and P^- are the probabilities for obtaining the error syndromes "even" (code space) and "odd" (error space), respectively (they correspond to the trace of the respective expression in squared brackets, i.e. each unnormalized conditional state). The worst-case fidelity is defined as

$$
\begin{aligned}
F_{wc} &= \min_{a,b} \left[\langle \bar{\psi} | \hat{\rho}^{(+)} | \bar{\psi} \rangle P^+ + \langle \bar{\psi}' | \hat{\rho}^{(-)} | \bar{\psi}' \rangle P^- \right] \\
&= \min_{a,b} \left[\widetilde{p}_0(a,b) + \widetilde{p}_2(a,b) \left| \langle \bar{\psi} | \left(\frac{a|\bar{0}_+\rangle - b|\bar{1}_+\rangle}{\sqrt{1 - 2\,\mathrm{Re}(ab^*)\frac{\cos(\alpha^2)}{\cosh(\alpha^2)}}} \right) \right|^2 \right. \\
&\qquad \left. + \widetilde{p}_1(a,b) + \widetilde{p}_3(a,b) \left| \langle \bar{\psi}' | \left(\frac{a|\bar{0}_+\rangle - ib|\bar{1}_+\rangle}{\sqrt{1 - 2\,\mathrm{Re}(iab^*)\frac{\cos(\alpha^2)}{\cosh(\alpha^2)}}} \right) \right|^2 \right],
\end{aligned}
\tag{B.23}
$$

where $|\bar{\psi}'\rangle = \frac{a|\bar{0}_+\rangle + ib|\bar{1}_+\rangle}{\sqrt{1 - 2\,\mathrm{Re}(iab^*)\frac{\cos(\alpha^2)}{\cosh(\alpha^2)}}}$ (i.e., the reference input state for the odd syndrome has a fixed

phase gate applied to it compared to the original qubit input state $|\bar{\psi}\rangle = \frac{a|\bar{0}_+\rangle + b|\bar{1}_+\rangle}{\sqrt{1 + 2\,\mathrm{Re}(ab^*)\frac{\cos(\alpha^2)}{\cosh(\alpha^2)}}}$).

The second term in each of the last two lines of Eq. (B.23) is non-negative. If both terms vanish (i.e., we have $\alpha \to \infty$ and $a = \frac{1}{\sqrt{2}} = \pm b$), $\widetilde{p}_0$ and $\widetilde{p}_1$ no longer depend on a and b, and $F_{wc} = \widetilde{p}_0 + \widetilde{p}_1$ (more generally: $F_{wc} = \widetilde{p}_0(a^{wc}, b^{wc}) + \widetilde{p}_1(a^{wc}, b^{wc}) \geq \min_{a,b} (\widetilde{p}_0 + \widetilde{p}_1)$).

For the other case when the two relevant terms in Eq. (B.23) do not vanish, we have

$$
\begin{aligned}
F_{wc} &> \widetilde{p}_0(a^{wc}, b^{wc}) + \widetilde{p}_1(a^{wc}, b^{wc}) \\
&\geq \min_{a,b} (\widetilde{p}_0 + \widetilde{p}_1).
\end{aligned}
\tag{B.24}
$$

Thus, in general, we obtain the bound on F_{wc} as expressed by Eq. (6.15).

We show in the following that the probability for correct syndrome identification $F(a,b)$ for $L = 1$ and a logical qubit $a|\bar{0}_+\rangle + b|\bar{1}_+\rangle$ under the conditions $a, b \in \mathbb{R}$ is extremal for $|a| = |b| = \frac{1}{\sqrt{2}}$.

The fidelity can be cast in the following form:

$$
\begin{aligned}
F(a,b) &= \frac{1 + 2abc_1}{1 + 2abc_2} p_0 + \frac{1 - 2abc_3}{1 + 2abc_2} p_1 \\
&= \frac{1 + 2a\sqrt{1 - a^2}c_1}{1 + 2a\sqrt{1 - a^2}c_2} p_0 + \frac{1 - 2a\sqrt{1 - a^2}c_3}{1 + 2a\sqrt{1 - a^2}c_2} p_1 \\
&= \frac{p_0 + p_1 + 2a\sqrt{1 - a^2}(c_1 p_0 - c_3 p_1)}{1 + 2a\sqrt{1 - a^2}c_2} \\
&= F(a).
\end{aligned}
\tag{B.25}
$$

Here, the coefficients are short-hand for the overlaps of the codewords in the different error spaces, see Eqs. (13-15), and Eqs. (6.3) and (6.10). These coefficients are real and bounded by 1. To find the extremal value of the fidelity, we derive F with respect to a:

$$\frac{dF}{da} = \frac{(1 + 2a\sqrt{1-a^2}c_2)(c_1 p_0 - c_3 p_1)\frac{2-4a^2}{\sqrt{1-a^2}}}{(1 + 2a\sqrt{1-a^2}c_2)^2}$$
$$- \frac{(p_0 + p_1 + 2a\sqrt{1-a^2}(c_1 p_0 - c_3 p_1))c_2 \frac{2-4a^2}{\sqrt{1-a^2}}}{(1 + 2a\sqrt{1-a^2}c_2)^2} \qquad \text{(B.26)}$$
$$\propto 2 - 4a^2.$$

This vanishes for $a^2 = \frac{1}{2}$ and therefore we find the two solutions $a = \pm\frac{1}{\sqrt{2}}$. One solution corresponds to a maximum and the other to a minimum. The second derivative can resolve this and the solution depends on the signs of the coefficients c_i. To be safe and to avoid complicated formulae, one can clearly set

$$f_{min}(a) := \min\{F(a = \frac{1}{\sqrt{2}}), F(a = -\frac{1}{\sqrt{2}})\}, \qquad \text{(B.27)}$$

which then corresponds to the lower bound F on the worst-case fidelity F_{wc}, as shown in Eq. (6.15).

B.3 Derivation of codewords in the Fock basis

To solve the system of equations (6.16), we set $|\bar{0}\rangle = \sum_{n=0}^{\infty} c_n |n\rangle$. We have

$$
\begin{aligned}
\hat{a}^{L+1}|\bar{0}\rangle &= \sum_{n=L+1}^{\infty} c_n \sqrt{n}\sqrt{n-1}\cdots\sqrt{n-L}|n-L-1\rangle \\
&= \sum_{k=0}^{\infty} c_{k+L+1}\sqrt{k+L+1}\sqrt{k+L}\cdots\sqrt{k+1}|k\rangle \\
&= \alpha^{L+1}\sum_{k=0}^{\infty} c_k |k\rangle.
\end{aligned}
\tag{B.28}
$$

One obtains a recursive definition of the coefficients:

$$
c_{k+L+1} = \frac{\alpha^{L+1} c_k}{\sqrt{k+L+1}\sqrt{k+L}\cdots\sqrt{k+1}}.
\tag{B.29}
$$

To solve the series, one of the first parameters, c_0 or c_1, has to be fixed.

Before determining the general solution, let us examine the easiest example, $L = 0$. Here, the parity condition is trivial and the other two equations are just the defining equations for coherent states. Therefore, the system of equations leads to $|\bar{0}\rangle = |\alpha\rangle$ and $|\bar{1}\rangle = |-\alpha\rangle$.

As another illustrative example, we choose $L = 1$. Then we find the series:

$$
c_{k+2} = \frac{\alpha^2 c_k}{\sqrt{k+2}\sqrt{k+1}}.
\tag{B.30}
$$

If we set c_0 as given, this series is resolved by

$$
c_{2k} = \frac{\alpha^{2k} c_0}{\sqrt{(2k)!}}.
\tag{B.31}
$$

However, c_0 is not arbitrary, because it follows from the normalization constraint

$$
\sum_{k=0}^{\infty} |c_{2k}|^2 = \sum_{k=0}^{\infty} \frac{(\alpha^2)^{2k}}{(2k)!}|c_0|^2 = 1 \Rightarrow |c_0|.
\tag{B.32}
$$

The coefficient c_0 is then determined up to a irrelevant phase which leads to a global phase because of (B.31). The corresponding recursion formula for $|\bar{1}\rangle$ is given by

$$
c_{2k} = \frac{(-1)^k \alpha^{2k} c_0}{\sqrt{(2k)!}},
\tag{B.33}
$$

where c_0 can be determined through normalization. Therefore, in the Fock basis, the basis codewords read:

$$|\bar{0}\rangle = \frac{1}{\sqrt{\cosh(\alpha^2)}} \sum_{n=0}^{\infty} \frac{\alpha^{2n}}{\sqrt{(2n)!}} |2n\rangle,$$
$$|\bar{1}\rangle = \frac{1}{\sqrt{\cosh(\alpha^2)}} \sum_{n=0}^{\infty} (-1)^n \frac{\alpha^{2n}}{\sqrt{(2n)!}} |2n\rangle. \tag{B.34}$$

This can be expressed in terms of coherent states

$$|\bar{0}\rangle = \frac{1}{\sqrt{N_+}} (|\alpha\rangle + |-\alpha\rangle),$$
$$|\bar{1}\rangle = \frac{1}{\sqrt{N_+}} (|i\alpha\rangle + |-i\alpha\rangle), \tag{B.35}$$

as given in Section 6.1.

If we fix c_1, a completely analogous calculation leads to

$$|\bar{0}\rangle = \frac{1}{\sqrt{\sinh(\alpha^2)}} \sum_{n=0}^{\infty} \frac{\alpha^{2n+1}}{\sqrt{(2n+1)!}} |2n+1\rangle,$$
$$|\bar{1}\rangle = \frac{1}{\sqrt{\sinh(\alpha^2)}} \sum_{n=0}^{\infty} (-1)^n \frac{\alpha^{2n+1}}{\sqrt{(2n+1)!}} |2n+1\rangle. \tag{B.36}$$

Since the parity condition for $L = 1$ reads as $(-1)^{\hat{n}} |\bar{\psi}\rangle = |\bar{\psi}\rangle$, the first pair of codewords is the solution of the determining system of equations.

For general L, it is easy to verify that the solutions of the defining equations in the Fock basis are given by

$$|\bar{0}\rangle = \sum_{k=0}^{\infty} \frac{\alpha^{(L+1)k}}{\sqrt{([L+1]k)!}} |(L+1)k\rangle,$$
$$|\bar{1}\rangle = \sum_{k=0}^{\infty} \frac{(-1)^k \alpha^{(L+1)k}}{\sqrt{([L+1]k)!}} |(L+1)k\rangle. \tag{B.37}$$

We show in the following these states can be rewritten in terms of coherent states as presented in the main text:

$$|\bar{0}\rangle = \sum_{k=0}^{L} |\alpha \exp\left(\frac{2\pi i k}{L+1}\right)\rangle,$$
$$|\bar{1}\rangle = \sum_{k=1}^{L+1} |\alpha \exp\left(\frac{(2k-1)\pi i}{L+1}\right)\rangle. \tag{B.38}$$

Expressed in the Fock basis, we have

$$|\bar{0}\rangle = \sum_{k=0}^{L} \sum_{r=0}^{\infty} \frac{\alpha^r \exp\left(\frac{\pi i 2 k}{L+1}\right)^r}{\sqrt{r!}} |r\rangle \tag{B.39}$$

106

$$= \sum_{r=0}^{\infty} \frac{\alpha^r}{\sqrt{r!}} |r\rangle \sum_{k=0}^{L} \exp\left(\frac{\pi i 2 r}{L+1}\right)^k$$

$$= \sum_{r=0}^{\infty} \frac{\alpha^r}{\sqrt{r!}} |r\rangle \frac{1 - \exp\left(\pi i 2 r\right)}{1 - \exp\left(\frac{\pi i 2 r}{L+1}\right)}$$

$$= \sum_{r=0}^{\infty} \frac{\alpha^r}{\sqrt{r!}} |r\rangle \delta_r^{(L+1)m}$$

$$= \sum_{m=0}^{\infty} \frac{\alpha^{(L+1)m}}{\sqrt{[(L+1)m]!}} |(L+1)m\rangle.$$

The calculation for the other codeword is similar,

$$|\bar{1}\rangle = \sum_{k=1}^{L+1} \sum_{r=0}^{\infty} \frac{\alpha^r \exp\left(\frac{\pi i (2k-1)}{L+1}\right)^r}{\sqrt{r!}} |r\rangle \qquad \text{(B.40)}$$

$$= \sum_{r=0}^{\infty} \frac{\alpha^r}{\sqrt{r!}} |r\rangle \sum_{k=1}^{L+1} \exp\left(\frac{\pi i r}{L+1}\right)^{2k-1}$$

$$= \sum_{r=0}^{\infty} \frac{\alpha^r}{\sqrt{r!}} |r\rangle \exp\left(-\frac{\pi i r}{L+1}\right) \sum_{k=1}^{L+1} \exp\left(\frac{2\pi i r}{L+1}\right)^k$$

$$= \sum_{r=0}^{\infty} \frac{\alpha^r}{\sqrt{r!}} |r\rangle \exp\left(\frac{\pi i r}{L+1}\right) \sum_{j=0}^{L} \exp\left(\frac{2\pi i r}{L+1}\right)^j$$

$$= \sum_{r=0}^{\infty} \frac{\alpha^r}{\sqrt{r!}} |r\rangle \exp\left(\frac{\pi i r}{L+1}\right) \frac{1 - \exp\left(\pi i 2 r\right)}{1 - \exp\left(\frac{\pi i 2 r}{L+1}\right)}$$

$$= \sum_{r=0}^{\infty} \frac{\alpha^r}{\sqrt{r!}} |r\rangle \exp\left(\frac{\pi i r}{L+1}\right) \delta_r^{(L+1)m}$$

$$= \sum_{m=0}^{\infty} \frac{(-1)^m \alpha^{(L+1)m}}{\sqrt{[(L+1)m]!}} |(L+1)m\rangle.$$

Up to normalization, the basic codewords in the $L + 1$ error spaces in terms of coherent states are defined as

$$|\bar{0}_q\rangle_L := \sum_{k=0}^{L} \exp\left(\frac{2qki\pi}{L+1}\right) |\alpha \exp\left(\frac{2ki\pi}{L+1}\right)\rangle,$$

$$|\bar{1}_q\rangle_L := \sum_{k=1}^{L+1} \exp\left(\frac{2q(k-1)i\pi}{L+1}\right) |\alpha \exp\left(\frac{(2k-1)i\pi}{L+1}\right)\rangle, \qquad \text{(B.41)}$$

for $q = 0, .., L$. In the Fock basis, these can be expressed as

$$|\bar{0}_q\rangle_L := \sum_{k=1}^{\infty} \frac{\alpha^{(L+1)k-q}}{\sqrt{[(L+1)k-q]!}}|(L+1)k-q\rangle,$$

$$|\bar{1}_q\rangle_L := \sum_{k=1}^{\infty} \frac{(e^{\frac{i\pi}{L+1}}\alpha)^{(L+1)k-q}}{\sqrt{[(L+1)k-q]!}}|(L+1)k-q\rangle.$$

(B.42)

The code-defining equations, including both the code space and all error spaces, then become

$$\exp\left(\frac{2\pi i\hat{n}}{L+1}\right)|\bar{0}_q\rangle_L = \exp\left(\frac{2\pi iq}{L+1}\right)|\bar{0}_q\rangle_L,$$

(B.43)

$$\exp\left(\frac{2\pi i\hat{n}}{L+1}\right)|\bar{1}_q\rangle_L = \exp\left(\frac{2\pi iq}{L+1}\right)|\bar{1}_q\rangle_L,$$

$$(\hat{a}^{L+1} - \alpha^{L+1})|\bar{0}_q\rangle_L = 0,$$

$$(\hat{a}^{L+1} + \alpha^{L+1})|\bar{1}_q\rangle_L = 0,$$

$\forall q = 0, 1, 2, ..., L$. The evolution of a logical qubit $|\bar{\Psi}\rangle = \frac{a|\bar{0}\rangle + b|\bar{1}\rangle}{\sqrt{1 + 2\operatorname{Re}(ab^*\langle\bar{0}|\bar{1}\rangle)}}$ under AD can then be described as an (unnormalized) mixture of $2(L+1)$ components:

$$\begin{aligned}\bar{\rho} = &\; p_0(a|\widetilde{0}_0\rangle + b|\widetilde{1}_0\rangle) \times H.c. + p_1(a|\widetilde{0}_1\rangle + e^{\frac{i\pi}{L+1}}b|\widetilde{1}_1\rangle) \times H.c. + p_2(a|\widetilde{0}_2\rangle + e^{\frac{2i\pi}{L+1}}b|\widetilde{1}_2\rangle) \times H.c. \\ &+ p_3(a|\widetilde{0}_3\rangle + e^{\frac{3i\pi}{L+1}}b|\widetilde{1}_3\rangle) \times H.c. + ... + p_L(a|\widetilde{0}_L\rangle + e^{\frac{Li\pi}{L+1}}b|\widetilde{1}_L\rangle) \times H.c. \\ &+ p_{L+1}(a|\widetilde{0}_0\rangle_1 - b|\widetilde{1}_0\rangle_1) \times H.c. + p_{L+2}(a|\widetilde{0}_1\rangle - e^{\frac{i\pi}{L+1}}b|\widetilde{1}_1\rangle) \times H.c. \\ &+ p_{L+3}(a|\widetilde{0}_2\rangle - e^{\frac{2i\pi}{L+1}}b|\widetilde{1}_2\rangle_2) \times H.c. + ... + p_{2L+1}(a|\widetilde{0}_L\rangle - e^{\frac{Li\pi}{L+1}}b|\widetilde{1}_L\rangle) \times H.c.\end{aligned}$$

(B.44)

B.4 Full loss channel and KL conditions for the two-loss code

The normalized $L = 2$ codewords read in the Fock basis as:

$$|\bar{0}\rangle = \frac{1}{\sqrt{N}} \sum_{k=0}^{\infty} \frac{\alpha^{3k}}{\sqrt{(3k)!}} |3k\rangle,$$
$$|\bar{1}\rangle = \frac{1}{\sqrt{N}} \sum_{k=0}^{\infty} \frac{(-\alpha)^{3k}}{\sqrt{(3k)!}} |3k\rangle, \tag{B.45}$$

where $N = \frac{1}{3}\left(\exp(\alpha^2) + 2\exp\left(\frac{-\alpha^2}{2}\right)\cos\left(\frac{\sqrt{3}\alpha^2}{2}\right)\right)$. The codeword overlap is given by

$$\langle\bar{1}|\bar{0}\rangle = \frac{\exp(-\alpha^2) + 2\exp\left(\frac{\alpha^2}{2}\right)\cos\left(\frac{\sqrt{3}\alpha^2}{2}\right)}{\exp(\alpha^2) + 2\exp\left(\frac{-\alpha^2}{2}\right)\cos\left(\frac{\sqrt{3}\alpha^2}{2}\right)} \xrightarrow{\alpha\to\infty} 0. \tag{B.46}$$

Based on the results obtained in Section 6.2 for the simplified error model, we expect a similar cyclic behavior of the code under the full AD channel. It is therefore advantageous to consider the action of the operators $\{A_{3k}, A_{3k+1}, A_{3k+2}\}$ on the codewords:

$$A_{3k}|\bar{0}\rangle = \frac{1}{\sqrt{N}}\frac{\sqrt{1-\gamma}^{3k}\alpha^{3k}}{\sqrt{(3k)!}}\sum_{n=0}^{\infty}\frac{(\alpha\sqrt{\gamma})^{3n}}{\sqrt{(3n)!}}|3n\rangle,$$

$$A_{3k}|\bar{1}\rangle = \frac{(-1)^k}{\sqrt{N}}\frac{\sqrt{1-\gamma}^{3k}\alpha^{3k}}{\sqrt{(3k)!}}\sum_{n=0}^{\infty}\frac{(-\alpha\sqrt{\gamma})^{3n}}{\sqrt{(3n)!}}|3n\rangle,$$

$$A_{3k+1}|\bar{0}\rangle = \frac{1}{\sqrt{N}}\frac{\sqrt{1-\gamma}^{3k+1}\alpha^{3k+1}}{\sqrt{(3k+1)!}}\sum_{n=1}^{\infty}\frac{(\alpha\sqrt{\gamma})^{3n-1}}{\sqrt{(3n-1)!}}|3n-1\rangle,$$

$$A_{3k+1}|\bar{1}\rangle = \frac{(-1)^{k+1}}{\sqrt{N}}\frac{\sqrt{1-\gamma}^{3k+1}\alpha^{3k+1}e^{\frac{\pi i}{3}}}{\sqrt{(3k+1)!}}\sum_{n=1}^{\infty}\frac{(e^{\frac{\pi i}{3}}\alpha\sqrt{\gamma})^{3n-1}}{\sqrt{(3n-1)!}}|3n-1\rangle, \tag{B.47}$$

$$A_{3k+2}|\bar{0}\rangle = \frac{1}{\sqrt{N}}\frac{\sqrt{1-\gamma}^{3k+2}\alpha^{3k+2}}{\sqrt{(3k+2)!}}\sum_{n=1}^{\infty}\frac{(\alpha\sqrt{\gamma})^{3n-2}}{\sqrt{(3n-2)!}}|3n-2\rangle,$$

$$A_{3k+2}|\bar{1}\rangle = \frac{(-1)^k}{\sqrt{N}}\frac{\sqrt{1-\gamma}^{3k+2}\alpha^{3k+2}e^{\frac{2\pi i}{3}}}{\sqrt{(3k+2)!}}\sum_{n=1}^{\infty}\frac{(e^{\frac{\pi i}{3}}\alpha\sqrt{\gamma})^{3n-2}}{\sqrt{(3n-2)!}}|3n-2\rangle.$$

Following the notation introduced after Eq. (6.20), the basic codewords in the three orthogonal error spaces read

$$\widetilde{|0_0\rangle}_2 \propto \sum_{k=0}^{\infty} \frac{(\alpha\sqrt{\gamma})^{3k}}{\sqrt{(3k)!}} |3k\rangle,$$

$$\widetilde{|1_0\rangle}_2 \propto \sum_{k=0}^{\infty} \frac{(-\alpha\sqrt{\gamma})^{3k}}{\sqrt{(3k)!}} |3k\rangle,$$

$$\widetilde{|0_1\rangle}_2 \propto \sum_{k=1}^{\infty} \frac{(\alpha\sqrt{\gamma})^{3k-1}}{\sqrt{(3k-1)!}} |3k-1\rangle,$$

$$\widetilde{|1_1\rangle}_2 \propto \sum_{k=1}^{\infty} \frac{(e^{\frac{\pi i}{3}}\alpha\sqrt{\gamma})^{3k-1}}{\sqrt{(3k-1)!}} |3k-1\rangle, \tag{B.48}$$

$$\widetilde{|0_2\rangle}_2 \propto \sum_{k=1}^{\infty} \frac{(\alpha\sqrt{\gamma})^{3k-2}}{\sqrt{(3k-2)!}} |3k-2\rangle,$$

$$\widetilde{|1_2\rangle}_2 \propto \sum_{k=1}^{\infty} \frac{(e^{\frac{\pi i}{3}}\alpha\sqrt{\gamma})^{3k-2}}{\sqrt{(3k-2)!}} |3k-2\rangle,$$

where $\sim$ again indicates the damped amplitude. Obviously, the different error spaces are orthogonal and the codewords in each error space become orthogonal for large α.

Furthermore, we define the following logical states ($\sim$ denotes again damped logical states),

$$|\widetilde{\Psi}_0\rangle \propto a\widetilde{|0_0\rangle}_2 + b\widetilde{|1_0\rangle}_2,$$

$$|\widetilde{\Psi}_1\rangle \propto a\widetilde{|0_1\rangle}_2 + e^{\frac{\pi i}{3}}b\widetilde{|1_1\rangle}_2,$$

$$|\widetilde{\Psi}_2\rangle \propto a\widetilde{|0_2\rangle}_2 + e^{\frac{2\pi i}{3}}b\widetilde{|1_2\rangle}_2,$$

$$|\widetilde{\Psi}_3\rangle \propto a\widetilde{|0_0\rangle}_2 - b\widetilde{|1_0\rangle}_2, \tag{B.49}$$

$$|\widetilde{\Psi}_4\rangle \propto a\widetilde{|0_1\rangle}_2 - e^{\frac{\pi i}{3}}b\widetilde{|1_1\rangle}_2,$$

$$|\widetilde{\Psi}_5\rangle \propto a\widetilde{|0_2\rangle}_2 - e^{\frac{2\pi i}{3}}b\widetilde{|1_2\rangle}_2.$$

The final mixture for a logical qubit $|\bar{\Psi}\rangle = \frac{a|\bar{0}\rangle + b|\bar{1}\rangle}{\sqrt{1 + 2\,\mathrm{Re}(a^*b\langle\bar{0}|\bar{1}\rangle)}}$ can thus be written in the form,

$$\bar{\rho} = p_0 \left(\frac{1 + 2\,\mathrm{Re}(a^*b\langle\widetilde{0}_0|\widetilde{1}_0\rangle)}{1 + 2\,\mathrm{Re}(a^*b\langle\bar{0}_0|\bar{1}_0\rangle)} \right) |\widetilde{\Psi}_0\rangle\langle\widetilde{\Psi}_0|, + p_1 \left(\frac{1 + 2\,\mathrm{Re}(a^*be^{\frac{\pi i}{3}}\langle\widetilde{0}_1|\widetilde{1}_1\rangle)}{1 + 2\,\mathrm{Re}(a^*b\langle\bar{0}_0|\bar{1}_0\rangle)} \right) |\widetilde{\Psi}_1\rangle\langle\widetilde{\Psi}_1|$$

$$+ p_2 \left(\frac{1 + 2\,\mathrm{Re}(a^*be^{\frac{2\pi i}{3}}\langle\widetilde{0}_2|\widetilde{1}_2\rangle)}{1 + 2\,\mathrm{Re}(a^*b\langle\bar{0}_0|\bar{1}_0\rangle)} \right) |\widetilde{\Psi}_2\rangle\langle\widetilde{\Psi}_2| + p_3 \left(\frac{1 - 2\,\mathrm{Re}(a^*b\langle\widetilde{0}_0|\widetilde{1}_0\rangle)}{1 + 2\,\mathrm{Re}(a^*b\langle\bar{0}_0|\bar{1}_0\rangle)} \right) |\widetilde{\Psi}_3\rangle\langle\widetilde{\Psi}_3| \tag{B.50}$$

$$+ p_4 \left(\frac{1 - 2\,\mathrm{Re}(a^*be^{\frac{\pi i}{3}}\langle\widetilde{0}_1|\widetilde{1}_1\rangle)}{1 + 2\,\mathrm{Re}(a^*b\langle\bar{0}_0|\bar{1}_0\rangle)} \right) |\widetilde{\Psi}_4\rangle\langle\widetilde{\Psi}_4| + p_5 \left(\frac{1 - 2\,\mathrm{Re}(a^*be^{\frac{2\pi i}{3}}\langle\widetilde{0}_2|\widetilde{1}_2\rangle)}{1 + 2\,\mathrm{Re}(a^*b\langle\bar{0}_0|\bar{1}_0\rangle)} \right) |\widetilde{\Psi}_5\rangle\langle\widetilde{\Psi}_5|,$$

where we also omitted the index indicating $L = 2$ at the state vectors. For this code, the codeword probabilities p_i, $i = 0, ..., 5$, are given by

$$p_i = \frac{1}{\sqrt{N}} \sum_{m=0}^{\infty} \frac{(\alpha^2(1-\gamma))^{6m+i}}{(6m+i)!}. \tag{B.51}$$

From the mixed final state in Eq. (B.50), the non-deformation of the codewords becomes also manifest. Therefore, the KL-conditions are approximately fulfilled. A recovery is therefore also approximately possible, provided the amplitudes are chosen large enough.

B.5 Amplitude restoration

One effect of the realistic photon loss channel on the basic codewords is the damping of their amplitude. Consequently, the initial amplitude of the incoming logical state has to be restored. The first step in our quantum error correction process is a parity measurement that determines a certain error space. We have referred to this step as qubit recovery. For simplicity, the amplitude-damped codewords in the respective error space are denoted as $|\widetilde{0}\rangle$ and $|\widetilde{1}\rangle$ in the following. The goal of amplitude restoration, the second step of our QEC, is to turn back the damped amplitudes $\sqrt{\gamma}\alpha$ to the initial amplitude for every codeword, $|\widetilde{0}\rangle \to |\bar{0}\rangle$, $|\widetilde{1}\rangle \to |\bar{1}\rangle$. Later we will choose to map the qubit with restored amplitudes from the error space back into the code space (where this step is not a necessity, but helpful w.r.t. our one-way communication scheme).

Our strategy is to teleport the damped qubit into a space spanned by undamped codewords using an encoded, asymmetric Bell state with one half a damped qubit and the other half an undamped qubit (see Eq. (B.61)). In order to perform the Bell measurement onto a Bell basis expressed by non-orthogonal codewords, we propose to first apply a probabilistic "filter operation" and then do a standard Bell measurement. Let us now describe this filter [150]. Since the codewords are not orthogonal for finite α, they are not perfectly distinguishable. However, they can be written in some orthonormal basis $\{|x\rangle, |y\rangle\}$ as

$$
\begin{aligned}
|\bar{0}\rangle &= b_0|x\rangle + b_1|y\rangle, \\
|\bar{1}\rangle &= e^{i\phi}(b_0|x\rangle - b_1|y\rangle),
\end{aligned}
\tag{B.52}
$$

where $b_0^2 + b_1^2 = 1$ and $b_0, b_1 \in \mathbb{R}$ with $b_0 > b_1$ without loss of generality. Furthermore, one has $\langle\bar{0}|\bar{1}\rangle = e^{i\phi}(2b_0^2 - 1)$, such that

$$
\begin{aligned}
b_0 &= \sqrt{\frac{1 + e^{-i\phi}\langle\bar{0}|\bar{1}\rangle}{2}}, \\
b_1 &= \sqrt{\frac{1 - e^{-i\phi}\langle\bar{0}|\bar{1}\rangle}{2}}.
\end{aligned}
\tag{B.53}
$$

Furthermore, we define the following operators:

$$
A_s = \begin{pmatrix} \frac{b_1}{b_0} & 0 \\ 0 & 1 \end{pmatrix}, \; A_f = \begin{pmatrix} \sqrt{1 - \left(\frac{b_1}{b_0}\right)^2} & 0 \\ 0 & 0 \end{pmatrix}.
\tag{B.54}
$$

As can easily be checked, one has $A_s^\dagger A_s + A_f^\dagger A_f = \mathbb{1}$ and we refer to the non-unitary operations expressed by A_s and A_f as a successful and a failed filter operation, respectively. A successful filter on the codewords leads to

$$A_s|\bar{0}\rangle = b_1(|x\rangle + |y\rangle),$$
$$A_s|\bar{1}\rangle = e^{i\phi}b_1(|x\rangle - |y\rangle), \tag{B.55}$$

i.e. it maps the non-orthogonal codewords onto orthogonal states. Because the codewords cannot be perfectly distinguished, this cannot be done deterministically. In fact, the success probability for the filter operation is

$$P_{succ} = \langle\bar{0}|A_s^\dagger A_s|\bar{0}\rangle = \langle\bar{1}|A_s^\dagger A_s|\bar{1}\rangle = 2 - 2b_0^2 = 1 - |\langle\bar{0}|\bar{1}\rangle|. \tag{B.56}$$

Before proceeding, we illustrate the idea using the $L = 0$ cat code, whose codewords are $|\bar{0}\rangle = |\alpha\rangle$ and $|\bar{1}\rangle = |-\alpha\rangle$ with real overlap $\langle\alpha|-\alpha\rangle = e^{-2\alpha^2}$. The corresponding orthogonal basis is the cat state basis

$$|x\rangle = \frac{1}{\sqrt{N_+}}(|\alpha\rangle + |-\alpha\rangle),$$
$$|y\rangle = \frac{1}{\sqrt{N_-}}(|\alpha\rangle - |-\alpha\rangle). \tag{B.57}$$

Since the overlap is real, we have $\phi = 0$ and find

$$b_0 = \sqrt{\frac{1 + \exp(-2\alpha^2)}{2}},$$
$$b_1 = \sqrt{\frac{1 - \exp(-2\alpha^2)}{2}}. \tag{B.58}$$

The probability for successfully distinguishing $|\bar{0}\rangle$ and $|\bar{1}\rangle$ is therefore $P_{succ} = 1 - \exp(-2\alpha^2)$ (so-called unambiguous state discrimination).

For the teleportation-based amplitude restoration scheme, we need the Bell states in the (known) error space (note the normalization factor due to the non-orthogonality of the codewords):

$$|\widetilde{\phi}_+\rangle = \frac{1}{\sqrt{N_{\widetilde{\phi}_+}}}\frac{|\widetilde{0}\rangle|\widetilde{0}\rangle + |\widetilde{1}\rangle|\widetilde{1}\rangle}{\sqrt{2}},$$

$$|\widetilde{\phi}_-\rangle = \frac{1}{\sqrt{N_{\widetilde{\phi}_-}}}\frac{|\widetilde{0}\rangle|\widetilde{0}\rangle - |\widetilde{1}\rangle|\widetilde{1}\rangle}{\sqrt{2}},$$

$$|\widetilde{\psi}_+\rangle = \frac{1}{\sqrt{N_{\widetilde{\psi}_+}}}\frac{|\widetilde{0}\rangle|\widetilde{1}\rangle + |\widetilde{1}\rangle|\widetilde{0}\rangle}{\sqrt{2}},$$

$$|\widetilde{\psi}_-\rangle = \frac{1}{\sqrt{N_{\widetilde{\psi}_-}}}\frac{|\widetilde{0}\rangle|\widetilde{1}\rangle - |\widetilde{1}\rangle|\widetilde{0}\rangle}{\sqrt{2}}. \tag{B.59}$$

For later use for the "Bennett decomposition" in the teleportation step, one rearranges the former equations into

$$|\widetilde{0}\rangle|\widetilde{0}\rangle = \frac{1}{\sqrt{2}}(\sqrt{N_{\widetilde{\phi}_+}}|\widetilde{\phi}_+\rangle + \sqrt{N_{\widetilde{\phi}_-}}|\widetilde{\phi}_-\rangle),$$

$$|\widetilde{1}\rangle|\widetilde{1}\rangle = \frac{1}{\sqrt{2}}(\sqrt{N_{\widetilde{\phi}_+}}|\widetilde{\phi}_+\rangle - \sqrt{N_{\widetilde{\phi}_-}}|\widetilde{\phi}_-\rangle),$$

$$|\widetilde{0}\rangle|\widetilde{1}\rangle = \frac{1}{\sqrt{2}}(\sqrt{N_{\widetilde{\psi}_+}}|\widetilde{\psi}_+\rangle + \sqrt{N_{\widetilde{\psi}_-}}|\widetilde{\psi}_-\rangle),$$ (B.60)

$$|\widetilde{1}\rangle|\widetilde{0}\rangle = \frac{1}{\sqrt{2}}(\sqrt{N_{\widetilde{\psi}_+}}|\widetilde{\psi}_+\rangle - \sqrt{N_{\widetilde{\psi}_-}}|\widetilde{\psi}_-\rangle).$$

The amplitude restoration works as follows: an encoded qubit is sent through the channel whose output is a mixed state. As pointed out in the main text, the first step in the error correction procedure is the parity measurement which determines the corresponding error space, i.e. the input qubit of our amplitude restoration is of the form $|\omega\rangle = \frac{c_0|\widetilde{0}\rangle + c_1|\widetilde{1}\rangle}{\sqrt{N_\omega}}$ with unknown coefficients c_0 and c_1. According to the result of the parity measurement, the following state must be generated:

$$|\hat{\phi}^+\rangle = \frac{1}{\sqrt{N_{\hat{\phi}_+}}}\frac{|\widetilde{0}\rangle|\widetilde{0}\rangle + |\widetilde{1}\rangle|\widetilde{1}\rangle}{\sqrt{2}}.$$ (B.61)

In total, we then have

$$|\omega\rangle \otimes |\hat{\phi}^+\rangle = \frac{1}{\sqrt{N_\omega N_{\hat{\phi}^+}}}\frac{1}{\sqrt{2}}(c_0|\widetilde{0}\rangle|\widetilde{0}\rangle|\widetilde{0}\rangle + c_0|\widetilde{0}\rangle|\widetilde{1}\rangle|\widetilde{1}\rangle + c_1|\widetilde{1}\rangle|\widetilde{0}\rangle|\widetilde{0}\rangle + c_1|\widetilde{1}\rangle|\widetilde{1}\rangle|\widetilde{1}\rangle)$$ (B.62)

$$= \frac{1}{\sqrt{N_\omega N_{\hat{\phi}^+}}}\frac{1}{2}[c_0\sqrt{N_{\widetilde{\phi}_+}}|\widetilde{\phi}_+\rangle|\widetilde{0}\rangle + c_0\sqrt{N_{\widetilde{\phi}_-}}|\widetilde{\phi}_-\rangle|\widetilde{0}\rangle + c_0\sqrt{N_{\widetilde{\psi}_+}}|\widetilde{\psi}_+\rangle|\widetilde{1}\rangle + c_0\sqrt{N_{\widetilde{\psi}_-}}|\widetilde{\psi}_-\rangle|\widetilde{1}\rangle$$

$$+ c_1\sqrt{N_{\widetilde{\psi}_+}}|\widetilde{\psi}_+\rangle|\widetilde{0}\rangle - c_1\sqrt{N_{\widetilde{\psi}_-}}|\widetilde{\psi}_-\rangle|\widetilde{0}\rangle + c_1\sqrt{N_{\widetilde{\phi}_+}}|\widetilde{\phi}_+\rangle|\widetilde{1}\rangle - c_1\sqrt{N_{\widetilde{\phi}_-}}|\widetilde{\phi}_-\rangle|\widetilde{0}\rangle]$$

$$= \frac{1}{\sqrt{N_\omega N_{\hat{\phi}^+}}}\frac{1}{2}[\sqrt{N_{\widetilde{\phi}_+}}|\widetilde{\phi}_+\rangle(c_0|\widetilde{0}\rangle + c_1|\widetilde{1}\rangle) + \sqrt{N_{\widetilde{\phi}_-}}|\widetilde{\phi}_-\rangle(c_0|\widetilde{0}\rangle - c_1|\widetilde{1}\rangle)$$

$$+ \sqrt{N_{\widetilde{\psi}_+}}|\widetilde{\psi}_+\rangle(c_0|\widetilde{1}\rangle + c_1|\widetilde{0}\rangle) + \sqrt{N_{\widetilde{\psi}_-}}|\widetilde{\psi}_-\rangle(c_0|\widetilde{1}\rangle - c_1|\widetilde{0}\rangle)]$$

$$= \frac{\sqrt{N_{\chi_1}}}{\sqrt{N_\omega N_{\hat{\phi}^+}}}\frac{1}{2}\sqrt{N_{\widetilde{\phi}^+}}|\widetilde{\phi}_+\rangle\left(\frac{c_0|\widetilde{0}\rangle + c_1|\widetilde{1}\rangle}{\sqrt{N_{\chi_1}}}\right) + \frac{\sqrt{N_{\chi_2}}}{\sqrt{N_\omega N_{\hat{\phi}^+}}}\frac{1}{2}\sqrt{N_{\widetilde{\phi}^-}}|\widetilde{\phi}_-\rangle\left(\frac{c_0|\widetilde{0}\rangle - c_1|\widetilde{1}\rangle}{\sqrt{N_{\chi_2}}}\right)$$

$$+ \frac{\sqrt{N_{\chi_3}}}{\sqrt{N_\omega N_{\hat{\phi}^+}}}\frac{1}{2}\sqrt{N_{\widetilde{\psi}^+}}|\widetilde{\psi}_+\rangle\left(\frac{c_0|\widetilde{1}\rangle + c_1|\widetilde{0}\rangle}{\sqrt{N_{\chi_3}}}\right) + \frac{\sqrt{N_{\chi_4}}}{\sqrt{N_\omega N_{\hat{\phi}^+}}}\frac{1}{2}\sqrt{N_{\widetilde{\psi}^-}}|\widetilde{\psi}_-\rangle\left(\frac{c_0|\widetilde{1}\rangle - c_1|\widetilde{0}\rangle}{\sqrt{N_{\chi_4}}}\right)$$

$$= \frac{\sqrt{N_{\chi_1}}}{\sqrt{N_\omega N_{\hat{\phi}^+}}}\frac{1}{2}\sqrt{N_{\widetilde{\phi}^+}}\left(\frac{|\widetilde{0}\rangle|\widetilde{0}\rangle + |\widetilde{1}\rangle|\widetilde{1}\rangle}{\sqrt{2}}\right)\left(\frac{c_0|\widetilde{0}\rangle + c_1|\widetilde{1}\rangle}{\sqrt{N_{\chi_1}}}\right)$$

$$+ \frac{\sqrt{N_{\chi_2}}}{\sqrt{N_\omega N_{\hat{\phi}^+}}}\frac{1}{2}\sqrt{N_{\widetilde{\phi}^-}}\left(\frac{|\widetilde{0}\rangle|\widetilde{0}\rangle - |\widetilde{1}\rangle|\widetilde{1}\rangle}{\sqrt{2}}\right)\left(\frac{c_0|\widetilde{0}\rangle - c_1|\widetilde{1}\rangle}{\sqrt{N_{\chi_2}}}\right)$$

$$+ \frac{\sqrt{N_{\chi_3}}}{\sqrt{N_\omega N_{\hat{\phi}^+}}}\frac{1}{2}\sqrt{N_{\widetilde{\psi}^+}}\left(\frac{|\widetilde{0}\rangle|\widetilde{1}\rangle + |\widetilde{1}\rangle|\widetilde{0}\rangle}{\sqrt{2}}\right)\left(\frac{c_0|\widetilde{1}\rangle + c_1|\widetilde{0}\rangle}{\sqrt{N_{\chi_3}}}\right)$$

$$+ \frac{\sqrt{N_{\chi_4}}}{\sqrt{N_\omega N_{\hat\phi^+}}} \frac{1}{2} \sqrt{N_{\widetilde\psi^-}} \left(\frac{|\widetilde 0\rangle |\widetilde 1\rangle - |\widetilde 1\rangle |\widetilde 0\rangle}{\sqrt 2} \right) \left(\frac{c_0 |\bar 1\rangle - c_1 |\bar 0\rangle}{\sqrt{N_{\chi 4}}} \right).$$

Note that each of the four different output qubits requires a different normalization factor which we denote as $N_{\chi_i}, i = 1, 2, 3, 4$. Like in a usual teleportation scheme, we have a superposition of tensor products of four Bell states and four different output qubits. Because the codewords $|\widetilde 0\rangle$ and $|\widetilde 1\rangle$ are not orthogonal, the Bell measurement in this basis cannot be performed deterministically. Therefore, we apply the filter operation on the first two modes individually which leads, after an additional Hadamard gate in $\{|x\rangle, |y\rangle\}$, to

$$\begin{aligned}
|\omega\rangle \otimes |\hat\phi^+\rangle \to &\frac{b_1^2 \sqrt{N_{\chi_1}} \sqrt{N_{\widetilde\phi^+}}}{\sqrt{N_\omega N_{\hat\phi^+}}} \left(\frac{|x\rangle |x\rangle + e^{2i\phi} |y\rangle |y\rangle}{\sqrt 2} \right) \left(\frac{c_0 |\bar 0\rangle + c_1 |\bar 1\rangle}{\sqrt{N_{\chi_1}}} \right) \\
&+ \frac{b_1^2 \sqrt{N_{\chi_2}} \sqrt{N_{\widetilde\phi^-}}}{\sqrt{N_\omega N_{\hat\phi^+}}} \left(\frac{|x\rangle |x\rangle - e^{2i\phi} |y\rangle |y\rangle}{\sqrt 2} \rangle \right) \left(\frac{c_0 |\bar 0\rangle - c_1 |\bar 1\rangle}{\sqrt{N_{\chi_2}}} \right) \\
&+ e^{i\phi} \frac{b_1^2 \sqrt{N_{\chi_3}} \sqrt{N_{\widetilde\psi^+}}}{\sqrt{N_\omega N_{\hat\phi^+}}} \left(\frac{|x\rangle |y\rangle + |y\rangle |x\rangle}{\sqrt 2} \right) \left(\frac{c_0 |\bar 1\rangle + c_1 |\bar 0\rangle}{\sqrt{N_{\chi_3}}} \right) \\
&+ e^{i\phi} \frac{b_1^2 \sqrt{N_{\chi_4}} \sqrt{N_{\widetilde\psi^-}}}{\sqrt{N_\omega N_{\hat\phi^+}}} \left(\frac{|x\rangle |y\rangle - |y\rangle |x\rangle}{\sqrt 2} \right) \left(\frac{c_0 |\bar 1\rangle - c_1 |\bar 0\rangle}{\sqrt{N_{\chi_4}}} \right) =: |\nu\rangle.
\end{aligned} \tag{B.63}$$

Note that compared to Eq. (B.52) the $\{|x\rangle, |y\rangle\}$-basis is now that which expresses the damped states $|\widetilde 0\rangle$ and $|\widetilde 1\rangle$.

Since $|x\rangle$ and $|y\rangle$ are orthogonal, the Bell measurement can be performed. Because the filter operation is non-deterministic, the whole teleportation scheme has a non-unit success probability which corresponds to the norm of the state in Eq. (B.63),

$$\begin{aligned}
P_{succ} = \langle \nu | \nu \rangle &= \frac{b_1^4}{N_\omega N_{\hat\phi^+}} (N_{\chi_1} N_{\widetilde\phi^+} + N_{\chi_2} N_{\widetilde\phi^-} + N_{\chi_3} N_{\widetilde\psi^+} + N_{\chi_4} N_{\widetilde\psi^-}) \\
&= \frac{(1 - b_0^2)^2}{N_\omega N_{\hat\phi^+}} (N_{\chi_1} N_{\widetilde\phi^+} + N_{\chi_2} N_{\widetilde\phi^-} + N_{\chi_3} N_{\widetilde\psi^+} + N_{\chi_4} N_{\widetilde\psi^-}) \\
&= \frac{(1 - e^{-i\phi} \langle \widetilde 0 | \widetilde 1 \rangle)^2}{4 N_\omega N_{\hat\phi^+}} (N_{\chi_1} N_{\widetilde\phi^+} + N_{\chi_2} N_{\widetilde\phi^-} + N_{\chi_3} N_{\widetilde\psi^+} + N_{\chi_4} N_{\widetilde\psi^-}) \\
&= \frac{(1 - e^{-i\phi} \langle \widetilde 0 | \widetilde 1 \rangle)^2}{4(1 + 2\operatorname{Re}(c_0^* c_1 \langle \widetilde 0 | \widetilde 1 \rangle))(1 + \operatorname{Re}(\langle \widetilde 0 | \widetilde 1 \rangle \langle \widetilde 0 | \widetilde 1 \rangle))} (N_{\chi_1} N_{\widetilde\phi^+} + N_{\chi_2} N_{\widetilde\phi^-} + N_{\chi_3} N_{\widetilde\psi^+} + N_{\chi_4} N_{\widetilde\psi^-}).
\end{aligned} \tag{B.64}$$

For an L-encoded qubit with coefficients a and b (i.e., now we replace $c_0 \to a$, $c_1 \to b$), the total success probability for the one-way scheme is (see Section 7.3.2)

$$P_{ow} = \left(\sum_{k=0}^{2L+1} \widetilde{p}_k(a,b) \cdot P_{succ} \left[a|\widetilde{0}_k\rangle_L + \exp\left(\frac{k\pi i}{L+1} \right) b|\widetilde{1}_k\rangle_L \right] \right)^{\mathcal{L}/d_0}, \tag{B.65}$$

where $\mathcal{L}$ is the total distance, d_0 is the regular interval at which AR is performed, and the index "k" in the codewords is to be understood as modulo $L+1$ to obtain the corresponding error space codewords (recall $q = 0, ..., L$). Furthermore, $P_{succ}[\circ]$ is to be understood as P_{succ} from Eq. (B.64) with the respective incoming qubit state $\circ$. Note that the sum goes over all components in the incoming mixed state because this probability does not correspond to the success probability of qubit QEC (as our QR is deterministic and imperfect, as expressed by the non-unit fidelity of the scheme) but to the probability for the filters (and hence each AR) to succeed.

Note that at every AR step, we may obtain one of four possible qubit states, as expressed by Eq. (B.63). From the Bell measurement result it is known which one of the four. This "Pauli-frame" can be recorded, however, without any additional operations, we may have an input qubit at the next station that differs from the original qubit at the sending station. For large α, this will not matter much in Eq. (B.65) (see e.g. $\widetilde{p}_k(a,b)$ in Eq. (6.12)).

Appendix C

Appendices to Chapter 7

C.1 Rate analysis

In this appendix, we show several tables summarizing the results on the rates and fidelities for our qutrit quantum repeater scheme ($d = 3$), as described in Section 7.1.1. We consider various total distances up to 1280 km, two possible elementary distances ($L_0 = 5, 10$ km), between zero and three rounds of entanglement purification directly after the initial entanglement distribution, and the two possible detection schemes (homodyne, USD).

	rounds of purification	no	one	two	three
	initial fidelity	0.652	0.87	0.987	0.999
	effective probability	0.414	0.147	0.078	0.05
rate [Hz]	20 km	3020	1010	524	343
	40 km	2271	738	380	248
	80 km	1788	570	293	191
	160 km	1463	461	236	156
	320 km	1234	385	197	128
	640 km	1065	331	169	110
	1280 km	936	289	147	96
fidelity	20 km	0.420	0.76	0.974	0.999
	40 km	0.18	0.57	0.95	0.999
	80 km	0.03	0.33	0.9	0,999
	160 km	0.001	0.1	0.814	0.998
	320 km	0	0.01	0.66	0.996
	640 km	0	0	0.436	0.992
	1280 km	0	0	0.19	0.984

Table C.1: L_0=10 km (USD), $\alpha = 1.2$, $L \leq 1280$ km

	rounds of purification	no	one	two	three
	initial fidelity	0.73	0.93	0.997	0.999997
	effective probability	0.38	0.15	0.09	0.0619534
rate [Hz]	10 km	5496	2056	1219	835
	20 km	4117	1502	885	605
	40 km	3233	1161	682	465
	80 km	2641	939	550	375
	160 km	2225	785	459	313
	320 km	1919	674	394	267
	640 km	1686	589	344	234
fidelity	10 km	0.53	0.86	0.995	0.999994
	20 km	0.28	0.75	0.990	0.999987
	40 km	0.08	0.56	0.980	0.999975
	80 km	0.01	0.31	0.961	0.99995
	160 km	0.00	0.10	0.923	0.9999
	320 km	0.00	0.01	0.852	0.9998
	640 km	0.00	0.00	0.726	0.9996

Table C.2: L_0=5 km (homodyne), $\alpha \approx 1$, $L \leq 640$ km

	rounds of purification	no	one	two	three
	initial fidelity	0.6	0.81	0.974	0.9996
	effective probability	0.39	0.12	0.057	0.037
rate [Hz]	20 km	2828	817	384	246
	40 km	2121	595	278	178
	80 km	1667	460	214	137
	160 km	1362	371	172	110
	320 km	1148	310	144	92
	640 km	990	266	123	79
	1280 km	870	233	107	69
fidelity	20 km	0.360	0.656	0.949	0.999
	40 km	0.130	0.430	0.900	0.999
	80 km	0.017	0.185	0.810	0.997
	160 km	0.000	0.034	0.656	0.994
	320 km	0.000	0.001	0.430	0.989
	640 km	0	0	0.184	0.978
	1280 km	0	0	0.03	0.957

Table C.3: L_0=10 km (homodyne), $\alpha \approx 1$, $L \leq 1280$ km

rounds of purification		no	one	two
	initial fidelity	0.861808	0.986275	0.999876
	effective probability	0.0137597	0.0069238	0.0044958
rate [Hz]	40 km	92	46	30
	80 km	33	17	11
	160 km	26	13	9
	320 km	21	11	7
	640 km	17	9	6
	1280 km	15	8	5
fidelity	20 km	0.86180	0.986275	0.9999
	40 km	0.7427	0.9727	0.9998
	80 km	0.5516	0.9462	0.9995
	160 km	0.3043	0.8953	0.9990
	320 km	0.09259	0.8016	0.9980
	640 km	0.008573	0.6426	0.9960
	1280 km	0	0.4129	0.9921

Table C.4: L_0=20 km (USD), $\alpha = 0.5$, $L \leq 1280$ km

C.2   Ququart hybrid repeater

The dispersive interaction acting on a ququart-light system is defined by the unitary transformation

$$U_4(\theta)\left[\frac{1}{2}(|0\rangle + |1\rangle + |2\rangle + |3\rangle)|\alpha\rangle\right] = \frac{1}{2}(|0\rangle|\alpha\rangle + |1\rangle|\alpha e^{i\theta}\rangle + |2\rangle|\alpha e^{2i\theta}\rangle + |3\rangle|\alpha e^{3i\theta}\rangle), \qquad (C.1)$$

which is induced by the Hamiltonian $H_{int}^{(4)} = \hbar g \hat{S}_z^{(4)} \hat{a}^\dagger \hat{a}$ with $\hat{S}_z^{(4)}|k\rangle = \left(\frac{2k-3}{2}\right)|k\rangle$ for $k \in \{0,1,2,3\}$. Thus, the ququart (4-level system) may be represented by a spin-$\frac{3}{2}$ particle. The case of a strong interaction is obtained by choosing $\theta = \frac{\pi}{2}$.

As before, the first step in the protocol is the generation of an entangled ququart-light state via the strong dispersive interaction, i.e.,

$$\frac{1}{2}(|0\rangle|\alpha\rangle + |1\rangle|i\alpha\rangle + |2\rangle|-\alpha\rangle + |3\rangle|-i\alpha\rangle), \qquad (C.2)$$

of which the light part is then sent through the optical channel over a distance L_0, suffering from loss.

The output density matrix is again determined by mixing the light mode with an ancilla vacuum state and tracing out the light mode. It is again useful to transform the coherent states of the light field into an orthogonal basis. The adapted orthogonal basis in this case reads

119

$$|u\rangle = \frac{1}{\sqrt{N_u(\alpha)}}(|\alpha\rangle + |-\alpha\rangle + |i\alpha\rangle + |-i\alpha\rangle),$$

$$|v\rangle = \frac{1}{\sqrt{N_v(\alpha)}}(|\alpha\rangle + i|-\alpha\rangle - |i\alpha\rangle - i|-i\alpha\rangle),$$

$$|w\rangle = \frac{1}{\sqrt{N_w(\alpha)}}(|\alpha\rangle - |-\alpha\rangle + |i\alpha\rangle - |-i\alpha\rangle),$$

$$|z\rangle = \frac{1}{\sqrt{N_z(\alpha)}}(|\alpha\rangle - i|-\alpha\rangle - |i\alpha\rangle + i|-i\alpha\rangle),$$

(C.3)

with normalization constants $N_u(\alpha), N_v(\alpha), N_w(\alpha)$, and $N_z(\alpha)$. We can therefore write

$$|\alpha\rangle = \frac{1}{4}(\sqrt{N_u(\alpha)}|u\rangle + \sqrt{N_v(\alpha)}|v\rangle + \sqrt{N_w(\alpha)}|w\rangle + \sqrt{N_z(\alpha)}|z\rangle),$$

$$|-\alpha\rangle = \frac{1}{4}(\sqrt{N_u(\alpha)}|u\rangle - i\sqrt{N_v(\alpha)}|v\rangle - \sqrt{N_w(\alpha)}|w\rangle + i\sqrt{N_z(\alpha)}|z\rangle),$$

$$|i\alpha\rangle = \frac{1}{4}(\sqrt{N_u(\alpha)}|u\rangle - \sqrt{N_v(\alpha)}|v\rangle + \sqrt{N_w(\alpha)}|w\rangle - \sqrt{N_z(\alpha)}|z\rangle),$$

$$|-i\alpha\rangle = \frac{1}{4}(\sqrt{N_u(\alpha)}|u\rangle + i\sqrt{N_v(\alpha)}|v\rangle - \sqrt{N_w(\alpha)}|w\rangle - i\sqrt{N_z(\alpha)}|z\rangle).$$

(C.4)

The resulting output density matrix,

$$\rho_{out} = \frac{N_u(\sqrt{1-\gamma}\alpha)}{16} \times \left[\frac{1}{2}(|0\rangle|\sqrt{\gamma}\alpha\rangle + |1\rangle|-\sqrt{\gamma}\alpha\rangle + |2\rangle|i\sqrt{\gamma}\alpha\rangle + |3\rangle|-i\sqrt{\gamma}\alpha\rangle)\right] \times H.c.$$

$$+ \frac{N_v(\sqrt{1-\gamma}\alpha)}{16} \times \left[\frac{1}{2}(|0\rangle|\sqrt{\gamma}\alpha\rangle - i|1\rangle|-\sqrt{\gamma}\alpha\rangle - |2\rangle|i\sqrt{\gamma}\alpha\rangle + i|3\rangle|-i\sqrt{\gamma}\alpha\rangle)\right] \times H.c.$$

$$+ \frac{N_w(\sqrt{1-\gamma}\alpha)}{16} \times \left[\frac{1}{2}(|0\rangle|\sqrt{\gamma}\alpha\rangle - |1\rangle|-\sqrt{\gamma}\alpha\rangle + |2\rangle|i\sqrt{\gamma}\alpha\rangle - |3\rangle|-i\sqrt{\gamma}\alpha\rangle)\right] \times H.c.$$

$$+ \frac{N_z(\sqrt{1-\gamma}\alpha)}{16} \times \left[\frac{1}{2}(|0\rangle|\sqrt{\gamma}\alpha\rangle + i|1\rangle|-\sqrt{\gamma}\alpha\rangle - |2\rangle|i\sqrt{\gamma}\alpha\rangle - i|3\rangle|-i\sqrt{\gamma}\alpha\rangle)\right] \times H.c.,$$

(C.5)

is now a four-component mixture. This entangled ququart-light state can be further simplified by switching to the orthogonal basis (Eq. (C.3)) for the light mode and to the X-Basis

$$|\widetilde{0}\rangle = \frac{1}{2}(|0\rangle + |1\rangle + |2\rangle + |3\rangle),$$

$$|\widetilde{1}\rangle = \frac{1}{2}(|0\rangle + i|1\rangle - |2\rangle - i|3\rangle),$$

$$|\widetilde{2}\rangle = \frac{1}{2}(|0\rangle - |1\rangle + |2\rangle - |3\rangle),$$

$$|\widetilde{3}\rangle = \frac{1}{2}(|0\rangle - i|1\rangle - |2\rangle + i|3\rangle),$$

(C.6)

for the matter system. Using these bases, Eq. (C.5) can be rewritten as

$$\rho_{out} = \frac{N_u(\sqrt{1-\gamma}\alpha)}{16} \times \left[\frac{1}{4} \left(\sqrt{N_u(\sqrt{\gamma}\alpha)}|\widetilde{0}\rangle|\widetilde{u}\rangle + \sqrt{N_v(\sqrt{\gamma}\alpha)}|\widetilde{1}\rangle|\widetilde{v}\rangle + \sqrt{N_w(\sqrt{\gamma}\alpha)}|\widetilde{2}\rangle|\widetilde{w}\rangle \right. \right.$$

$$\left. \left. + \sqrt{N_z(\sqrt{\gamma}\alpha)}|\widetilde{3}\rangle|\widetilde{z}\rangle \right) \right] \times H.c.$$

$$+ \frac{N_v(\sqrt{1-\gamma}\alpha)}{16} \times \left[\frac{1}{4} \left(\sqrt{N_u(\sqrt{\gamma}\alpha)}|\widetilde{3}\rangle|\widetilde{u}\rangle + \sqrt{N_v(\sqrt{\gamma}\alpha)}|\widetilde{2}\rangle|\widetilde{v}\rangle + \sqrt{N_w(\sqrt{\gamma}\alpha)}|\widetilde{1}\rangle|\widetilde{w}\rangle \right. \right.$$

$$\left. \left. + \sqrt{N_z(\sqrt{\gamma}\alpha)}|\widetilde{0}\rangle|\widetilde{z}\rangle \right) \right] \times H.c.$$

$$+ \frac{N_w(\sqrt{1-\gamma}\alpha)}{16} \times \left[\frac{1}{4} \left(\sqrt{N_u(\sqrt{\gamma}\alpha)}|\widetilde{2}\rangle|\widetilde{u}\rangle + \sqrt{N_v(\sqrt{\gamma}\alpha)}|\widetilde{1}\rangle|\widetilde{v}\rangle + \sqrt{N_w(\sqrt{\gamma}\alpha)}|\widetilde{0}\rangle|\widetilde{w}\rangle \right. \right.$$

$$\left. \left. + \sqrt{N_z(\sqrt{\gamma}\alpha)}|\widetilde{3}\rangle|\widetilde{z}\rangle \right) \right] \times H.c.$$

$$+ \frac{N_z(\sqrt{1-\gamma}\alpha)}{16} \times \left[\frac{1}{4} \left(\sqrt{N_u(\sqrt{\gamma}\alpha)}|\widetilde{1}\rangle|\widetilde{u}\rangle + \sqrt{N_v(\sqrt{\gamma}\alpha)}|\widetilde{0}\rangle|\widetilde{v}\rangle + \sqrt{N_w(\sqrt{\gamma}\alpha)}|\widetilde{3}\rangle|\widetilde{w}\rangle \right. \right.$$

$$\left. \left. + \sqrt{N_z(\sqrt{\gamma}\alpha)}|\widetilde{2}\rangle|\widetilde{z}\rangle \right) \right] \times H.c. \tag{C.7}$$

where $\sim$ again indicates basis vectors with damped amplitudes for the light-mode states. The light mode of the state in Eq. (C.5) finally interacts with a second matter system via the inverse dispersive interaction with $\theta = -\frac{\pi}{2}$. The resulting state reads

$$\rho = \frac{N_u(\sqrt{1-\gamma}\alpha)}{16}|D_0\rangle\langle D_0| + \frac{N_v(\sqrt{1-\gamma}\alpha)}{16}|D_1\rangle\langle D_1|$$
$$+ \frac{N_w(\sqrt{1-\gamma}\alpha)}{16}|D_2\rangle\langle D_2| + \frac{N_z(\sqrt{1-\gamma}\alpha)}{16}|D_3\rangle\langle D_3|, \tag{C.8}$$

with the components

$$|D_0\rangle = \frac{1}{2}\left(\frac{1}{2}(|00\rangle + |11\rangle + |22\rangle + |33\rangle)|\sqrt{\gamma}\alpha\rangle \right.$$
$$+ \frac{1}{2}(|01\rangle + |10\rangle + |23\rangle + |32\rangle)| - \sqrt{\gamma}\alpha\rangle$$
$$+ \frac{1}{2}(|03\rangle + |12\rangle + |20\rangle + |31\rangle)|i\sqrt{\gamma}\alpha\rangle$$
$$\left. + \frac{1}{2}(|02\rangle + |13\rangle + |21\rangle + |30\rangle)| - i\sqrt{\gamma}\alpha\rangle \right), \tag{C.9}$$

$$|D_1\rangle = \frac{1}{2}\left(\frac{1}{2}(|00\rangle - i|11\rangle - |22\rangle + i|33\rangle)\,|\sqrt{\gamma}\alpha\rangle\right.$$
$$+ \frac{1}{2}(|01\rangle - i|10\rangle - |23\rangle + i|32\rangle)|-\sqrt{\gamma}\alpha\rangle$$
$$+ \frac{1}{2}(|03\rangle - i|12\rangle - |20\rangle + i|31\rangle)|i\sqrt{\gamma}\alpha\rangle$$
$$\left.+ \frac{1}{2}(|02\rangle - i|13\rangle - |21\rangle + i|30\rangle)|-i\sqrt{\gamma}\alpha\rangle\right),$$

(C.10)

$$|D_2\rangle = \frac{1}{2}\left(\frac{1}{2}(|00\rangle - i|11\rangle - |22\rangle + i|33\rangle)|\sqrt{\gamma}\alpha\rangle\right.$$
$$+ \frac{1}{2}(|01\rangle - i|10\rangle - |23\rangle + i|32\rangle)|-\sqrt{\gamma}\alpha\rangle$$
$$+ \frac{1}{2}(|03\rangle - i|12\rangle - |20\rangle + i|31\rangle)|i\sqrt{\gamma}\alpha\rangle$$
$$\left.+ \frac{1}{2}(|02\rangle - i|13\rangle - |21\rangle + i|30\rangle)|-i\sqrt{\gamma}\alpha\rangle\right),$$

(C.11)

$$|D_3\rangle = \frac{1}{2}\left(\frac{1}{2}(|00\rangle + i|11\rangle - |22\rangle - i|33\rangle)|\sqrt{\gamma}\alpha\rangle\right.$$
$$+ \frac{1}{2}(|01\rangle + i|10\rangle - |23\rangle - i|32\rangle)|-\sqrt{\gamma}\alpha\rangle$$
$$+ \frac{1}{2}(|03\rangle + i|12\rangle - |20\rangle - i|31\rangle)|i\sqrt{\gamma}\alpha\rangle$$
$$\left.+ \frac{1}{2}(|02\rangle + i|13\rangle - |21\rangle - i|30\rangle)|-i\sqrt{\gamma}\alpha\rangle\right).$$

(C.12)

The remaining task is then to project onto the coherent states $|\sqrt{\gamma}\alpha\rangle, |-\sqrt{\gamma}\alpha\rangle, |i\sqrt{\gamma}\alpha\rangle$ and $|-i\sqrt{\gamma}\alpha\rangle$ to establish a maximally entangled state in each of the components. Due to the special structure of the coherent states under consideration, homodyne detection in the ququart case is more problematic than in the qutrit case.

The states $|\pm\sqrt{\gamma}\alpha\rangle$ have Gaussian position distribution around $\pm\sqrt{\gamma}\alpha$, whereas $|\pm i\sqrt{\gamma}\alpha\rangle$ are both distributed around zero and therefore cannot be distinguished by an $\hat{x}$-measurement. The same is true for a $\hat{p}$-measurement, where $|\pm\sqrt{\gamma}\alpha\rangle$ have now both average zero and $|\pm i\sqrt{\gamma}\alpha\rangle$ have means $\sqrt{\gamma}\alpha$ and $-\sqrt{\gamma}\alpha$, respectively. Therefore, deterministic entanglement generation is not possible and the corresponding terms in the superposition have to be discarded.

If we choose the $\hat{x}$-measurement, the selection windows are then the same as in the qubit case: $w_0 = [\sqrt{\gamma}\alpha - \Delta, \infty]$ with $\Delta > 0$ corresponds to a projection onto $\frac{1}{2}(|00\rangle + |11\rangle + |22\rangle + |33\rangle)$, whereas a measurement result in $w_1 = [-\infty, -\sqrt{\gamma}\alpha + \Delta]$ leads to $\frac{1}{2}(|01\rangle + |10\rangle + |23\rangle + |32\rangle)$. In both cases, of course, an error due to the non-orthogonality of the coherent states has to be taken into account.

The probability for optimally distinguishing the four coherent states via USD as well as entan-

glement purification and swapping are addressed in Section 7.1.1 as a special case of the general qudit.

Appendix D

Heralded creation of photonic qudits from parametric down conversion using linear optics

D.1 Overview

The proposed scheme aims at generating arbitrary superpositions of two-mode optical states with fixed photon number. The key observation in this scheme from the theoretical side is that any such state can be written as a product of first order polynomials for the creation operators $\hat{a}_1^\dagger$ and $\hat{a}_2^\dagger$ of the two modes. A trivial example for total photon number one is

$$\frac{1}{\sqrt{2}}(|10\rangle + |01\rangle) = \frac{1}{\sqrt{2}}(\hat{a}_1^\dagger + \hat{a}_2^\dagger)|00\rangle =: p(\hat{a}_1^\dagger, \hat{a}_2^\dagger)|00\rangle, \tag{D.1}$$

where the polynomial reads $p(x, y) = \frac{1}{\sqrt{2}}(x + y)$.

From the experimental point of view, it can be shown that any state of the form

$$\prod_{i=0}^{q}(t_i\hat{a}_1^\dagger + r_i\hat{a}_2^\dagger)|00\rangle \tag{D.2}$$

can be experimentally generated by two two-mode squeezed resource states by sending one mode of each state through a network of beam splitters with some additional vacuum inputs and final photon detections.

The coefficients t_i and r_i in Eq. (D.2) correspond to the transmission and reflections of the individual beam splitters in the linear optical network. For finding these parameters for specific states, decompositions of polynomials are required which is the topic of the next three sections. More detailed information can be found in the corresponding publication (arXiv: 1710.08906).

D.2 Examples

D.2.1 Generation of a one-loss code

An important possible application of our general superposition states is possibility to create a general logical qubit encoded by the loss code given in Eq. (3.5).

Assuming $\alpha, \beta \neq 0$, the logical qubit state $|\bar{\psi}\rangle$ can be expressed in terms of creation operators,

$$
\begin{aligned}
|\bar{\psi}\rangle = \frac{\alpha}{\sqrt{2}}(|40\rangle + |04\rangle) + \beta|22\rangle &= \left(\frac{\alpha}{\sqrt{2}} \left(\frac{\hat{a}_1^{\dagger 4}}{\sqrt{4!}} + \frac{\hat{a}_2^{\dagger 4}}{\sqrt{4!}} \right) + \frac{\beta}{2} \hat{a}_1^{\dagger 2} \hat{a}_2^{\dagger 2} \right) |00\rangle \\
&= \left(\frac{\alpha}{\sqrt{48}} \hat{a}_1^{\dagger 4} + \frac{\alpha}{\sqrt{48}} \hat{a}_2^{\dagger 4} + \frac{\beta}{2} \hat{a}_1^{\dagger 2} \hat{a}_2^{\dagger 2} \right) |00\rangle \\
&=: p(\hat{a}_1^{\dagger}, \hat{a}_2^{\dagger})|00\rangle.
\end{aligned} \tag{D.3}
$$

To find the transmittance and the reflection coefficients in Eq. (D.2), one has to determine the decomposition of $p(\hat{a}_1^{\dagger}, \hat{a}_2^{\dagger})$ into linear factors. A short calculation shows

$$
p(\hat{a}_1^{\dagger}, \hat{a}_2^{\dagger})|00\rangle = \frac{\alpha}{\sqrt{48}} \left(\hat{a}_1^{\dagger} - \hat{a}_2^{\dagger} \sqrt{\left(-\frac{\sqrt{3}\beta}{\alpha} + \sqrt{\frac{3\beta^2}{\alpha^2} - 1} \right)} \right) \left(\hat{a}_1^{\dagger} - \hat{a}_2^{\dagger} \sqrt{\left(-\frac{\sqrt{3}\beta}{\alpha} - \sqrt{\frac{3\beta^2}{\alpha^2} - 1} \right)} \right)
\tag{D.4}
$$

$$
\times \left(\hat{a}_1^{\dagger} + \hat{a}_2^{\dagger} \sqrt{\left(-\frac{\sqrt{3}\beta}{\alpha} + \sqrt{\frac{3\beta^2}{\alpha^2} - 1} \right)} \right) \left(\hat{a}_1^{\dagger} + \hat{a}_2^{\dagger} \sqrt{\left(-\frac{\sqrt{3}\beta}{\alpha} - \sqrt{\frac{3\beta^2}{\alpha^2} - 1} \right)} \right) |00\rangle.
\tag{D.5}
$$

The expression is not yet in the form of Eq. (D.2). This is done by rescaling each linear factor to obtain the transmission and reflection coefficients:

$$
t_1 = t_3 = \frac{1}{\sqrt{1 + \left| -\frac{\sqrt{3}\beta}{\alpha} + \sqrt{\frac{3\beta^2}{\alpha^2} - 1} \right|^2}}, \qquad r_1 = r_3 = \frac{-\frac{\sqrt{3}\beta}{\alpha} + \sqrt{\frac{3\beta^2}{\alpha^2} - 1}}{\sqrt{1 + \left| -\frac{\sqrt{3}\beta}{\alpha} + \sqrt{\frac{3\beta^2}{\alpha^2} - 1} \right|^2}}, \tag{D.6}
$$

$$
t_2 = t_4 = \frac{1}{\sqrt{1 + \left| \frac{\sqrt{3}\beta}{\alpha} + \sqrt{\frac{3\beta^2}{\alpha^2} - 1} \right|^2}}, \qquad r_2 = r_4 = \frac{-\frac{\sqrt{3}\beta}{\alpha} - \sqrt{\frac{3\beta^2}{\alpha^2} - 1}}{\sqrt{1 + \left| \frac{\sqrt{3}\beta}{\alpha} + \sqrt{\frac{3\beta^2}{\alpha^2} - 1} \right|^2}}. \tag{D.7}
$$

The success probability for the heralded generation is found to be

$$P_{\text{succ}}(\alpha, \beta) = \frac{48}{\alpha^2} \frac{q^8}{256} (1 - q^2)^2 \left(1 + \left|-\frac{\sqrt{3}\beta}{\alpha} + \sqrt{\frac{3\beta^2}{\alpha^2} - 1}\right|^2\right)^{-1} \left(1 + \left|\frac{\sqrt{3}\beta}{\alpha} + \sqrt{\frac{3\beta^2}{\alpha^2} - 1}\right|^2\right)^{-1}.$$

$$\text{(D.8)}$$

D.2.2 NOON states

(a) $N = 2$

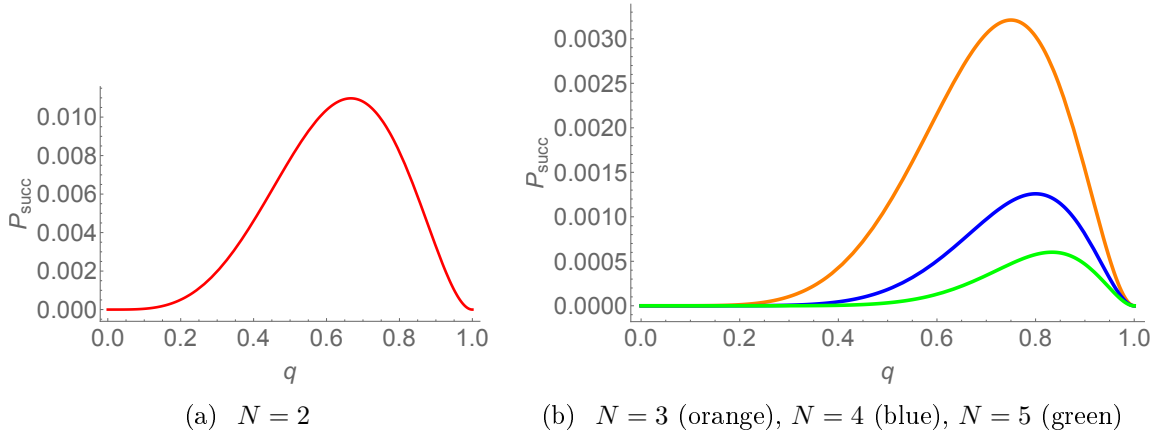(b) $N = 3$ (orange), $N = 4$ (blue), $N = 5$ (green)

Figure D.1: Success probability for creating $\frac{1}{\sqrt{2}}(|N0\rangle + |0N\rangle)$ for various N in dependence of q (using photon number resolving detectors). Note that the $N = 2$ NOON state can be also directly obtained from two single-photon states using a beam splitter.

A general NOON state is given by

$$\frac{1}{\sqrt{2}}(|N0\rangle + |0N\rangle) = \frac{1}{\sqrt{2}} \left(\frac{\hat{a}_1^{\dagger N}}{\sqrt{N!}} + \frac{\hat{a}_2^{\dagger N}}{\sqrt{N!}}\right) |00\rangle.$$

$$\text{(D.9)}$$

To be able to apply our scheme for their creation, the polynomial

$$p(x, y) = \frac{1}{\sqrt{2N!}} \left(x^N + y^N\right)$$

$$\text{(D.10)}$$

has to be decomposed into linear factors. The decomposition is given by

$$p(x, y) := \frac{1}{\sqrt{2N!}} \prod_{k=0}^{N-1} \left(x - \zeta_N^k y\right)$$

$$\text{(D.11)}$$

where $\zeta_N^k = \exp\left(\frac{(2k+1)\pi i}{N}\right)$, $k = 0, 1, .., N - 1$, are the N-th roots of minus unity. Therefore, one can write

$$p(\hat{a}_1^\dagger, \hat{a}_2^\dagger)|00\rangle = \frac{1}{\sqrt{2N!}} \prod_{k=0}^{N-1} \left(\hat{a}_1^\dagger - \zeta_N^k \hat{a}_2^\dagger \right)|00\rangle \tag{D.12}$$

$$= \frac{1}{\sqrt{2N!}} \sqrt{2}^N \prod_{k=0}^{N-1} \left(t_k \hat{a}_1^\dagger + r_k \hat{a}_2^\dagger \right)|00\rangle, \tag{D.13}$$

where the corresponding transmission and reflection coefficients are

$$t_k = \frac{1}{\sqrt{2}} \quad \text{and} \quad r_k = -\frac{\zeta_N^k}{\sqrt{2}}. \tag{D.14}$$

The corresponding success probability is

$$p_N = q^{2N}(1-q^2)^2 \frac{2N!}{2^N} \frac{1}{N^{N/2}}. \tag{D.15}$$

In Fig. D.1, the success probability is shown for various values of N.

D.2.3   Two-photon states

Let us consider the balanced superposition $\frac{1}{\sqrt{3}}(|20\rangle + |02\rangle + |11\rangle)$, which cannot be obtained by linear optics alone. We can write

$$\frac{1}{\sqrt{3}}(|20\rangle + |02\rangle + |11\rangle) \tag{D.16}$$

$$= \frac{1}{\sqrt{3}} \left(\frac{\hat{a}_1^{\dagger 2}}{\sqrt{2}} + \frac{\hat{a}_2^{\dagger 2}}{\sqrt{2}} + \hat{a}_1^\dagger \hat{a}_2^\dagger \right)|00\rangle \tag{D.17}$$

$$= \sqrt{\frac{1}{6}} \left(\hat{a}_1^\dagger + \frac{1}{\sqrt{2}}(1-i)\hat{a}_2^\dagger \right) \left(\hat{a}_1^\dagger + \frac{1}{\sqrt{2}}(1+i)\hat{a}_2^\dagger \right)|00\rangle \tag{D.18}$$

$$= \sqrt{\frac{2}{3}} \left(\frac{\hat{a}_1^\dagger}{\sqrt{2}} + \frac{1}{2}(1-i)\hat{a}_2^\dagger \right) \left(\frac{\hat{a}_1^\dagger}{\sqrt{2}} + \frac{1}{2}(1+i)\hat{a}_2^\dagger \right)|00\rangle. \tag{D.19}$$

The probability for successful generation is thus $P_{\text{succ}} = \frac{3}{8}q^4(1-q^2)^2$, which is plotted in Fig. D.2. A general superposition of two-photon states can be decomposed as follows:

$$\alpha|20\rangle + \beta|02\rangle + \gamma|11\rangle = (\frac{\alpha}{\sqrt{2}}\hat{a}_1^{\dagger 2} + \frac{\beta}{\sqrt{2}}\hat{a}_2^{\dagger 2} + \gamma\hat{a}_1^\dagger\hat{a}_2^\dagger)|00\rangle \tag{D.20}$$

$$= \frac{\alpha}{\sqrt{2}} \left(\hat{a}_1^\dagger - \hat{a}_2^\dagger \left(-\frac{\gamma}{\sqrt{2}\alpha} + \sqrt{\frac{\gamma^2}{2\alpha^2} - \frac{\beta}{\alpha}} \right) \right) \left(\hat{a}_1^\dagger - \hat{a}_2^\dagger \left(-\frac{\gamma}{\sqrt{2}\alpha} - \sqrt{\frac{\gamma^2}{2\alpha^2} - \frac{\beta}{\alpha}} \right) \right)|00\rangle \tag{D.21}$$
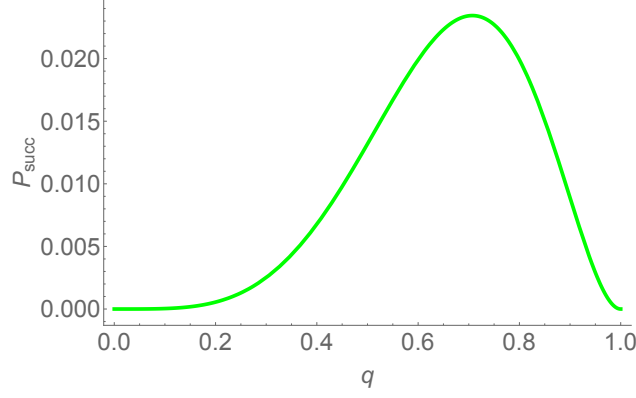
Figure D.2:   Success probability for creating $\frac{1}{\sqrt{3}}(|20\rangle + |02\rangle + |11\rangle)$ in dependence of q (using photon number resolving detectors).

The corresponding transmission and reflection coefficients are

$$t_1 = \frac{1}{\sqrt{1 + \left| -\frac{\gamma}{\sqrt{2}\alpha} + \sqrt{\frac{\gamma^2}{2\alpha^2} - \frac{\beta}{\alpha}} \right|^2}}, \tag{D.22a}$$

$$r_1 = \frac{-\frac{\gamma}{\sqrt{2}\alpha} + \sqrt{\frac{\gamma^2}{2\alpha^2} - \frac{\beta}{\alpha}}}{\sqrt{1 + \left| -\frac{\gamma}{\sqrt{2}\alpha} + \sqrt{\frac{\gamma^2}{2\alpha^2} - \frac{\beta}{\alpha}} \right|^2}} \tag{D.22b}$$

$$t_2 = \frac{1}{\sqrt{1 + \left| \frac{\gamma}{\sqrt{2}\alpha} + \sqrt{\frac{\gamma^2}{2\alpha^2} - \frac{\beta}{\alpha}} \right|^2}}, \tag{D.22c}$$

$$r_2 = -\frac{\frac{\gamma}{\sqrt{2}\alpha} + \sqrt{\frac{\gamma^2}{2\alpha^2} - \frac{\beta}{\alpha}}}{\sqrt{1 + \left| \frac{\gamma}{\sqrt{2}\alpha} + \sqrt{\frac{\gamma^2}{2\alpha^2} - \frac{\beta}{\alpha}} \right|^2}}. \tag{D.22d}$$

D.2.4   Three-mode states

Using the methods described above, as an example of a three-mode state that can be indeed created, we present the following state,

$$\frac{1}{2\sqrt{3}}(\hat{a}_1^\dagger + \hat{a}_2^\dagger)(\hat{a}_1^\dagger + \hat{a}_3^\dagger)(\hat{a}_2^\dagger - \hat{a}_3^\dagger)|000\rangle \tag{D.23}$$

$$= \frac{1}{2\sqrt{3}}(\hat{a}_1^{\dagger 2}\hat{a}_2^\dagger - \hat{a}_1^{\dagger 2}\hat{a}_3^\dagger - \hat{a}_1^{\dagger 2}\hat{a}_3^\dagger + \hat{a}_2^{\dagger 2}\hat{a}_1^\dagger + \hat{a}_2^{\dagger 2}\hat{a}_3^\dagger - \hat{a}_3^{\dagger 2}\hat{a}_2^\dagger)|000\rangle \tag{D.24}$$

$$= \frac{1}{\sqrt{3}}\left(|2\rangle\frac{|10\rangle - |01\rangle}{\sqrt{2}} + |1\rangle\frac{|20\rangle - |02\rangle}{\sqrt{2}} + |0\rangle\frac{|21\rangle - |12\rangle}{\sqrt{2}} \right). \tag{D.25}$$

128

Bibliography

[1] H. J. Kimble, "The quantum internet," *Nature*, vol. 453, pp. 1023–1030, Jun 2008.

[2] C. Simon, "Towards a global quantum network," *Nature Photonics*, vol. 11, no. 11, pp. 678–680, 2017.

[3] R. V. Meter and S. J. Devitt, "The path to scalable distributed quantum computing," *Computer*, vol. 49, pp. 31–42, Sept 2016.

[4] V. Giovannetti, S. Lloyd, and L. Maccone, "Quantum-enhanced positioning and clock synchronization," *Nature*, vol. 412, pp. 417–419, Jul 2001.

[5] D. Gottesman, T. Jennewein, and S. Croke, "Longer-baseline telescopes using quantum repeaters," *Phys. Rev. Lett.*, vol. 109, p. 070503, Aug 2012.

[6] V. Scarani, H. Bechmann-Pasquinucci, N. J. Cerf, M. Dušek, N. Lütkenhaus, and M. Peev, "The security of practical quantum key distribution," *Rev. Mod. Phys.*, vol. 81, pp. 1301–1350, Sep 2009.

[7] H.-K. Lo, M. Curty, and K. Tamaki, "Secure quantum key distribution," *Nat Photon*, vol. 8, pp. 595–604, Aug 2014. Review.

[8] P. Xue, K. Wang, and X. Wang, "Efficient multiuser quantum cryptography network based on entanglement," *Scientific Reports*, vol. 7, pp. 45928 EP –, Apr 2017.

[9] T. C. Ralph, "Quantum optical systems for the implementation of quantum information processing," *Reports on Progress in Physics*, vol. 69, no. 4, p. 853, 2006.

[10] P. Kok, W. J. Munro, K. Nemoto, T. C. Ralph, J. P. Dowling, and G. J. Milburn, "Linear optical quantum computing with photonic qubits," *Rev. Mod. Phys.*, vol. 79, pp. 135–174, Jan 2007.

[11] E. Knill, R. Laflamme, and G. J. Milburn, "A scheme for efficient quantum computation with linear optics," *Nature*, vol. 409, pp. 46–52, Jan 2001.

[12] G. Vallone, D. Bacco, D. Dequal, S. Gaiarin, V. Luceri, G. Bianco, and P. Villoresi, "Experimental satellite quantum communications," *Phys. Rev. Lett.*, vol. 115, p. 040502, Jul 2015.

[13] R. Ursin, F. Tiefenbacher, T. Schmitt-Manderbach, H. Weier, T. Scheidl, M. Lindenthal, B. Blauensteiner, T. Jennewein, J. Perdigues, P. Trojek, B. Omer, M. Furst, M. Meyenburg, J. Rarity, Z. Sodnik, C. Barbieri, H. Weinfurter, and A. Zeilinger, "Entanglement-based quantum communication over 144 km," *Nat Phys*, vol. 3, pp. 481–486, Jul 2007.

[14] W. K. Wootters and W. H. Zurek, "A single quantum cannot be cloned," *Nature*, vol. 299, pp. 802–803, Oct 1982.

[15] D. Dieks, "Communication by EPR devices," *Physics Letters A*, vol. 92, no. 6, pp. 271 – 272, 1982.

[16] H.-J. Briegel, W. Dür, J. I. Cirac, and P. Zoller, "Quantum repeaters: The role of imperfect local operations in quantum communication," *Phys. Rev. Lett.*, vol. 81, pp. 5932–5935, Dec 1998.

[17] W. Dür, H.-J. Briegel, J. I. Cirac, and P. Zoller, "Quantum repeaters based on entanglement purification," *Phys. Rev. A*, vol. 59, pp. 169–181, Jan 1999.

[18] N. Sangouard, C. Simon, H. de Riedmatten, and N. Gisin, "Quantum repeaters based on atomic ensembles and linear optics," *Rev. Mod. Phys.*, vol. 83, pp. 33–80, Mar 2011.

[19] S. Muralidharan, L. Li, J. Kim, N. Lütkenhaus, M. D. Lukin, and L. Jiang, "Optimal architectures for long distance quantum communication," *Scientific Reports*, vol. 6, pp. 20463 EP –, Feb 2016.

[20] D. Bruss and G. Leuchs, *Lectures on quantum information.* Wiley-VCH, 2007.

[21] M. Żukowski, A. Zeilinger, M. A. Horne, and A. K. Ekert, ""Event-ready-detectors" Bell experiment via entanglement swapping," *Phys. Rev. Lett.*, vol. 71, pp. 4287–4290, Dec 1993.

[22] M. Nielsen and I. Chuang, *Quantum Computation and Quantum Information: 10th Anniversary Edition.* Cambridge University Press, 2010.

[23] S. Muralidharan, J. Kim, N. Lütkenhaus, M. D. Lukin, and L. Jiang, "Ultrafast and fault-tolerant quantum communication across long distances," *Phys. Rev. Lett.*, vol. 112, p. 250501, Jun 2014.

[24] D. Lidar and T. Brun, *Quantum Error Correction.* Cambridge University Press, 2013.

[25] E. Knill, R. Laflamme, and L. Viola, "Theory of quantum error correction for general noise," *Phys. Rev. Lett.*, vol. 84, pp. 2525–2528, Mar 2000.

[26] B. E. Kane, "A silicon-based nuclear spin quantum computer," *Nature*, vol. 393, pp. 133–137, May 14 1998.

[27] J. I. Cirac and P. Zoller, "Quantum computations with cold trapped ions," *Phys. Rev. Lett.*, vol. 74, pp. 4091–4094, May 1995.

[28] C. H. Bennett and S. J. Wiesner, "Communication via one- and two-particle operators on Einstein-Podolsky-Rosen states," *Phys. Rev. Lett.*, vol. 69, pp. 2881–2884, Nov 1992.

[29] C. H. Bennett, G. Brassard, C. Crépeau, R. Jozsa, A. Peres, and W. K. Wootters, "Teleporting an unknown quantum state via dual classical and Einstein-Podolsky-Rosen channels," *Phys. Rev. Lett.*, vol. 70, pp. 1895–1899, Mar 1993.

[30] L. Vaidman, "Teleportation of quantum states," *Phys. Rev. A*, vol. 49, pp. 1473–1476, Feb 1994.

[31] R. Raussendorf and H. J. Briegel, "A one-way quantum computer," *Phys. Rev. Lett.*, vol. 86, pp. 5188–5191, May 2001.

[32] R. Horodecki, P. Horodecki, M. Horodecki, and K. Horodecki, "Quantum entanglement," *Rev. Mod. Phys.*, vol. 81, pp. 865–942, Jun 2009.

[33] O. Gühne and G. Tóth, "Entanglement detection," *Physics Reports*, vol. 474, no. 1–6, pp. 1 – 75, 2009.

[34] B. P. Lanyon, M. Barbieri, M. P. Almeida, T. Jennewein, T. C. Ralph, K. J. Resch, G. J. Pryde, J. L. O/'Brien, A. Gilchrist, and A. G. White, "Simplifying quantum logic using higher-dimensional Hilbert spaces," *Nat Phys*, vol. 5, pp. 134–140, Feb 2009.

[35] Z. Gedik, I. A. Silva, B. Çakmak, G. Karpat, E. L. G. Vidoto, D. O. Soares-Pinto, E. R. deAzevedo, and F. F. Fanchini, "Computational speed-up with a single qudit," vol. 5, pp. 14671 EP –, Oct 2015.

[36] N. J. Cerf, M. Bourennane, A. Karlsson, and N. Gisin, "Security of quantum key distribution using d-level systems," *Phys. Rev. Lett.*, vol. 88, p. 127902, Mar 2002.

[37] M. Erhard, R. Fickler, M. Krenn, and A. Zeilinger, "Twisted photons: New quantum perspectives in high dimensions," 2017. arXiv:1708.06101.

[38] T. Vértesi, S. Pironio, and N. Brunner, "Closing the detection loophole in Bell experiments using qudits," *Phys. Rev. Lett.*, vol. 104, p. 060401, Feb 2010.

[39] H.-P. Lo, C.-M. Li, A. Yabushita, Y.-N. Chen, C.-W. Luo, and T. Kobayashi, "Experimental violation of Bell inequalities for multi-dimensional systems," *Sci Rep*, vol. 6, p. 22088, Feb 2016.

[40] M. Kues, C. Reimer, P. Roztocki, L. R. Cortés, S. Sciara, B. Wetzel, Y. Zhang, A. Cino, S. T. Chu, B. E. Little, D. J. Moss, L. Caspani, J. Azaña, and R. Morandotti, "On-chip generation of high-dimensional entangled quantum states and their coherent control," *Nature*, vol. 546, pp. 622–626, Jun 2017.

[41] M. Yukawa, K. Miyata, T. Mizuta, H. Yonezawa, P. Marek, R. Filip, and A. Furusawa, "Generating superposition of up-to three photons for continuous variable quantum information processing," *Opt. Express*, vol. 21, pp. 5529–5535, Mar 2013.

[42] G. Adesso, S. Ragy, and A. R. Lee, "Continuous variable quantum information: Gaussian states and beyond," *Open Syst. Inf. Dyn.*, vol. 21, p. 1440001, Jun 2014.

[43] S. L. Braunstein and P. van Loock, "Quantum information with continuous variables," *Rev. Mod. Phys.*, vol. 77, pp. 513–577, Jun 2005.

[44] M. Mirrahimi, Z. Leghtas, V. V. Albert, S. Touzard, R. J. Schoelkopf, L. Jiang, and M. H. Devoret, "Dynamically protected cat-qubits: a new paradigm for universal quantum computation," *New Journal of Physics*, vol. 16, no. 4, p. 045014, 2014.

[45] Z. Leghtas, G. Kirchmair, B. Vlastakis, R. J. Schoelkopf, M. H. Devoret, and M. Mirrahimi, "Hardware-efficient autonomous quantum memory protection," *Phys. Rev. Lett.*, vol. 111, p. 120501, Sep 2013.

[46] N. Ofek, A. Petrenko, R. Heeres, P. Reinhold, Z. Leghtas, B. Vlastakis, Y. Liu, L. Frunzio, S. M. Girvin, L. Jiang, M. Mirrahimi, M. H. Devoret, and R. J. Schoelkopf, "Extending the lifetime of a quantum bit with error correction in superconducting circuits," *Nature*, vol. 536, pp. 441 EP –, Jul 2016.

[47] M. H. Michael, M. Silveri, R. T. Brierley, V. V. Albert, J. Salmilehto, L. Jiang, and S. M. Girvin, "New class of quantum error-correcting codes for a bosonic mode," *Phys. Rev. X*, vol. 6, p. 031006, Jul 2016.

[48] M. Schlosshauer, "Decoherence, the measurement problem, and interpretations of quantum mechanics," *Rev. Mod. Phys.*, vol. 76, pp. 1267–1305, Feb 2005.

[49] H. Breuer and F. Petruccione, *The Theory of Open Quantum Systems*. Oxford University Press, 2002.

[50] W. F. Stinespring, "Positive functions on C^*-algebras," *Proc. Amer. Math. Soc.*, vol. 6, pp. 211–216, 1955.

[51] K.-E. Hellwig and K. Kraus, "Operations and measurements. ii," *Comm. Math. Phys.*, vol. 16, no. 2, pp. 142–147, 1970.

[52] J. S. Ivan, K. K. Sabapathy, and R. Simon, "Operator-sum representation for bosonic Gaussian channels," *Phys. Rev. A*, vol. 84, p. 042311, Oct 2011.

[53] I. L. Chuang, D. W. Leung, and Y. Yamamoto, "Bosonic quantum codes for amplitude damping," *Phys. Rev. A*, vol. 56, pp. 1114–1125, Aug 1997.

[54] C. H. Bennett, G. Brassard, S. Popescu, B. Schumacher, J. A. Smolin, and W. K. Wootters, "Purification of noisy and faithful teleportation via noisy channels," *Phys. Rev. Lett.*, vol. 78, pp. 2031–2031, Mar 1997.

[55] R. F. Werner, "Quantum states with Einstein-Podolsky-Rosen correlations admitting a hidden-variable model," *Phys. Rev. A*, vol. 40, pp. 4277–4281, Oct 1989.

[56] D. Deutsch, A. Ekert, R. Jozsa, C. Macchiavello, S. Popescu, and A. Sanpera, "Quantum privacy amplification and the security of quantum cryptography over noisy channels," *Phys. Rev. Lett.*, vol. 77, pp. 2818–2821, Sep 1996.

[57] J.-W. Pan, C. Simon, C. Brukner, and A. Zeilinger, "Entanglement purification for quantum communication," *Nature*, vol. 410, pp. 1067–1070, Apr 2001.

[58] J.-W. Pan, S. Gasparoni, R. Ursin, G. Weihs, and A. Zeilinger, "Experimental entanglement purification of arbitrary unknown states," *Nature*, vol. 423, pp. 417–422, May 2003.

[59] M. Horodecki and P. Horodecki, "Reduction criterion of separability and limits for a class of distillation protocols," *Phys. Rev. A*, vol. 59, pp. 4206–4216, Jun 1999.

[60] G. Alber, A. Delgado, N. Gisin, and I. Jex, "Efficient bipartite quantum state purification in arbitrary dimensional Hilbert spaces," *Journal of Physics A: Mathematical and General*, vol. 34, no. 42, p. 8821, 2001.

[61] W. Wasilewski and K. Banaszek, "Protecting an optical qubit against photon loss," *Phys. Rev. A*, vol. 75, p. 042316, Apr 2007.

[62] T. C. Ralph, A. J. F. Hayes, and A. Gilchrist, "Loss-tolerant optical qubits," *Phys. Rev. Lett.*, vol. 95, p. 100501, Aug 2005.

[63] D. W. Leung, M. A. Nielsen, I. L. Chuang, and Y. Yamamoto, "Approximate quantum error correction can lead to better codes," *Phys. Rev. A*, vol. 56, pp. 2567–2573, Oct 1997.

[64] R. Laflamme, C. Miquel, J. P. Paz, and W. H. Zurek, "Perfect quantum error correcting code," *Phys. Rev. Lett.*, vol. 77, pp. 198–201, Jul 1996.

[65] C. H. Bennett, D. P. DiVincenzo, J. A. Smolin, and W. K. Wootters, "Mixed-state entanglement and quantum error correction," *Phys. Rev. A*, vol. 54, pp. 3824–3851, Nov 1996.

[66] D. Gottesman, A. Kitaev, and J. Preskill, "Encoding a qubit in an oscillator," *Phys. Rev. A*, vol. 64, p. 012310, Jun 2001.

[67] S. L. Braunstein, "Error correction for continuous quantum variables," *Phys. Rev. Lett.*, vol. 80, pp. 4084–4087, May 1998.

[68] S. Lloyd and J.-J. E. Slotine, "Analog quantum error correction," *Phys. Rev. Lett.*, vol. 80, pp. 4088–4091, May 1998.

[69] S. L. Braunstein, "Quantum error correction for communication with linear optics," *Nature*, vol. 394, pp. 47–49, Jul 1998.

[70] P. van Loock, "A note on quantum error correction with continuous variables," *Journal of Modern Optics*, vol. 57, no. 19, pp. 1965–1971, 2010.

[71] T. Aoki, G. Takahashi, T. Kajiya, J.-i. Yoshikawa, S. L. Braunstein, P. van Loock, and A. Furusawa, "Quantum error correction beyond qubits," *Nat Phys*, vol. 5, pp. 541–546, Aug 2009.

[72] J. Niset, J. Fiurášek, and N. J. Cerf, "No-go theorem for Gaussian quantum error correction," *Phys. Rev. Lett.*, vol. 102, p. 120501, Mar 2009.

[73] R. Namiki, O. Gittsovich, S. Guha, and N. Lütkenhaus, "Gaussian-only regenerative stations cannot act as quantum repeaters," *Phys. Rev. A*, vol. 90, p. 062316, Dec 2014.

[74] S. Glancy and E. Knill, "Error analysis for encoding a qubit in an oscillator," *Phys. Rev. A*, vol. 73, p. 012325, Jan 2006.

[75] N. Sangouard, R. Dubessy, and C. Simon, "Quantum repeaters based on single trapped ions," *Phys. Rev. A*, vol. 79, p. 042340, Apr 2009.

[76] M. Razavi and J. H. Shapiro, "Long-distance quantum communication with neutral atoms," *Phys. Rev. A*, vol. 73, p. 042303, Apr 2006.

[77] B. Scharfenberger, H. Kosaka, W. J. Munro, and K. Nemoto, "Absorption-based quantum communication with nv centres," *New Journal of Physics*, vol. 17, no. 10, p. 103012, 2015.

[78] L.-M. Duan, M. D. Lukin, J. I. Cirac, and P. Zoller, "Long-distance quantum communication with atomic ensembles and linear optics," *Nature*, vol. 414, pp. 413–418, Nov 2001.

[79] L. Jiang, J. M. Taylor, and M. D. Lukin, "Fast and robust approach to long-distance quantum communication with atomic ensembles," *Phys. Rev. A*, vol. 76, p. 012301, Jul 2007.

[80] B. Zhao, Z.-B. Chen, Y.-A. Chen, J. Schmiedmayer, and J.-W. Pan, "Robust creation of entanglement between remote memory qubits," *Phys. Rev. Lett.*, vol. 98, p. 240502, Jun 2007.

[81] Z.-B. Chen, B. Zhao, Y.-A. Chen, J. Schmiedmayer, and J.-W. Pan, "Fault-tolerant quantum repeater with atomic ensembles and linear optics," *Phys. Rev. A*, vol. 76, p. 022329, Aug 2007.

[82] C. Simon, H. de Riedmatten, M. Afzelius, N. Sangouard, H. Zbinden, and N. Gisin, "Quantum repeaters with photon pair sources and multimode memories," *Phys. Rev. Lett.*, vol. 98, p. 190503, May 2007.

[83] N. Sangouard, C. Simon, B. Zhao, Y.-A. Chen, H. de Riedmatten, J.-W. Pan, and N. Gisin, "Robust and efficient quantum repeaters with atomic ensembles and linear optics," *Phys. Rev. A*, vol. 77, p. 062301, Jun 2008.

[84] P. van Loock, N. Lütkenhaus, W. J. Munro, and K. Nemoto, "Quantum repeaters using coherent-state communication," *Phys. Rev. A*, vol. 78, p. 062319, Dec 2008.

[85] P. van Loock, T. D. Ladd, K. Sanaka, F. Yamaguchi, K. Nemoto, W. J. Munro, and Y. Yamamoto, "Hybrid quantum repeater using bright coherent light," *Phys. Rev. Lett.*, vol. 96, p. 240501, Jun 2006.

[86] U. L. Andersen, J. S. Neergaard-Nielsen, P. van Loock, and A. Furusawa, "Hybrid discrete- and continuous-variable quantum information," *Nat Phys*, vol. 11, pp. 713–719, Sep 2015. Progress Article.

[87] A. D. Pfister, M. Salz, M. Hettrich, U. G. Poschinger, and F. Schmidt-Kaler, "A quantum repeater node with trapped ions: a realistic case example," *Applied Physics B*, vol. 122, no. 4, p. 89, 2016.

[88] J. B. Brask, I. Rigas, E. S. Polzik, U. L. Andersen, and A. S. Sørensen, "Hybrid long-distance entanglement distribution protocol," *Phys. Rev. Lett.*, vol. 105, p. 160501, Oct 2010.

[89] Y. Lim, J. Joo, T. P. Spiller, and H. Jeong, "Loss-resilient photonic entanglement swapping using optical hybrid states," *Phys. Rev. A*, vol. 94, p. 062337, Dec 2016.

[90] E. T. Jaynes and F. W. Cummings, "Comparison of quantum and semiclassical radiation theories with application to the beam maser," *Proceedings of the IEEE*, vol. 51, pp. 89–109, Jan 1963.

[91] C. Gerry and P. Knight, *Introductory Quantum Optics*. Cambridge University Press, 2005.

[92] M. B. Plenio and S. Virmani, "An introduction to entanglement measures," *Quantum Info. Comput.*, vol. 7, pp. 1–51, Jan. 2007.

[93] K. Banaszek, "Optimal receiver for quantum cryptography with two coherent states," *Physics Letters A*, vol. 253, no. 1–2, pp. 12 – 15, 1999.

[94] L. Jiang, J. M. Taylor, K. Nemoto, W. J. Munro, R. Van Meter, and M. D. Lukin, "Quantum repeater with encoding," *Phys. Rev. A*, vol. 79, p. 032325, Mar 2009.

[95] E. Knill, "Quantum computing with realistically noisy devices," *Nature*, vol. 434, pp. 39–44, Mar 2005.

[96] N. K. Bernardes and P. van Loock, "Hybrid quantum repeater with encoding," *Phys. Rev. A*, vol. 86, p. 052301, Nov 2012.

[97] W. J. Munro, K. A. Harrison, A. M. Stephens, S. J. Devitt, and K. Nemoto, "From quantum multiplexing to high-performance quantum networking," *Nat Photon*, vol. 4, pp. 792–796, Nov 2010.

[98] R. Raussendorf, D. E. Browne, and H. J. Briegel, "Measurement-based quantum computation on cluster states," *Phys. Rev. A*, vol. 68, p. 022312, Aug 2003.

[99] A. Blais, R.-S. Huang, A. Wallraff, S. M. Girvin, and R. J. Schoelkopf, "Cavity quantum electrodynamics for superconducting electrical circuits: An architecture for quantum computation," *Phys. Rev. A*, vol. 69, p. 062320, Jun 2004.

[100] F. Ewert, M. Bergmann, and P. van Loock, "Ultrafast long-distance quantum communication with static linear optics," *Phys. Rev. Lett.*, vol. 117, p. 210501, Nov 2016.

[101] F. Ewert and P. van Loock, "Ultrafast fault-tolerant long-distance quantum communication with static linear optics," *Phys. Rev. A*, vol. 95, p. 012327, Jan 2017.

[102] S. Muralidharan, C.-L. Zou, L. Li, J. Wen, and L. Jiang, "Overcoming erasure errors with multilevel systems," *New Journal of Physics*, vol. 19, no. 1, p. 013026, 2017.

[103] W. J. Munro, A. M. Stephens, S. J. Devitt, K. A. Harrison, and K. Nemoto, "Quantum communication without the necessity of quantum memories," *Nat Photon*, vol. 6, pp. 777–781, Nov 2012.

[104] K. Azuma, K. Tamaki, and H.-K. Lo, "All-photonic quantum repeaters," *Nature Communications*, vol. 6, pp. 6787 EP –, Apr 2015.

[105] B. C. Sanders, "Quantum dynamics of the nonlinear rotator and the effects of continual spin measurement," *Phys. Rev. A*, vol. 40, pp. 2417–2427, Sep 1989.

[106] P. Kok, H. Lee, and J. P. Dowling, "Creation of large-photon-number path entanglement conditioned on photodetection," *Phys. Rev. A*, vol. 65, p. 052104, Apr 2002.

[107] M. W. Mitchell, J. S. Lundeen, and A. M. Steinberg, "Super-resolving phase measurements with a multiphoton entangled state," *Nature*, vol. 429, pp. 161–164, May 2004.

[108] P. Walther, J.-W. Pan, M. Aspelmeyer, R. Ursin, S. Gasparoni, and A. Zeilinger, "De broglie wavelength of a non-local four-photon state," *Nature*, vol. 429, pp. 158–161, May 2004.

[109] J. J. . Bollinger, W. M. Itano, D. J. Wineland, and D. J. Heinzen, "Optimal frequency measurements with maximally correlated states," *Phys. Rev. A*, vol. 54, pp. R4649–R4652, Dec 1996.

[110] N. Gisin and R. Thew, "Quantum communication," *Nat Photon*, vol. 1, pp. 165–171, Mar 2007.

[111] V. Giovannetti, S. Lloyd, and L. Maccone, "Advances in quantum metrology," *Nat Photon*, vol. 5, pp. 222–229, Apr 2011.

[112] A. N. Boto, P. Kok, D. S. Abrams, S. L. Braunstein, C. P. Williams, and J. P. Dowling, "Quantum interferometric optical lithography: Exploiting entanglement to beat the diffraction limit," *Phys. Rev. Lett.*, vol. 85, pp. 2733–2736, Sep 2000.

[113] K. R. Motes, J. P. Olson, E. J. Rabeaux, J. P. Dowling, S. J. Olson, and P. P. Rohde, "Linear optical quantum metrology with single photons: Exploiting spontaneously generated entanglement to beat the shot-noise limit," *Phys. Rev. Lett.*, vol. 114, p. 170802, Apr 2015.

[114] C. C. Gerry and R. A. Campos, "Generation of maximally entangled photonic states with a quantum-optical fredkin gate," *Phys. Rev. A*, vol. 64, p. 063814, Nov 2001.

[115] K. T. Kapale and J. P. Dowling, "Bootstrapping approach for generating maximally path-entangled photon states," *Phys. Rev. Lett.*, vol. 99, p. 053602, Aug 2007.

[116] H. Lee, P. Kok, N. J. Cerf, and J. P. Dowling, "Linear optics and projective measurements alone suffice to create large-photon-number path entanglement," *Phys. Rev. A*, vol. 65, p. 030101, Mar 2002.

[117] N. M. VanMeter, P. Lougovski, D. B. Uskov, K. Kieling, J. Eisert, and J. P. Dowling, "General linear-optical quantum state generation scheme: Applications to maximally path-entangled states," *Phys. Rev. A*, vol. 76, p. 063808, Dec 2007.

[118] H. Cable and J. P. Dowling, "Efficient generation of large number-path entanglement using only linear optics and feed-forward," *Phys. Rev. Lett.*, vol. 99, p. 163604, Oct 2007.

[119] M. Bohmann, J. Sperling, and W. Vogel, "Entanglement and phase properties of noisy NOON states," *Phys. Rev. A*, vol. 91, p. 042332, Apr 2015.

[120] V. Potoček, F. M. Miatto, M. Mirhosseini, O. S. Magaña Loaiza, A. C. Liapis, D. K. L. Oi, R. W. Boyd, and J. Jeffers, "Quantum Hilbert Hotel," *Phys. Rev. Lett.*, vol. 115, p. 160505, Oct 2015.

[121] H. Fearn and R. Loudon, "Quantum theory of the lossless beam splitter," *Optics Communications*, vol. 64, no. 6, pp. 485 – 490, 1987.

[122] A. V. Sharypov and B. He, "Generation of arbitrary symmetric entangled states with conditional linear optical coupling," *Phys. Rev. A*, vol. 87, p. 032323, Mar 2013.

[123] A. P. Lund, T. C. Ralph, and H. L. Haselgrove, "Fault-tolerant linear optical quantum computing with small-amplitude coherent states," *Phys. Rev. Lett.*, vol. 100, p. 030503, Jan 2008.

[124] S. Glancy, H. M. Vasconcelos, and T. C. Ralph, "Transmission of optical coherent-state qubits," *Phys. Rev. A*, vol. 70, p. 022317, Aug 2004.

[125] R. Wickert and P. van Loock, "Quantum error correction and detection: Quantitative analysis of a coherent-state amplitude-damping code," *Phys. Rev. A*, vol. 89, p. 052309, May 2014.

[126] R. Wickert, N. K. Bernardes, and P. van Loock, "Entanglement properties of optical coherent states under amplitude damping," *Phys. Rev. A*, vol. 81, p. 062344, Jun 2010.

[127] D. Gottesman, "Stabilizer codes and quantum error correction," 1997. Caltech Ph. D. thesis.

[128] B. M. Terhal, "Quantum error correction for quantum memories," *Rev. Mod. Phys.*, vol. 87, pp. 307–346, Apr 2015.

[129] V. V. Albert, C. Shu, S. Krastanov, C. Shen, R.-B. Liu, Z.-B. Yang, R. J. Schoelkopf, M. Mirrahimi, M. H. Devoret, and L. Jiang, "Holonomic quantum control with continuous variable systems," *Phys. Rev. Lett.*, vol. 116, p. 140502, Apr 2016.

[130] U. L. Andersen and T. C. Ralph, "High-fidelity teleportation of continuous-variable quantum states using delocalized single photons," *Phys. Rev. Lett.*, vol. 111, p. 050504, Aug 2013.

[131] S. Dogra, K. Dorai, and Arvind, "Experimental demonstration of quantum contextuality on an NMR qutrit," *Physics Letters A*, vol. 380, no. 22, pp. 1941 – 1946, 2016.

[132] A. Chefles, "Unambiguous discrimination between linearly independent quantum states," *Physics Letters A*, vol. 239, no. 6, pp. 339 – 347, 1998.

[133] S. J. van Enk, "Unambiguous state discrimination of coherent states with linear optics: Application to quantum cryptography," *Phys. Rev. A*, vol. 66, p. 042313, Oct 2002.

[134] S. Croke, S. M. Barnett, and G. Weir, "Optimal sequential measurements for bipartite state discrimination," *Phys. Rev. A*, vol. 95, p. 052308, May 2017.

[135] M. Dušek, "Discrimination of the Bell states of qudits by means of linear optics," *Optics Communications*, vol. 199, no. 1–4, pp. 161 – 166, 2001.

[136] N. K. Bernardes, L. Praxmeyer, and P. van Loock, "Rate analysis for a hybrid quantum repeater," *Phys. Rev. A*, vol. 83, p. 012323, Jan 2011.

[137] J. Dias and T. C. Ralph, "Quantum repeaters using continuous-variable teleportation," *Phys. Rev. A*, vol. 95, p. 022312, Feb 2017.

[138] W. Munro and F. Furrer, "Designing quantum repeaters for continuous variable quantum communication," in *Conference on Lasers and Electro-Optics*, p. FM2E.7, Optical Society of America, 2017.

[139] K. Hammerer, A. S. Sørensen, and E. S. Polzik, "Quantum interface between light and atomic ensembles," *Rev. Mod. Phys.*, vol. 82, pp. 1041–1093, Apr 2010.

[140] D. P. DiVincenzo, "The physical implementation of quantum computation," *Fortschritte der Physik*, vol. 48, no. 9-11, pp. 771–783, 2000.

[141] D. A. Lidar, *Review of Decoherence-Free Subspaces, Noiseless Subsystems, and Dynamical Decoupling*, pp. 295–354. John Wiley & Sons, Inc., 2014.

[142] E. G. Carnio, A. Buchleitner, and M. Gessner, "Generating and protecting correlated quantum states under collective dephasing," *New Journal of Physics*, vol. 18, no. 7, p. 073010, 2016.

[143] D. Kielpinski, V. Meyer, M. A. Rowe, C. A. Sackett, W. M. Itano, C. Monroe, and D. J. Wineland, "A decoherence-free quantum memory using trapped ions," *Science*, vol. 291, no. 5506, pp. 1013–1015, 2001.

[144] M. Zwerger, B. P. Lanyon, T. E. Northup, C. A. Muschik, W. Dür, and N. Sangouard, "Quantum repeaters based on trapped ions with decoherence-free subspace encoding," *Quantum Science and Technology*, vol. 2, no. 4, p. 044001, 2017.

[145] M. Takeoka, S. Guha, and M. M. Wilde, "Fundamental rate-loss tradeoff for optical quantum key distribution," *Nature Communications*, vol. 5, pp. 5235 EP –, Oct 2014.

[146] Y.-W. Cho, G. T. Campbell, J. L. Everett, J. Bernu, D. B. Higginbottom, M. T. Cao, J. Geng, N. P. Robins, P. K. Lam, and B. C. Buchler, "Highly efficient optical quantum memory with long coherence time in cold atoms," *Optica*, vol. 3, pp. 100–107, Jan 2016.

[147] V. V. Albert, K. Noh, K. Duivenvoorden, R. T. Brierley, P. Reinhold, C. Vuillot, L. Li, C. Shen, S. M. Girvin, B. M. Terhal, and L. Jiang, "Performance and structure of bosonic codes," 2017. arXiv:1708.05010.

[148] M. Y. Niu, I. L. Chuang, and J. H. Shapiro, "Hardware-efficient bosonic quantum error-correcting codes based on symmetry operators," 2017. arXiv:1709.05302.

[149] D. Su and T. C. Ralph, "Quantum communication in the presence of a horizon," *Phys. Rev. D*, vol. 90, p. 084022, Oct 2014.

[150] M. Dušek, M. Jahma, and N. Lütkenhaus, "Unambiguous state discrimination in quantum cryptography with weak coherent states," *Phys. Rev. A*, vol. 62, p. 022306, Jul 2000.

Aus Datenschutzgründen entfernt.